Winter 12-22-2021

Fine Scales, Broad Consequences: Drivers and Effects of Microclimatic Variation in Great Smoky Mountains National Park

Jordan Rebecca Stark
Syracuse University

Abstract

Climate is highly variable at scales that are not captured by most weather and climate models due to local effects of topography and living systems. This variation in microclimate has been noted for many decades but has been difficult to incorporate into quantitative understanding of ecological systems and processes due to the large amount of data and complex models required to adequately describe fine-scale patterns across complex landscapes. In recent years, models of thermal microclimate variation have been developed using low-cost temperature sensors, but few of these models have been used to predict the effects of microclimatic variation on ecological processes and patterns such as species distributions. In addition, no similar low-cost tools have been commercialized for soil moisture measurements, limiting the ability of microclimate models to fully describe the conditions experienced by organisms. In Chapter 1, I compare species distribution models for the plants of Great Smoky Mountains National Park (GSMNP) generated using broad-scale climate drivers to those generated using an existing thermal microclimate model. While model fit was similar, microclimate projections of future suitable habitat under climate change were very different from macroclimate projections, highlighting the need to consider local buffering of climate when planning for the future. In Chapter 2, I develop, test, and deploy new low-cost soil moisture sensors across GSMNP and describe the effects of topographic, vegetation, and weather-related drivers on soil moisture. Local variation in moisture was high and was not fully explained by the gradient of precipitation or other proxies for moisture availability across the Park, indicating that better models are needed to describe the moisture available to organisms across the landscape. Together, these results demonstrate the need to consider the effects of microclimate on ecological systems and provide new tools for understanding multiple axes of microclimatic variation.

Fine scales, broad consequences: drivers and effects of microclimatic variation in Great Smoky Mountains National Park

By

Jordan Rebecca Stark

B.A. Skidmore College 2015

THESIS

Submitted in partial fulfillment of the requirements for the degree of

Master of Science in Biology

Syracuse University

December 2021

Acknowledgements

This project would not have been possible without the generous assistance of many people. First and foremost, the support and mentorship of my advisor, Jason Fridley, has been invaluable. Thank you for sharing your expertise and for giving me the guidance, encouragement, and space I needed—I really cannot imagine a better graduate school experience than working in your lab. My committee members John Stella, Martin Dovciak, and Doug Frank have also provided excellent advice on this work. Two amazing research assistants, Minhein Htet and Sophia Cohen, contributed to a wide array of projects including sensor design, construction, fieldwork, and data processing. Thank you for your brilliant ideas and for putting up with many steep miles of hiking with me in the Smokies. Work in the Park was facilitated by Paul Super – thank you for your guidance on the science as well as everything from permits to keeping sensors safe from curious bears. Paul Super and two anonymous reviewers also provided comments on drafts of Chapter 1.

I owe a great debt to the graduate students in the biology department who have answered all of my silly questions and supported me when things were difficult, especially Neha Mohan Babu, Alex Ebert, Sarah Araldi-Brondolo, Julie LeVonne, Anne Curé, and Sarah Weiss. I would also like to thank the many supervisors, co-workers, and colleagues who taught me how to do ecological research and encouraged me on my path to graduate school, including Zoe Cardon, Suzanne Thomas, Elena Lopez Peredo, Rich McHorney, Christine O'Connell, Omar Gutiérrez del Arroyo Santiago, Carla López Lloreda, Sarah Hamman, and Ben Blonder.

This work was supported by a grant from the National Park Service. Additional funding was provided by Friends of Great Smoky Mountains National Park. Vegetation archival activities were supported by the National Parks Ecological Research Fellowship program, a

partnership between the National Park Service, the Ecological Society of America, and the National Park Foundation, and funded through a generous grant from the Andrew W. Mellon Foundation. The vegetation database used in Chapter 1 was created by Jason Fridley with assistance from M. Jenkins, K. Langdon, P. Super, P. White, and the many researchers that contributed vegetation data.

Table of Contents

List of Illustrative Materials

Chapter 1

Chapter 2

Appendices

Introduction

Climate is a key driver of many ecological and environmental processes. However, measurements and models of climate are usually generated from weather station data which can describe only broad-scale patterns driven by widespread processes such as weather fronts and continental drivers of climate such as latitude. These measurements are made in environments selected to be representative of the conditions in open, non-forested areas rather than capturing the heterogeneity of natural systems. The mismatch between the climate measured by weather stations (macroclimate) and the climates experienced by organisms near the ground (microclimate) has been recognized for decades (Geiger, 1966). Differences between local climate and climate interpolated from weather stations can be driven by physical factors including radiative load, hillslope position, and local topographic position (Bramer et al., 2018; Geiger, 1966). Biotic communities can also shape their own climatic conditions: under forest canopies, temperatures are generally more buffered than at open weather stations, with summer high temperatures several degrees cooler and winter low temperature several degrees warmer under forest canopies than in the open (De Frenne et al., 2019; Haesen et al., 2021). These local differences in temperature, equivalent to hundreds of miles of latitude, are often ignored in models of ecological and environmental processes.

Understanding the effects of microclimatic variation will be critical for predicting ecological processes across space and time, especially in the context of global change. To date, while several studies have found effects of microclimatic conditions on species responses to warming (De Frenne et al., 2013; Graae et al., 2018; Zellweger et al., 2020), few studies have compared predictions of habitat stability and species distributions using macroclimate and locally-validated microclimate drivers. The effects of other axes of microclimatic variation, such

as variation in moisture availability, are even more poorly described. Microclimatic research has overwhelmingly focused on thermal variables (Bramer et al., 2018). Thermal microclimate variation has been quantified in large part due to low-cost, easily-deployed sensor technology for measuring temperature; sensors needed to take equivalent timeseries measurements of soil moisture are generally expensive, bulky, hard to maintain, and have high power requirements. This makes deployment of large numbers of sensors difficult, particularly in landscapes where sensors could be damaged or destroyed or must be deployed in remote areas. New tools for monitoring environmental conditions have been developed that could help to address these issues, including the environmental microcontroller units (EMUs) described by Mickley et al (2019). These sensor and datalogger units have low power requirements, can be assembled inexpensively from commercially available electronic components, and can measure a wide range of conditions including temperature, light, humidity, and soil moisture for tens, rather than hundreds or thousands, of dollars. However, several issues in the use and calibration of these sensors, including temperature-dependency of soil moisture measurements and robustness of long-term sensor deployments, have not been resolved by previous work.

Local variation in moisture and temperature is high across a wide range of environments, but short gradients of temperature and moisture are particularly evident in some forested, topographically complex systems. Here, I examine drivers and effects of microclimatic variation in Great Smoky Mountains National Park (GSMNP; NC and TN, USA). This area is among the earliest sites where local climate variation was described as shaping plant distributions, with completely different plant community composition in sheltered coves than on adjacent exposed ridges. This cove-to-ridge gradient is associated with local variation in moisture availability (Whittaker, 1956), and also leads to strong local variation in below-canopy temperatures (Fridley

2009). Plant communities in the Park are diverse and include, at the highest elevations, spruce-fir forests more commonly associated with boreal regions. Rainfall is high throughout the Park, increasing from about 150 cm at low elevation to about 230 cm at high elevation (Shanks, 1954). Previous work has described high local variation in below-canopy temperature, with differences on hot summer days of up to 4 °C from coves to adjacent exposed ridges (Fridley, 2009). However, quantitative measurements of microclimate across the Park have been limited to thermal variables, and while effects of microclimate on individual species have been examined (Ulrey, Quintana-Ascencio, Kauffman, Smith, & Menges, 2016), Whittaker's (1956) description of local topography as a key driver of species distributions across the Park has not been revisited with fine-scale climate data that would allow a more mechanistic understanding of the relationship between plant distributions and particular climate variables. Since global change may affect some microclimatic variables differently than others, developing a quantitative understanding of the effects of multiple microclimatic drivers on species and processes will be key to understanding which species and areas are most at risk.

Here, I use existing thermal microclimate models, species occurrence records, and newly-developed soil moisture and temperature sensors to describe effects of thermal microclimate on plant communities and measure local variation in moisture across GSMNP. While existing microclimate models, short climatic gradients, and extensive species records lend themselves to this work in the Park, similar processes likely occur in topographically complex and forested regions throughout the world. In Chapter 1, I use projections of climate based on interpolated weather station data (Fick & Hijmans, 2017) and an existing thermal microclimate model (Fridley, 2009) to develop species distribution models for plant species across GSMNP. Below-canopy temperatures in the Park are buffered compared to weather station predictions, with the

strongest effects on very hot days (Fridley, 2009; Lesser & Fridley, 2015). Therefore, plants occurring in some areas may be more exposed to atmospheric conditions and risks associated with climate change. In Chapter 2, I describe development, deployment, and results of a new low-cost, low-power, soil moisture and temperature sensor. These new sensors, which cost more than an order of magnitude less than commercial soil moisture sensors and dataloggers, can allow distributed monitoring of soil moisture that allows measurement of another axis of microclimatic variation. Using these sensors, I describe landscape-wide variation in soil moisture conditions in GSMNP. In total, these two chapters examine the variability of microclimatic conditions across the complex topography of GSMNP and explore the effects of this microclimatic variability on species which have adapted to particular climates and are now under threat from climatic changes.

References

Bramer, I., Anderson, B. J., Bennie, J., Bladon, A. J., De Frenne, P., Hemming, D., … Gillingham, P. K. (2018). Advances in Monitoring and Modelling Climate at Ecologically Relevant Scales. *Advances in Ecological Research*, 58, 101–161. https://doi.org/10.1016/bs.aecr.2017.12.005

De Frenne, P., Rodríguez-Sánchez, F., Coomes, D. A., Baeten, L., Verstraeten, G., Vellen, M., … Verheyen, K. (2013). Microclimate moderates plant responses to macroclimate warming. *Proceedings of the National Academy of Sciences of the United States of America*, 110(46), 18561–18565. https://doi.org/10.1073/pnas.1311190110

De Frenne, P., Zellweger, F., Rodríguez-Sánchez, F., Scheffers, B. R., Hylander, K., Luoto, M., … Lenoir, J. (2019). Global buffering of temperatures under forest canopies. *Nature Ecology and Evolution*, 3(5), 744–749. https://doi.org/10.1038/s41559-019-0842-1

Fick, S. E., & Hijmans, R. J. (2017). WorldClim 2: new 1-km spatial resolution climate surfaces for global land areas. *International Journal of Climatology*, 37(12), 4302–4315. https://doi.org/10.1002/joc.5086

Fridley, J. D. (2009). Downscaling climate over complex terrain: High finescale (<1000 m) spatial variation of near-ground temperatures in a montane forested landscape (Great Smoky Mountains). *Journal of Applied Meteorology and Climatology*, 48(5), 1033–1049. https://doi.org/10.1175/2008JAMC2084.1

Geiger, R. (1966). The climate near the ground (Translated). Cambridge, MA: Harvard University Press.

Graae, B. J., Vandvik, V., Armbruster, W. S., Eiserhardt, W. L., Svenning, J. C., Hylander, K., … Lenoir, J. (2018). Stay or go – how topographic complexity influences alpine plant population and community responses to climate change. *Perspectives in Plant Ecology, Evolution and Systematics*, 30(February 2018), 41–50. https://doi.org/10.1016/j.ppees.2017.09.008

Haesen, S., Lembrechts, J. J., De Frenne, P., Lenoir, J., Aalto, J., Ashcroft, M. B., … Van Meerbeek, K. (2021). ForestTemp – Sub-canopy microclimate temperatures of European forests. *Global Change Biology*, (September), 1–13. https://doi.org/10.1111/gcb.15892

Lesser, M. R., & Fridley, J. D. (2015). Global change at the landscape level: Relating regional and landscape-scale drivers of historical climate trends in the Southern Appalachians. *International Journal of Climatology*, 36(3), 1197–1209. https://doi.org/10.1002/joc.4413

Mickley, J. G., Moore, T. E., Schlichting, C. D., DeRobertis, A., Pfisterer, E. N., & Bagchi, R. (2019). Measuring microenvironments for global change : DIY environmental microcontroller units (EMUs). *Methods in Ecology and Evolution*, 10(November 2018), 578–584. https://doi.org/10.1111/2041-210X.13128

Shanks, R. E. (1954). Climates of the Great Smoky Mountains. *Ecology*, 35(3), 354–361. https://doi.org/10.2307/1930098

Ulrey, C., Quintana-Ascencio, P. F., Kauffman, G., Smith, A. B., & Menges, E. S. (2016). Life at the top: Long-term demography, microclimatic refugia, and responses to climate change for a high-elevation southern Appalachian endemic plant. *Biological Conservation*, 200, 80–92. https://doi.org/10.1016/j.biocon.2016.05.028

Whittaker, R. H. (1956). Vegetation of the Great Smoky Mountains. *Ecological Monographs*, 26(1), 1–80.

Zellweger, F., de Frenne, P., Lenoir, J., Vangansbeke, P., Verheyen, K., Bernhardt-Römermann, M., … Coomes, D. (2020). Forest microclimate dynamics drive plant responses to warming. *Science*, 368(6492), 772–775. https://doi.org/10.1126/science.aba6880

Chapter 1: Microclimate-based species distribution models in complex terrain indicate widespread cryptic refugia under climate change

Jordan R. Stark and Jason Fridley

Currently in review at *Global Ecology and Biogeography*

Supplemental figures and tables are available in the Appendix

Abstract

Aim: Species' climatic niches may be poorly predicted by regional climate estimates used in species distribution models (SDMs) due to microclimatic buffering of local conditions. Here, we compare SDMs generated using a locally validated below-canopy microclimate model to those based on interpolated weather station data at two spatial scales to determine the effects of scale, topography, and forest cover on potential future ground-level warming and species distributions.

Location: Great Smoky Mountains National Park (2090 km^2; NC, TN, USA)

Time period: 1970 – 2006, late-century warming

Major taxa: Vascular plant species of the Southern Appalachians

Methods: We compared the fit and spatiotemporal predictions of SDMs generated using a database of plant occurrences and three climate models: macroclimate (1 km, WorldClim), fine-scale (30 m) interpolation of macroclimate with elevation, and fine-scale below-canopy microclimate from a ground-level sensor network. We projected microclimatic warming with 4 °C of regional warming to predict future habitat suitability.

Results: We found that, although SDM fit (area under the curve) was similar across models, microclimate-derived SDMs predicted substantially greater species persistence with warming, with a difference of 50% of the species pool in some areas. Microclimate SDMs predicted higher stability of mid-elevation species, particularly in thermally buffered areas near streams, and

critically, less change in species composition at high elevation. In contrast, predictions of macroclimate and interpolation models were similar despite improved resolution.
Main conclusions: Our results demonstrate that careful selection of climate drivers, including local near-ground validation rather than interpolation, is critical for projecting species distributions. They also suggest that some species at risk from climate change might persist, even with 4 °C of macroclimate warming, in cryptic refugia buffered by microclimate, pointing to the roles of forest cover and topography in explaining slower-than-expected changes in understory communities. However, certain species, such as those currently occurring on low-elevation ridges that are sensitive to atmospheric changes, may be at more risk than macroclimate or interpolated SDMs suggest.

Introduction

The role of climate in constraining plant species distributions is a foundational ecological concept that has taken on new urgency in light of anthropogenic climate change. While the relationship between plant distributions and climate has historically been considered at regional to continental scales, local climate variation on scales of tens of meters can also be strong, with microclimate conditions varying in complex ways that are sometimes decoupled from regional climate (Geiger, 1966). The effects of this small-scale variation in climate on plant species distributions are not well understood, although ecologists have long noted steep local gradients in climate and species composition in topographically complex terrain. For example, in Great Smoky Mountains National Park (GSMNP, NC and TN, USA) the topographic transition from coves to ridges is associated with complete turnover of plant species composition in the Park across distances less than 500 m (Whittaker, 1956). In contrast, regional climate estimates (≥1

km resolution) based on interpolated weather station data largely reflect broad-scale gradients such as those generated by latitude, continentality, and the movement of synoptic air masses. The effect of local climate variability on plant distributions is particularly important to understand in a global change context, since organisms that inhabit relatively warm microclimates under current conditions may be able to escape the warming effects of climate change by moving into cooler microclimates without needing to disperse over the long distances projected by macroclimate models (Graae et al., 2018). In addition, historical data suggest that the difference between microclimate and macroclimate temperatures could increase as macroclimate temperatures warm (De Frenne et al., 2021).

Recent evidence supports the idea that the buffering effect of forest canopies on temperature is related to slower-than-expected responses of some species to climate change (De Frenne et al., 2013; Suggitt et al., 2018; Zellweger et al., 2020). Understory microclimate measurements indicate that thermal buffering is strongest on the hottest days (Fridley, 2009; Lesser & Fridley, 2015), suggesting that the forest canopy may limit the warming experienced in the understory in some systems. This microclimate buffering happens when local terrain and physiognomic elements (e.g. topography, canopy structure, and cold-air drainage) drive differences between microclimate and macroclimate temperatures, leading to an uneven distribution of microclimatic conditions in macroclimate space (Geiger, 1966). In general, buffering has its strongest effects on climate extremes (De Frenne et al., 2021). If buffered areas are common or increasing with climate change, microclimate-derived models of species distributions could allow identification of "cryptic refugia", defined here as locations where climatically sensitive species can persist despite incompatibility with regional climate (Rull, 2010; Stewart, Lister, Barnes & Dalen, 2010). Cryptic refugia have been proposed as important

in understanding the recovery of species distributions following glaciation (Cruzan & Templeton, 2000).

The need for locally validated, biophysically-based microclimate models in predicting species distributions under climate change has been widely acknowledged (e.g. Opedal, Armbruster, & Graae, 2015; Scherrer & Körner, 2011), but there are few studies that include locally-validated microclimate drivers in species distribution models (SDMs). Slavich et al. (2014) modelled climate variation at 25 m resolution and found fewer predicted species extinctions with climate change than in a downscaled regional climate model. However, they projected warming evenly across the landscape, potentially missing complex patterns of warming due to the relationship between microclimatic buffering and above-canopy temperatures (De Frenne et al., 2021; Fridley, 2009; Lesser & Fridley, 2015). Two other studies compared SDMs driven by measured microclimate and other climate products, but did not project climate change impacts: Storlie et al. (2013) found improved model fit and patchier species distributions with a local climate model, and Lembrechts et al. (2019) found best model fit with local soil temperature (compared to several other drivers). As a result, although the importance of microclimate in driving species distributions is widely acknowledged, quantitative understanding of its role in predicting species responses to climate change remains poor.

Several studies have modelled the effect of climate change on species distributions using spatially downscaled models based on elevation or other proxies for fine-scale landscape heterogeneity. However, as these models do not account for any differences between temperatures measured at weather stations and temperature in buffered habitats (such as near streams or under forest canopies), they may not accurately describe future climatic refugia (Dobrowski, 2011). Spatial downscaling has had variable effects depending on the study: Randin

et al. (2009), Maclean et al. (2015), and Meineri and Hylander (2017) found increased predicted species persistence under climate change, while Trivedi et al. (2008) and Franklin et al. (2013) found decreased persistence. The different results of these tests may relate to true ecological differences between species and sites or to specific model choices, including accounting for incomplete climate gradients and variable spatial resolution. In most other SDMs, predictions have been generated using low-resolution gridded climate estimates (≥ 1 km), although microclimate variation is increasingly acknowledged as needing further study (Lembrechts, Nijs, & Lenoir, 2019; Potter, Arthur Woods, & Pincebourde, 2013; Seo, Thorne, Hannah, & Thuiller, 2009).

GSMNP is particularly well suited to analysis of relationships between species distributions and climatic factors. Located near the southern end of the Appalachian Mountains with >1700 m of elevation change within 2090 km^2, the gradients of GSMNP capture much of the range of both climatic conditions and species composition present in Eastern North America (Braun, 1950). This variation has inspired a long history of compositional gradient analysis, including some of the earliest work mapping species habitats onto climatic and topographic conditions (Whittaker, 1956). Short topographic gradients are associated with both complete turnover of species and strong variability in local climatic conditions driven by biophysical processes. When temperatures are warm, the effects of landform can be as strong as the effects of elevation, with variation in ground-level temperature between protected coves and adjacent exposed ridges of up to 4 °C, or about half of the variation in mean annual temperature due to latitude in the continental United States (Fridley, 2009). Historical weather station records allow estimation of these local climatic conditions since ca. 1900 (Lesser & Fridley, 2015), so that microclimate conditions can be directly compared with commonly used global macroclimate

summaries. Park-wide quantitative assessments of the relationship between microclimate conditions and species distributions have never been conducted, although work on some rare species indicates that particular microclimates are needed for their survival (Ulrey et al., 2016).

Here, we quantify differences between historical and warmed climate scenarios based on three models of the climate in GSMNP: macroclimate conditions from WorldClim 2.1 (Fick & Hijmans, 2017; 1 km resolution); interpolation of macroclimate conditions using local variation in elevation (30 m resolution); and a locally-validated below-canopy microclimate model (Fridley, 2009; 30 m resolution). For each climate model, we estimate future warming using a 4 °C regional warming scenario based on late-century global climate models (GCMs). For the microclimate model, we also account for effects of microclimatic buffering and historical relationships between regional temperature and elevational lapse rates to describe expected below-canopy warming rates. We use these climate models as drivers of GSMNP-wide plant SDMs and analyze differences in current and future predicted habitat suitability to understand the species and regions of GSMNP that may be particularly susceptible or resistant to the effects of regional climate warming. We address three broad questions. First, how well do macroclimate and interpolated climate describe microclimate conditions? Are there particular areas that are poorly described, especially in terms of their warming potential? Second, does building SDMs with microclimate drivers improve model accuracy compared to macroclimate or interpolated climate drivers? Finally, how do future habitat suitability predictions differ in SDMs based on the three climate models with 4 °C of regional warming? Are the predictions with elevation-based interpolation sufficient to identify cryptic refugia, or is the validated microclimate model necessary?

Methods

Study area

GSMNP includes 2090 km^2 of primary and secondary forest and is among the most diverse biotic regions in North America (Shanks, 1954; Whittaker, 1956). The elevation gradient spans over 1700 m (256-2024 m a.s.l.), in some places across distances less than 10 km, and is associated with a 10-15 °C ground-level temperature difference during the growing season (Fridley, 2009). GSMNP lacks a climatic treeline but most species reach their upper or lower climatic limits in the Park. High elevation communities of boreal forest experience heavy cloud cover and annual precipitation > 250 cm/year, while the lowest elevations are characterized by deciduous oak-hickory vegetation of the southern piedmont with annual precipitation < 150 cm (Shanks, 1954), increasing by 10% over the 20^{th} century (Lesser & Fridley, 2015). A steep terrain of narrow ridges and rocky coves is associated with a secondary microclimatic gradient that Fridley (2009), using a network of ground-level temperature sensors, found to be associated with both site water content and radiation exposure; cove sites less than 500 m distant from adjacent ridges are as much as 2 °C warmer at night and 4 °C colder during the day, depending on season.

Vegetation data

We compiled a database of vegetation surveys in GSMNP from 1970-2006, including a standardized taxonomy for all geo-located observations of vascular plants (Weakley, 2006), allowing spatial inferences of both presences and absences. Plot sizes were most often 600-1000 m^2 (range 1-15,000 m^2). In total, this dataset includes 36,494 records of plants across 971 plots, some of which were surveyed multiple times. While most studies included all vascular plants at

each location, two studies (94 total plots) surveyed only trees. Before analysis, data were transformed into matrices of presence-absence data. For sites that were surveyed multiple times, only the most recent survey was used since there were not enough data to compare change over time within sites. Taxa that were not identified to the species level were removed. In addition, rare species (<50 occurrences in the database) were removed. This resulted in a final database of 154 species of vascular plants recorded across 956 plots. Species that were not recorded in plots that had surveyed all vascular plants were treated as absent, while species not recorded in plots which surveyed only trees were converted to 'NA' values.

Climate data

We estimated recent historical (1970-2000) climate based on three different models. First, macroclimate mean annual temperature (MAT) was obtained from the bioclimatic variables dataset of WorldClim 2.1 (Fick & Hijmans, 2017). This dataset uses interpolated weather station records, elevation, and remote-sensing covariates to estimate climate. Variables related to seasonal and diurnal fluctuations in temperature are also included in the dataset; however, for GSMNP these were highly correlated with MAT and with each other, so separating their effects in models was not possible. We used the finest resolution data available from WorldClim: 0.5 x 0.5 arc-minutes or about 1 km resolution. Second, we interpolated WorldClim macroclimate using a 30 m grid of elevation as a covariate. To do this, we calculated the slope of a linear model relating each climate variable to the 0.5 arc-minute DEM from WorldClim. Then, we determined the difference between the elevation of each 30 m grid cell and its corresponding 0.5 arc-minute grid cell and applied the overall slope to adjust the macroclimate climate estimate for the difference in elevation, resulting in a smoothed surface. Third, we estimated below-

canopy microclimate conditions at the same 30 m resolution using the microclimate model developed by Fridley (2009) for GSMNP. In brief, this model was developed and validated using temperature data (1 m above ground height) recorded over 400 days at 120 locations in GSMNP in 2005-2006. The model estimates below-canopy daily minimum and maximum temperatures using above-canopy temperature (calculated from daily lapse rates and intercepts based on weather station records; historical data from Lesser & Fridley 2015), topographic variables including stream distance and radiation input, and their interactions with seasonality (sine- and cosine- transformed day of year; see Table 1 for description of spatial data and Fridley, 2009 for full model details). We summarized these below-canopy temperatures to 1970-2000 MAT using the same methodology as WorldClim with historical data.

We also predicted future (late century) climate under a climate-change scenario for the three climate drivers. For the macroclimate and above-canopy models, we uniformly added 4 °C to MAT. To check that this climate scenario was reasonable, we examined predicted rates of warming in GSMNP for 2080-2100 under Shared Socioeconomic Pathway SSP3-7.0, a middle-of-the-road, business-as-usual climate change scenario used in the CMIP6 multi-model ensemble (Gidden et al., 2019). These data were downscaled from nine global climate models (GCMs) by WorldClim to 2.5 arc-minutes (see Table S1 for GCM details). The mean change in MAT from the 1970-2000 historical dataset (Fig. S1) varied between models from 3.5 to 6.3 °C , but variation in the Park within a single GCM was limited to 0.3 °C in MRI-ESM2-0 and less than 0.1 °C in each of the eight other models (Table S1). Therefore, we applied a uniform 4 °C warming scenario to the macroclimate predictions as a likely scenario. For the microclimate model, we added 4 °C to the intercept of the daily regional climate estimates for 1970-2000. We then adjusted lapse rates based on the historical relationship between intercept and lapse rate. In

the 1970-2000 data, each degree increase in the regional maximum temperature was associated with 0.207 ± 0.003 °C decrease in temperature per km elevation, while each degree increase in regional minimum temperature was associated with 0.134 ± 0.003 °C decrease temperatures per km elevation (Fig. S2). When applied to the climate change scenario, this meant that the mean lapse rate for daily minimum temperatures decreased from -4.7 °C/km to -5.2 °C/km, and the mean lapse rate for daily maximum temperatures decreased from -5.0 °C/km to -5.9 °C/km. After adjusting the intercepts and lapse rates of the 1970-2000 regional climate data to simulate climate change, we re-estimated microclimate MAT using the model from Fridley (2009) and summarization procedure from WorldClim.

We compared the three climate models to determine how well macroclimate describes microclimate conditions. For each 30 m pixel we calculated the difference between MAT estimates from the microclimate, interpolated climate, and macroclimate models. For the microclimate model and interpolation models, we calculated the range of temperatures present within 1 km^2 areas to compare with the macroclimate model. In addition, we calculated expected warming under the 4 °C scenario for each grid cell to determine variation across the Park.

Species distribution models

We modeled species distributions using the hierarchical modelling of species communities approach implemented in the R package 'Hmsc' version 3 (Ovaskainen et al., 2017; Tikhonov et al., 2020). Species interactions likely play a role in structuring communities here; however, given the lack of knowledge about how these interactions will change in the future, we chose not to include parameters for species interactions in these SDMs. While this means that we are not using the full range of tools available from Hmsc, this framework allowed fitting of

SDMs for all species at the same time and facilitated comparison of overall model fit for all species. For each climate scenario, we fit a generalized linear model of species presence using a probit error distribution. SDMs were fit using Bayesian inference with default weakly regularizing priors. Posterior distributions were sampled using three chains for a total of 900 samples with 500,000 burn-in values discarded and thinning of 1000 values between each sample. All potential scale reduction factors were less than 1.1, indicating good model convergence (Gelman & Rubin, 1992). For each climate model we fit SDMs with their own estimate of MAT, including a quadratic term to allow for species with maximum occurrence at moderate temperatures. Each SDM also included two topographic covariates—annual (above-canopy) radiation and log-transformed topographic convergence index (TCI; ln(upslope area/tan(slope); Bevin & Kirkby, 1979)—and their interactions with MAT. All SDMs also included log-transformed plot size to control for sampling effort, and UTM Easting and Northing values to control for linear spatial trends. We compared the fit and predictions of these SDMs with two simpler model structures: first, an SDM based only on elevation, plot size, and spatial location; and second, an SDM with all of the covariates included in our main SDMs but no interactions. We scaled all covariates to a mean of zero and standard deviation of one before fitting models. We compared overall fit of the SDMs using WAIC and mean AUC. We also compared AUC between species to determine which species had poor model fit (AUC < 0.8).

To predict the distribution of species across the park, we calculated the probability of species presence for each 30 m pixel by applying the median SDM parameters to climate, topographic, and spatial predictors, with plot size set to 900 m^2 to match pixel size. We used the same parameters to model distributions and future suitable habitat in climate change scenarios (current topographic data, projected future climate data). In order to avoid biased estimates

created by suitability thresholds (Benito, Cayuela, & Albuquerque, 2013), we calculated expected area occupied by each species as the sum of occurrence probabilities (corrected for pixel area) across the park. In addition, we summed probabilities within each pixel for all species to determine the expected number of species present (following Slavich et al., 2014). We then calculated expected probability of occurrence using the same methods under the climate change scenario. For two high-elevation species with positive quadratic effects of elevation on occurrence probability, this extrapolation resulted in the nonsensical effect of predicted presence in the climate change scenario at low elevations. We removed one of these species (*Athyrium filix-femina*) from further calculations due to low sample size. The other species, *Abies fraseri*, is the highest-elevation tree species in the park and its future distribution is of considerable interest. Therefore, we applied a correction to its predicted future distribution by only including predicted suitability in areas where future suitability is predicted to be lower than current suitability (a reasonable assumption since its distribution is currently limited to the coldest areas in the Park). This removed only low-elevation areas that were incorrectly predicted to be suitable under climate change. The results presented here include predicted species distributions across GSMNP only for those species with highly accurate SDMs (AUC >0.8), although we also included predictions based on models of all species to ensure that this criterion did not affect overall conclusions.

For all species, we calculated two estimates of future habitat distributions. First, we calculated expected occupied area and number of species present based on an unlimited dispersal scenario with the raw outputs of applying historical SDM coefficients to climate change scenario data. Second, we calculated stable habitat as the minimum probability of occurrence in each grid cell based on the historical and climate change scenarios. The distributions predicted using this

approach simulate a no-dispersal scenario, since species can only be as common (or less common) in future predictions than in historical predictions. For each species, we used this index to estimate the fraction of current area that would remain suitable given climate change as the summed probability of the no-dispersal scenario divided by the historical expected occupied area, and we estimated the maximum future distribution as the summed probability of the full dispersal scenario. To ensure that any differences between models were not driven by incomplete climatic gradients from species which do not have low elevation/warm climate limits in our datasets, we examined the relationship between expected stability and species mean occurrence elevation. We also identified potential microclimatic refugia that could not be detected by interpolation by calculating the difference between the fraction of species that would remain stable in each grid cell in the interpolation SDM and the microclimate SDM.

All analyses were conducted using R version 4.0.3 (R Core Team, 2020). Spatial analyses were conducted using packages 'raster' (Hijmans, 2020), 'sp' (R. S. Bivand & Pebesma, 2013), and 'rgdal' (R. Bivand, Keitt, & Rowlingson, 2020). The packages 'lubridate' (Grolemund & Wickham, 2011), 'parallel', and 'tidyr' (Wickham, 2020) were used in some analyses to improve processing efficiency. The packages 'ggplot2' (Wickham, 2016), 'patchwork' (Pedersen, 2020), 'RColorBrewer' (Neuwirth, 2014), 'ggrepel' (Slowikowski, 2020), and 'rasterVis' (Perpiñán & Hijmans, 2020) were used to create figures.

Results

Present and future temperature regimes

Microclimate and macroclimate estimates of MAT varied across space, with the microclimate model up to 3.1 °C warmer or 3.0 °C colder than the macroclimate model,

depending on location, and the highest overall range of MAT in the microclimate model (Figure 1). While average MAT across the Park was similar in all models (macroclimate=10.9 °C, interpolation mean=11.0 °C, microclimate mean=11.1 °C), variability within a single 1 km^2 grid cell was up to 5.3 °C in the microclimate model (mean variation=2.9 °C). Interpolation based on elevation reduced the temperature discrepancy in some areas but increased the discrepancy in others; the microclimate model was up to 2.9 °C warmer and 3.4 °C colder than the interpolated model (Figure 1F), and the maximum variability within 1 km^2 in the interpolation model was only 2.4 °C (mean variation=1.2 °C). With 4 °C of macroclimate warming, the microclimate model predicted that areas near high elevation streams would warm the least (1.9 °C), while low-elevation ridgelines would warm the most (3.8 °C; Figure 2). The overall range of microclimate MAT increased from 11.0 °C in the historical scenario to 12.8 °C in the warming scenario because the areas that were warmest historically were also least buffered from regional climate. Since uniform warming of 4 °C was applied to both the macroclimate and interpolation models (with variable warming in the microclimate model due to changes in lapse rates and microclimatic buffering), the variation in temperature across the park was the same in the historical and climate change scenarios.

Species distribution models

Overall fit was similar across SDMs (mean AUC between 0.80 and 0.81). In general, SDMs of high-elevation, range-limited species had the highest AUC scores, while SDMs of widespread, mid-elevation species had the lowest scores (Fig. S3). All three models performed better than the elevation-only baseline model for predicting species occurrence (elevation model AUC = 0.72, delta WAIC from full models = 4.4 – 4.6). SDM fit was similar across climate

models regardless of whether interactions were included; adding interactions improved fit only slightly (delta WAIC=0.2-0.4; Table S2). Given previous work demonstrating that topographic effects on plant distributions vary with elevation (e.g. Whittaker, 1956), we conducted the rest of this analysis using the SDMs with interactions between climate and topographic variables. This choice had little influence on results; predictions of species occurrences from the full models and the models without interactions were highly correlated (Pearson's R=0.97).

Eighty-five species had AUC values > 0.8 in all three SDMs and were included in spatial predictions of species distribution. While goodness-of-fit statistics were similar across models, predictions were very different, especially with projected climate change. Some low-elevation species were predicted to have nearly completely stable habitat in all models, likely due to the lack of information in the model about their probability of occurrence in areas warmer than the warmest climates currently found in the Park. However, this was true for a limited number of species and did not drive differences between models; predicted stability for all mid- to high-elevation species was highest in the microclimate SDM (Figure 3).

The macroclimate SDM predicted that 18 species currently found in the Park would nearly disappear (<10 km^2 suitable habitat area) in the climate change scenario, but the microclimate SDM predicted near disappearance of only two species (*Abies fraseri* and *Acer spicatum*). More generally, the microclimate SDM predicted that a larger fraction of currently occupied habitat would be stable for all mid- to high-elevation species, and the ratio of future to current area was usually closest to one when dispersal was allowed (Figure 4, Table S3). Species stability and dispersal predictions were qualitatively identical when including SDMs with AUC <0.8 (Figs. S4-S7). In addition to effects on high elevation species, differences between the SDMs were particularly evident along streams, where microclimate conditions were predicted to

be cooler and more resistant to change. For example, *Liriodendron tulipifera* was predicted to have suitable habitat in the climate change scenario only along mid- and high-elevation ridges based on the macroclimate and interpolated SDMs, but to retain much of its current low- and mid-elevation habitat, especially along streams, based on the microclimate SDM (Figure 5; and see Figs. S8-S93 for historical suitability and +4 °C predicted dispersal and stability for all species).

Expected regions of greatest compositional change

The differences between the three climate models were not evenly distributed across the range of environmental conditions in the Park. Although high elevation streamside areas were predicted to warm most slowly according to the microclimate model (Figure 6, row 2), the proportion of species in stable habitat and the change in richness if species were able to disperse freely to suitable habitat were predicted to be highest at mid-elevations in the microclimate SDM (Figure 6, rows 3-4). This is because current high-elevation species have narrow thermal niches, so even the lower predicted warming of high elevation streams would render much of the currently occupied area unsuitable. However, the microclimate SDM did predict some persistence of high elevation species which would disappear from the Park in interpolated or macroclimate scenarios. For example, *Abies fraseri* was predicted to disappear in the macroclimate and interpolation SDMs but to keep 5 km^2 of stable area in the microclimate SDM. Similarly, *Picea rubens* was predicted to retain only 2-3 km^2 of its occupied area in the macroclimate and interpolation SDMs, but 55 km^2 in the microclimate SDM (Fig. S57). Community-wide stability was highest in the microclimate SDM except on low-elevation ridges, where the interpolated SDM predicted lower temperatures and higher stability. Cryptic refugia,

especially at mid- to high- elevations, were only identified using the microclimate model (not the interpolation model), and could lead to increased persistence of half of the species currently present in some locations (Figure 7).

Discussion

We found strong effects of climate model choice on the predictions, but not the goodness of fit, of SDMs for common plant species in the Great Smoky Mountains. In general, there were large differences between the interpolation and microclimate SDM predictions, while the interpolation and macroclimate SDM predictions were similar. This demonstrates the need for local climate models that incorporate drivers of microclimatic buffering, rather than just improving resolution with spatial interpolation. The difference between the interpolation and microclimate models here was particularly evident on low elevation ridges. The interpolation model predicted that these ridges would be cooler and their plant communities more stable than the macroclimate model since they are at higher elevation than the 1 km^2 pixel averages. However, the microclimate model predicted that the same ridges would be warmer and their plant communities less stable than the macroclimate model because their exposed location is not as buffered from atmospheric conditions as other habitats. Differences in warming potential were also evident at high elevations; according to the microclimate model, MAT in high elevation areas, particularly along streams, may warm only about half as much as regional climate. Based on these differential effects of warming, we identified potential cryptic refugia for many species across the park which could persist in buffered microhabitats even as the climate warms. If species are able to persist in these buffered habitats, the number of species lost or nearly lost

from the Park will be much lower than predicted by macroclimate SDMs, and some cryptic refugia may be able to protect 50% more species than the interpolation SDMs would suggest.

The SDMs presented here are by necessity a simplification of the actual drivers of species distributions. First, climatic extremes are generally thought to be more closely related to species distributions than climatic means, although they are infrequently included in SDMs (Mod, Scherrer, Luoto, & Guisan, 2016). We could not include models based on climatic extremes due to high collinearity in the season-specific data available from WorldClim in GSMNP (ie models could not distinguish between effects of MAT and effects of annual maximum temperature because they were highly correlated). However, the microclimate dataset presented here could be used to compare climatic extremes and seasonal or annual variability (Lesser & Fridley, 2015), supporting further SDM development. In addition, our models do not include an estimate of current or future moisture conditions, which can support or constrain species ranges at local scales in some environments (McLaughlin et al., 2017). Predictions of climate change in the Southeastern U.S. include a small (<10%) increase in spring through fall precipitation and a 10-20% increase in winter precipitation, as well as an increase in extreme precipitation events (Easterling et al., 2017), but little is known about the effects on local availability of water to plants. Finally, many non-climatic drivers of species distributions have already been demonstrated in GSMNP including biotic interactions with insects and pathogens (Cofer, Elliott, Bush, & Miniat, 2018; Smith & Nicholas, 1998; Woods & Shanks, 1959), human disturbance including fires, historical clearcutting, and exotic species introduction (Delcourt & Delcourt, 1998; Duffy & Meier, 1992; Harmon, Bratton, & White, 1983), geographic location (Mackenzie & White, 1998), and soil pH (Golden, 1981). These drivers can operate in very different ways than climate change; for example, in other systems, recovery from disturbance has been linked to

downslope shifts in the range of some tree species (Wason & Dovciak, 2017). To the extent that these factors are geographically stable or change in ways that are not correlated with changes in temperature, they may also have strong impacts on the future distribution of species in GSMNP.

Our results indicate the need to explicitly consider microclimatic conditions when projecting future climates to understand organismal responses. Theoretically, plants that occupy particular microclimates could be modelled accurately by coarse resolution SDMs constructed with macroclimate data, assuming that microclimate and macroclimate conditions are well correlated so that the microclimates necessary for a species are always present in areas with similar macroclimates (Bennie, Wilson, Maclean, & Suggitt, 2014). However, two considerations suggest that this is rare in many landscapes. First, regional climate estimates may be biased towards climates that occupy more land area (i.e., low-elevation climates in mountainous regions; Trivedi et al., 2008). Second, macroclimate and microclimate are often poorly correlated due to the mechanisms that lead to buffering or decoupling of microclimates from regional macroclimate (De Frenne et al., 2021; Dobrowski, 2011; Hylander, Ehrlen, Luoto, & Meineri, 2015). As demonstrated here, macroclimate conditions will not accurately predict species responses if microclimates respond to overall warming in different ways. While interpolation is a less effort intensive way to estimate microclimate than developing locally validated models, SDMs based on interpolated climate data did not strongly change predictions in this system compared to macroclimate SDMs. Previous studies have also found that SDMs driven by interpolated macroclimate do not approximate SDMs driven by measured microclimate (Lembrechts, Lenoir, et al., 2019; Slavich et al., 2014). Given the difficulty of measuring local variation in climate, additional tools, such as mechanistic models for estimating

microclimatic conditions (Kearney, Gillingham, Bramer, Duffy, & Maclean, 2020; Kearney & Porter, 2017), would be valuable if more widely used and validated.

Understanding interacting effects of multiple global change drivers on microclimate buffering is a critical area for future research; while our historical data (and that from other sites; De Frenne et al., 2021) suggest that microclimate buffering may become stronger with increasing regional temperatures, changes in forest canopy (e.g. Zellweger et al., 2020), moisture regimes, or other drivers of thermal conditions may disrupt this pattern and affect both local climate and suitable habitat availability. For example, high elevation forests of GSMNP are often above the cloud base, which contributes to thermal buffering, cools overall temperatures, and leads to high moisture availability, potentially stabilizing the presence of spruce-fir forests at the southern edge of their typical range (Berry & Smith, 2013; Cogbill & White, 1991). If cloud base heights in GSMNP change (e.g. due to urbanization; Williams et al., 2015), the climate currently supporting high-elevation forests may change much more than we predict here.

The response of species to microclimatic effects is also more complex than presented here, with different species responding to changes in climate in different ways. Many herbaceous and subcanopy species spend their whole life-cycle in buffered understory microclimatic conditions. While the leaves of canopy trees can exist in a very different thermal and light environment, the distribution of these trees could still be influenced by below-canopy microclimate during the seedling/sapling stages or through the effects of thermal microclimate on local variation in soil moisture (e.g. Oren & Pataki, 2001). The relative influence of these differing above- and below-canopy conditions is not well understood, but some evidence indicates that canopy and subcanopy individuals, even within the same species, respond differently to changing environmental conditions (Rollinson et al., 2020). The ability of a species

to persist in microrefugia may depend on its traits and the particular climatic drivers that are most tightly tied to its distribution (Hylander et al., 2015), suggesting that while thermal microclimate conditions may predict suitable habitat for more species than macroclimate conditions, the accuracy of these predictions will vary by species. Given similar model fit but widely divergent predictions of response to climate change, improved understanding of which species are likely to benefit from microrefugia will be critical for providing recommendations on conservation.

In summary, we found that species that are influenced by below-canopy microclimate conditions in GSMNP may respond very differently to climate change than macroclimate SDMs predict. We also demonstrated that interpolation of macroclimate using fine-scale variation in elevation does not capture the effects of microclimate on species distributions, particularly in terms of response to climate change. Our analysis supports improved theoretical understanding of the effects of local climate variation on plant community composition and species distribution as well as improved risk assessment and planning for conservation of species and landscapes affected by climate change. In the coming decades, we predict that even though the coldest environments in GSMNP will disappear, the range of microclimatic niches will increase, as the low-elevation ridges that are currently the warmest areas of the park are also least buffered from atmospheric warming. Species that occupy mesic habitats, especially at mid-elevations, may be less sensitive to climate change than otherwise predicted. This raises the possibility that low elevation species may not be able to recruit in their current thermal habitats upslope if mid-elevation forests remain relatively intact. Understanding the effects of this band of relatively stable forest on the distribution of other species would require a more thorough understanding of species interactions in these diverse forests. These mesic cryptic refugia may also become

unstable if the conditions that lead to buffering (e.g., high elevation immersion in clouds and dense forest canopy) change in the Park, with unexpected effects on species distributions. Additional work focused on the particular climate drivers that constrain different species and life stages, and how those drivers will vary over both space and time, is critical to predicting species distributions and responses to climate change in GSMNP and other climatically complex landscapes.

Tables

Table 1. Description of spatial data used in climate and SDM models

Dataset	Units	Resolution (m)	Data source
Macroclimate MAT	°C	1000[a]	WorldClim 2.1
Interpolated MAT	°C	30	Calculated from macroclimate, WorldClim elevation, and 30 m elevation
Microclimate MAT	°C	30	Calculated using model from Fridley (2009)
WorldClim Elevation	m a.s.l.	1000[a]	WorldClim 2.1
Elevation	m a.s.l.	30	Fridley 2009; DEM
Annual radiation	W / m2	30	Fridley 2009; sum of daily radiation
Topographic convergence index	unitless	30	Fridley 2009; r.topidx routine in GRASS GISb
Stream distance[c]	m	30	Fridley 2009; calculated from stream locations
Daily radiation	W / m2	30	Fridley 2009; r.sun routine in GRASS GIS[b]
Maximum synoptic temperature[c]	°C	30	Calculated from weather records and elevation
Minimum synoptic temperature[c]	°C	30	Calculated from weather records and elevation

a: approximately; resolution is 0.5 arc-minutes

b: GRASS development team (2006)

c: used only in microclimate calculation

Figures

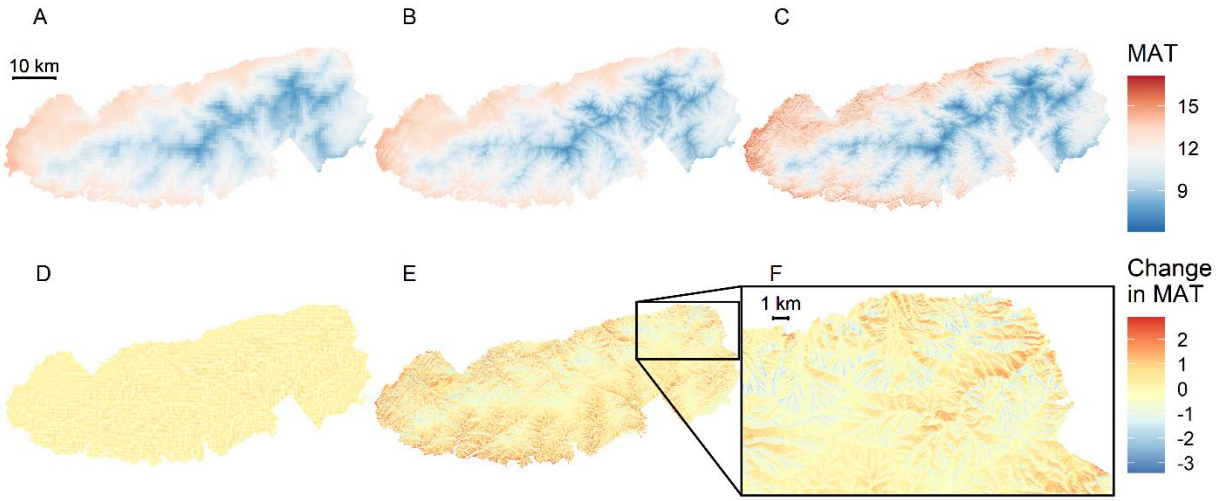

Figure 1. Comparison of historical climate estimates of mean annual temperature from 1970-2000 across climate models. (A) macroclimate; WorldClim 1 km resolution grid, (B) interpolated climate; lapse-rate correction of WorldClim data to 30 m resolution, (C) microclimate; locally validated below-canopy climate model, (D) difference between interpolated climate and macroclimate, (E) difference between validated microclimate and interpolated climate, (F) closer image of northeastern corner of panel E (location indicated by box in panel E). Differences between macroclimate and interpolated climate are small, but differences between interpolated climate and microclimate are often >2 °C cooler along north-facing streams and warmer along south-facing ridges.

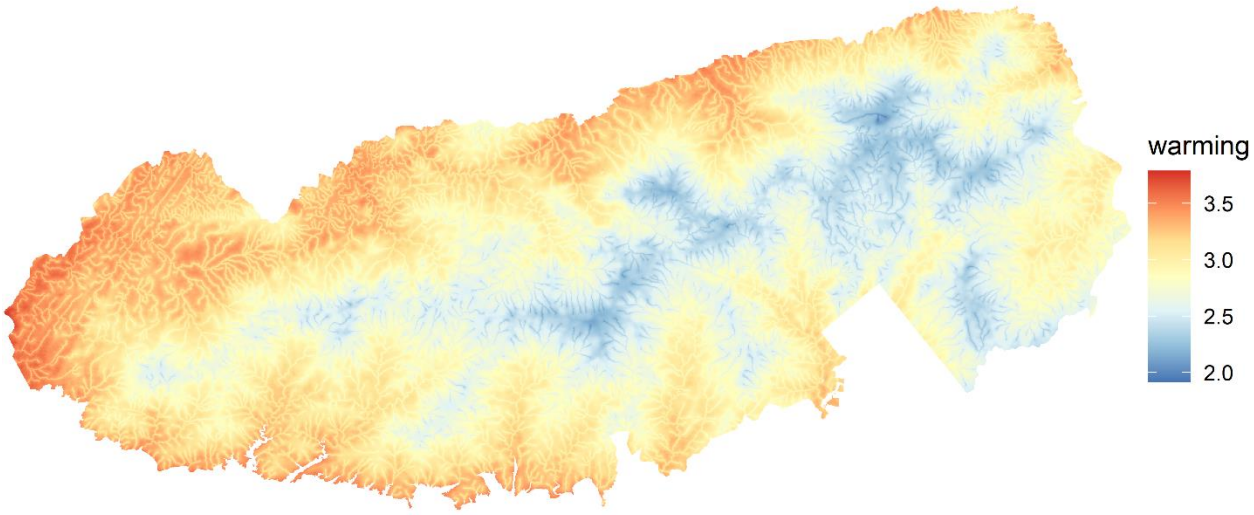

Figure 2**.** Projected ground-level warming (°C increase in MAT) across GSMNP based on a locally validated microclimate model with 4 °C of macroclimate warming. The most buffered sites, near high-elevation streams, warm only half as much as regional temperatures, while the least buffered sites, along low-elevation exposed ridges, warm nearly the same amount as regional temperatures.

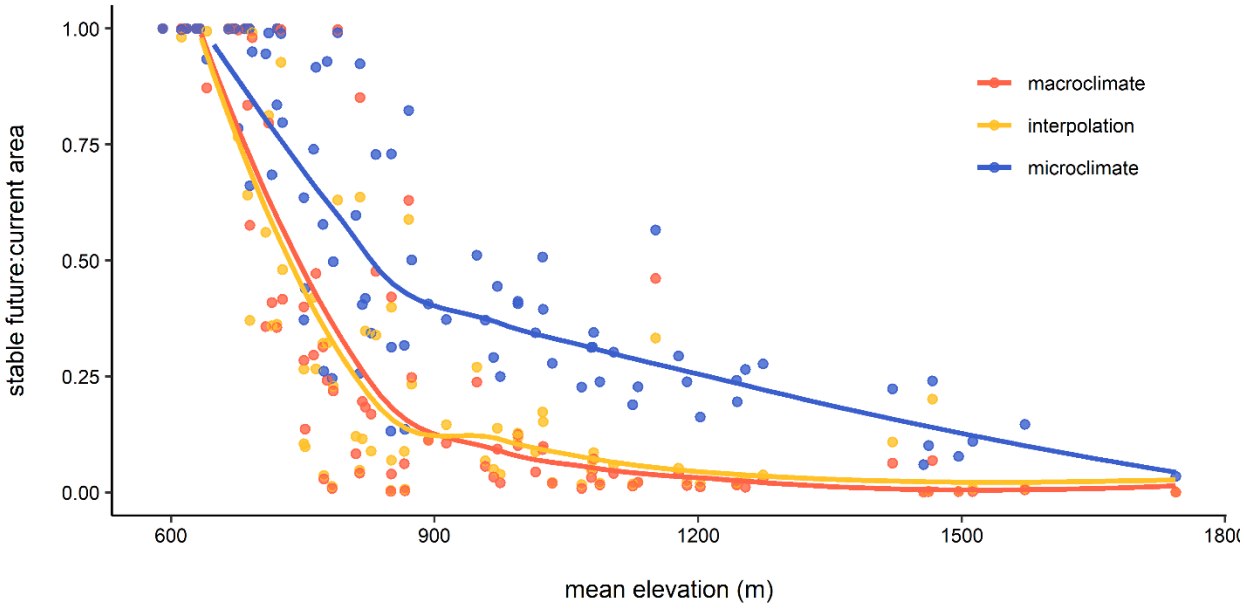

Figure 3**.** Proportion of current suitable habitat area that will remain suitable according to SDMs driven by the three different climate models. Points are arranged on the x axis according to species current mean elevation; lines are loess smoothing across the points for each climate model. Low elevation species may have erroneously high predicted stability due to lack of maximum temperature limits in our dataset; however, differences in stability between models occur in mid- to high-elevation species which do have thermal limits in GSMNP.

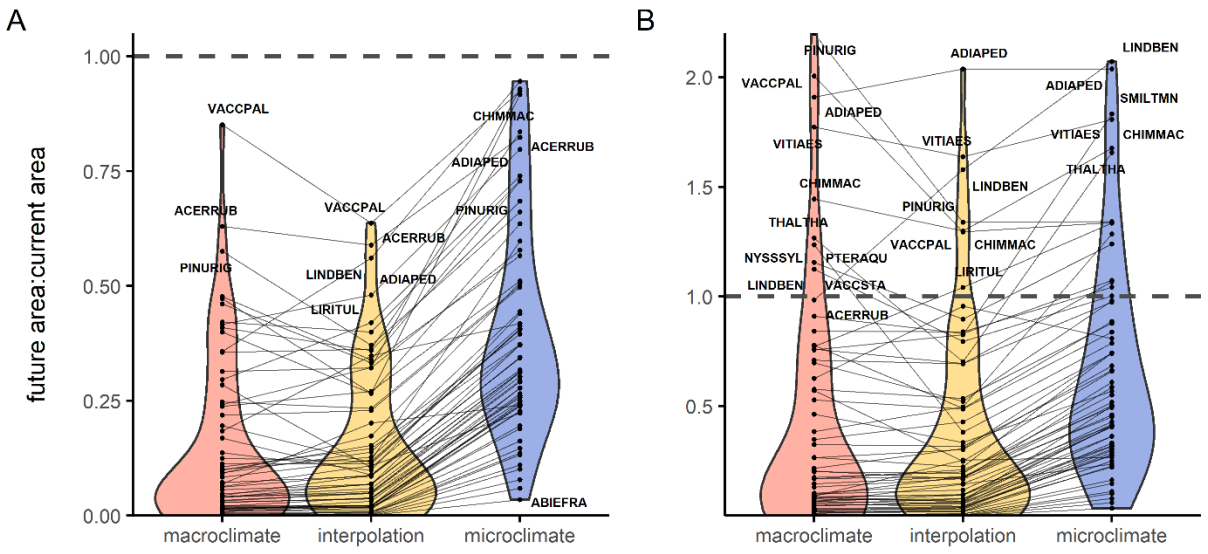

Figure 4**.** Responses of plant species to 4 °C of regional warming. In both panels, the Y axis is the ratio of future species area to current species area. Panel A shows the ratio for a no-dispersal scenario; points represent the fraction of current area that will still be suitable. Panel B shows the ratio for an unlimited dispersal scenario; points represent the change in suitable habitat area with climate change. The grey line in both panels indicates an equal area of future and current habitat; lower values represent a reduction in habitat area (note different scales of Y-axes). Species which had >98% stable habitat in any SDM were removed for visualization. Full species names and area projections can be found in Table S3.

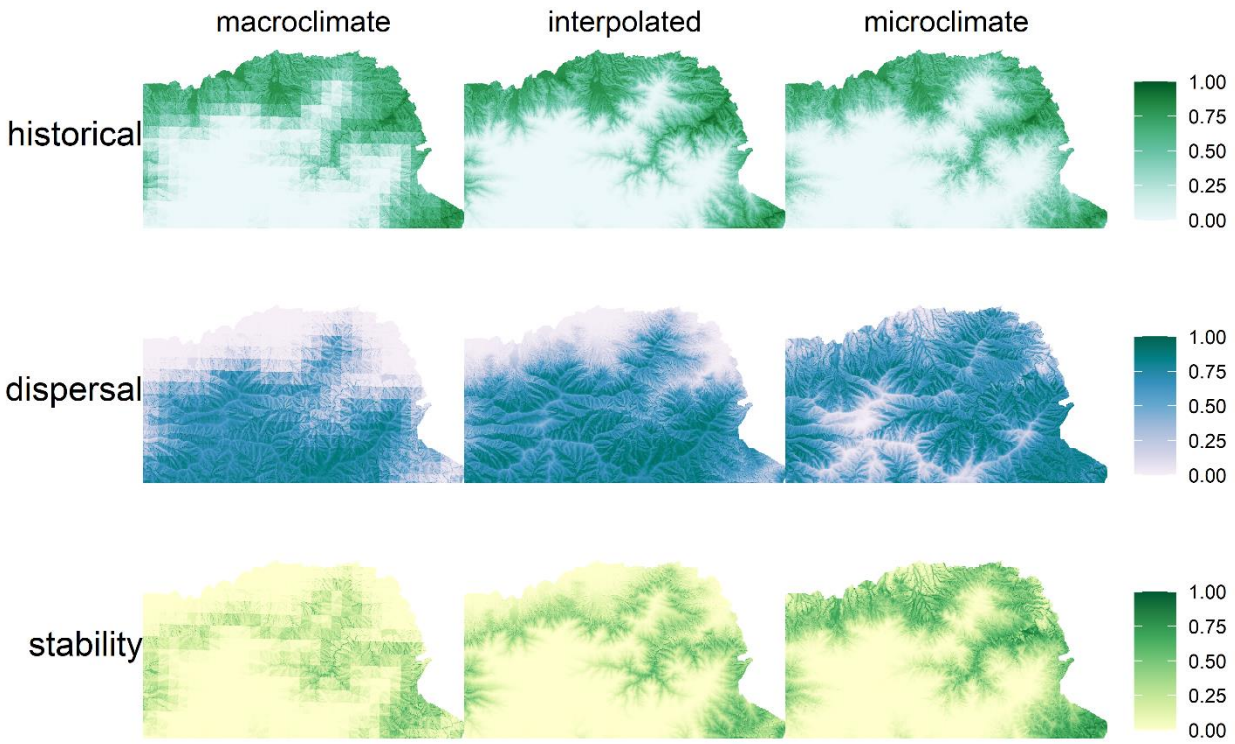

Figure 5**.** Historical (first row), future suitable (second row), and stable (third row) habitat area projection for *Liriodendron tulipifera* in macroclimate (left column; AUC=0.85), interpolated climate (middle column; AUC=0.86), and microclimate (right column; AUC=0.86) SDMs in the northeast corner of GSMNP (see Figure 1 for location). Darker colors indicate more suitable habitat. Stable habitat in macroclimate and interpolated climate habitats is at mid elevations; low elevation habitat remains stable in the microclimate model near streams. In the macroclimate and interpolated SDMs, dispersal occurs up to the highest elevations, but in the microclimate SDM the highest ridges remain too cold.

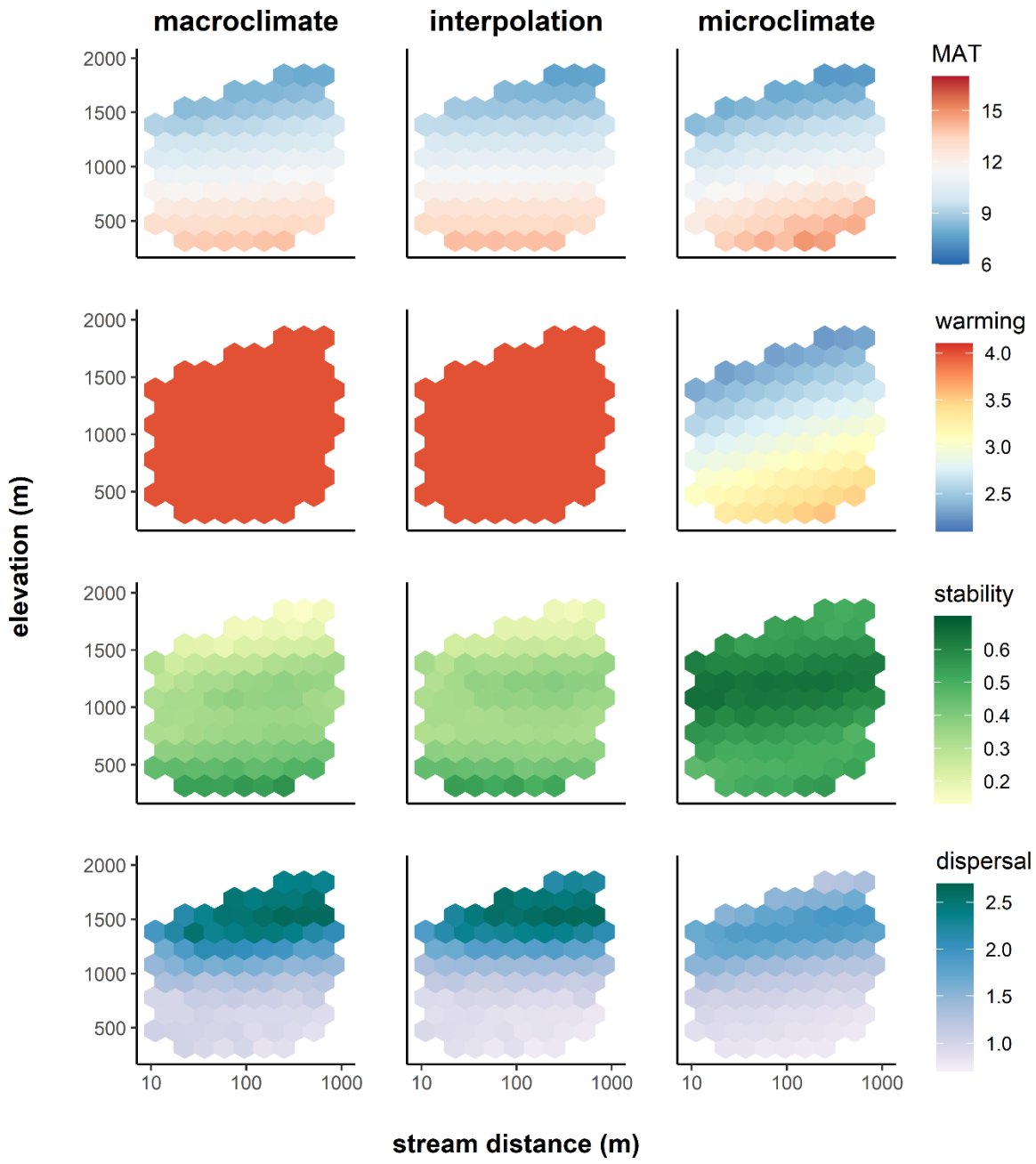

Figure 6**.** Effect of climate model and topographic position on warming and species response to warming. Colors show binned mean values of MAT (°C, row 1), change in MAT with warming scenario (row 2), fraction of current species that will still be within suitable habitat (row 3), and number of future species/number of current species with unlimited dispersal (row 4). Values are

based on 10,000 regularly sampled points within the Park; bins are shown only if they contain at least 10 values.

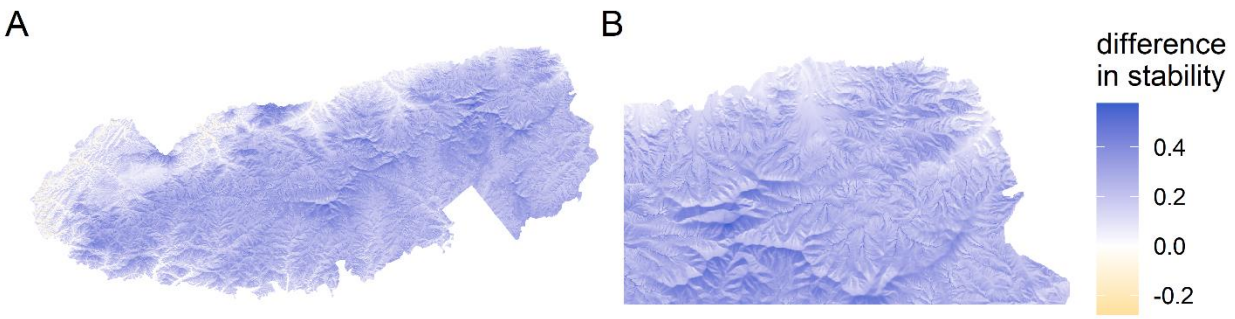

Figure 7**.** Potential cryptic refugia in GSMNP: geographic differences in the effect of below-canopy microclimate on stable habitat (additional proportion of species that are still within stable habitat) in each 30 m pixel. Blue indicates areas where the microclimate model predicts greater stability; red indicates areas where the interpolation model predicts greater stability. Panel (A) shows all of GSMNP, panel (B) shows the northeast corner. See Figure 1 for exact spatial location of panel B.

References

Benito, B. M., Cayuela, L., & Albuquerque, F. S. (2013). The impact of modelling choices in the predictive performance of richness maps derived from species-distribution models: Guidelines to build better diversity models. *Methods in Ecology and Evolution*, 4, 327–335. https://doi.org/10.1111/2041-210x.12022

Bennie, J., Wilson, R. J., Maclean, I. M. D., & Suggitt, A. J. (2014). Seeing the woods for the trees - when is microclimate important in species distribution models? *Global Change Biology*, 20(9), 2699–2700.

Berry, Z. C., & Smith, W. K. (2013). Ecophysiological importance of cloud immersion in a relic spruce-fir forest at elevational limits, southern Appalachian Mountains, USA. *Oecologia*, 173(3), 637–648. https://doi.org/10.1007/s00442-013-2653-4

Bivand, R., Keitt, T., & Rowlingson, B. (2020). rgdal: Bindings for the "Geospatial" Data Abstraction Library. Retrieved from https://cran.r-project.org/package=rgdal

Bivand, R. S., & Pebesma, E. (2013). Applied spatial data analysis with R (Second). NY: Springer. Retrieved from https://asdar-book.org/

Braun, E. L. (1950). Deciduous Forests of Eastern North America. Philadelphia: Blakiston.

Cofer, T. M., Elliott, K. J., Bush, J. K., & Miniat, C. F. (2018). Rhododendron maximum impacts seed bank composition and richness following Tsuga canadensis loss in riparian forests. *Ecosphere*, 9(4). https://doi.org/10.1002/ecs2.2204

Cogbill, C. V, & White, P. S. (1991). The Latitude-Elevation Relationship for Spruce-Fir Forest and Treeline along the Appalachian Mountain Chain. *Vegetatio*, 94(2), 153–175.

Cruzan, M. B., & Templeton, A. R. (2000). Paleoecology and coalescence: Phylogeographic analysis of hypotheses from the fossil record. *Trends in Ecology and Evolution*, 15(12), 491–496. https://doi.org/10.1016/S0169-5347(00)01998-4

De Frenne, P., Lenoir, J., Luoto, M., Scheffers, B. R., Zellweger, F., Aalto, J., … Hylander, K. (2021). Forest microclimates and climate change: Importance, drivers and future research agenda. *Global Change Biology*. https://doi.org/10.1111/gcb.15569

De Frenne, P., Rodríguez-Sánchez, F., Coomes, D. A., Baeten, L., Verstraeten, G., Vellen, M., … Verheyen, K. (2013). Microclimate moderates plant responses to macroclimate warming. *Proceedings of the National Academy of Sciences of the United States of America*, 110(46), 18561–18565. https://doi.org/10.1073/pnas.1311190110

Delcourt, P. A., & Delcourt, H. R. (1998). The Influence of Prehistoric Human-Set Fires on Oak-Chestnut Forests in the Southern Appalachians. Castanea, 63(3), 337–345.

Dobrowski, S. Z. (2011). A climatic basis for microrefugia: The influence of terrain on climate. *Global Change Biology*, 17(2), 1022–1035. https://doi.org/10.1111/j.1365-2486.2010.02263.x

Duffy, D. C., & Meier, A. J. (1992). Do Appalachian Herbaceous Understories Ever Recover from Clearcutting? *Conservation Biology*, 6(2), 196–201. https://doi.org/10.1046/j.1523-1739.1992.620196.x

Easterling, D. R., Kunkel, K. E., Arnold, J. R., Knutson, T. R., LeGrande, A. N., Leung, L. R., … Wehner, M. (2017). Precipitation change in the United States. In: Climate Science Special Report: Fourth National Climate Assessment. Fourth National Climate Assessment, Volume I, 207–230. https://doi.org/10.7930/J0H993CC.U.S.

Fick, S. E., & Hijmans, R. J. (2017). WorldClim 2: new 1-km spatial resolution climate surfaces for global land areas. *International Journal of Climatology*, 37(12), 4302–4315. https://doi.org/10.1002/joc.5086

Franklin, J., Davis, F. W., Ikegami, M., Syphard, A. D., Flint, L. E., Flint, A. L., & Hannah, L. (2013). Modeling plant species distributions under future climates: How fine scale do climate projections need to be? *Global Change Biology*, 19(2), 473–483. https://doi.org/10.1111/gcb.12051

Fridley, J. D. (2009). Downscaling climate over complex terrain: High finescale (<1000 m) spatial variation of near-ground temperatures in a montane forested landscape (Great Smoky Mountains). *Journal of Applied Meteorology and Climatology*, 48(5), 1033–1049. https://doi.org/10.1175/2008JAMC2084.1

Geiger, R. (1966). The climate near the ground (Translated). Cambridge, MA: Harvard University Press.

Gelman, A., & Rubin, D. B. (1992). Inference from iterative simulation using multiple sequences. *Statistical Science*, 7, 457–472.

Gidden, M. J., Riahi, K., Smith, S. J., Fujimori, S., Luderer, G., Kriegler, E., … Takahashi, K. (2019). Global emissions pathways under different socioeconomic scenarios for use in CMIP6: A dataset of harmonized emissions trajectories through the end of the century. *Geoscientific Model Development*, 12(4), 1443–1475. https://doi.org/10.5194/gmd-12-1443-2019

Golden, M. S. (1981). An Integrated Multivariate Analysis of Forest Communities of the Central Great Smoky Mountains. *The American Midland Naturalist*, 106(1), 37–53.

Graae, B. J., Vandvik, V., Armbruster, W. S., Eiserhardt, W. L., Svenning, J. C., Hylander, K., … Lenoir, J. (2018). Stay or go – how topographic complexity influences alpine plant population and community responses to climate change. *Perspectives in Plant Ecology, Evolution and Systematics*, 30(February 2018), 41–50. https://doi.org/10.1016/j.ppees.2017.09.008

GRASS Development Team. (2006). Geographic Resources Analysis Support System (GRASS) software.

Grolemund, G., & Wickham, H. (2011). Dates and Times Made Easy with {lubridate}. *Journal of Statistical Software*, 40(3), 1–25. Retrieved from https://www.jstatsoft.org/v40/i03/

Harmon, M. E., Bratton, S. P., & White, P. S. (1983). Disturbance and vegetation response in relation to environmental gradients in the Great Smoky Mountains. Vegetatio, 55(3), 129–139. https://doi.org/10.1007/BF00045013

Hijmans, R. J. (2020). Raster: Geographic Data Analysis and Modeling.

Hylander, K., Ehrlen, J., Luoto, M., & Meineri, E. (2015). Microrefugia : Not for everyone. *AMBIO*, 44((Suppl.1)), S60–S68. https://doi.org/10.1007/s13280-014-0599-3

Kearney, M. R., Gillingham, P. K., Bramer, I., Duffy, J. P., & Maclean, I. M. D. (2020). A method for computing hourly, historical, terrain-corrected microclimate anywhere on earth. *Methods in Ecology and Evolution*, 11(1), 38–43. https://doi.org/10.1111/2041-210X.13330

Kearney, M. R., & Porter, W. P. (2017). NicheMapR – an R package for biophysical modelling: the microclimate model. *Ecography*, 40(5), 664–674. https://doi.org/10.1111/ecog.02360

Lembrechts, J. J., Lenoir, J., Roth, N., Hattab, T., Milbau, A., Haider, S., … Nijs, I. (2019). Comparing temperature data sources for use in species distribution models: From in-situ

logging to remote sensing. *Global Ecology and Biogeography*, 28(11), 1578–1596. https://doi.org/10.1111/geb.12974

Lembrechts, J. J., Nijs, I., & Lenoir, J. (2019). Incorporating microclimate into species distribution models. *Ecography*, 42(7), 1267–1279. https://doi.org/10.1111/ecog.03947

Lesser, M. R., & Fridley, J. D. (2015). Global change at the landscape level: Relating regional and landscape-scale drivers of historical climate trends in the Southern Appalachians. *International Journal of Climatology*, 36(3), 1197–1209. https://doi.org/10.1002/joc.4413

Mackenzie, M. D., & White, P. S. (1998). Vegetation of Great Smoky Mountains National Park , 1935-1938. *Castanea*, 63(3), 323–336.

Maclean, I. M. D., Hopkins, J. J., Bennie, J., Lawson, C. R., & Wilson, R. J. (2015). Microclimates buffer the responses of plant communities to climate change. *Global Ecology and Biogeography*, 24(11), 1340–1350. https://doi.org/10.1111/geb.12359

McLaughlin, B. C., Ackerly, D. D., Klos, P. Z., Natali, J., Dawson, T. E., & Thompson, S. E. (2017). Hydrologic refugia, plants, and climate change. *Global Change Biology*, 23(8), 2941–2961. https://doi.org/10.1111/gcb.13629

Meineri, E., & Hylander, K. (2017). Fine-grain, large-domain climate models based on climate station and comprehensive topographic information improve microrefugia detection. *Ecography*, 40(8), 1003–1013. https://doi.org/10.1111/ecog.02494

Mod, H. K., Scherrer, D., Luoto, M., & Guisan, A. (2016). What we use is not what we know: environmental predictors in plant distribution models. *Journal of Vegetation Science*, 27(6), 1308–1322. https://doi.org/10.1111/jvs.12444

Neuwirth, E. (2014). RColorBrewer: ColorBrewer Palettes. Retrieved from https://cran.r-project.org/package=RColorBrewer

Opedal, Ø. H., Armbruster, W. S., & Graae, B. J. (2015). Linking small-scale topography with microclimate, plant species diversity and intra-specific trait variation in an alpine landscape. *Plant Ecology & Diversity*, 8(3), 305–315. https://doi.org/10.1080/17550874.2014.987330

Oren, R., & Pataki, D. E. (2001). Transpiration in response to variation in microclimate and soil moisture in southeastern deciduous forests. *Oecologia*, 127(4), 549–559. https://doi.org/10.1007/s004420000622

Ovaskainen, O., Tikhonov, G., Norberg, A., Guillaume Blanchet, F., Duan, L., Dunson, D., … Abrego, N. (2017). How to make more out of community data? A conceptual framework and its implementation as models and software. *Ecology Letters*, 20(5), 561–576. https://doi.org/10.1111/ele.12757

Pedersen, T. L. (2020). patchwork: The Composer of Plots. Retrieved from https://cran.r-project.org/package=patchwork

Perpiñán, O., & Hijmans, R. (2020). rasterVis. Retrieved from https://oscarperpinan.github.io/rastervis/

Potter, K. A., Arthur Woods, H., & Pincebourde, S. (2013). Microclimatic challenges in global change biology. *Global Change Biology*, 19(10), 2932–2939. https://doi.org/10.1111/gcb.12257

R Core Team. (2020). R: A Language and Environment for Statistical Computing. Vienna, Austria. Retrieved from https://www.r-project.org/

Randin, C. F., Engler, R., Normand, S., Zappa, M., Zimmermann, N. E., Pearman, P. B., … Guisan, A. (2009). Climate change and plant distribution: Local models predict high-

elevation persistence. *Global Change Biology*, 15(6), 1557–1569. https://doi.org/10.1111/j.1365-2486.2008.01766.x

Rollinson, C. R., Alexander, M. R., Dye, A. W., Moore, D. J. P., Pederson, N., & Trouet, V. (2020). Climate sensitivity of understory trees differs from overstory trees in temperate mesic forests. *Ecology*, 102(3), 1–11. https://doi.org/10.1002/ecy.3264

Rull. V. (2010). On microrefugia and cryptic refugia. *Journal of Biogeography*, 27(8), 1623-1625.

Scherrer, D., & Körner, C. (2011). Topographically controlled thermal-habitat differentiation buffers alpine plant diversity against climate warming. *Journal of Biogeography*, 38(2), 406–416. https://doi.org/10.1111/j.1365-2699.2010.02407.x

Seo, C., Thorne, J. H., Hannah, L., & Thuiller, W. (2009). Scale effects in species distribution models: Implications for conservation planning under climate change. *Biology Letters*, 5(1), 39–43. https://doi.org/10.1098/rsbl.2008.0476

Shanks, R. E. (1954). Climates of the Great Smoky Mountains. *Ecology*, 35(3), 354–361. https://doi.org/10.2307/1930098

Slavich, E., Warton, D. I., Ashcroft, M. B., Gollan, J. R., & Ramp, D. (2014). Topoclimate versus macroclimate: How does climate mapping methodology affect species distribution models and climate change projections? *Diversity and Distributions*, 20(8), 952–963. https://doi.org/10.1111/ddi.12216

Slowikowski, K. (2020). ggrepel: Automatically Position Non-Overlapping Text Labels with "ggplot2." Retrieved from https://cran.r-project.org/package=ggrepel

Smith, G. F., & Nicholas, N. (1998). Patterns of Overstory Composition in the Fir and Fir-Spruce Forests of the Great Smoky Mountains After Balsam Woolly Adelgid Infestation. *The American Midland Naturalist*, 139(2), 340–352.

Stewart, J.R., Lister, A.M., Barnes, I., & Dalen, L. (2010). Refugia revisited: Individualistic responses of species in space and time. *Proceedings of the Royal Society B: Biological Sciences.* 277(1682): 661-671.

Storlie, C. J., Phillips, B. L., Vanderwal, J. J., & Williams, S. E. (2013). Improved spatial estimates of climate predict patchier species distributions. *Diversity and Distributions*, 19(9), 1106–1113. https://doi.org/10.1111/ddi.12068

Suggitt, A. J., Wilson, R. J., Isaac, N. J. B., Beale, C. M., Auffret, A. G., August, T., … Maclean, I. M. D. (2018). Extinction risk from climate change is reduced by microclimatic buffering. *Nature Climate Change*, 8(8), 713–717. https://doi.org/10.1038/s41558-018-0231-9

Tikhonov, G., Opedal, Ø. H., Abrego, N., Lehikoinen, A., de Jonge, M. M. J., Oksanen, J., & Ovaskainen, O. (2020). Joint species distribution modelling with the r-package Hmsc. *Methods in Ecology and Evolution*, 11(3), 442–447. https://doi.org/10.1111/2041-210X.13345

Trivedi, M. R., Berry, P. M., Morecroft, M. D., & Dawson, T. P. (2008). Spatial scale affects bioclimate model projections of climate change impacts on mountain plants. *Global Change Biology*, 14(5), 1089–1103. https://doi.org/10.1111/j.1365-2486.2008.01553.x

Ulrey, C., Quintana-Ascencio, P. F., Kauffman, G., Smith, A. B., & Menges, E. S. (2016). Life at the top: Long-term demography, microclimatic refugia, and responses to climate change

for a high-elevation southern Appalachian endemic plant. *Biological Conservation*, 200, 80–92. https://doi.org/10.1016/j.biocon.2016.05.028

Wason JW & Dovciak M (2017) Tree demography suggests multiple directions and drivers for species range shifts in mountains of Northeastern United States. Global Change Biology, 23: 3335–3347.

Weakley, A. S. (2006). Flora of the Carolinas, Virginia, Georgia and surrounding areas. University of North Carolina Herbarium (NCU), North Carolina Botanical Garden, University of North Carolina at Chapel Hill.

Whittaker, R. H. (1956). Vegetation of the Great Smoky Mountains. *Ecological Monographs*, 26(1), 1–80.

Wickham, H. (2016). ggplot2: Elegant Graphics for Data Analysis. Springer-Verlag New York. Retrieved from https://ggplot2.tidyverse.org

Wickham, H. (2020). tidyr: Tidy Messy Data. Retrieved from https://cran.r-project.org/package=tidyr

Williams, A. P., Schwartz, R. E., Iacobellis, S., Seager, R., Cook, B. I., Still, C. J., … Michaelsen, J. (2015). Urbanization causes increased cloud base height and decreased fog in coastal Southern California. *Geophysical Research Letters*, 42(5), 1527–1536. https://doi.org/10.1002/2015GL063266

Woods, F. W., & Shanks, R. E. (1959). Natural Replacement of Chestnut by Other Species in the Great Smoky Mountains National Park. *Ecology*, 40(3), 349–361. https://doi.org/10.2307/1929751

Zellweger, F., de Frenne, P., Lenoir, J., Vangansbeke, P., Verheyen, K., Bernhardt-Römermann, M., … Coomes, D. (2020). Forest microclimate dynamics drive plant responses to warming. *Science*, 368(6492), 772–775. https://doi.org/10.1126/science.aba6880

Chapter 2: Low-cost sensor networks allow description of spatial and temporal variation in soil moisture across the complex forested terrain of the Great Smoky Mountains (USA)

Jordan R. Stark and Jason Fridley

Introduction

Research on microclimate, or the variation in climate at scales experienced by organisms, has increased dramatically in the past several decades (Bramer et al., 2018). Ecologically important climate variables include temperature, moisture, seasonality, and other factors, but microclimate research has focused primarily on temperature rather than moisture (Maclean, Bennie, Scott, & Wilson, 2012; Robinson et al., 2008; Vereecken et al., 2014). Soil moisture is a key driver of species distributions (Engelbrecht et al., 2007), carbon balance (Green et al., 2019), soil respiration (Curiel Yuste et al., 2018; Orchard & Cook, 1983), and risk for extreme events including floods and fires. Fine-scale, landscape-wide descriptions of soil moisture variability would be valuable for understanding and predicting these processes, but the cost and difficulty of using commercial soil moisture sensors has prevented deployment of sufficient numbers of sensors to capture the range of conditions in topographically complex regions. To address this challenge, we have developed a new low-cost, low-power sensor designed for distributed soil moisture monitoring and used data collected with these sensors to describe patterns of soil moisture availability across the complex forested landscape of Great Smoky Mountains National Park (GSMNP).

Several variables, including annual precipitation and topographic position, have been used as proxies for moisture availability in the absence of distributed moisture measurements. On the scale of hillslopes to watersheds, a common metric for potential wetness is topographic convergence index (TCI; ln(upslope area/tan(slope)); Beven & Kirkby, 1979). Sites with high

TCI values should be wetter because they collect more water from upslope areas and lose less water to drainage. However, the strength of the relationship between this index and soil moisture may depend on overall landscape wetness, seasonality, and other variables, depending on the site (Burt & Butcher, 1985; Tromp-van Meerveld & Mcdonnell, 2006; Western, Grayson, Blöschl, Willgoose, & McMahon, 1999). Other indices, such as radiation intensity, may also be related to transpiration or direct evaporation. On the highly local scale, site slope or local topographic position (TPI; difference between elevation of a raster cell and its surrounding cells; Wilson, O'Connell, Brown, Guinan, & Grehan, 2007) could influence plant communities, drainage and water retention. Finally, plant density and canopy cover can affect soil moisture in complex ways. Increased transpiration and interception with canopy cover can reduce soil moisture availability under canopies (Breshears, Rich, Barnes, & Campbell, 1997; Peck, Zenner, & Palik, 2012; Scharenbroch & Bockheim, 2007), but the cooling and shading effects of canopy cover can also reduce direct evaporation and increase soil moisture (Walsh et al., 2017). Highly local effects have been recognized as drivers of soil moisture for decades (Ball & Williams, 1968; Krumbach, 1959), but quantitative estimates of their strength are still rare.

Current products predicting soil moisture in most areas are at broad scales and generally not locally validated (e.g. SMAP L4 Surface Soil Moisture, 9km; Zhang, Zhang, Zhou, Shao, & Gao, 2017). In contrast, local temperature variation can be predicted at scales of tens of meters using mechanistic models globally (e.g. Kearney et al., 2020; Maclean & Klinges, 2021) and using locally validated statistical models across many regions (e.g. Fridley, 2009; Haesen et al., 2021; Holden et al., 2016; Vanwalleghem & Meentemeyer, 2009; Von Arx et al., 2012). Development of similar fine-scale models of soil moisture has been limited by both physical and logistical factors. Variation in moisture even at scales of centimeters to meters can be high,

leading to difficulty in scaling up from sensors to landscapes (Robinson et al., 2008). Constraints on the deployment of large commercial sensor networks have limited the development of landscape-level fine-scale soil moisture models (Robinson et al., 2008; Vereecken et al., 2014). Low-cost, low-power sensor technology for monitoring soil moisture has lagged behind similar technology for monitoring temperature (e.g. the iButton; Maxim integrated; San Jose, CA). Commercial moisture sensors are often hundreds of dollars and many require separate expensive dataloggers powered by large batteries. Developing accurate microclimate models in complex terrain generally requires deployment of extensive sensor networks, which can be expensive and logistically challenging using these existing tools.

Here, we have modified the design of inexpensive, self-contained environmental microcontroller units (EMUs) developed by Mickley et al. (2019) to improve durability and allow long-term deployment in the wet climate of GSMNP. While these sensors and dataloggers are more labor intensive to set up than commercially available soil moisture equipment (about two hours of work to construct each sensor), they have several major advantages. First, the total cost is more than an order of magnitude less than commonly used sensor and datalogger combinations at about $20 per unit including sensors, housing, batteries, and data storage. Second, the sensors have very low power usage, running on 4-AAA batteries and one watch battery for more than a year, which allows deployment of a large number of sensors in remote locations. Third, the sensors are re-useable, with replaceable batteries and rewritable memory. Finally, the design is easily modified for particular projects that may require different microcontroller housing or sensors. The low cost of these sensor units enables deployment of the large numbers needed to describe patterns of moisture variation across environmental gradients, including in areas where some sensors are likely to be damaged or destroyed during deployment.

Local gradients of moisture in GSMNP have been proposed as a key driver of ecological processes for decades (Whittaker, 1956). Here, we present the first landscape-wide timeseries data describing this variation. We address several broad questions. First, we test the performance and calibration of new low-cost, low-power soil moisture sensors. Second, we examine relationships of commonly used landscape proxies of moisture availability to measured soil moisture data across the complex landscape of GSMNP. Finally, we compare the magnitude of soil moisture variation in GSMNP to the magnitude of precipitation variation, and discuss the implications for moisture variability under a changing climate. These new tools and data demonstrate the feasibility of monitoring fine-scale variation in soil moisture across a complex landscape and will allow the development of new models at similar scales to thermal microclimate models, improving our understanding of the role of local climate in determining ecological function.

Methods

Sensor design

We developed environmental microcontrollers based on the components and design from Mickley et al. (2019) with modifications to improve durability in the field and allow storage of data in microcontroller internal memory (Serial Peripheral Interface Flash File System or SPIFFS). Major components of the system were (1) an Arduino-like microcontroller (Wemos d1 mini) to run a sensing program and store data; (2) a real-time clock (ds3231) and MOSFET to activate the system once per hour and prevent battery drainage when the system was off; (3) two solder-plated generic volumetric moisture sensors (resistance-based) and an analog-to-digital converter (ads1115) to read the sensor outputs; (4) a digital soil temperature probe (ds18b20); (5) a battery holder and 4-AAA batteries; (5) a custom printed circuit board; and (6) a sensor

housing constructed from PVC fittings. The microcontrollers were programmed in C++ via the Arduino IDE to read sensor values once per hour and store data to internal memory for later download. Sensor construction details are found in Appendix 2; for a full sensor construction protocol, microcontroller code, and bill of materials see https://github.com/jordanstark/Soil_temp_moisture_EMU. Total cost of components was approximately $20 per sensor.

Soil moisture calibration

Soil resistance probes were calibrated to volumetric moisture content (vmc) using two complementary methods: mass balance and comparison with commercial (Decagon EC-5) soil moisture probes. While a previous calibration for these resistance probes has been published (Mickley et al. 2019), that calibration did not account for effects of temperature on resistance which were large across the temperatures measured in this study. Temperature sensitivity of soil moisture probes is common, and is in part due to the changes in electrical conductivity of soils with temperature; commercial sensors including the Decagon EC-5 are sensitive to temperature variation and several procedures have been developed for removing the signal of temperature from moisture data (Saito, Fujimaki, Yasuda, Inosako, & Inoue, 2013).

Mass balance calibration was conducted using kitchen scales (Ozeri ZK14-S) retrofitted with a microcontroller that logged data hourly from the load cell as well as a soil resistance probe and a soil temperature probe. For each trial, a small pot of soil (142 mL) from GSMNP was mixed with water until saturated. Soil moisture and temperature probes were installed in the pot, and both the pot and a datalogger (Wemos d1 mini ESP8266) were placed on the modified scales in a growth chamber. Soils were then allowed to air dry for several days to weeks

(depending on temperature). Drying trials were conducted at every 5 degrees C from 10-35 degrees, with two replicates at each temperature. One replicate at 10 degrees was removed because of a balance malfunction; another replicate at 35 degrees was removed because final soil weight was not correctly recorded. Readings from the scales' load cells were converted to weight using known values and balances were tared with the empty pot and datalogger at each temperature. After air drying, each pot was removed from the balance and the soil was dried at 50 °C for at least 48 hours to determine the dry weight. Hourly volumetric soil moisture values were then calculated as [(wet soil weight – dry soil weight)/pot volume] for each time point.

Calibration against commercial moisture probes was conducted using Decagon EC-5 loggers and EM-50 datalogger. Three pots of pool sand were saturated with water and placed in a growth chamber. In each pot, one EC-5 sensor, two resistance sensors, and one soil temperature sensor were installed (~4cm apart; increasing distances were checked and did not have any effect on EC-5 readings). Data from the resistance and temperature sensors were stored hourly on dataloggers identical to those used in the field; data from the EC-5 sensors were stored hourly on an EM-50 datalogger. Three trials were conducted using this method – first at 25 degrees; then at variable temperatures from 10-35 degrees during each 24 hour period, and finally at variable temperatures from 10-25 degrees during each 24 hour period. Data from the EC-5 sensors exhibited some temperature sensitivity; therefore, these data were smoothed using a 24-hour rolling mean before comparison with the resistance probe data.

Based on the over- and under-fitting at the ends of the range in Mickley et al. (2019) and initial testing at different temperatures, a maximal model of soil moisture as a cubic function of resistance plus a cubic function of temperature and an interaction of resistance and temperature was fit to the data. The model also included a random intercept for each trial to account for

differences in installation or other effects. This model was fit to the data using the 'lmer' function in the 'lme4' package in R; AIC was then compared with all nested models using the 'dredge' function in the 'MuMIn' package. Only models that included lower power terms for all variables with interactions or higher power terms were accepted.

Sensor installation

23 proof-of-concept sensors were deployed at locations along low-, mid- and high-elevation trails in the eastern portions of GSMNP in October 2019. Site locations for sensors deployed after October 2019 (March and June-July 2020, n=63) were stratified according to the distribution of three factors in the Park: elevation, log-transformed TCI, and annual potential relative radiation (Pierce, Lookingbill, & Urban, 2005). To determine the strata, a raster layer of each environmental variable was sampled across a 250 m^2 grid throughout the Park, and then boundaries were determined to split points into 27 equal groups (low, middle, and high values for each of the three factors) based on these gradients. Once strata were calculated, three points in each stratum in each of two watersheds (Big Creek and Cosby) were randomly selected from a 100 m^2 sampling grid masked to areas within 5 km of parking and between 25 and 150 m of trails. After each point was selected, the nearest 25 points were checked and removed if they were from the same stratum to reduce local spatial effects. Stratification and point selection were conducted in R 3.6 using the 'sf' and 'raster' packages; TCI was calculated using the 'topmodel' package; potential relative radiation was calculated using the 'hillshade' function in the 'raster' package and the 'solartime' package.

Sites selected based on the stratified random sampling protocol were screened in the field based on (1) difficulty of access – sites that were inaccessible on foot were excluded; (2)

availability of soil – sites where a 2” PVC tube could not be installed to a depth of 6” were excluded; (3) consistency with research permit – sites in broad flat areas or historical sites were not permitted, and (4) canopy cover – since the processes governing soil moisture may be very different between open and forested sites, only sites with closed canopies in the summer were selected. When sites were rejected, an effort was made to find a nearby site (generally within 100 m and always within 250 m) to install the sensor. If a suitable site was not found nearby, the point was skipped. In March 2020, 23 sensors were installed following these guidelines, primarily in low- and mid-elevation sites. In June and July 2020, an additional 40 sensors were installed following these guidelines. 13 more sensors were deployed in the central part of the Park (along US Hwy 441, Newfound Gap Road, Clingmans Dome Road, and Lakeview Drive) for model validation. Their distribution was not determined through stratified random sampling but they were spaced across elevation in both NC and TN, and in vegetation representative of wet and dry areas.

At each site where sensors were installed, leaf litter was removed and a 6” deep core of soil was taken with a tulip bulb planter. The datalogger housing was installed in this hole and covered. Soil moisture and temperature sensors were installed ~15 cm upslope of the datalogger housing. One soil moisture sensor and the soil temperature sensor were installed vertically just below the leaf litter layer (measuring depths of 0-5 cm), while the other soil moisture sensor was installed 10 cm deeper (measuring depths of 10-15 cm). A shallow trench connecting the sensors and datalogger housing was created to protect sensor wires. Sensors which were damaged when examined in March or June 2020 were replaced at the same locations. All other sensors were collected in July or early August 2021. In total, 114 sensors were deployed across 99 sites (including some sites that had sensors replaced), with data collected between October 2019 and

July 2021 (Figure 9). We tested whether sensor success rates (fraction of deployed days with sensors collecting data) were related to the stratification gradients of elevation, TCI, and radiation using a linear model.

Data processing and cleaning

Following download of data from sensors, we checked all records to remove invalid points. Raw resistance and temperature values were converted to soil moisture based on the laboratory calibration. We then manually checked data from each sensor for anomalous readings, including sensor removal from soil, disconnected wires, or odd readings immediately after installation. Some data were removed from 31 sensors; most of these were damaged enough to stop recording soil conditions but still collected some data after sensors were not attached to the datalogger (visible in the data as a sudden change, followed by near stability of readings) or not in the ground (visible in the data as a sudden drop in soil moisture or increase in daily soil temperature range). Since soil temperature was used to calibrate soil moisture readings, any readings where soil temperature was not accurately recorded were also removed from the soil moisture datasets.

Meteorological and vegetation data

Daily below-canopy mean temperatures were estimated using the microclimate model developed in Fridley (2009). In brief, above-canopy minimum and maximum temperatures were calculated based on the relationship between elevation and weather-station temperatures using a 30 m DEM. These above-canopy temperatures were then used to calculate below-canopy minimum and maximum temperatures based on relationships between temperature, seasonality,

and topographic factors developed using a 120-sensor, 400-day dataset in 2005-2006. Here, we took the average of each day's below-canopy thermal minima and maxima to represent the mean conditions for direct soil evaporation below the canopy throughout the day.

Precipitation and vapor pressure deficit (VPD) estimates were obtained from PRISM at 4 km scale in October 2021 (PRISM climate group, 2021). Using the 4 km PRISM DEM, we calculated the daily slope and intercept of a regression predicting VPD based on elevation at 10,000 randomly sampled sites in the Park (we did not downscale precipitation due to the lack of strong relationships between daily precipitation and elevation). Most daily regressions had strong explanatory power ($r^2>0.8$). Regressions with lower r^2 values were on days with little variation in VPD across the Park that would be adequately predicted based on the intercept of the line. To estimate the VPD at each sensor site, we applied the daily regressions to a 30 m DEM of the park and extracted values at each point location. To determine the elevation gradient of precipitation in the Park, we also downloaded precipitation data from the weather stations used in thermal microclimate modelling. Mean annual precipitation was calculated for each weather station and linear regression was used to determine expected precipitation at high and low elevations in the Park.

Seasonality was estimated using the MODIS yearly land cover dynamics (MCD12Q2) product version 6 at 500 m resolution (Friedl, Gray, & Sulla-Menashe, 2019). We downloaded estimates of maturity and senescence (first and last cross of 90% of annual maximum enhanced vegetation index) for the years 2010-2019 (most recent available decade). After removing all pixels that were designated as less than 'best' quality for the given variable, we calculated the decadal mean maturity and senescence times for each raster cell. These dates were used to screen data for description of summer soil moisture variation when forest canopies were most active.

Using the same dataset, we also calculated maximum annual Enhanced Vegetation Index (EVI) values by adding minimum EVI values and the amplitude of EVI at each site for each year, and then taking the mean over the 2010-2019 decade. A full list of spatial data products used in this paper is found in Table 2.

Description of soil moisture patterns across spatial gradients

We describe the variation in soil moisture mean and variation over time across spatial gradients present in the Park. Site effects and local variability appeared higher in surface moisture sensors so we used data from the 10-15 cm deep sensors only for this analysis (Figure 8). Since sensors were deployed and functioning for different amounts of time, including during differentially wet and dry periods, we first used the subset of sensors that were all deployed and took at least 90% of readings between July 11 2020 and July 10 2021 (the one-year period with the most useable sensors, n=42). For each sensor, we calculated the median annual soil moisture and the coefficient of variation (CV) in annual soil moisture. We then used linear models to determine the effects of elevation and slope (the topographic factors that appeared most strongly related to soil moisture) on median annual moisture and the effects of elevation and topographic indices on CV of soil moisture. Moisture values were logit-transformed to improve normality. We also compared variation in soil moisture over elevation to the gradient of precipitation in the Park. To determine whether effects of topography and climatic conditions varied seasonally, we developed linear mixed models on the effect of topographic conditions on soil moisture (logit-transformed) including interactions with sine- and cosine-transformed day of year using the same subset of sensors which functioned from summer 2020 – summer 2021. A random intercept for each site was included to account for site effects

To examine the effects of topography, weather, and vegetation on soil moisture during the summer months when plant canopies are active, we extracted the subset of soil moisture values between EVI-derived canopy maturity and senescence (Table 2) and developed a linear mixed model of the effects of elevation, TCI, slope, TPI, maximum annual EVI, precipitation, VPD, radiation, and below-canopy temperature. Soil moisture was logit-transformed to improve normality. All predictors were standardized to a mean of zero and standard deviation of one before model fitting. This model also included random intercepts for site effects. Conditional (fixed effects) and marginal (full model) r^2 values were calculated following Nakagawa and Schielzeth (Nakagawa, Johnson, & Schielzeth, 2017; Nakagawa & Schielzeth, 2013). Collinearity was checked using variance inflation factors with the function 'vif' from the package 'car'. Data analysis was conducted in R 4.1.0; all scripts are available at github.com/jordanstark/GSMNP_moisture_drivers.

Results

Sensor calibration

There were three calibration models with equivalent AIC values (delta AIC <2): a model with all terms except for cubed soil temperature, a model with all terms except for cubed soil temperature and squared soil temperature, and the full model with all terms (Table 3). Of these three models with similar AIC, the most parsimonious model without higher-order terms for soil temperature was selected (Table 4). Using the same process with data from only the mass-balance or only the commercial probe trials resulted in similar predicted values in the regions where data was collected in both trials; however, the pool sand did not retain as much water so high-moisture points were not present in those trials and the extrapolated calibration was

somewhat different at the wet end. Combining both methods allowed the greatest range of data to be included; temperature could not be varied during individual mass-balance trials due to the strong temperature sensitivity of the balances. When applied back to the data without the random intercepts, the best model had a mean absolute error (MAE) of 0.034 and a root mean square error (RMSE) of 0.040. All residuals were less than 0.102. The calibration published by Mickley et al. (2019) fell within the range of values here for higher resistance values but slightly below the range of model predictions when very wet; since soil temperature was not reported during that trial direct comparison is not straightforward (Figure 10). The full calibration model presented here had comparable accuracy to commercial probes (RMSE=0.04; reported accuracy of Decagon EC-5 probes ± 0.03) and worked well across soils ranging from pool sand to organic duff.

Sensor performance under field conditions

Out of 114 sensor deployments, 56 sensors recorded for their entire deployment period, 12 sensors were not found, 2 sensors never recorded data, and 22 were destroyed or sufficiently damaged (by wildlife, humans, frost-heave, or other physical causes) to stop recording data. This left 22 sensors which failed for unknown reasons; after testing we were able to determine that about half of these failed due to loss of battery power in the real-time clock. No sensors ran out of main battery power. Data were successfully downloaded from all but two sensors (both badly damaged and corroded) that ran and were collected; even sensors that had some water infiltrate into the sensor housing generally did not have data loss. Three other sensors collected some data but the data were not useable due to very short collection periods or faulty sensors. For the sensors that recorded data and were collected, 77% of deployed days had recorded soil moisture

measurements (Figure 11). Sensor deployment adequately covered the major elevation and topographic gradients of the Park over time (Figure 12). There were no significant relationships between topography (elevation, TCI and radiation) and the fraction of possible data recorded by a sensor ($p>0.5$).

Topographic, meteorological, and seasonal gradients of annual soil moisture

Median 10-15 cm deep soil moisture within sites for the subset of sensors functioning between July 11 2020 and July 10 2021 ranged from 0.04 to 0.33 (v/v). The strongest single topographic driver of soil moisture was elevation; based on a linear model of the effect of elevation only on logit-transformed annual median soil moisture, sites at the highest elevations (2025 m) in the Park had about 4.7x higher median volumetric water content than sites at the lowest elevations (267 m) in the Park ($p=0.0001$, $r^2=0.301$). Over the same gradient, the highest elevations of the Park received about 1.5x more annual precipitation than the lowest elevations in the Park, so this relationship is not explained entirely by precipitation.

After controlling for the effect of elevation, slope had the strongest relationship with soil moisture. A linear model of the effect of slope and elevation on logit-transformed annual median soil moisture explained additional variance ($r^2=0.339$) compared to the elevation-only model. The effect of slope (coefficient=-0.14; $p=0.138$) was about 40% as strong as the effect of elevation (coefficient=0.42, $p<0.001$) across the dataset after centering and standardizing predictors. Based on this model, a high elevation site with a 40° slope would have the same median annual soil moisture as a flat site more than 700 m lower (Figure 13). Adding an interaction between slope and elevation to the model did not explain additional variance.

A linear model of the effects of topographic variables on within-site variability in soil moisture (CV) found that elevation was negatively correlated with variability (standardized coefficient=-0.07, $p<0.001$), while slope (standardized coefficient=0.03, $p=0.038$) and TPI (coefficient=0.04, $p=0.018$) were positively correlated with variability. Maximum EVI and TCI were not correlated with variability in moisture ($p>0.2$).

Examining effects of slope and elevation over time revealed interactions between season and spatial variation. A model of the effects of seasonality (sine- and cosine-transformed day of year), elevation, and slope on soil moisture values showed that the strongest seasonal effects occurred at low elevations and on steep slopes, where moisture was generally low (Figure 14). The effects of elevation (positive) and slope (negative) were strongest in the summer and fall (Table 5). The marginal (fixed effects) r^2 was 0.33 and the conditional (full model) r^2 was 0.95. Variance inflation factors for all variables were less than 1.1, indicating no problems with collinearity.

In a linear mixed model of the effects of all topographic, weather, and vegetation drivers on logit-transformed summer soil moisture, the strongest single driver was elevation (coefficient=0.36, $p<0.001$). Several daily drivers had significant relationships with soil moisture ($p<0.001$ in all cases): moisture decreased with VPD, radiation, and below canopy temperature, and increased with precipitation (Figure 15). None of the site variables had significant relationships with soil moisture but after elevation, the next strongest effects were negative relationships between soil moisture and slope (coefficient=-0.14, $p=0.095$), and between soil moisture and EVI (coefficient=-0.1, $p=0.213$; Table 6). The marginal (fixed effects) r^2 was 0.31 and the conditional (full model) r^2 was 0.94. Variance inflation factors for all variables were less than 1.7, indicating no problems with collinearity.

Discussion

Soil moisture variation at local scales is high, but has rarely been quantified across complex landscapes. Using new low-cost, low-power sensors, we have described patterns of moisture variation across the complex forested landscape of GSMNP. Across sites, we found that elevation has the strongest topographic relationship with soil moisture; high-elevation sites in the park have 4.8x higher median soil moisture than low-elevation sites. Local effects, including slope, are also strongly related to soil moisture, with steep (40°) slopes having moisture equivalent to flat areas that are 700 m lower in elevation. Within sites, the coefficient of variation in soil moisture availability was highest in low-elevation, high-slope, and high-TPI areas. The strongest effects of both slope and elevation in the 2020-2021 season occurred in late summer and fall. When considering all summer data, the strongest driver of moisture was elevation (+) followed by slope (-), maximum annual EVI (-), precipitation (+), radiation (-) and below-canopy temperature (-). TCI, an index commonly used to predict moisture distributions, was not strongly related to measured soil moisture across the whole dataset, although it may be more predictive during wet or dry periods. The elevation gradient in precipitation was significantly weaker than the elevation gradient in soil moisture, suggesting that evapotranspiration or soil properties are critical to local moisture availability.

The implications of local moisture variation across a landscape are not yet well understood, but water availability is a critical factor for a wide range of ecological processes. Since there have been many fewer measurements and models of fine-scale variation in moisture than temperature, research on the effects of local moisture variability have lagged behind

research on thermal microclimate. However, several case studies indicate that local moisture regimes could play an important role in determining species distributions and responses to global change (Crimmins, Dobrowski, Greenberg, Abatzoglou, & Mynsberge, 2011; e.g. Mcdowell et al., 2019; McLaughlin et al., 2017). Below-canopy variation in moisture and temperature are linked, with high soil and plant moisture levels contributing to buffered below-canopy temperatures (Fridley, 2009; Von Arx, Graf Pannatier, Thimonier, & Rebetez, 2013), so changes to moisture availability may exacerbate change in understory temperatures under climate change (Davis, Dobrowski, Holden, Higuera, & Abatzoglou, 2019). Some effects of fine-scale variation in temperature, such regulation of species distributions (Lembrechts, Nijs, et al., 2019; Slavich et al., 2014; Storlie et al., 2013) and responses to global change (De Frenne et al., 2013; Dobrowski, 2011; Zellweger et al., 2020) may be partly related to variation in moisture; additional work disentangling effects of local moisture and temperature variation will require fine-scale predictions of both variables over space and time. With improved tools for measuring local soil moisture availability, it may be possible to develop models capturing additional ecological patterns that are driven by non-thermal climate trends and better predict below-canopy conditions of the future.

Several dimensions of global change may influence local water availability in GSMNP. Precipitation is predicted to increase by 10-20% (depending on season) in the southeastern United States under climate change (Easterling et al., 2017). However, more of the precipitation is predicted to fall in the winter and during extreme events. Full consideration of the overall effects of climate change on moisture availability across the landscape must consider both the timing of rainfall and the spatial distribution of evapotranspiration. Even if more rainfall occurs over the course of a year, soil moisture levels may decrease overall during the growing season

between storms, particularly if drivers of evapotranspiration such as temperature and vapor pressure deficit also rise. If current moisture patterns continue into the future, low elevation and high slope areas may be most susceptible to drought conditions. However, the effects of some soil moisture drivers, particularly those related to transpiration (EVI, VPD), may also change as plant communities adapt to new climatic conditions and are affected by other aspects of global change. For example, forest declines following infestation by hemlock woolly adelgid have led to different effects on transpiration and soil moisture at different sites; long-term changes likely depend on the species that replace hemlock forests (Brantley, Ford, & Vose, 2013; Orwig, Cobb, D'Amato, Kizlinski, & Foster, 2008).

Future changes in multiple climatic conditions (e.g. precipitation and temperature) may not occur simultaneously in the same direction, leading to broad-scale reductions in suitable habitat for species (Oldfather, Kling, Sheth, Emery, & Ackerly, 2020). Novel microclimatic conditions may similarly influence community structure and ecological processes across scales in areas with complex relationships between topography, climate, and species distributions. While many studies have projected that thermal microclimate variability could reduce the need for species range shifts under climate change (e.g. Graae et al., 2018; Chapter 1), the presence of analogous thermal environments in nearby locations may not be enough to maintain suitable habitat if the distribution of moisture and other climatic factors change in ways that are not the same as temperature. In addition to effects on species distributions, ecosystem function can be impacted strongly by the combined effects of multiple climate drivers; for example, several experiments have found that warming leads to different consequences for ecosystem productivity under different moisture regimes (Töpper et al., 2018; Winkler, Chapin, & Kueppers, 2016).

More work is needed to predict local variability across multiple climate factors, changes in microclimate under climate change, and effects on species and ecosystems.

Multiple approaches have been proposed for predicting soil moisture availability across space and time. One common approach to site- or watershed-scale models is modeling the water balance of a site, which requires detailed knowledge of precipitation inputs, evaporation, transpiration, and soil characteristics. While several studies have compared water balance models with topographic indices (e.g. Dyer, 2009; Hoylman et al., 2019), the distributions of many of the drivers of water balance models have been mapped only at broad scales that are not suitable as inputs for a fine-scale model. Water balance models also tend to deviate from on-the-ground conditions over time as model error compounds. Therefore, generating landscape-wide water balance models over time at fine scales in topographically complex areas is generally not possible. Another approach proposed by Pan (2012), the soil moisture diagnostic equation, avoids this issue of compounding error by modelling current moisture conditions with a declining effect of previous days' precipitation and evapotranspiration rather than using previous soil moisture as an input. This approach has been adapted to make predictions across sites or landscapes using spatial kriging or other interpolation techniques (Bell et al., 2015; Evan J. Coopersmith, Cosh, Petersen, Prueger, & Niemeier, 2015; Stillman et al., 2014). However, the large number of soil- and site-specific parameters in this model make prediction across a topographically variable landscape challenging. Several networks of sensors have been used to create soil moisture products in other sites (e.g. Chaney, Roundy, Herrera-Estrada, & Wood, 2015; Evan J. Coopersmith et al., 2015; Kang et al., 2017; Sheikh, Visser, & Stroosnijder, 2009; Stillman et al., 2014), but in general these use highly site- and time-specific methods for modeling soil moisture variation (e.g. spatial kriging) that do not allow prediction across

complex topographic gradients or over time. Other studies focused on fine-scale prediction across plots or hillslope have found that variation in moisture is linked to soil depth, slope position, local temperature, and transpiration rates (Tromp-van Meerveld & Mcdonnell, 2006; Walsh et al., 2017), but these results have not been generalized across landscapes.

In addition to the structural challenges in selecting a model to predict soil moisture, several physical factors limit the accuracy of predictive soil moisture models. Soil moisture varies at scales much smaller than those measured by remote-sensing techniques or interpolated from weather station precipitation data. The extremely fine scale of local variation presents challenges for scaling up from sensor measurements, which integrate over very small soil volumes, to landscape models (Robinson et al., 2008). While topographic indices can be generated at fine scales, our data suggest that none of these indices, on their own, explain a large fraction of the variation in soil moisture across the complex landscape of GSMNP. Developing models that can predict variation in moisture conditions across complex topography is still a critical task even if not all local variation can be explained; without this fine-scale, broad-extent understanding of soil moisture variation, it is difficult to determine whether soil moisture represents another critical axis of microclimatic conditions like local variation in temperature.

Given the central role of moisture availability in ecological processes at broader scales, it is likely that our understanding of the role of microclimatic conditions in determining ecological function is limited by a focus on thermal microclimates rather than a broader understanding of microclimatic conditions across multiple climatic axes. This work demonstrates the feasibility of using a network of low-cost custom sensors to monitor soil moisture in complex forested landscapes where existing soil moisture and precipitation products do not adequately describe the moisture available to organisms and provides insight on the drivers of soil moisture variation

across space and seasons. Our results, particularly the strong elevation gradient of moisture that is not entirely driven by the gradient of precipitation, indicate that local controls can be key predictors of moisture availability to organisms across a landscape.

Tables

Table 2. GIS data used in microclimate models

Variable	Resolution (m)	Source	Description
Elevation	30	Fridley 2009	Elevation in meters above sea level
Slope	30	terrain() from 'raster'	Slope of each cell in elevation raster
TPI	30	terrain() from 'raster'	Difference between cell elevation and mean elevation of 8 surrounding cells
TCI	30	Fridley 2009	ln(upslope area/tan(slope))
Mean T	30	Calculated from Fridley 2009 model	Mean daily below-canopy temperature
Precip	4000	PRISM[1]	Daily precipitation interpolated from weather station data using elevation
VPD	30	Interpolated from PRISM[1]	Daily maximum vapor pressure deficit; interpolated from 4km PRISM dataset using 30m elevation data
Max EVI	500	MODIS MCD12Q2v6	Maximum annual EVI; 10-year mean derived from minimum EVI and EVI amplitude
Maturity	500	MODIS MCD12Q2v6	Day of year when EVI first crosses 90% of maximum EVI; 10-year mean
Senescence	500	MODIS MCD12Q2v6	Day of year when EVI last crosses 90% of maximum EVI; 10-year mean

1: PRISM climate group (2021); downloaded October 2021

Table 3. AIC table for soil moisture calibration. This table shows only models with lower-order terms for soil resistance or temperature when higher-order terms were present. Each column shows model coefficients for a given model term; each row shows a different model.

Int	resistance	resistance^2	resistance^3	tempC	tempC^2	tempC^3	resistance *tempC	DF	AICc	delta
0.33	3.56E-05	-3.24E-09	5.64E-14	-0.0033			5.18E-08	8	-16560.6	0
0.35	3.48E-05	-3.20E-09	5.56E-14	-0.0042	2.39E-05		5.43E-08	9	-16559.8	0.76
0.38	3.50E-05	-3.21E-09	5.58E-14	-0.0095	3.08E-04	-4.97E-06	6.54E-08	10	-16559.8	0.81
0.30	4.02E-05	-3.44E-09	6.00E-14	-0.0023				7	-16557.0	3.56
0.30	3.98E-05	-3.41E-09	5.95E-14	-0.0029	1.86E-05			8	-16555.8	4.81
0.31	4.01E-05	-3.43E-09	5.98E-14	-0.0046	1.11E-04	-1.62E-06		9	-16554.0	6.58
0.67	-2.06E-05	-1.21E-10		-0.0049	3.49E-05		7.85E-08	8	-16523.1	37.49

Table 4. Calibration coefficients for soil volumetric moisture content

Parameter	value
Intercept	0.334876
Resistance	$3.56 * 10^{-5}$
Resistance^2	$-3.24 * 10^{-9}$
Resistance^3	$5.64 * 10^{-14}$
Soil temperature	-0.00327
Resistance * soil temperature	$5.18 * 10^{-8}$

Table 5. Effects of slope, elevation, day of year, and their interactions on 10-15 cm deep soil moisture in sensors which functioned for the entire period between summer 2020 and summer 2021. Slope and elevation were standardized to a mean of zero and standard deviation of one to allow comparison of effect sizes. Soil moisture was logit transformed.

Parameter	Standardized estimate	T value	P value
Intercept	-2.09	-22.0	<0.001
cosine(doy*0.0172)	0.12	63.0	<0.001
sine(doy*0.0172)	0.05	23.3	<0.001
Elevation	0.43	4.5	<0.001
Slope	-0.14	-1.5	0.141
cosine(doy*0.0172)*Elevation	-0.09	-43.3	<0.001
sine(doy*0.0172)*Elevation	-0.08	-38.7	<0.001
cosine(doy*0.0172)*Slope	0.01	3.9	<0.001
sine(doy*0.0172)*Slope	0.03	17.1	<0.001

Table 6. Effects of topographic and meteorological drivers on summer soil moisture across all sensors.

Parameter	Standardized estimate	T value	P value
Intercept	-2.29	-31.0	<0.001
Elevation	0.36	4.2	<0.001
Log(TCI)	-0.04	-0.5	0.635

Slope	-0.14	-1.7	0.095
TPI	-0.04	-0.5	0.628
Precipitation	0.07	20.0	<0.001
VPD	-0.04	-8.4	<0.001
Radiation	-0.07	-9.6	<0.001
Below-canopy temperature	-0.06	-12.6	<0.001
sqrt(Maximum EVI)	-0.10	-1.3	0.213

Figures

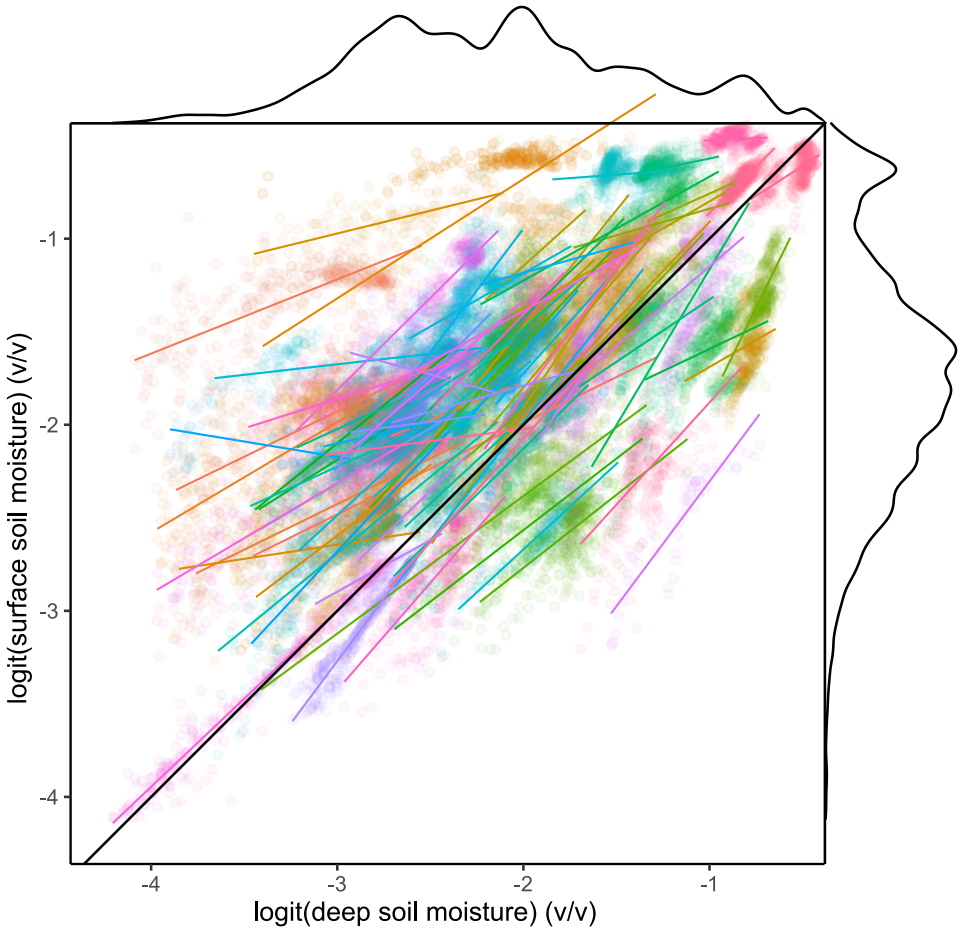

Figure 8. Relationships between surface (0-5 cm) and deep (10-15 cm) soil moisture measurements. Soil moisture measurements were logit-transformed for visualization. Point and line colors are different for each site. Lines represent beset-fit linear models for each site. The black line shows a 1:1 relationship. Marginal distributions show the probability distribution function for each dataset.

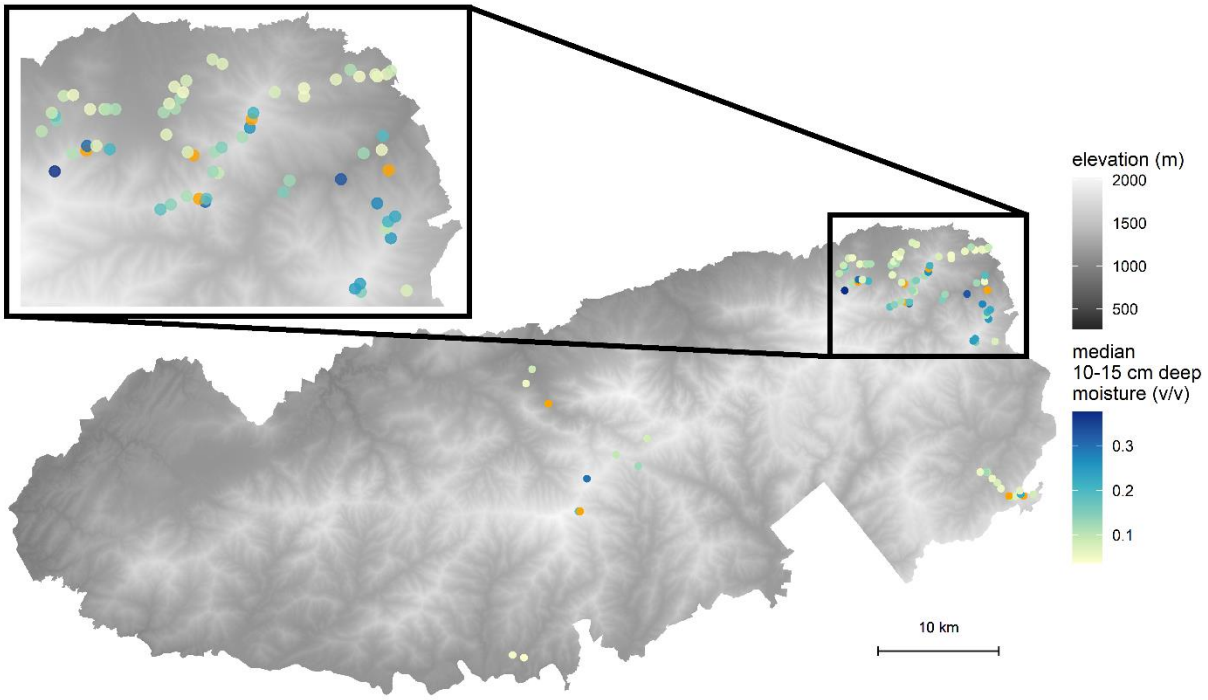

Figure 9. Map of locations where soil moisture and temperature sensors were installed in GSMNP. Only points where sensors were collected and some data were downloaded are shown. Orange points do not have any recorded 10-15 cm deep soil moisture values due to sensor damage. All other points are colored based on their median deep soil moisture content. The inset map includes Big Creek and Cosby watersheds where stratified random sampling was used to choose sensor locations.

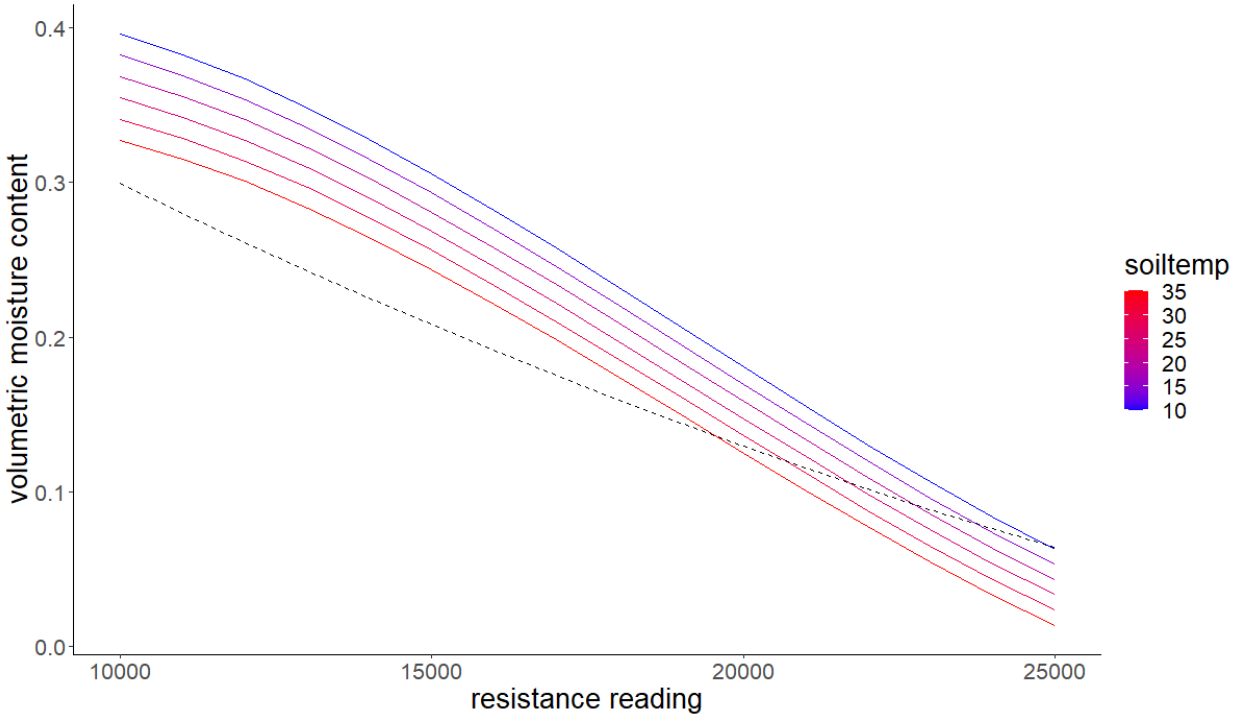

Figure 10. Predicted soil volumetric moisture content across resistance and temperature values. Solid lines represent model predictions at 5 degree temperature increments ranging from 10 degrees (blue) to 35 degrees (red). Dotted black line shows previously published calibration (Mickley et al 2019). Parameter values are in Table 4.

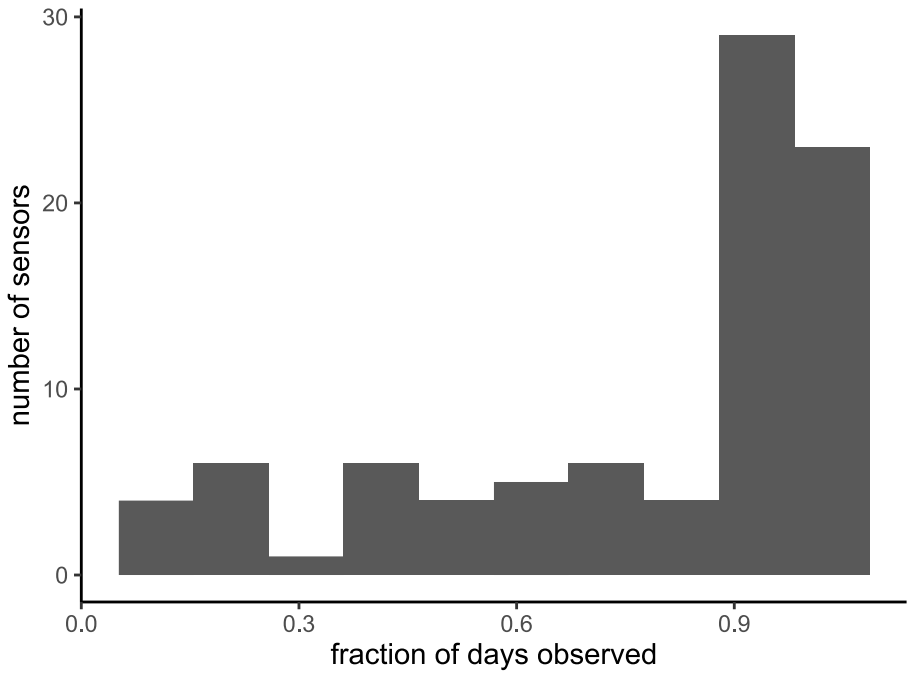

Figure 11. Sensor success rates in data collection. This figure shows only sensors which were collected and recorded some data. An additional 13 sensors were not relocated and five sensors collected no useable data.

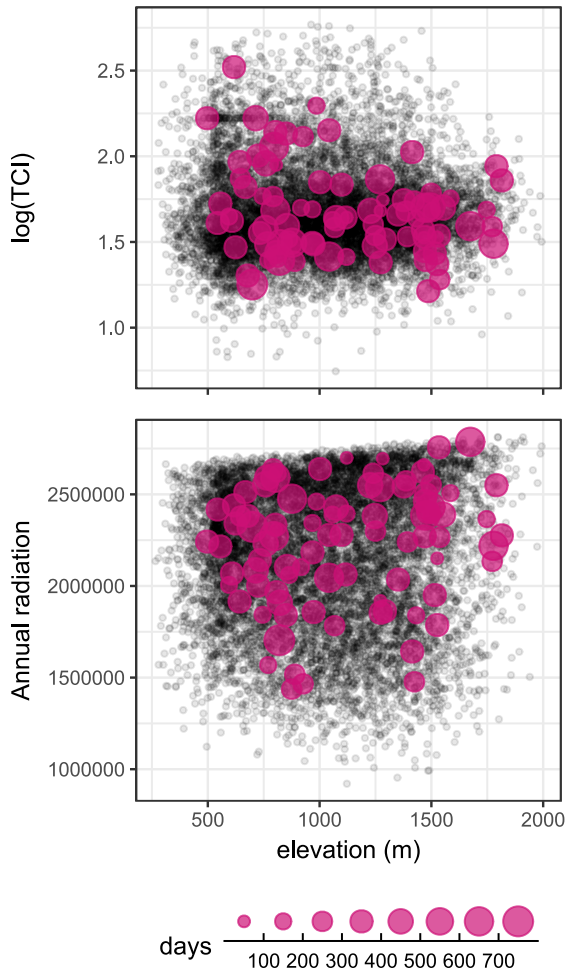

Figure 12. Distribution of sensors across environmental gradients within the Park. In each panel, black points are 10,000 points evenly spaced across the Park; purple points are sensor locations. Point size indicates the length of soil moisture sensor records.

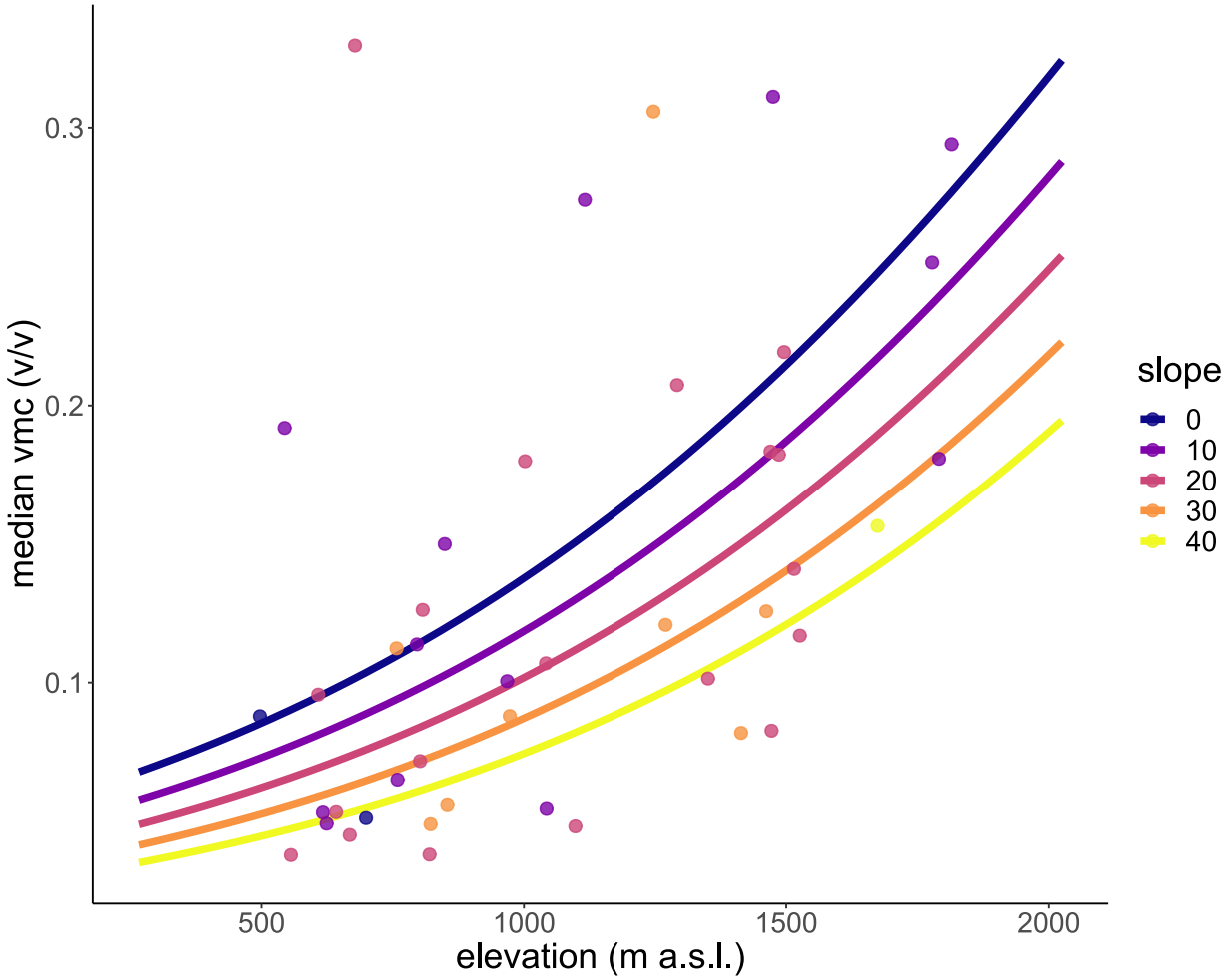

Figure 13. Effect of slope and elevation on median annual 10-15 cm deep soil moisture in sensors deployed from July 2020-July 2021. Lines represent predictions of an additive model of elevation and slope; points are measured median soil moisture values (color of points is based on slope rounded to the nearest 10 degrees). Soil moisture was logit-transformed to improve normality and back-transformed for visualization.

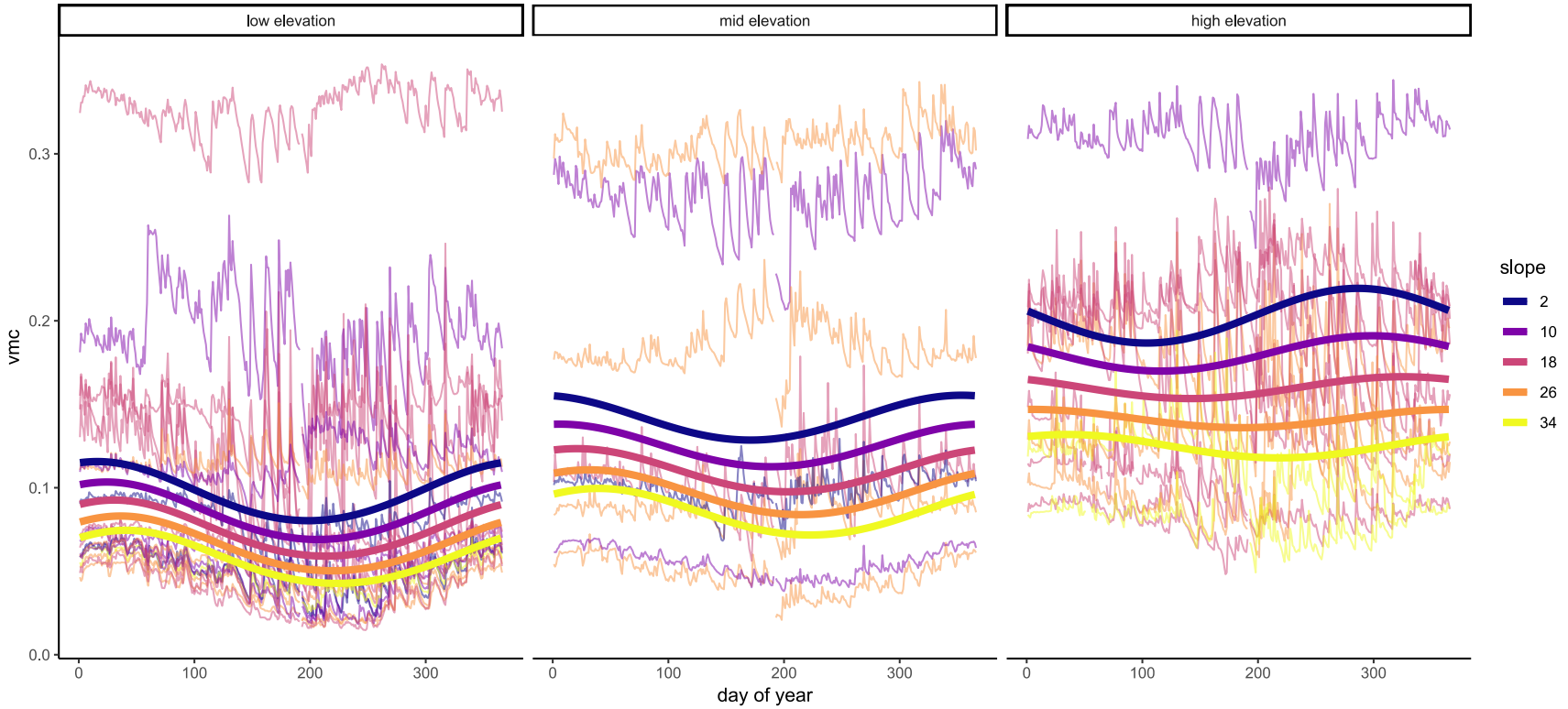

Figure 14. Annual variation 10-15 cm deep soil moisture in sensors deployed from July 2020-July 2021. Panels represent low (mean – sd), middle (mean) and high (mean + sd) elevation. Thin lines show data binned into nearest integer standard deviation from the mean for elevation and slope. Thick lines represent predictions of soil moisture from a linear model with sine- and cosine- transformed day of year, slope, elevation, and interactions between the topographic variables and the seasonal variables. Soil moisture was logit-transformed to improve normality and back-transformed for visualization

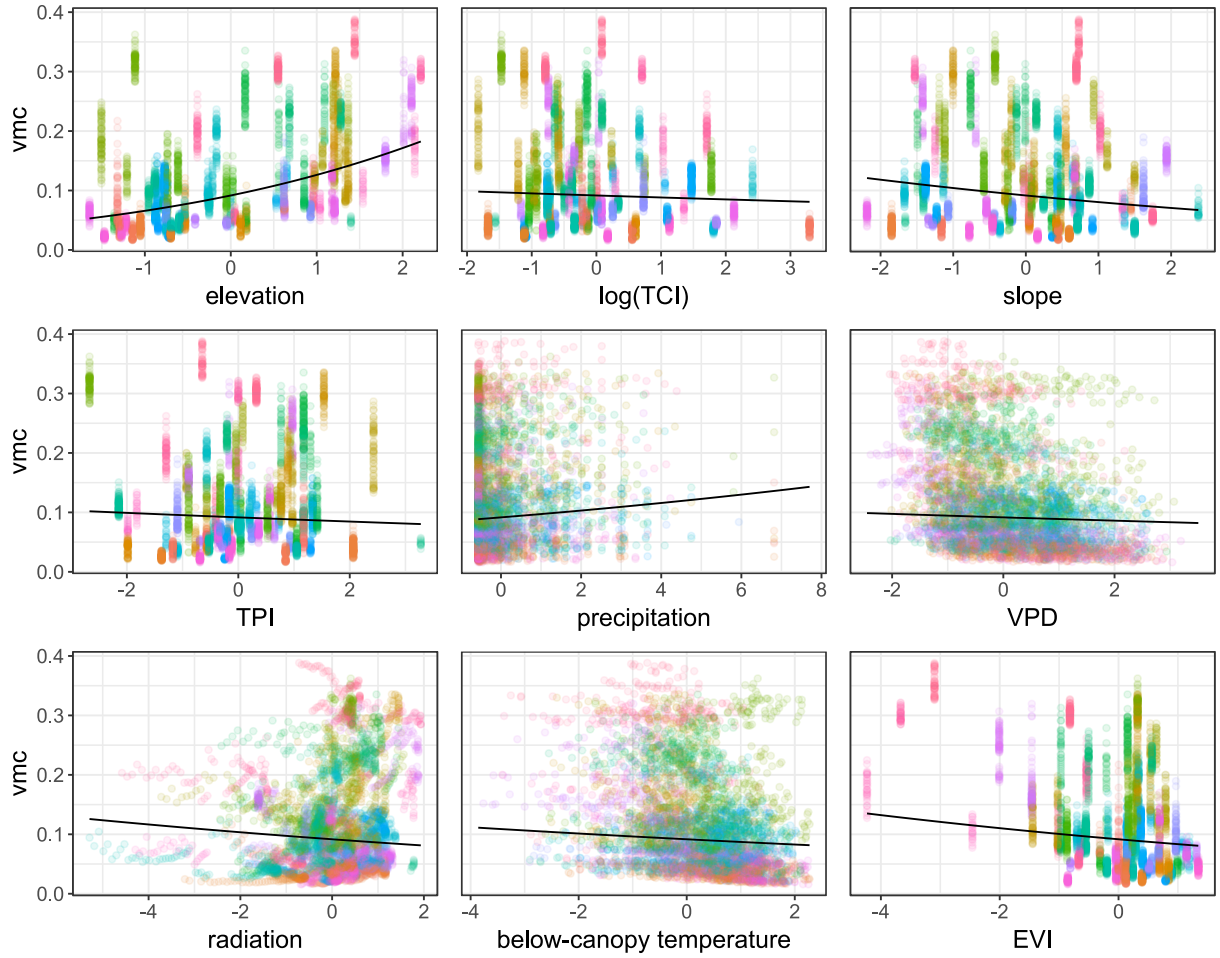

Figure 15. Effects of topographic and daily weather predictors on summer soil moisture across all measured sites. Lines show partial slopes from linear mixed model of the effect of all predictors and random site intercepts on logit-transformed vmc. All predictors were standardized to a mean of zero and standard deviation of one to allow comparison of effect sizes. Points show vmc values used in the model; only values when canopies were between maturity and senescence dates were used. The color of the points reflects site identity. Soil moisture was logit-transformed to improve normality and back-transformed for visualization. Full model results are in Table 6.

References

Ball, D., & Williams, W. (1968). Variability of soil chemical properties in two uncultivated brown earths. *Journal of Soil Science*, 19(2), 379–391.

Bell, J. E., Leeper, R. D., Palecki, M. A., Coopersmith, E., Wilson, T., Bilotta, R., & Embler, S. (2015). Evaluation of the 2012 Drought with a Newly Established National Soil Monitoring Network. *Vadose Zone Journal*, 14(11), vzj2015.02.0023. https://doi.org/10.2136/vzj2015.02.0023

Beven, K. J., & Kirkby, M. J. (1979). A physically based, variable contributing area model of basin hydrology. *Hydrological Sciences Bulletin*, 24(1), 43–69. https://doi.org/10.1080/02626667909491834

Bramer, I., Anderson, B. J., Bennie, J., Bladon, A. J., De Frenne, P., Hemming, D., … Gillingham, P. K. (2018). Advances in Monitoring and Modelling Climate at Ecologically Relevant Scales. *Advances in Ecological Research*, 58, 101–161. https://doi.org/10.1016/bs.aecr.2017.12.005

Brantley, S., Ford, C. R., & Vose, J. M. (2013). Future species composition will affect forest water use after loss of eastern hemlock from southern Appalachian forests. *Ecological Applications*, 23(4), 777–790. https://doi.org/10.1890/12-0616.1

Breshears, D. D., Rich, P. M., Barnes, F. J., & Campbell, K. (1997). Overstory-imposed heterogeneity in solar radiation and soil moisture in a semiarid woodland. *Ecological Applications*, 7(4), 1201–1215. https://doi.org/10.1890/1051-0761(1997)007[1201:OIHISR]2.0.CO;2

Burt, T. P., & Butcher, D. P. (1985). Topographic controls of soil moisture distributions. *Journal of Soil Science*, 36(3), 469–486. https://doi.org/10.1111/j.1365-2389.1985.tb00351.x

Chaney, N. W., Roundy, J. K., Herrera-Estrada, J. E., & Wood, E. F. (2015). High-resolution modeling of the spatial heterogeneity of soil moisture: Applications in network design. *Water Resources Research*, 51, 619–638. https://doi.org/10.1002/2013WR014964

Coopersmith, E. J., Cosh, M. H., Petersen, W. A., Prueger, J., & Niemeier, J. J. (2015). Soil moisture model calibration and validation: An ARS watershed on the South Fork Iowa River. *Journal of Hydrometeorology*, 16(3), 1087–1101. https://doi.org/10.1175/JHM-D-14-0145.1

Crimmins, S. M., Dobrowski, S. Z., Greenberg, J. A., Abatzoglou, J. T., & Mynsberge, A. R. (2011). Changes in climatic water balance drive downhill shifts in plant species' optimum elevations. *Science*, 331, 324–327. https://doi.org/10.1126/science.1199040

Curiel Yuste, J., Baldocchi, D., Gershenson, A., Goldstein, A., Misson, L., & Wong, S. (2018). Microbial soil respiration and its dependency on carbon inputs , soil temperature and moisture. *Global Change Biology*, 13(2007), 2018–2035. https://doi.org/10.1111/j.1365-2486.2007.01415.x

Davis, K. T., Dobrowski, S. Z., Holden, Z. A., Higuera, P. E., & Abatzoglou, J. T. (2019). Microclimatic buffering in forests of the future: the role of local water balance, *Ecography*, 1–11. https://doi.org/10.1111/ecog.03836

De Frenne, P., Rodríguez-Sánchez, F., Coomes, D. A., Baeten, L., Verstraeten, G., Vellen, M., … Verheyen, K. (2013). Microclimate moderates plant responses to macroclimate warming. *Proceedings of the National Academy of Sciences of the United States of America*, 110(46), 18561–18565. https://doi.org/10.1073/pnas.1311190110

Dobrowski, S. Z. (2011). A climatic basis for microrefugia: The influence of terrain on climate. *Global Change Biology*, 17(2), 1022–1035. https://doi.org/10.1111/j.1365-2486.2010.02263.x

Dyer, J. M. (2009). Assessing topographic patterns in moisture use and stress using a water balance approach. *Landscape Ecology*, 24, 391–403.

Easterling, D. R., Kunkel, K. E., Arnold, J. R., Knutson, T. R., LeGrande, A. N., Leung, L. R., … Wehner, M. (2017). Precipitation change in the United States. In: Climate Science Special Report: Fourth National Climate Assessment. Fourth National Climate Assessment, Volume I, 207–230. https://doi.org/10.7930/J0H993CC.U.S.

Engelbrecht, B. M. J., Comita, L. S., Condit, R., Kursar, T. A., Tyree, M. T., Turner, B. L., & Hubbell, S. P. (2007). Drought sensitivity shapes species distribution patterns in tropical forests, *Nature*, 447, 80–82. https://doi.org/10.1038/nature05747

Fridley, J. D. (2009). Downscaling climate over complex terrain: High finescale (<1000 m) spatial variation of near-ground temperatures in a montane forested landscape (Great Smoky Mountains). *Journal of Applied Meteorology and Climatology*, 48(5), 1033–1049. https://doi.org/10.1175/2008JAMC2084.1

Friedl, M., Gray, J., & Sulla-Menashe, D. (2019). MCD12Q2 MODIS/Terra+Aqua Land Cover Dynamics Yearly L3 Global 500m SIN Grid V006. NASA EOSDIS Land Processes DAAC. https://doi.org/10.5067/MODIS/MCD12Q2.006

Graae, B. J., Vandvik, V., Armbruster, W. S., Eiserhardt, W. L., Svenning, J. C., Hylander, K., … Lenoir, J. (2018). Stay or go – how topographic complexity influences alpine plant population and community responses to climate change. *Perspectives in Plant Ecology*,

Evolution and Systematics, 30(February 2018), 41–50. https://doi.org/10.1016/j.ppees.2017.09.008

Green, J. K., Seneviratne, S. I., Berg, A. M., Findell, K. L., Hagemann, S., Lawrence, D. M., & Gentine, P. (2019). Large influence of soil moisture on long-term terrestrial carbon uptake. *Nature*, 565, 476–481. https://doi.org/10.1038/s41586-018-0848-x

Haesen, S., Lembrechts, J. J., De Frenne, P., Lenoir, J., Aalto, J., Ashcroft, M. B., … Van Meerbeek, K. (2021). ForestTemp – Sub-canopy microclimate temperatures of European forests. *Global Change Biology*, (September), 1–13. https://doi.org/10.1111/gcb.15892

Holden, Z. A., Swanson, A., Klene, A. E., Abatzoglou, J. T., Dobrowski, S. Z., Cushman, S. A., … Oyler, J. W. (2016). Development of high-resolution (250 m) historical daily gridded air temperature data using reanalysis and distributed sensor networks for the US Northern Rocky Mountains. *International Journal of Climatology*, 36(10), 3620–3632. https://doi.org/10.1002/joc.4580

Hoylman, Z. H., Jencso, K. G., Hu, J., Holden, Z. A., Martin, J. T., & Gardner, W. P. (2019). The Climatic Water Balance and Topography Control Spatial Patterns of Atmospheric Demand, Soil Moisture, and Shallow Subsurface Flow. *Water Resources Research*, 55(3), 2370–2389. https://doi.org/10.1029/2018WR023302

Kang, J., Jin, R., Li, X., Ma, C., Qin, J., & Zhang, Y. (2017). High spatio-temporal resolution mapping of soil moisture by integrating wireless sensor network observations and MODIS apparent thermal inertia in the Babao River Basin, China. Remote Sensing of Environment, 191, 232–245. https://doi.org/10.1016/j.rse.2017.01.027

Kearney, M. R., Gillingham, P. K., Bramer, I., Duffy, J. P., & Maclean, I. M. D. (2020). A method for computing hourly, historical, terrain-corrected microclimate anywhere on

earth. *Methods in Ecology and Evolution*, 11(1), 38–43. https://doi.org/10.1111/2041-210X.13330

Krumbach, A. W. (1959). Effects of Microrelief on Distribution of Soil Moisture and Bulk Density. *Journal of Geophysical Research*, 64(10), 1587–1590.

Lembrechts, J. J., Nijs, I., & Lenoir, J. (2019). Incorporating microclimate into species distribution models. *Ecography*, 42(7), 1267–1279. https://doi.org/10.1111/ecog.03947

Maclean, I. M. D., Bennie, J. J., Scott, A. J., & Wilson, R. J. (2012). A high-resolution model of soil and surface water conditions. *Ecological Modelling*, 237–238, 109–119. https://doi.org/10.1016/j.ecolmodel.2012.03.029

Maclean, I. M. D., & Klinges, D. H. (2021). Microclimc: A mechanistic model of above, below and within-canopy microclimate. *Ecological Modelling*, 451(March), 109567. https://doi.org/10.1016/j.ecolmodel.2021.109567

Mcdowell, N. G., Grossiord, C., Adams, H. D., Pinzón-Navarro, S., Mackay, D. S., Breshears, D. D., … Xu, C. (2019). Mechanisms of a coniferous woodland persistence under drought and heat. *Environmental Res*, 14. https://doi.org/10.1088/1748-9326/ab0921

McLaughlin, B. C., Ackerly, D. D., Klos, P. Z., Natali, J., Dawson, T. E., & Thompson, S. E. (2017). Hydrologic refugia, plants, and climate change. *Global Change Biology*, 23(8), 2941–2961. https://doi.org/10.1111/gcb.13629

Mickley, J. G., Moore, T. E., Schlichting, C. D., Derobertis, A., Pfisterer, E. N., Bagchi, R., & Mickley, J. G. (2019). Measuring microenvironments for global change : DIY environmental microcontroller units (EMUs). *Methods in Ecology and Evolution*, 10(November 2018), 578–584. https://doi.org/10.1111/2041-210X.13128

Nakagawa, S., Johnson, P. C. D., & Schielzeth, H. (2017). The coefficient of determination R2 and intra-class correlation coefficient from generalized linear mixed-effects models revisited and expanded. *Journal of the Royal Society Interface*, 14(134). https://doi.org/10.1098/rsif.2017.0213

Nakagawa, S., & Schielzeth, H. (2013). A general and simple method for obtaining R2 from generalized linear mixed-effects models. *Methods in Ecology and Evolution*, 4(2), 133–142. https://doi.org/10.1111/j.2041-210x.2012.00261.x

Oldfather, M. F., Kling, M. M., Sheth, S. N., Emery, N. C., & Ackerly, D. D. (2020). Range edges in heterogeneous landscapes: Integrating geographic scale and climate complexity into range dynamics. *Global Change Biology*, 26(3), 1055–1067. https://doi.org/10.1111/gcb.14897

Orchard, V. A., & Cook, F. . (1983). Relationship between soil respiration and soil moisture. *Soil Biology and Biochemistry*, 15(4), 447–453.

Orwig, D. A., Cobb, R. C., D'Amato, A. W., Kizlinski, M. L., & Foster, D. R. (2008). Multi-year ecosystem response to hemlock woolly adelgid infestation in southern New England forests. *Canadian Journal of Forest Research*, 38(4), 834–843. https://doi.org/10.1139/X07-196

Pan, F. (2012). Estimating Daily Surface Soil Moisture Using a Daily Diagnostic Soil Moisture Equation. *Journal of Irrigation and Drainage Engineering*, 138(7), 625–631. https://doi.org/10.1061/(ASCE)IR.1943-4774.0000450

Peck, J. E., Zenner, E. K., & Palik, B. (2012). Variation in microclimate and early growth of planted pines under dispersed and aggregated overstory retention in mature managed red

pine in Minnesota. *Canadian Journal of Forest Research*, 42(2), 279–290. https://doi.org/10.1139/X11-186

Pierce, K. B., Lookingbill, T., & Urban, D. (2005). A simple method for estimating potential relative radiation (PRR) for landscape-scale vegetation analysis. *Landscape Ecology*, 20(2), 137–147. https://doi.org/10.1007/s10980-004-1296-6

PRISM climate group. (2021). No Title. Oregon State University. Retrieved from http://prism.oregonstate.edu

Robinson, D. A., Campbell, C. S., Hopmans, J. W., Hornbuckle, B. K., Jones, S. B., Knight, R., … Wendroth, O. (2008). Soil Moisture Measurement for Ecological and Hydrological Watershed-Scale Observatories: A Review. *Vadose Zone Journal*, 7(1), 358–389. https://doi.org/10.2136/vzj2007.0143

Saito, T., Fujimaki, H., Yasuda, H., Inosako, K., & Inoue, M. (2013). Calibration of Temperature Effect on Dielectric Probes Using Time Series Field Data. *Vadose Zone Journal*, 12(2). https://doi.org/10.2136/vzj2012.0184

Scharenbroch, B., & Bockheim, J. (2007). Impacts of forest gaps on soil properties and processes in old growth northern hardwood-hemlock forests. *Plant Soil*, 294, 219–233. https://doi.org/10.1007/s11104-007-9248-y

Sheikh, V., Visser, S., & Stroosnijder, L. (2009). A simple model to predict soil moisture: Bridging Event and Continuous Hydrological (BEACH) modelling. *Environmental Modelling and Software*, 24(4), 542–556. https://doi.org/10.1016/j.envsoft.2008.10.005

Slavich, E., Warton, D. I., Ashcroft, M. B., Gollan, J. R., & Ramp, D. (2014). Topoclimate versus macroclimate: How does climate mapping methodology affect species distribution

models and climate change projections? *Diversity and Distributions*, 20(8), 952–963. https://doi.org/10.1111/ddi.12216

Stillman, S., Ninneman, J., Zeng, X., Franz, T., Scott, R. L., Shuttleworth, W. J., & Cummins, K. (2014). Summer Soil Moisture Spatiotemporal Variability in Southeastern Arizona. *Journal of Hydrometeorology*, 15, 1473–1485. https://doi.org/10.1175/JHM-D-13-0173.1

Storlie, C. J., Phillips, B. L., Vanderwal, J. J., & Williams, S. E. (2013). Improved spatial estimates of climate predict patchier species distributions. *Diversity and Distributions*, 19(9), 1106–1113. https://doi.org/10.1111/ddi.12068

Töpper, J. P., Meineri, E., Olsen, S. L., Rydgren, K., Skarpaas, O., & Vandvik, V. (2018). The devil is in the detail: Nonadditive and context-dependent plant population responses to increasing temperature and precipitation. *Global Change Biology*, 24(10), 4657–4666. https://doi.org/10.1111/gcb.14336

Tromp-van Meerveld, H. J., & Mcdonnell, J. J. (2006). On the interrelations between topography , soil depth , soil moisture , transpiration rates and species distribution at the hillslope scale. *Advances in Water Resources*, 29, 293–310. https://doi.org/10.1016/j.advwatres.2005.02.016

Vanwalleghem, T., & Meentemeyer, R. K. (2009). Predicting forest microclimate in heterogeneous landscapes. *Ecosystems*, 12(7), 1158–1172. https://doi.org/10.1007/s10021-009-9281-1

Vereecken, H., Huisman, J. A., Pachepsky, Y., Montzka, C., van der Kruk, J., Bogena, H., … Vanderborght, J. (2014). On the spatio-temporal dynamics of soil moisture at the field scale. *Journal of Hydrology*, 516, 76–96. https://doi.org/10.1016/j.jhydrol.2013.11.061

Von Arx, G., Dobbertin, M., Rebetez, M., Arx, G. Von, Dobbertin, M., & Rebetez, M. (2012). Spatio-temporal effects of forest canopy on understory microclimate in a long-term experiment in Switzerland. *Agricultural and Forest Meteorology*, 166–167(April), 144–155. https://doi.org/10.1016/j.agrformet.2012.07.018

Von Arx, G., Graf Pannatier, E., Thimonier, A., & Rebetez, M. (2013). Microclimate in forests with varying leaf area index and soil moisture: Potential implications for seedling establishment in a changing climate. *Journal of Ecology*, 101(5), 1201–1213. https://doi.org/10.1111/1365-2745.12121

Walsh, S. F., Nyman, P., Sheridan, G. J., Baillie, C. C., Tolhurst, K. G., & Duff, T. J. (2017). Hillslope-scale prediction of terrain and forest canopy effects on temperature and near-surface soil moisture deficit. *International Journal of Wildland Fire*, 26(3), 191–208. https://doi.org/10.1071/WF16106

Western, A. W., Grayson, R. B., Blöschl, G., Willgoose, G. R., & McMahon, T. A. (1999). Observed spatial organization of soil moisture and its relation to terrain indices. *Water Resources Research*, 35(3), 797–810. https://doi.org/10.1029/1998WR900065

Whittaker, R. H. (1956). Vegetation of the Great Smoky Mountains. *Ecological Monographs*, 26(1), 1–80.

Wilson, M. F. J., O'Connell, B., Brown, C., Guinan, J. C., & Grehan, A. J. (2007). Multiscale terrain analysis of multibeam bathymetry data for habitat mapping on the continental slope. *Marine Geodesy* (Vol. 30). https://doi.org/10.1080/01490410701295962

Winkler, D. E., Chapin, K. J., & Kueppers, L. M. (2016). Soil moisture mediates alpine life form and community productivity responses to warming. *Ecology*, 97(6), 1553–1563. https://doi.org/10.1890/15-1197.1

Zellweger, F., de Frenne, P., Lenoir, J., Vangansbeke, P., Verheyen, K., Bernhardt-Römermann, M., … Coomes, D. (2020). Forest microclimate dynamics drive plant responses to warming. *Science*, 368(6492), 772–775. https://doi.org/10.1126/science.aba6880

Zhang, X., Zhang, T., Zhou, P., Shao, Y., & Gao, S. (2017). Validation analysis of SMAP and AMSR2 soil moisture products over the United States using ground-based measurements. *Remote Sensing*, 9(2). https://doi.org/10.3390/rs9020104

Conclusion

Local variation in moisture and temperature has been proposed as a key factor structuring the spatial variation in plant communities and ecological process in GSMNP since at least the 1950s (Whittaker, 1956). However, microclimate data at scales relevant to the cove-to-ridge gradients over which plant communities change dramatically were not available until recently. Sixty-five years after Whittaker's influential work qualitatively describing the relationship between local climate and plant communities in GSMNP, I quantitatively describe and model these patterns from two distinct angles. In Chapter 1, I used local temperature models (Fridley, 2009) to model the distribution of plant species throughout the Park. The current distribution of plant species in the Park was not predicted better by microclimate data than macroclimate data; however, microclimatic buffering suggested that some species, particularly those in near-stream or high-TCI areas at middle elevations, could persist in their current locations even under 4 °C of regional climate warming. On the other hand, focusing on the single axis of temperature variation does not fully capture the climatic niches of plants. In Chapter 2 I developed new soil moisture sensors and collected soil moisture data to allow exploration of local moisture variation. The elevation gradient of soil moisture was much stronger than the corresponding precipitation gradient, suggesting that local controls (evapotranspiration or soil depth/texture) are key drivers of moisture availability in the Park. In addition, while several potential topographic (slope), plant-related (EVI), and meteorological (VPD, below-canopy temperature) drivers were correlated with moisture, no single proxy explained a large amount of variation. This demonstrates the critical need to develop better local models of soil moisture dynamics across complex landscapes to improve understanding of the drivers and effects of microclimatic conditions.

Research on microclimate has always been limited by the available tools. Early studies of local variation in temperature and moisture relied on techniques that were labor-intensive and limited the ability of researchers to understand variation over time (e.g. Ball & Williams, 1968; Geiger, 1966). While tools for measuring thermal microclimate over time across landscapes are now commonly used in microclimate studies, many recent examinations of landscape-wide moisture variation still use techniques that require a person to be present to collect each sensor reading (e.g. Kaiser & McGlynn, 2018; Lookingbill & Urban, 2004). Soil moisture timeseries have been collected for other sites, but most examine single watersheds, sites selected for homogeneity across systems, or other areas where spatial kriging or other smoothing techniques can represent conditions between sparsely-placed sensors (e.g. E. J. Coopersmith, Minsker, & Sivapalan, 2014; Holden et al., 2016). New sensors such as those developed in Chapter 2 will facilitate increased sampling and improved understanding of the drivers and effects of local variation in soil moisture.

Global change threatens ecological communities around the world, but understanding the effects of warmer temperatures, changes to rainfall patterns, and increases in extreme events will require improved understanding of the climatic conditions actually experienced by organisms. In topographically complex regions and under forest canopies, the processes that control temperature and moisture are complex and not captured by the climate data collected at weather stations. Chapter 1 suggests that many species which respond to below-canopy temperature may be impacted less by warming temperatures than global circulation models would indicate. However, several important caveats exist. First, some of the drivers of microclimatic buffering may themselves be affected by climate change; for example, if forest canopies are disrupted by disease or pest outbreaks, below-canopy climatic conditions may change much more rapidly than

predicted by either fine- or broad-scale climate models. Second, chapter 2 demonstrates that soil moisture also varies strongly on local scales in GSMNP. If moisture and temperature gradients do not shift synchronously, the range of suitable habitats for species which occupy particular microclimatic niches on both of these (or other) axes may shrink. Finally, it is not clear whether (or which) species respond most strongly to buffered below-canopy microclimatic conditions rather than above-canopy temperatures. For example, if canopy tree species' distributions are most tightly linked to seedling survival, they may respond more strongly to below-canopy microclimates than if their distributions are linked to mature tree photosynthetic rates. Creating models that allow prediction of future microclimatic conditions based on weather data and other drivers will be critical for understanding the effects of global change on organisms and ecological processes.

References

Ball, D., & Williams, W. (1968). Variability of soil chemical properties in two uncultivated brown earths. *Journal of Soil Science*, 19(2), 379–391.

Coopersmith, E. J., Minsker, B. S., & Sivapalan, M. (2014). Using similarity of soil texture and hydroclimate to enhance soil moisture estimation. *Hydrology and Earth System Sciences*, 18(8), 3095–3107. https://doi.org/10.5194/hess-18-3095-2014

Fridley, J. D. (2009). Downscaling climate over complex terrain: High finescale (<1000 m) spatial variation of near-ground temperatures in a montane forested landscape (Great Smoky Mountains). *Journal of Applied Meteorology and Climatology*, 48(5), 1033–1049. https://doi.org/10.1175/2008JAMC2084.1

Geiger, R. (1966). The climate near the ground (Translated). Cambridge, MA: Harvard University Press.

Holden, Z. A., Swanson, A., Klene, A. E., Abatzoglou, J. T., Dobrowski, S. Z., Cushman, S. A., … Oyler, J. W. (2016). Development of high-resolution (250 m) historical daily gridded air temperature data using reanalysis and distributed sensor networks for the US Northern Rocky Mountains. *International Journal of Climatology*, 36(10), 3620–3632. https://doi.org/10.1002/joc.4580

Kaiser, K. E., & McGlynn, B. L. (2018). Nested Scales of Spatial and Temporal Variability of Soil Water Content Across a Semiarid Montane Catchment. *Water Resources Research*, 54(10), 7960–7980. https://doi.org/10.1029/2018WR022591

Lookingbill, T., & Urban, D. (2004). An empirical approach towards improved spatial estimates of soil moisture for vegetation analysis. *Landscape Ecology*, 19(4), 417–433. https://doi.org/10.1023/B:LAND.0000030451.29571.8b

Whittaker, R. H. (1956). Vegetation of the Great Smoky Mountains. *Ecological Monographs*, 26(1), 1–80.

Appendix 1: Supplemental material for Chapter 1

Tables

Table S1. Climate warming scenarios used as comparison for 4 – degree projected warming in GSMNP. All data obtained from 2.5 minute downscaling at worldclim.org. Warming is for the change in MAT from SSP3-7.0 in 2080-2100 compared to historical WorldClim data from 1970-2000 in GSMNP.

Model name	Citation	Institution	Mean warming	Range warming
BCC-CSM2-MR	(Zhang et al., 2019)	Beijing Climate Center, Beijing 100081, China	4.95	4.91-4.97
CanESM5	(Swart et al., 2019)	Canadian Centre for Climate Modelling and Analysis, Environment and Climate Change Canada, Victoria, BC V8P 5C2, Canada	6.34	6.30-6.39
CNRM-CM6-1	(Voldoire, 2019)	CNRM (Centre National de Recherches Meteorologiques, Toulouse 31057, France), CERFACS (Centre Europeen de Recherche et de Formation Avancee en Calcul Scientifique, Toulouse 31057, France)	4.41	4.40-4.43
CNRM-ESM2-1	(Seferian, 2019)	CNRM (Centre National de Recherches Meteorologiques, Toulouse 31057, France), CERFACS (Centre Europeen de Recherche et de Formation Avancee en Calcul Scientifique, Toulouse 31057, France)	4.18	4.13-4.22
GFDL-ESM4	(Horowitz et al., 2018)	National Oceanic and Atmospheric Administration, Geophysical Fluid Dynamics Laboratory, Princeton, NJ 08540, USA	3.49	3.46-3.52
IPSL-CM6A-LR	(Boucher et al., 2018)	Institut Pierre Simon Laplace, Paris 75252, France	5.41	5.37-5.44
MIROC-ES2L	(Hajima et al., 2019)	JAMSTEC (Japan Agency for Marine-Earth Science and Technology, Kanagawa 236-0001, Japan), AORI (Atmosphere and Ocean Research Institute, The University of Tokyo, Chiba 277-8564, Japan), NIES (National Institute for Environmental Studies, Ibaraki 305-8506, Japan), and R-CCS (RIKEN Center for Computational Science, Hyogo 650-0047, Japan)	4.37	4.33-4.40
MIROC6	(Takemura, 2019)	JAMSTEC (Japan Agency for Marine-Earth Science and Technology, Kanagawa 236-0001, Japan), AORI	4.17	4.13-4.21

		(Atmosphere and Ocean Research Institute, The University of Tokyo, Chiba 277-8564, Japan), NIES (National Institute for Environmental Studies, Ibaraki 305-8506, Japan), and R-CCS (RIKEN Center for Computational Science, Hyogo 650-0047, Japan)		
MRI-ESM2-0	(Yukimoto et al., 2019)	Meteorological Research Institute, Tsukuba, Ibaraki 305-0052, Japan	3.84	3.72-4.04

References for CMIP6 GCM data

We acknowledge the World Climate Research Programme, which, through its Working Group on Coupled Modelling, coordinated and promoted CMIP6. We thank the climate modeling groups for producing and making available their model output, the Earth System Grid Federation (ESGF) for archiving the data and providing access, and the multiple funding agencies who support CMIP6 and ESGF.

Boucher, O., Denvil, S., Levavasseur, G., Cozic, A., Caubel, A., Foujols, M.-A., … Ghattas, J. (2018). IPSL IPSL-CM6A-LR model output prepared for CMIP6 C4MIP. Earth System Grid Federation. https://doi.org/10.22033/ESGF/CMIP6.1521

Hajima, T., Kawamiya, M., Tachiiri, K., Abe, M., Arakawa, O., Suzuki, T., … Watanabe, S. (2019). MIROC MIROC-ES2L model output prepared for CMIP6 C4MIP. Earth System Grid Federation. https://doi.org/10.22033/ESGF/CMIP6.906

Horowitz, L. W., Naik, V., Sentman, L., Paulot, F., Blanton, C., McHugh, C., … Zeng, Y. (2018). NOAA-GFDL GFDL-ESM4 model output prepared for CMIP6 AerChemMIP. Earth System Grid Federation. https://doi.org/10.22033/ESGF/CMIP6.1404

Seferian, R. (2019). CNRM-CERFACS CNRM-ESM2-1 model output prepared for CMIP6 AerChemMIP. Earth System Grid Federation. https://doi.org/10.22033/ESGF/CMIP6.1389

Swart, N. C., Cole, J. N. S., Kharin, V. V, Lazare, M., Scinocca, J. F., Gillett, N. P., … Sigmond, M. (2019). CCCma CanESM5 model output prepared for CMIP6 C4MIP. Earth System Grid Federation. https://doi.org/10.22033/ESGF/CMIP6.1301

Takemura, T. (2019). MIROC MIROC6 model output prepared for CMIP6 AerChemMIP. Earth System Grid Federation. https://doi.org/10.22033/ESGF/CMIP6.9121

Voldoire, A. (2019). CNRM-CERFACS CNRM-CM6-1 model output prepared for CMIP6 CFMIP. Earth System Grid Federation. https://doi.org/10.22033/ESGF/CMIP6.1374

Yukimoto, S., Koshiro, T., Kawai, H., Oshima, N., Yoshida, K., Urakawa, S., … Adachi, Y. (2019). MRI MRI-ESM2.0 model output prepared for CMIP6 AerChemMIP. Earth System Grid Federation. https://doi.org/10.22033/ESGF/CMIP6.633

Zhang, F., Wu, T., Shi, X., Li, J., Chu, M., Liu, Q., … Wei, M. (2019). BCC BCC-CSM2MR model output prepared for CMIP6 C4MIP. Earth System Grid Federation. https://doi.org/10.22033/ESGF/CMIP6.1723

Table S2. Effects of model structure choice on model fit.

formula		Mean AUC			Overall WAIC		
Elevation	~ elev + Easting + Northing + log(Plotsize)	0.72			53.5		
		macro	interp	micro	macro	interp	micro
No interactions	~ MAT + MAT^2 + log(TCI) + totrad + Easting + Northing + log(Plotsize)	0.80	0.80	0.80	49.3	49.3	48.7
Full model	~ (MAT + MAT^2)*(log(TCI) + totrad) + Easting + Northing + log(Plotsize)	0.80	0.80	0.80	49.0	49.0	49.1

Table S3. Model fit and change in area for each species with AUC > 0.8

Species Code	Species Name	AUC				Stable future:current			Dispersal future:current		
		elev	macro	interp	micro	macro	interp	micro	macro	interp	micro
ABIEFRA	*Abies fraseri*	0.98	0.98	0.99	0.98	0.00	0.00	0.04	0.00	0.00	0.04
ACERRUB	*Acer rubrum*	0.79	0.83	0.82	0.82	0.63	0.59	0.82	0.91	0.83	1.07
ACERSPI	*Acer spicatum*	0.90	0.91	0.90	0.91	0.00	0.00	0.06	0.00	0.00	0.06
ACTARACR	*Actaea racemosa*	0.63	0.83	0.84	0.85	0.12	0.12	0.41	0.20	0.17	0.46
ADIAPED	*Adiantum pedatum*	0.72	0.89	0.90	0.90	0.41	0.48	0.79	1.91	2.04	2.03
AESCFLA	*Aesculus flava*	0.69	0.83	0.83	0.83	0.04	0.06	0.30	0.04	0.06	0.32
AGERALS	*Ageratina altissima*	0.81	0.83	0.83	0.84	0.01	0.02	0.16	0.01	0.02	0.16
ARISMAC	*Aristolochia macrophylla*	0.71	0.87	0.86	0.86	0.11	0.15	0.37	0.35	0.43	0.79
BETUALL	*Betula alleghaniensis*	0.82	0.86	0.86	0.87	0.03	0.04	0.28	0.03	0.04	0.28
CALYFLOG	*Calycanthus floridus*	0.83	0.89	0.89	0.88	0.00	0.01	0.14	0.08	0.07	0.41
CARDDIP	*Cardamine diphylla*	0.62	0.84	0.84	0.85	0.05	0.09	0.35	0.10	0.15	0.41
CAREDEB	*Carex debilis*	0.81	0.83	0.82	0.83	0.07	0.20	0.24	0.09	0.25	0.27
CARYALB	*Carya alba*	0.87	0.88	0.87	0.88	1.00	1.00	1.00	6.79	6.00	4.21
CARYGLA	*Carya glabra*	0.80	0.82	0.82	0.82	0.80	0.81	0.99	2.58	2.47	2.15
CASTDNT	*Castanea dentata*	0.70	0.81	0.81	0.81	0.06	0.07	0.37	0.13	0.17	0.59
CAULTHA	*Caulophyllum thalictroides*	0.66	0.87	0.88	0.89	0.02	0.02	0.24	0.06	0.06	0.36
CHIMMAC	*Chimaphila maculate*	0.79	0.84	0.84	0.85	0.36	0.36	0.84	1.45	1.30	1.68
CLINUMB	*Clintonia umbellulate*	0.72	0.80	0.82	0.82	0.02	0.02	0.24	0.02	0.03	0.30
COLLCAN	*Collinsonia canadensis*	0.80	0.84	0.85	0.86	0.01	0.02	0.23	0.03	0.04	0.27
COREMAJ	*Coreopsis major*	0.81	0.92	0.92	0.92	1.00	0.63	0.99	3.81	1.16	1.66
CORNFLO	*Cornus florida*	0.87	0.88	0.87	0.87	1.00	1.00	1.00	3.37	3.41	2.47
CYSTPRO	*Cystopteris protrusa*	0.66	0.80	0.80	0.81	0.11	0.11	0.40	0.20	0.20	0.61
DEPAACR	*Deparia acrostichoides*	0.68	0.87	0.88	0.88	0.01	0.02	0.19	0.02	0.03	0.22

DESMNUD	*Desmodium nudiflorum*	0.78	0.82	0.81	0.82	0.83	0.64	1.00	3.75	2.54	3.24
DICHCMM	*Dichanthelium commutatum*	0.80	0.88	0.88	0.88	0.99	0.77	0.78	5.57	2.66	1.51
DRYOINT	*Dryopteris intermedia*	0.73	0.84	0.84	0.84	0.04	0.05	0.29	0.05	0.06	0.30
DRYOMAR	*Dryopteris marginalis*	0.59	0.81	0.81	0.81	0.23	0.27	0.51	0.57	0.54	0.88
EPIGREP	*Epigaea repens*	0.71	0.86	0.86	0.86	0.17	0.09	0.34	0.57	0.25	0.66
EUONAME	*Euonymus americana*	0.85	0.86	0.86	0.85	1.00	1.00	1.00	4.64	5.13	3.25
GALAURC	*Galax urceolata*	0.65	0.84	0.82	0.83	0.06	0.09	0.32	0.33	0.32	0.66
GALICRC	*Galium circaezans*	0.83	0.86	0.85	0.85	1.00	1.00	1.00	12.27	11.68	7.13
GAULPRO	*Gaultheria procumbens*	0.62	0.82	0.81	0.83	0.19	0.35	0.42	0.63	0.95	0.81
GAYLBAC	*Gaylussacia baccata*	0.77	0.88	0.88	0.89	0.05	0.05	0.25	0.14	0.18	0.45
GAYLURS	*Gaylussacia ursina*	0.76	0.87	0.87	0.87	0.01	0.01	0.25	0.27	0.22	0.74
HALETETM	*Halesia tetraptera*	0.64	0.83	0.83	0.83	0.10	0.13	0.41	0.18	0.20	0.55
HOUSSER	*Houstonia serpyllifolia*	0.78	0.82	0.81	0.81	0.01	0.02	0.24	0.01	0.02	0.24
HUPELUC	*Huperzia lucidula*	0.78	0.81	0.81	0.81	0.46	0.33	0.57	0.46	0.33	0.57
ILEXOPAO	*Ilex opaca*	0.85	0.84	0.85	0.84	0.87	0.99	0.94	2.87	3.47	2.11
KALMLAT	*Kalmia latifolia*	0.64	0.82	0.80	0.81	0.25	0.23	0.50	0.53	0.49	0.84
LAPOCAN	*Laportea canadensis*	0.65	0.82	0.82	0.83	0.07	0.09	0.34	0.09	0.09	0.36
LINDBEN	*Lindera benzoin*	0.74	0.84	0.84	0.83	0.35	0.56	0.94	0.99	1.58	2.06
LIRITUL	*Liriodendron tulipifera*	0.82	0.85	0.85	0.84	0.30	0.42	0.74	0.77	1.04	1.34
MAGNACU	*Magnolia acuminata*	0.70	0.81	0.81	0.81	0.02	0.02	0.28	0.08	0.07	0.50
NYSSSYL	*Nyssa sylvatica*	0.80	0.88	0.88	0.88	0.40	0.27	0.64	1.16	0.90	1.24
OSMOCLA	*Osmorhiza claytonii*	0.58	0.84	0.85	0.86	0.02	0.04	0.25	0.17	0.17	0.50
OXALMON	*Oxalis montana*	0.80	0.86	0.86	0.86	0.06	0.11	0.22	0.06	0.14	0.24
OXYDARB	*Oxydendrum arboretum*	0.79	0.86	0.86	0.86	0.31	0.32	0.58	0.84	0.84	1.04
PARTQUI	*Parthenocissus quinquefolia*	0.79	0.82	0.82	0.81	1.00	1.00	1.00	3.92	4.20	3.08
PHEGHEX	*Phegopteris hexagonoptera*	0.66	0.82	0.83	0.83	0.04	0.07	0.32	0.27	0.31	0.68

PICERUB	*Picea rubens*	0.95	0.95	0.96	0.96	0.00	0.01	0.15	0.00	0.01	0.15
PINUPUN	*Pinus pungens*	0.74	0.91	0.90	0.90	0.00	0.00	0.13	0.07	0.08	0.41
PINURIG	*Pinus rigida*	0.81	0.89	0.89	0.89	0.58	0.37	0.66	2.21	1.34	1.34
PINUSTR	*Pinus strobus*	0.88	0.89	0.90	0.90	1.00	1.00	1.00	3.60	3.40	2.40
PINUVIR	*Pinus virginiana*	0.90	0.93	0.93	0.94	1.00	0.99	1.00	5.50	3.65	2.26
POLYPUB	*Polygonatum pubescens*	0.75	0.84	0.85	0.84	0.02	0.02	0.23	0.05	0.04	0.33
POTECND	*Potentilla canadensis*	0.76	0.81	0.82	0.82	1.00	1.00	1.00	7.20	7.04	3.93
PROSLAN	*Prosartes lanuginose*	0.64	0.82	0.83	0.84	0.10	0.15	0.39	0.17	0.21	0.49
PRUNPEN	*Prunus pensylvanica*	0.89	0.90	0.90	0.90	0.00	0.00	0.10	0.00	0.00	0.10
PTERAQU	*Pteridium aquilinum*	0.78	0.90	0.90	0.90	0.28	0.10	0.37	1.23	0.38	0.74
QUERALB	*Quercus alba*	0.81	0.85	0.85	0.85	1.00	1.00	1.00	4.14	3.87	2.85
QUERCOCC	*Quercus coccinea*	0.77	0.88	0.88	0.88	0.14	0.10	0.44	0.70	0.52	0.98
QUERMON	*Quercus montana*	0.72	0.87	0.87	0.86	0.20	0.12	0.41	0.78	0.49	0.89
QUERVEL	*Quercus velutina*	0.81	0.86	0.86	0.87	1.00	0.93	0.99	3.87	2.92	2.06
SANGCND	*Sanguinaria canadensis*	0.63	0.84	0.84	0.84	0.09	0.12	0.60	0.38	0.50	1.29
SANICANC	*Sanicula canadensis*	0.80	0.82	0.82	0.82	1.00	1.00	1.00	6.36	6.61	3.63
SASSALB	*Sassafras albidum*	0.77	0.84	0.84	0.84	0.22	0.23	0.50	0.76	0.69	0.97
SMILGLA	*Smilax glabra*	0.85	0.89	0.89	0.89	0.98	0.99	0.95	2.86	2.80	1.94
SMILHER	*Smilax herbacea*	0.77	0.81	0.81	0.81	0.01	0.03	0.26	0.01	0.03	0.29
SMILROT	*Smilax rotundifolia*	0.75	0.80	0.80	0.80	0.42	0.40	0.73	0.71	0.69	1.07
SMILTMN	*Smilax tamnoides*	0.78	0.82	0.81	0.80	0.24	0.32	0.94	0.75	0.83	1.84
STELPBR	*Stellaria pubera*	0.72	0.81	0.82	0.82	0.05	0.07	0.31	0.06	0.08	0.32
THALTHA	*Thalictrum thalictroides*	0.74	0.85	0.86	0.85	0.47	0.27	0.92	1.27	0.70	1.66
TIARCOR	*Tiarella cordifolia*	0.62	0.82	0.82	0.83	0.09	0.17	0.51	0.09	0.18	0.52
TILIAME	*Tilia americana*	0.77	0.84	0.83	0.83	0.09	0.14	0.44	0.22	0.31	0.74
TILIAMEH	*Tilia americana (heterophylla)*	0.58	0.82	0.83	0.84	0.03	0.05	0.29	0.10	0.12	0.43
TOXIRAD	*Toxicodendron radicans*	0.89	0.88	0.89	0.89	1.00	1.00	1.00	8.85	9.21	5.96

VACCERY	*Vaccinium erythrocarpum*	0.87	0.87	0.87	0.86	0.00	0.01	0.11	0.00	0.01	0.11
VACCHIR	*Vaccinium hirsutum*	0.84	0.89	0.89	0.89	0.03	0.04	0.26	0.08	0.10	0.41
VACCPAL	*Vaccinium pallidum*	0.75	0.86	0.86	0.86	0.85	0.64	0.92	2.01	1.29	1.34
VACCSIM	*Vaccinium simulatum*	0.76	0.82	0.82	0.81	0.02	0.02	0.19	0.02	0.02	0.23
VACCSTA	*Vaccinium stamineum*	0.72	0.85	0.85	0.85	0.48	0.34	0.73	1.12	0.80	1.00
VIBULAN	*Viburnum lantanoides*	0.89	0.91	0.91	0.90	0.00	0.00	0.08	0.00	0.00	0.08
VIOLROT	*Viola rotundifolia*	0.68	0.82	0.82	0.83	0.03	0.05	0.31	0.06	0.10	0.42
VIOLSOR	*Viola sororia*	0.85	0.88	0.88	0.87	1.00	1.00	1.00	12.25	12.53	5.68
VITIAES	*Vitis aestivalis*	0.76	0.81	0.80	0.81	0.41	0.36	0.68	1.77	1.63	1.81

Figures

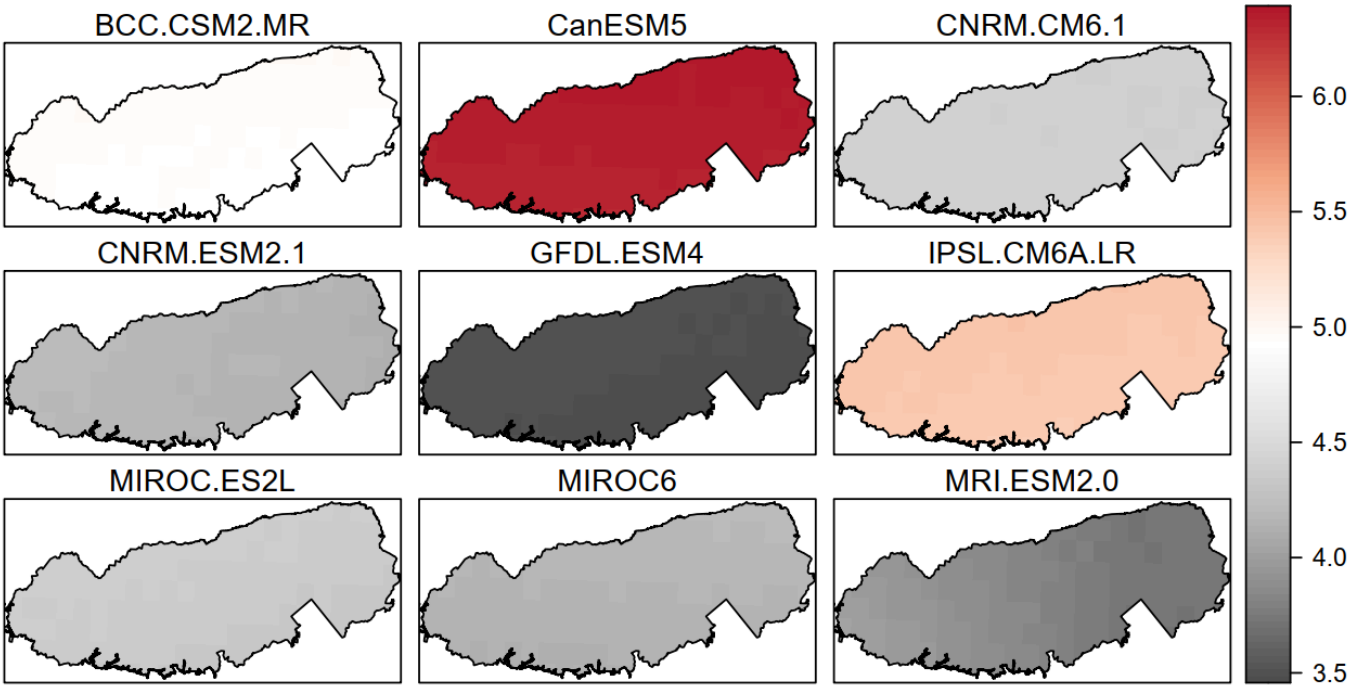

Figure S1. Projected warming from SSP3-7.0 for each of the nine GCMs downscaled by WorldClim 2.1 compared to 1970-2000 records.

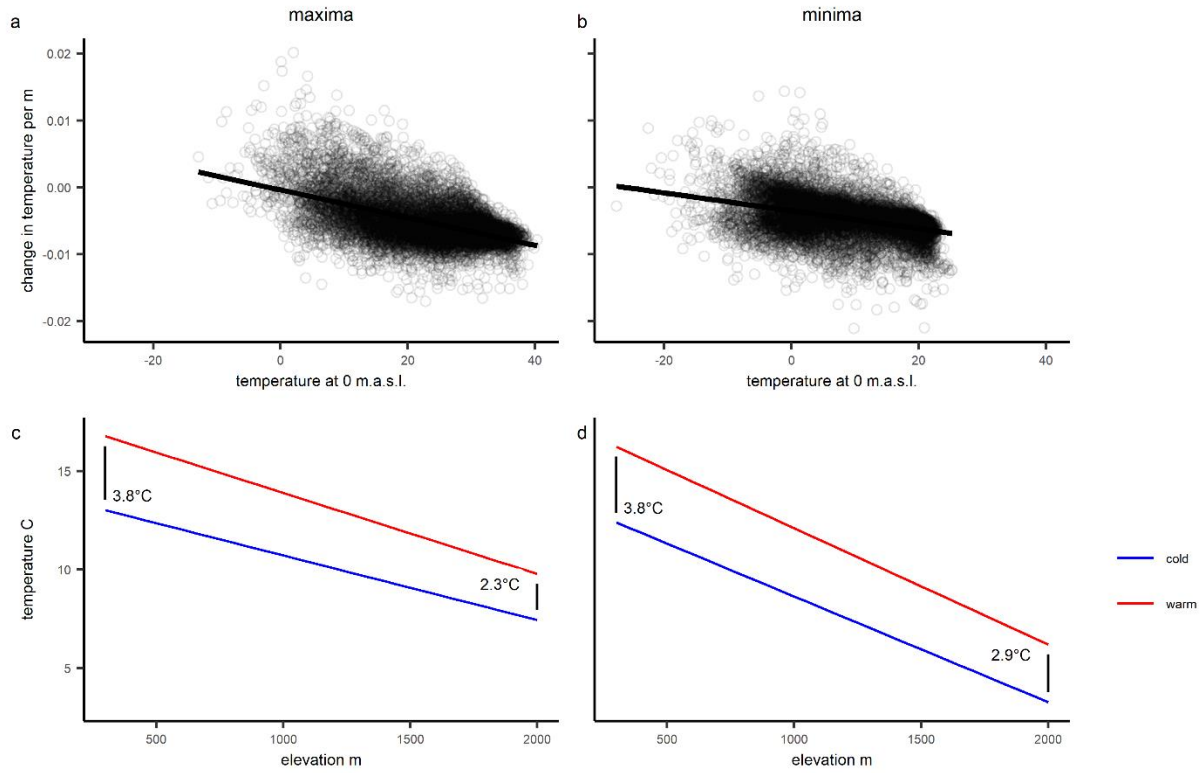

Figure S2. Relationship between regional temperature and thermal lapse rates. The first row shows the relationship between daily lapse rates and inferred temperatures at sea level (lapse rate model intercepts) for (a) thermal maxima and (b) thermal minima. Panel (c) shows the predicted above-canopy thermal maxima and panel (d) above-canopy thermal minima across elevation for a warm (18 °C at sea level) and cold (14 °C at sea level) day. Differences in temperature at low elevation (300 m) and high elevation (2000 m) are shown as black line segments. Since the slopes are less steep on cold days, increasing regional temperatures lead to larger predicted changes in temperature at lower elevations.

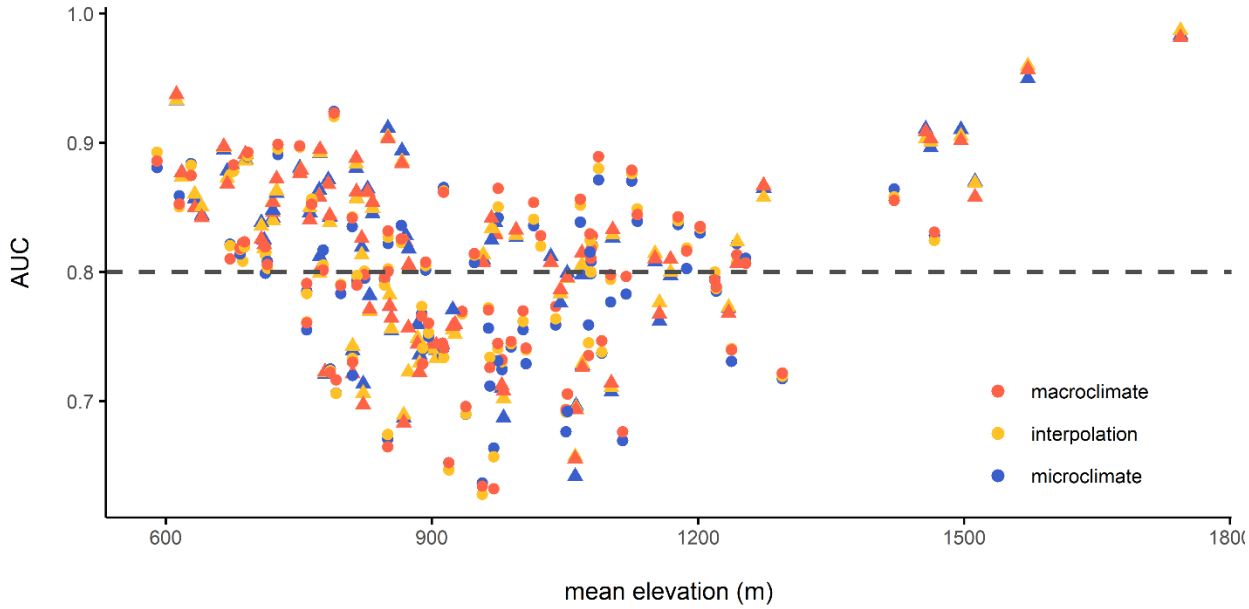

Figure S3. AUC scores for each model; species are arranged on the x-axis based on their mean elevation in sampled plots. Red points are macroclimate models, yellow points interpolation models, and blue points microclimate models. Triangles represent trees and shrubs; circles represent herbaceous species. The grey line at AUC=0.8 was the threshold used for including species in predictions. Species were only included in main paper predictions if all three models had AUC > 0.8.

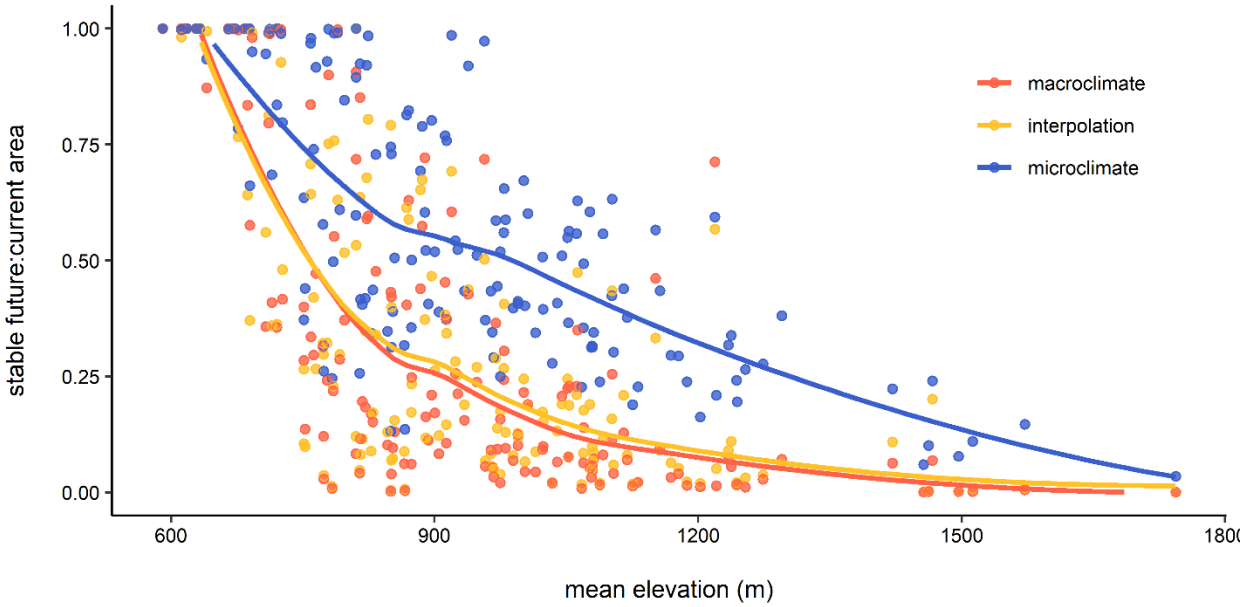

Figure S4. Proportion of current suitable habitat area that will remain suitable with 4 °C of macroclimate warming; without regard to model goodness-of-fit (this is equivalent to Fig. 3 in the main text but with more species) Points are arranged on the x axis according to species current mean elevation; lines are loess smoothing across the points for each climate model.

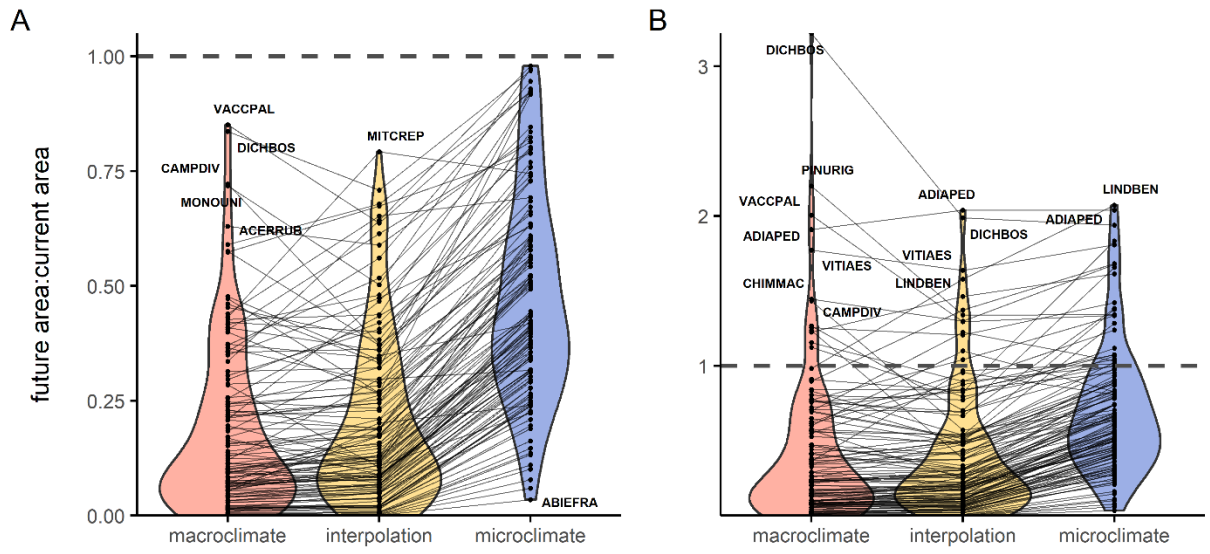

Figure S5. Responses of plant species to 4 °C of macroclimate warming; without regard to model goodness-of-fit (this is equivalent to Fig. 4 in the main text but with more species). Panel A shows the ratio for a no-dispersal scenario; points represent the fraction of current area that will still be suitable. Panel B shows the ratio for an unlimited dispersal scenario; points represent the change in suitable habitat area with climate change. The grey line in both panels indicates an equal area of future and current habitat; lower values represent a reduction in habitat area (note different scales of Y-axes). Species which had >98% stable habitat in any SDM were removed for visualization.

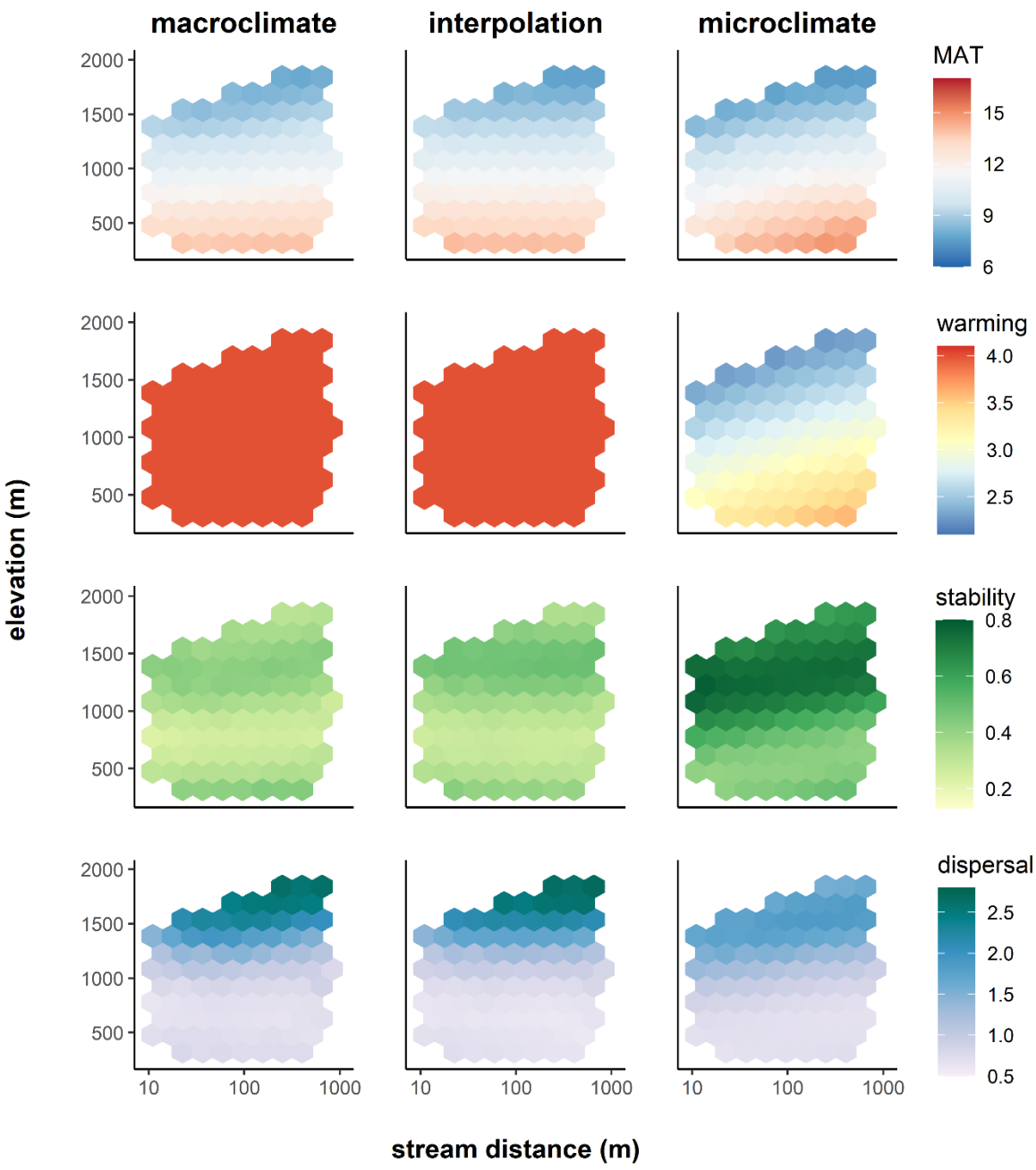

Figure S6. Effect of climate model and topographic position on warming and species response to warming; without regard to model goodness-of-fit (this is equivalent to Fig. 6 in the main text but with more species). Colors show binned mean values of MAT (row 1), change in MAT with warming scenario (row 2), fraction of current species that will still be within suitable habitat

(row 3), and number of future species/number of current species with unlimited dispersal (row 4). Values are based on 10,000 regularly sampled points within the Park; bins are shown only if they contain at least 10 values.

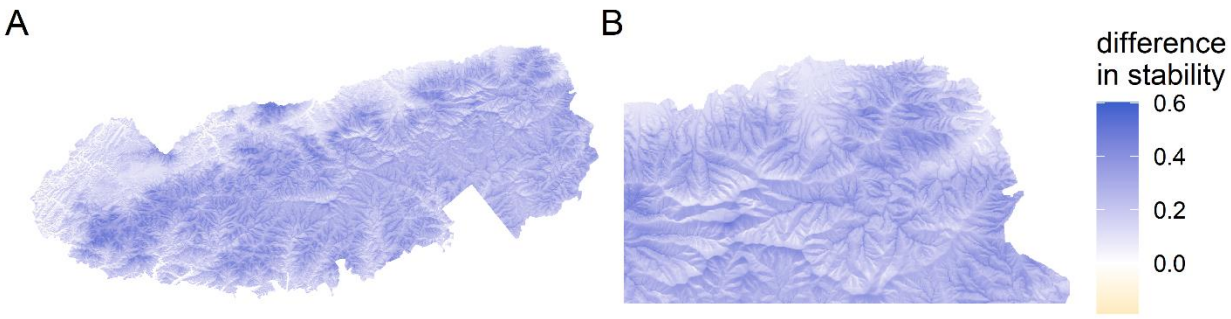

Figure S7. Potential cryptic refugia in GSMNP; without regard to model goodness-of-fit (this is equivalent to Fig. 7 in the main text but with more species). Geographic differences in the effect of below-canopy microclimate on stable habitat (additional proportion of species that are still within stable habitat) in each 30 m pixel. Blue indicates areas where the microclimate model predicts greater stability; red indicates areas where the interpolation model predicts greater stability. Panel (A) shows all of GSMNP, panel (B) shows the northeast corner. See Fig. 1 for exact spatial location of panel B.

Fig S8. Probability of ABIEFRA occurrence

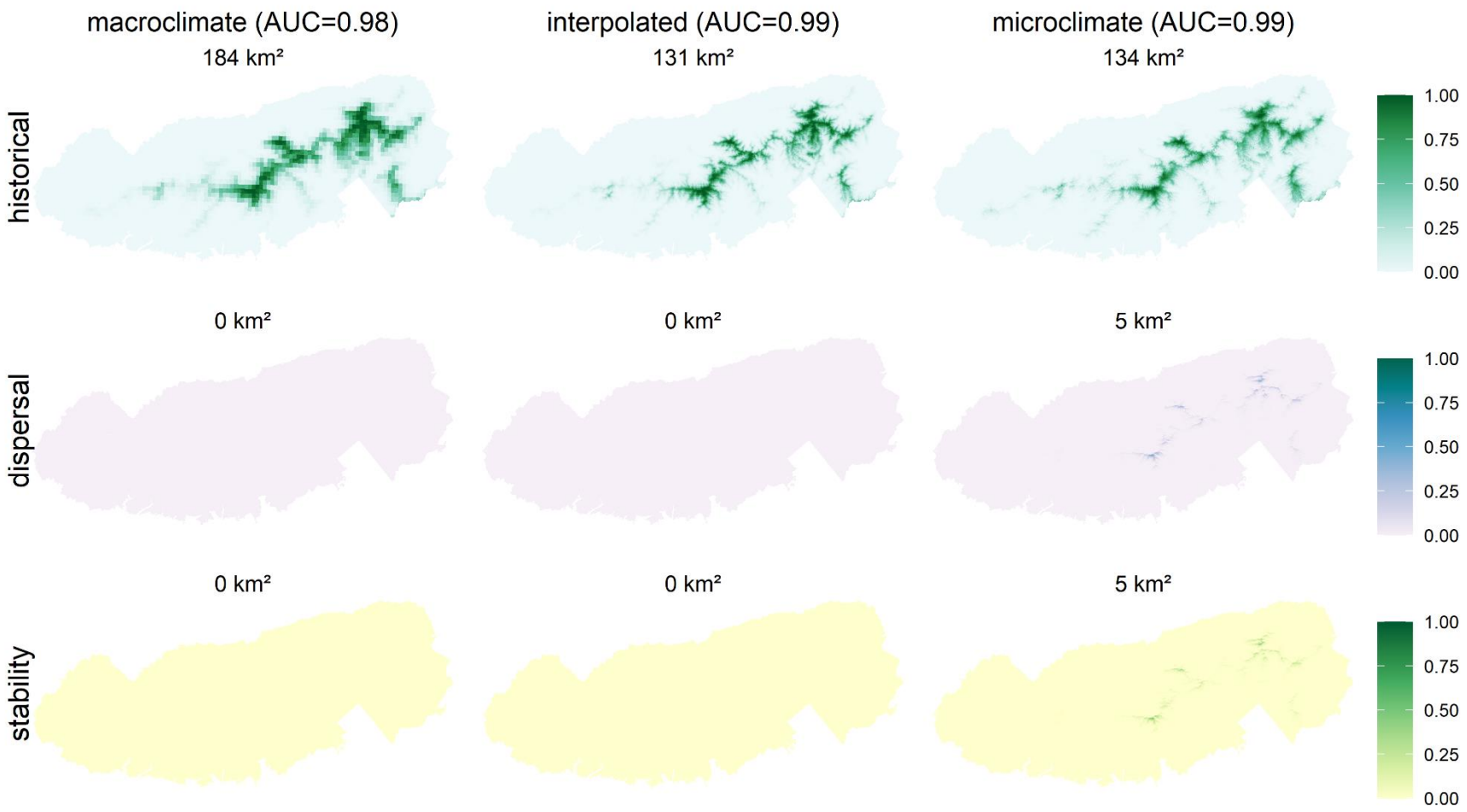

Fig S9. Probability of ACERRUB occurrence

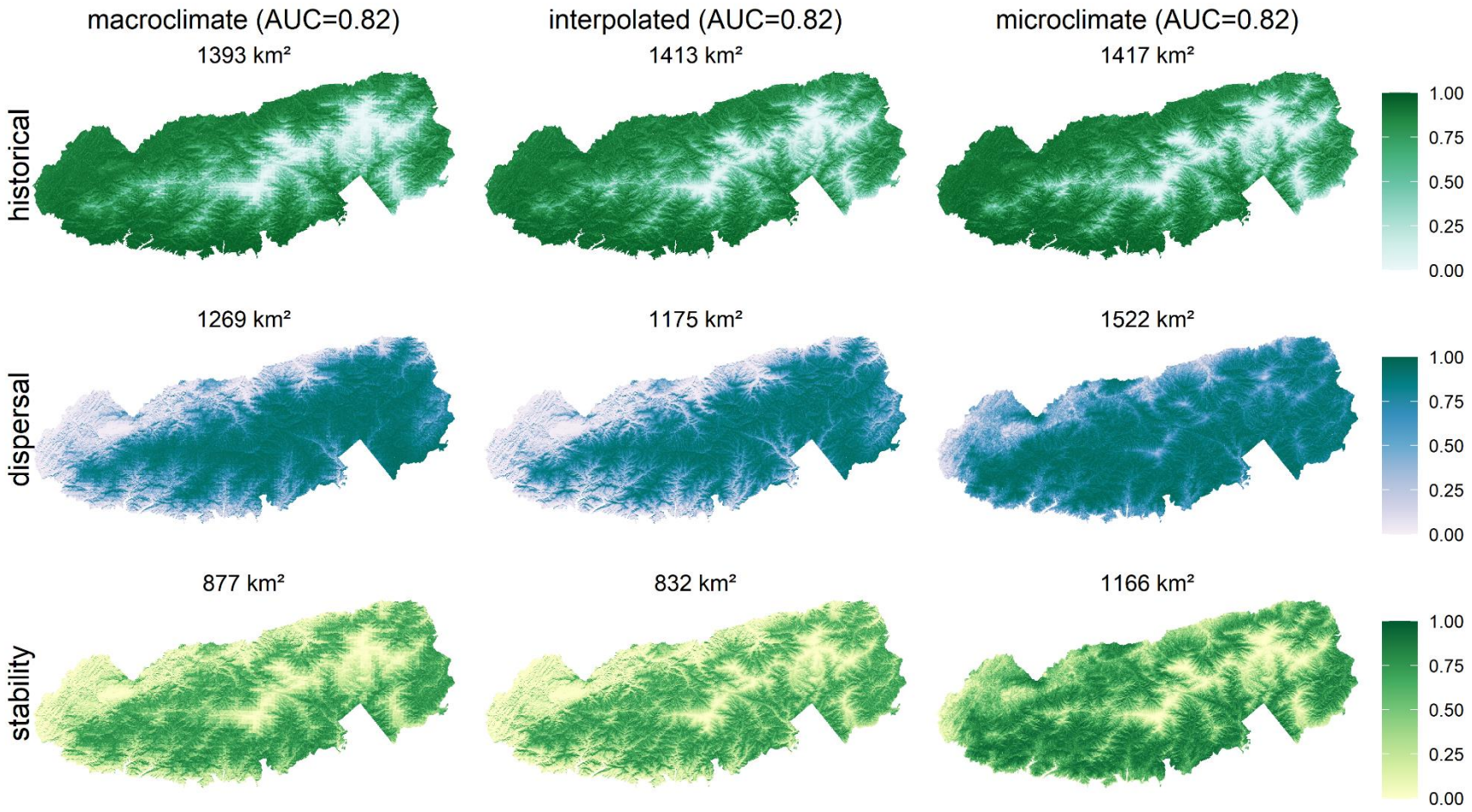

Fig S10. Probability of ACERSPI occurrence

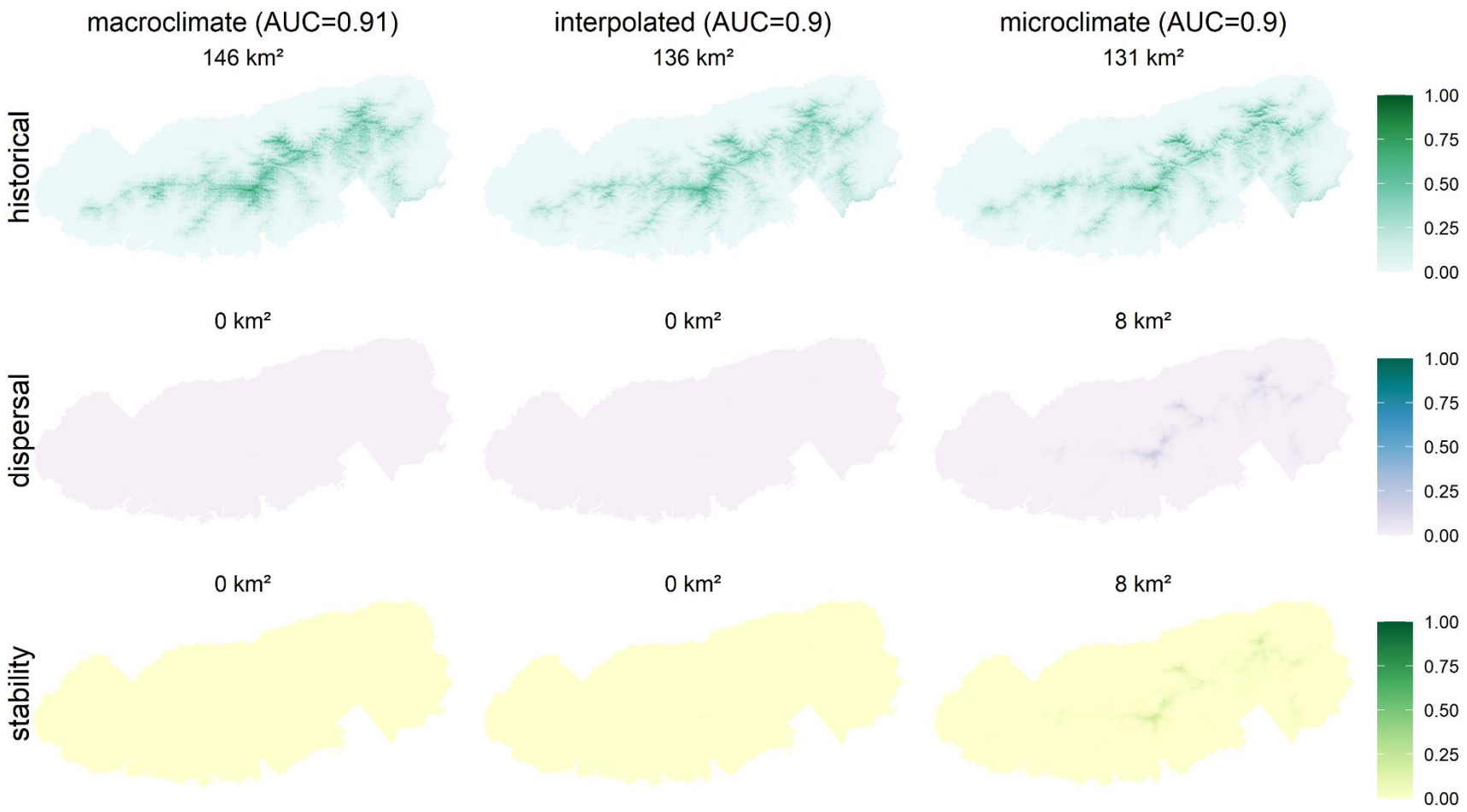

Fig S11. Probability of ACTARACR occurrence

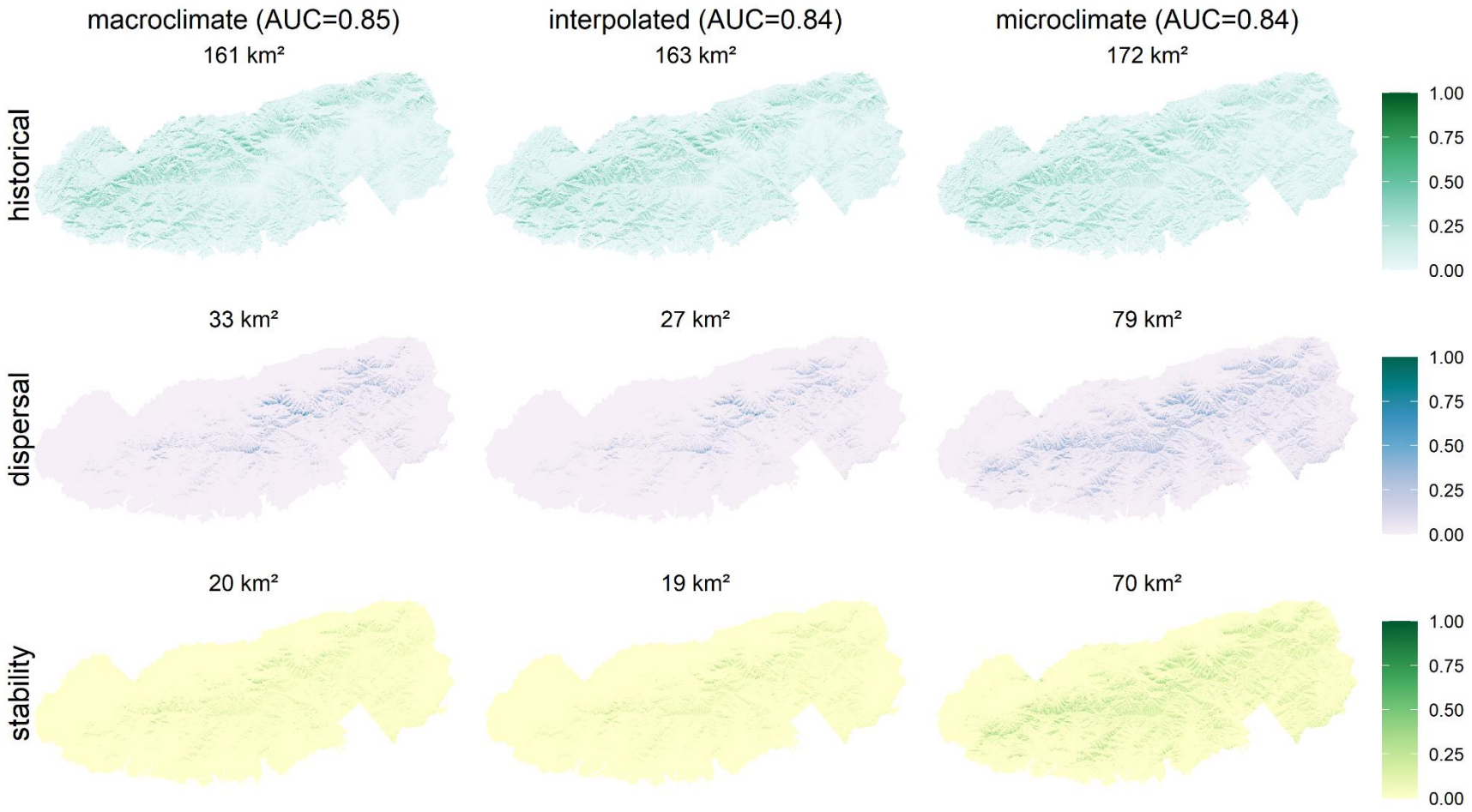

Fig S12. Probability of ADIAPED occurrence

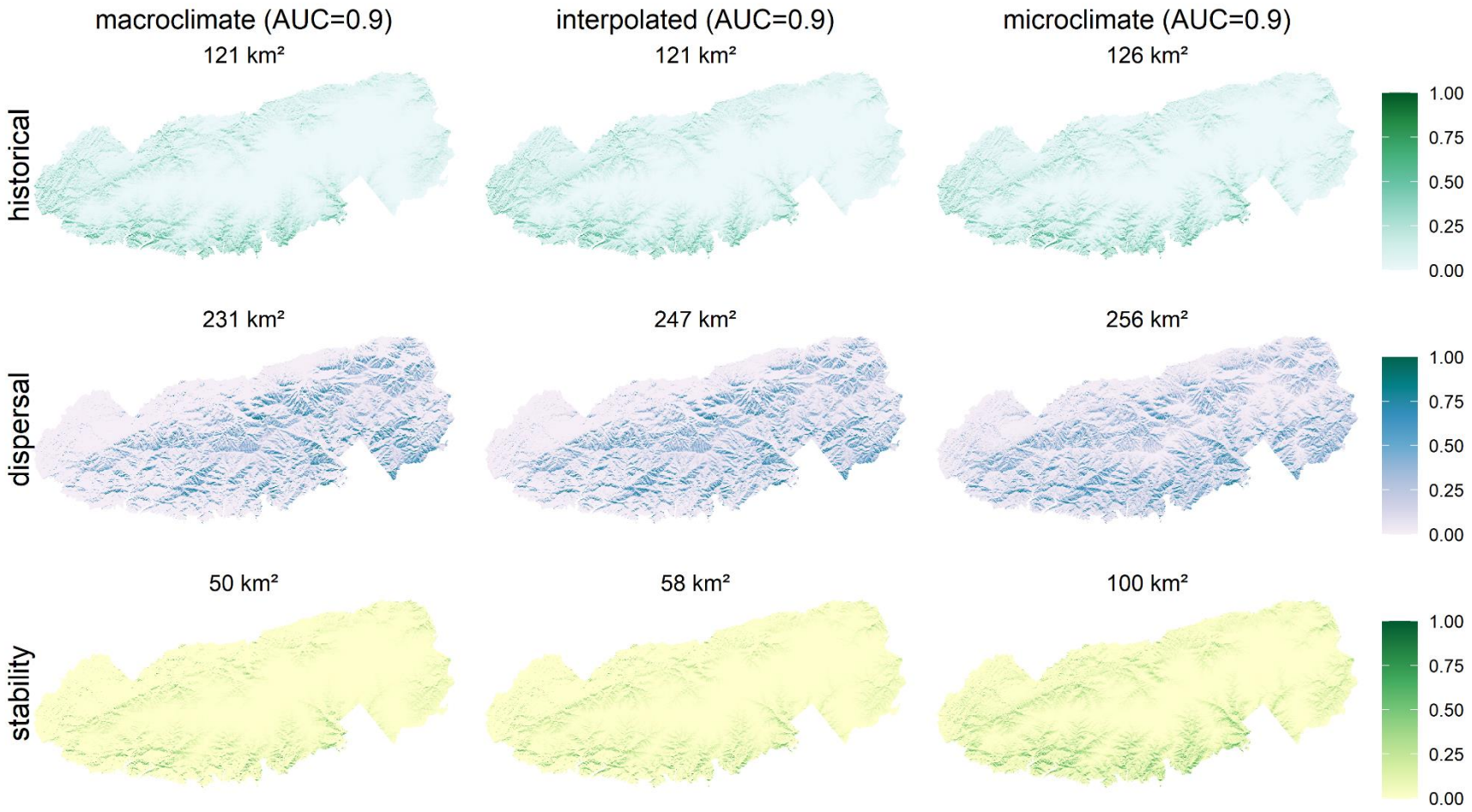

Fig S13. Probability of AESCFLA occurrence

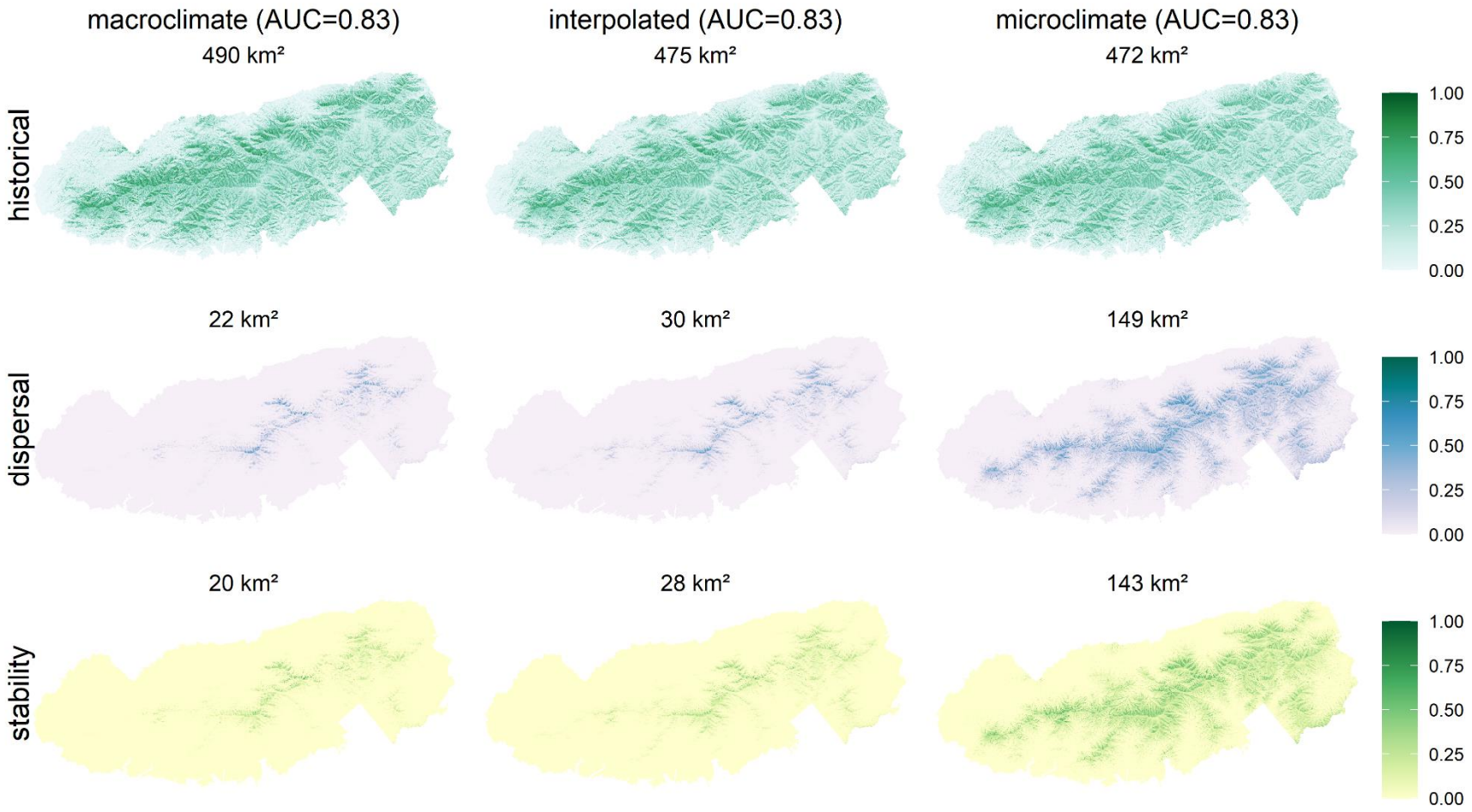

Fig S14. Probability of AGERALS occurrence

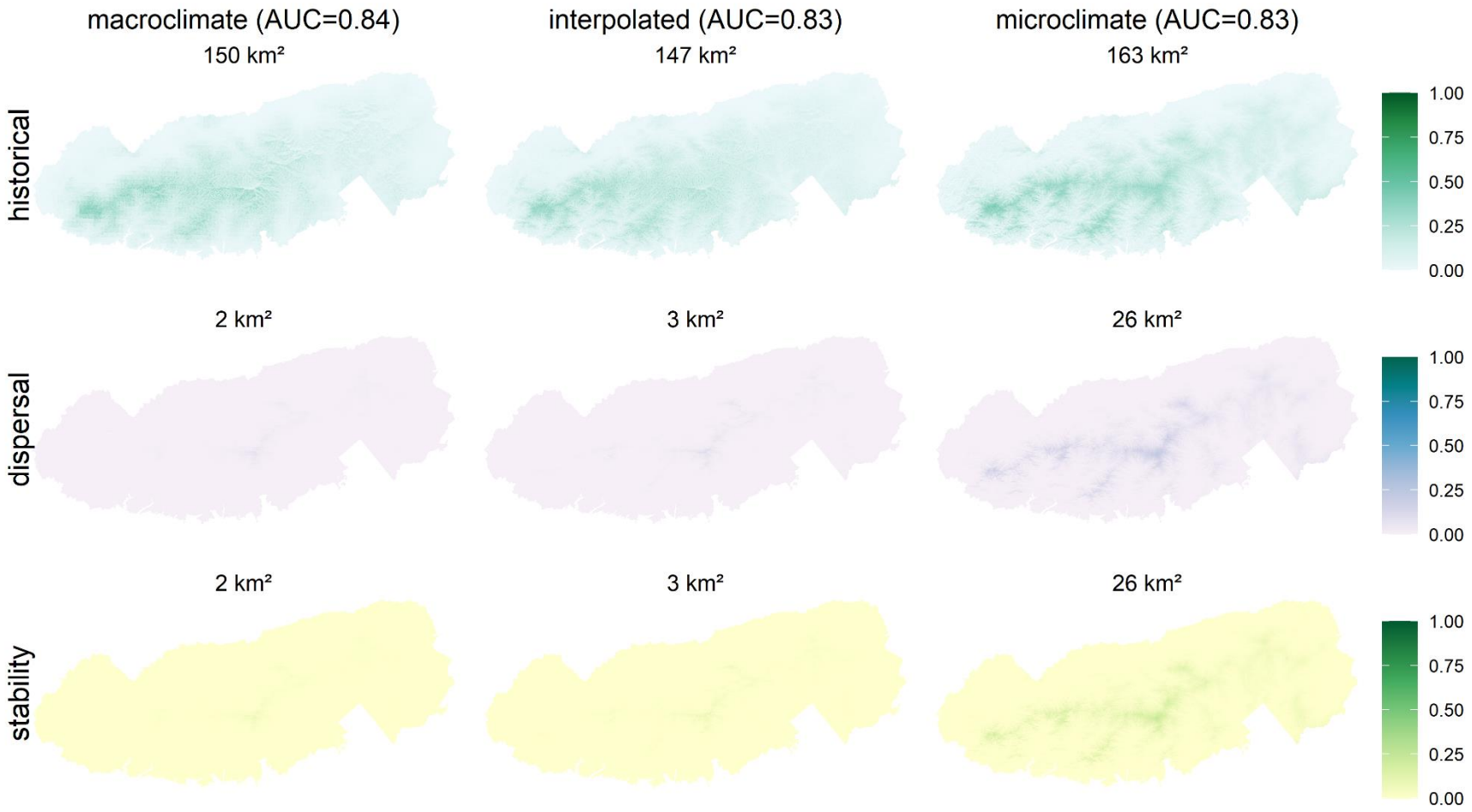

Fig S15. Probability of ARISMAC occurrence

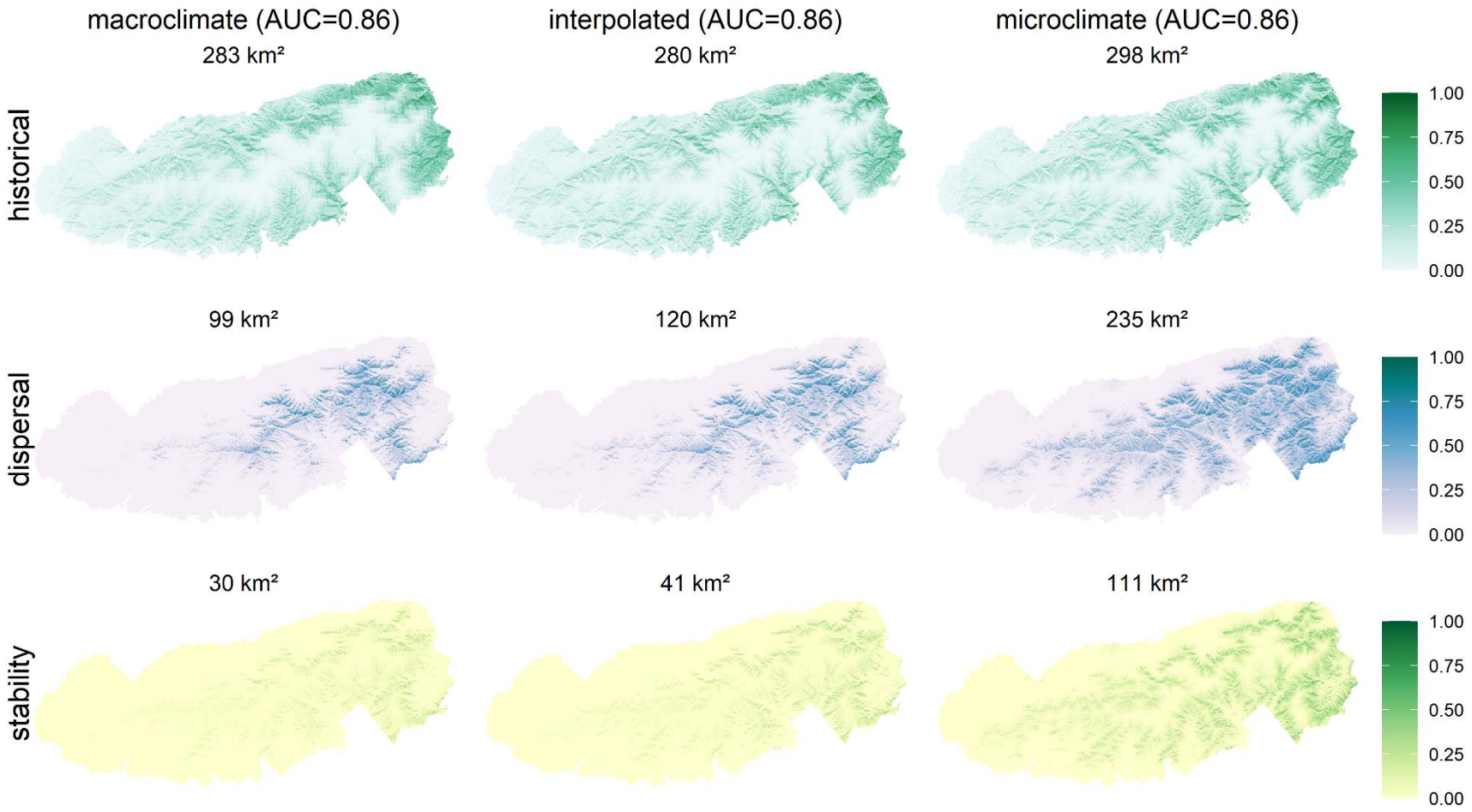

Fig S16. Probability of BETUALL occurrence

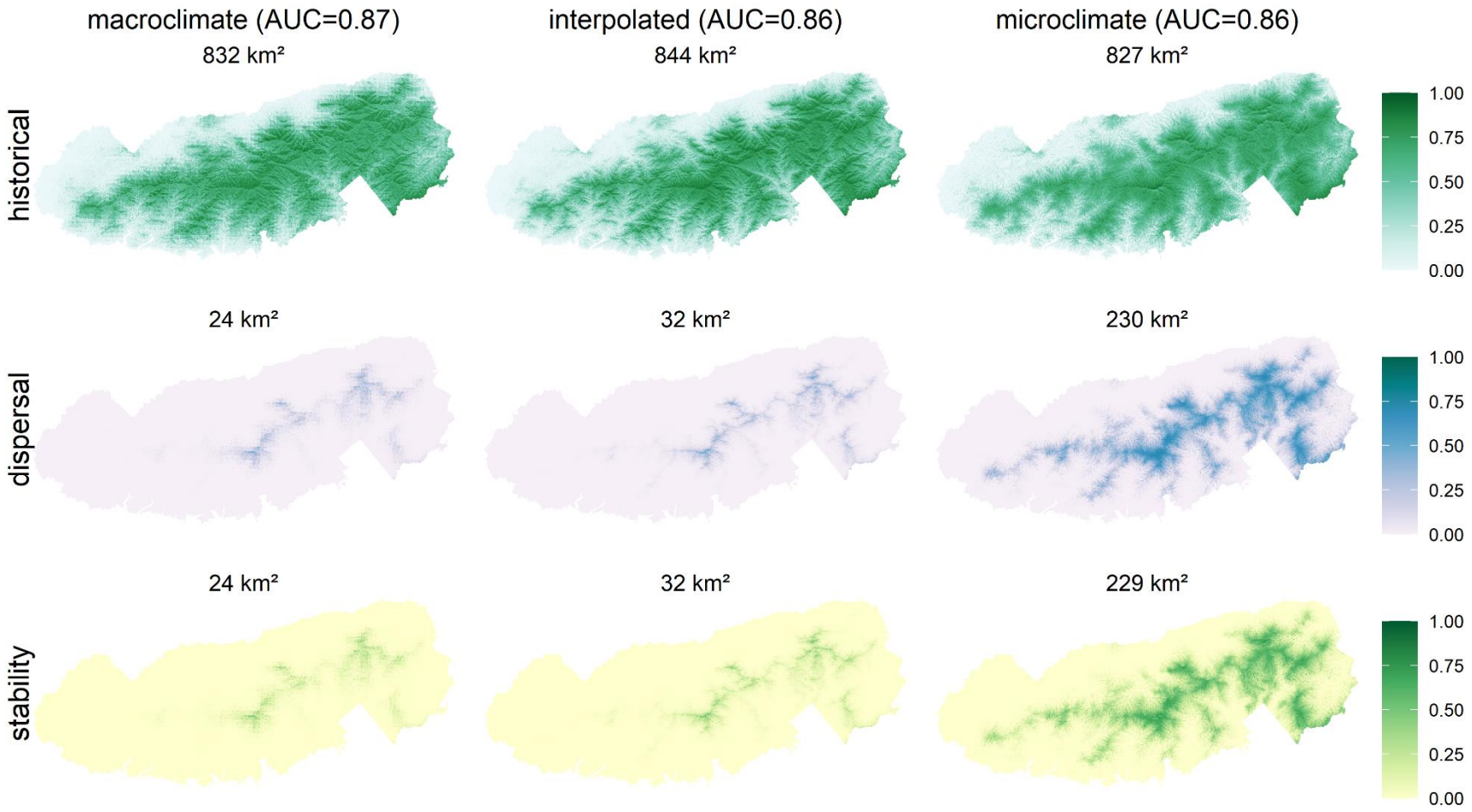

Fig S17. Probability of CALYFLOG occurrence

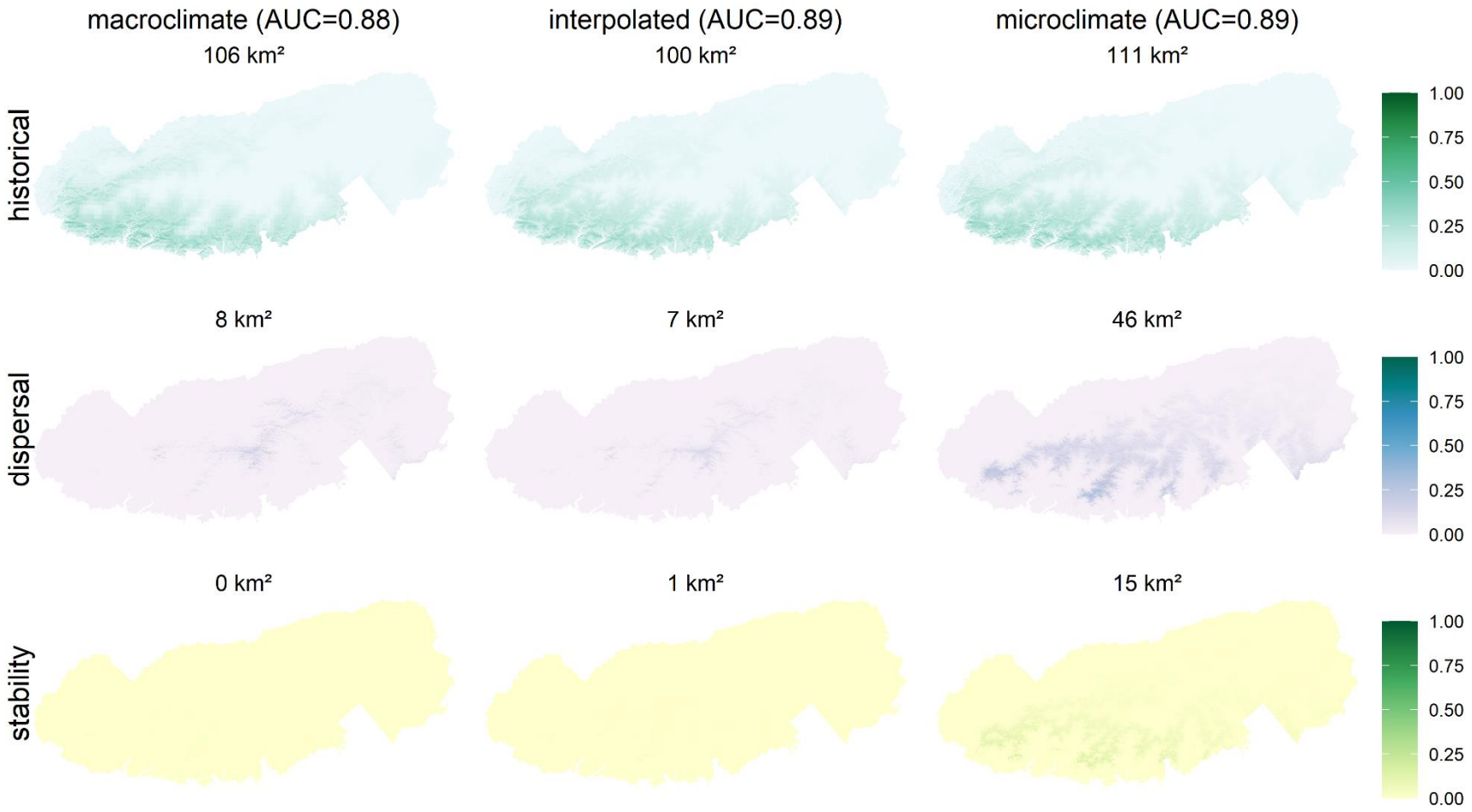

Fig S18. Probability of CARDDIP occurrence

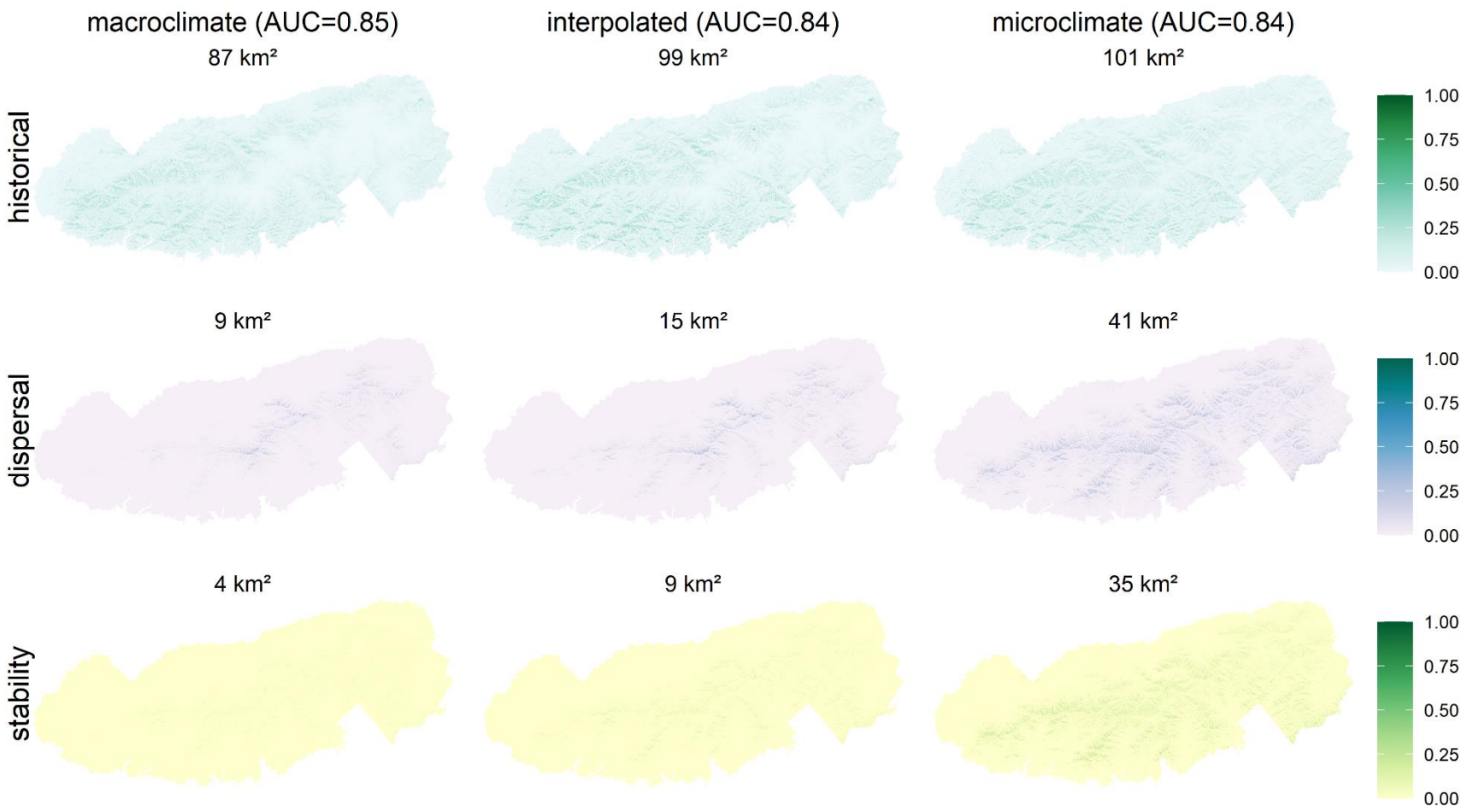

Fig S19. Probability of CAREDEB occurrence

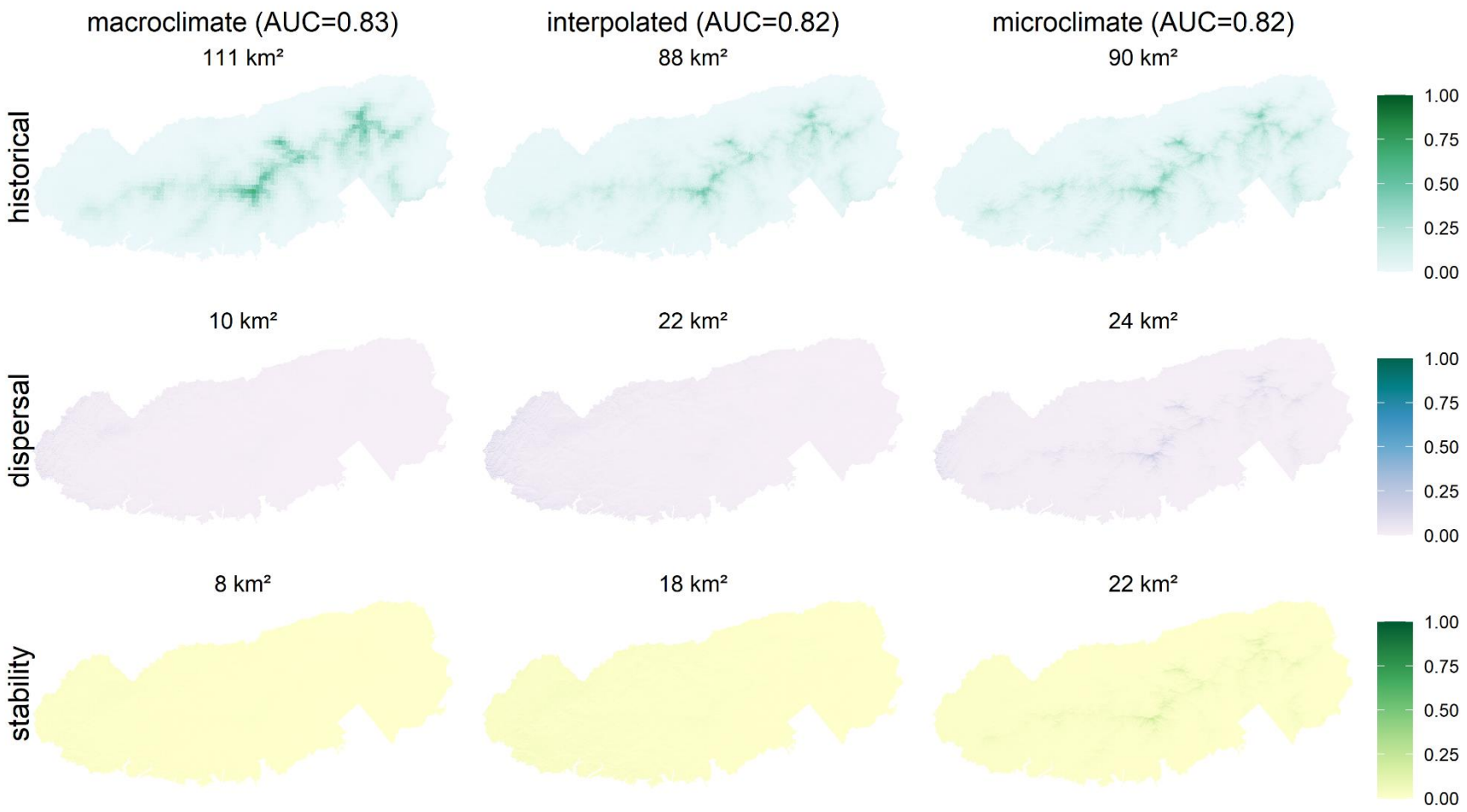

Fig S20. Probability of CARYALB occurrence

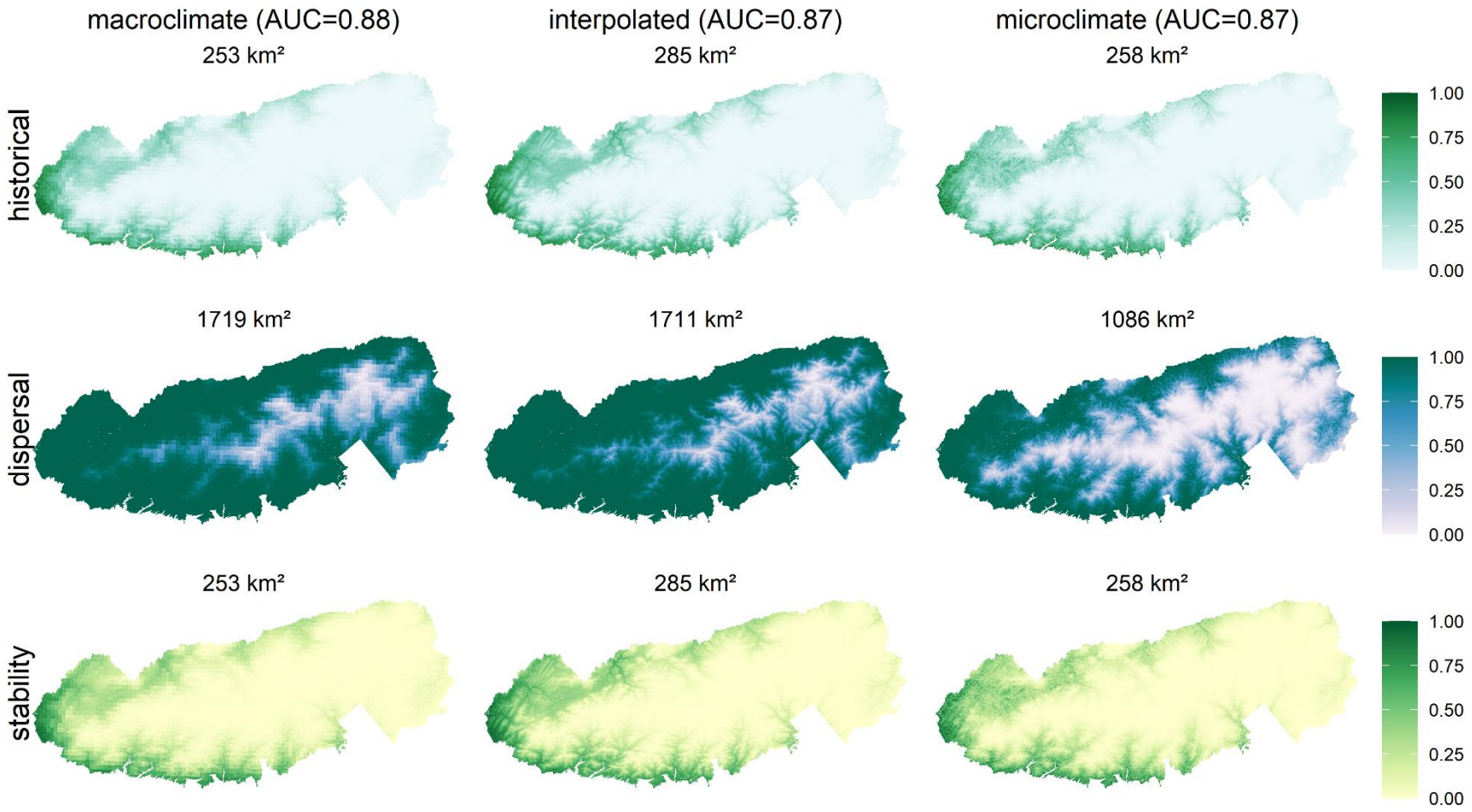

Fig S21. Probability of CARYGLA occurrence

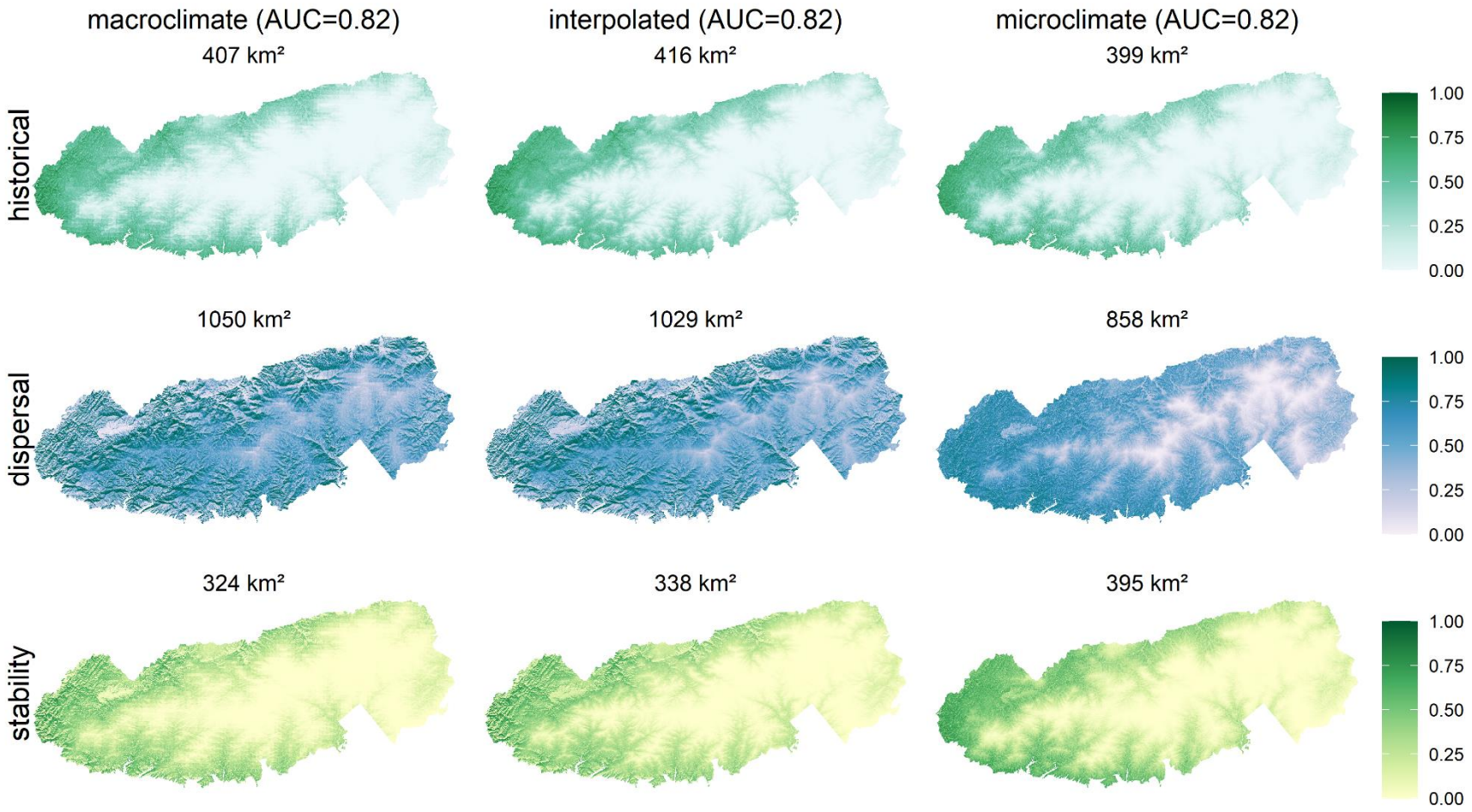

Fig S22. Probability of CASTDNT occurrence

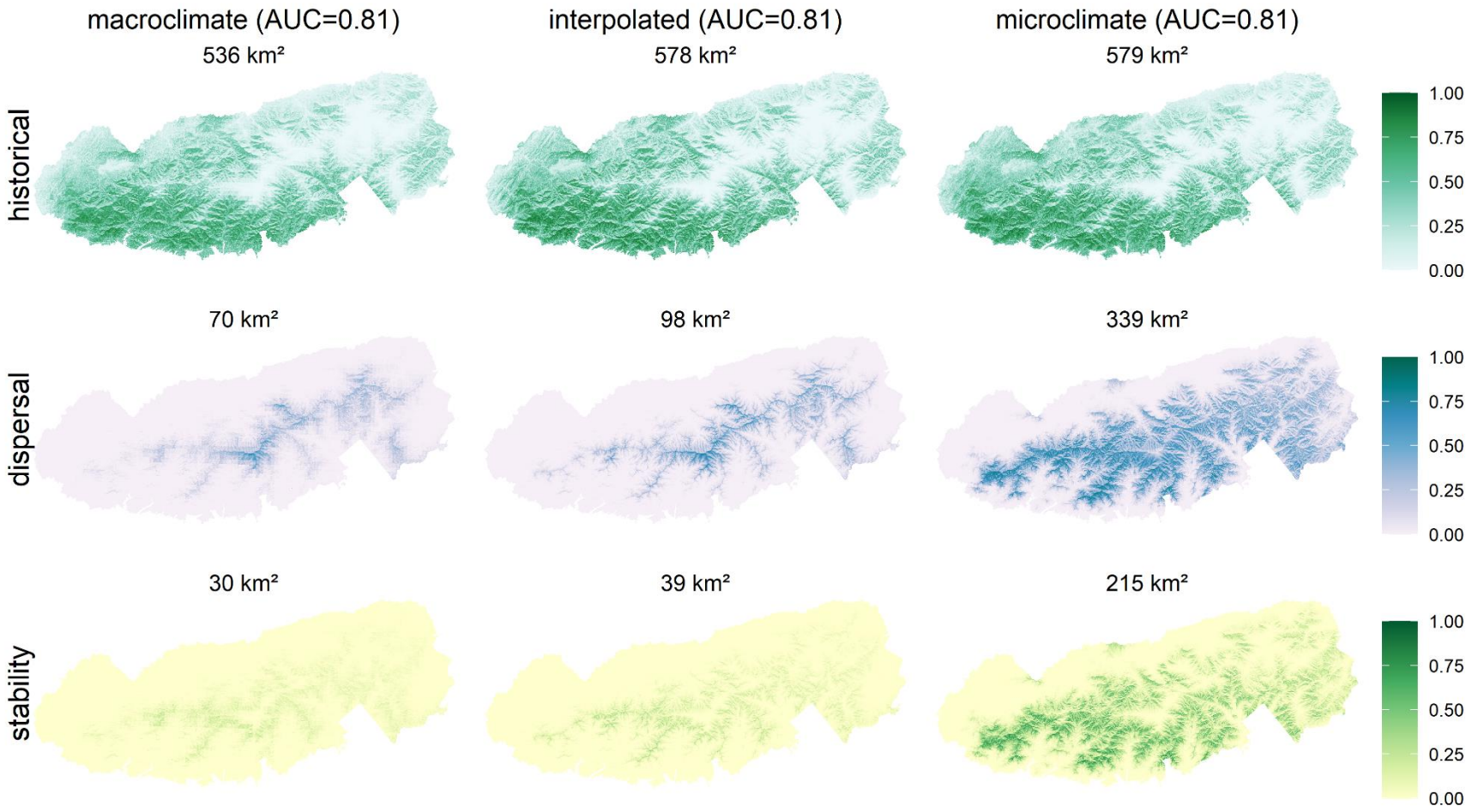

Fig S23. Probability of CAULTHA occurrence

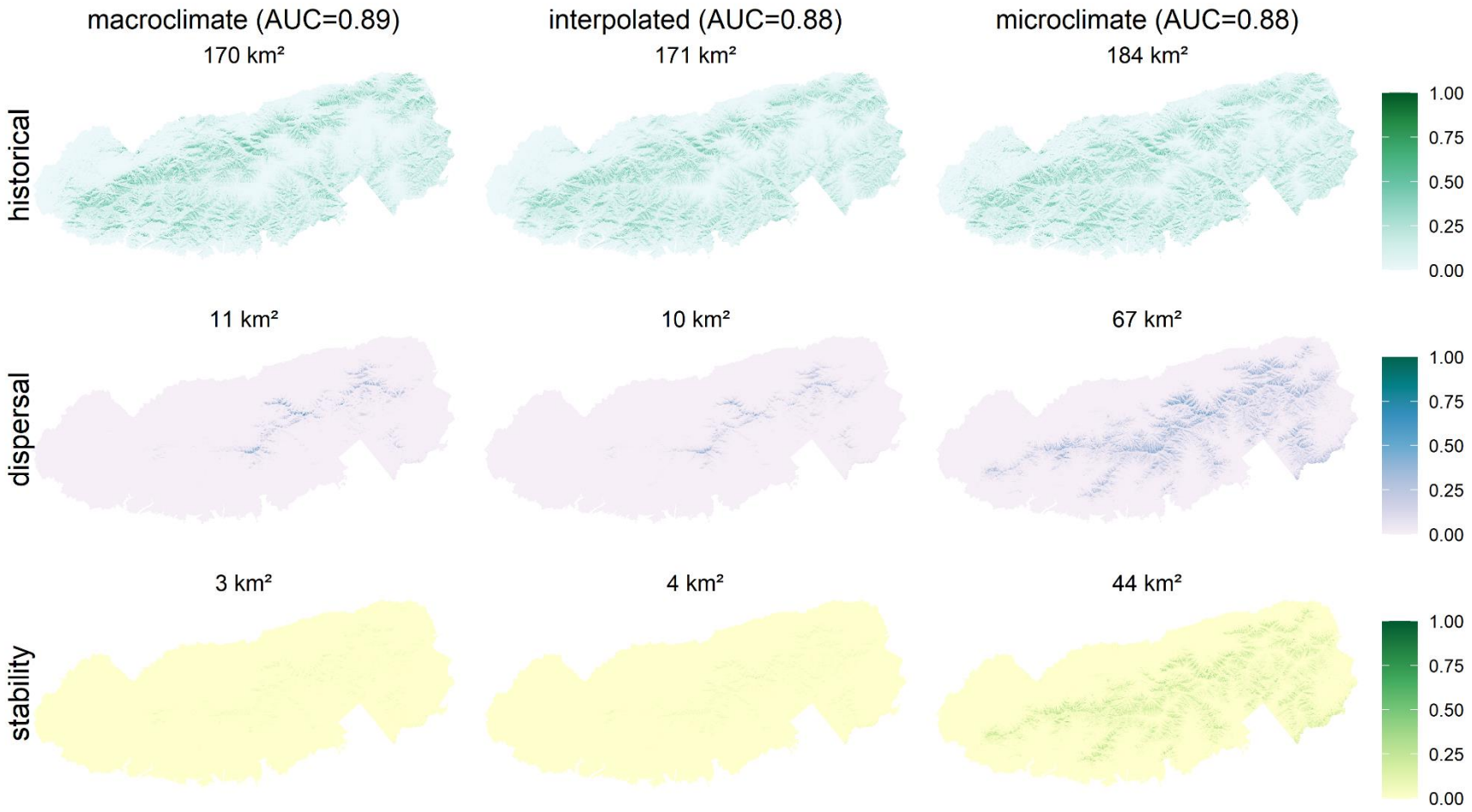

Fig S24. Probability of CHIMMAC occurrence

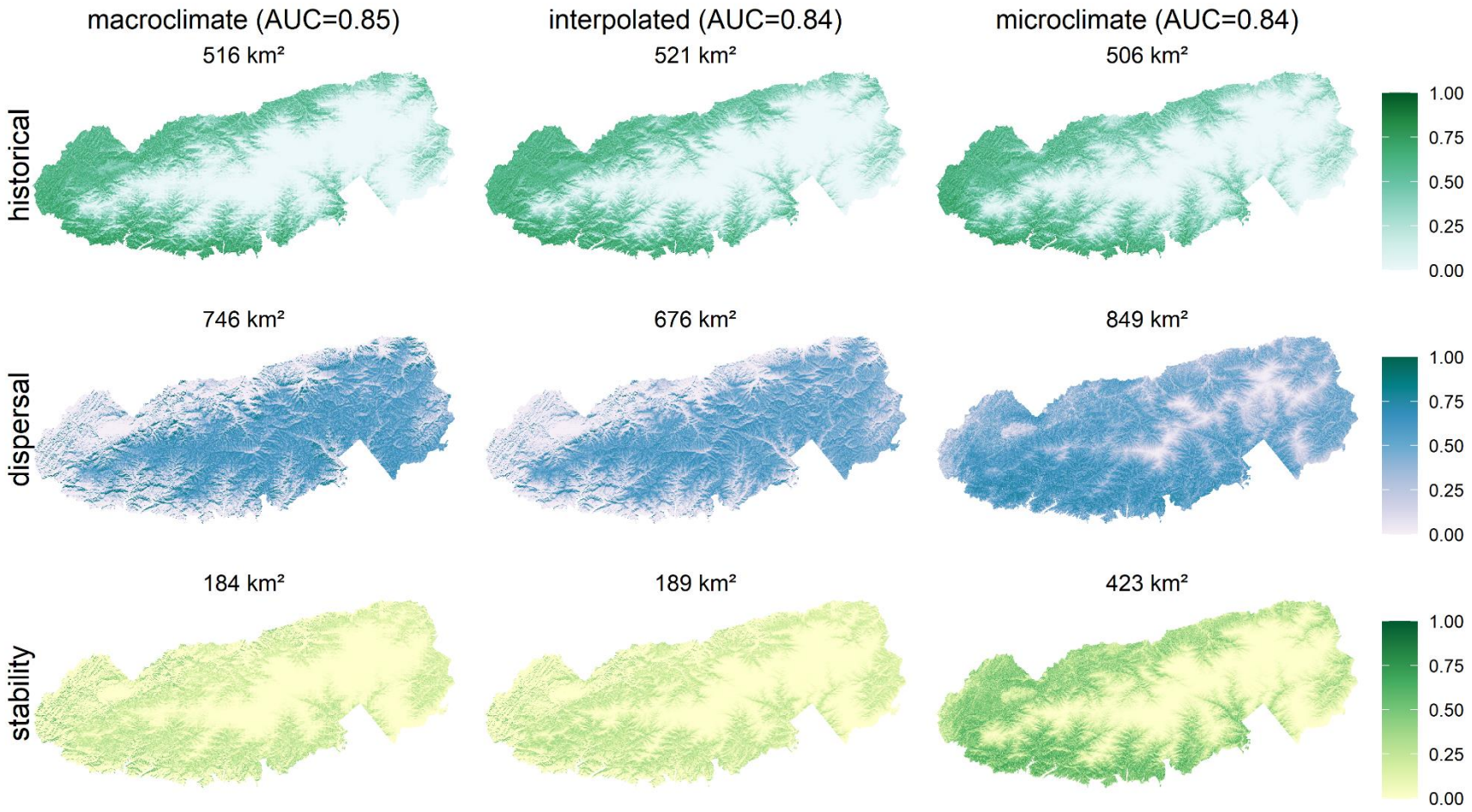

Fig S25. Probability of CLINUMB occurrence

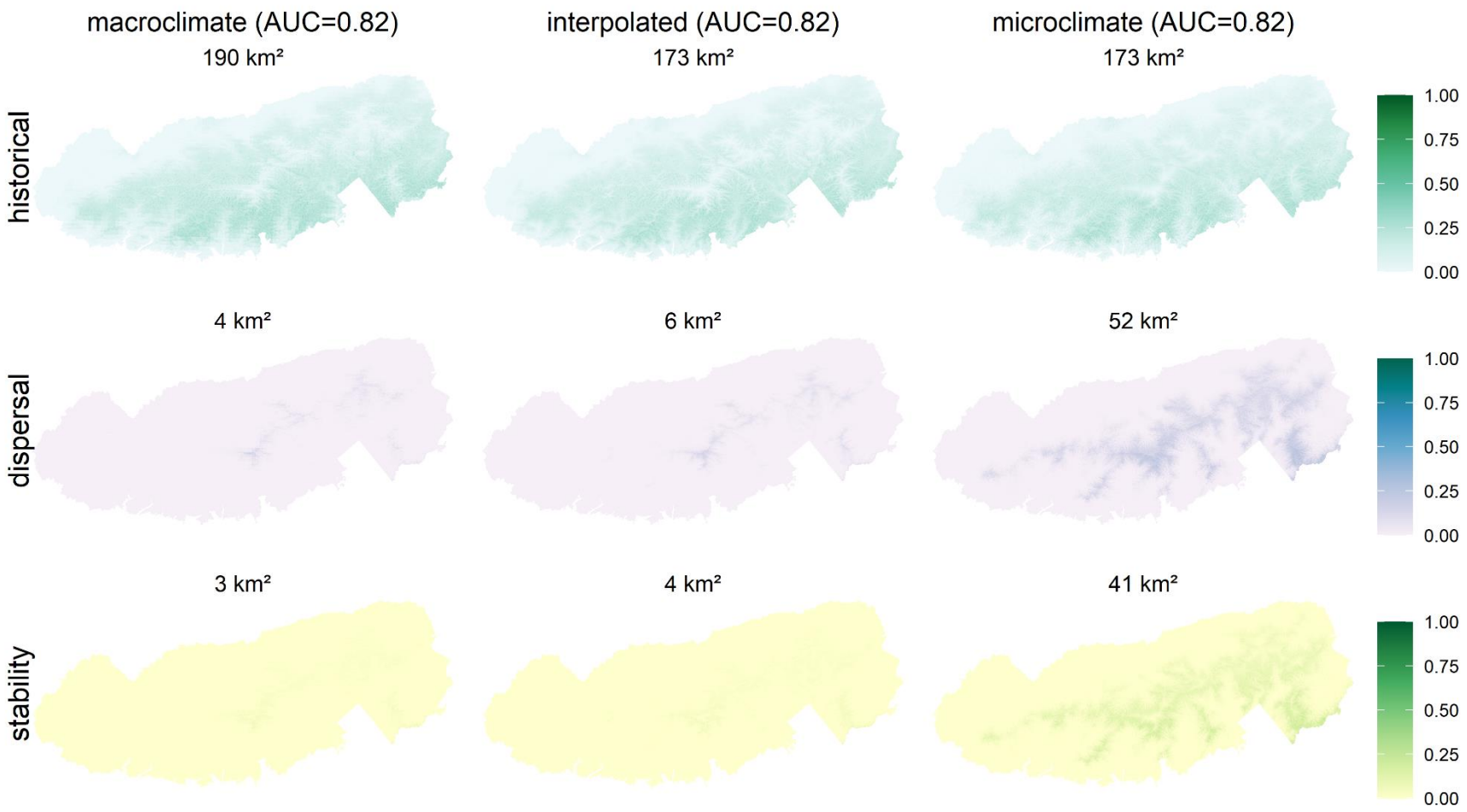

Fig S26. Probability of COLLCAN occurrence

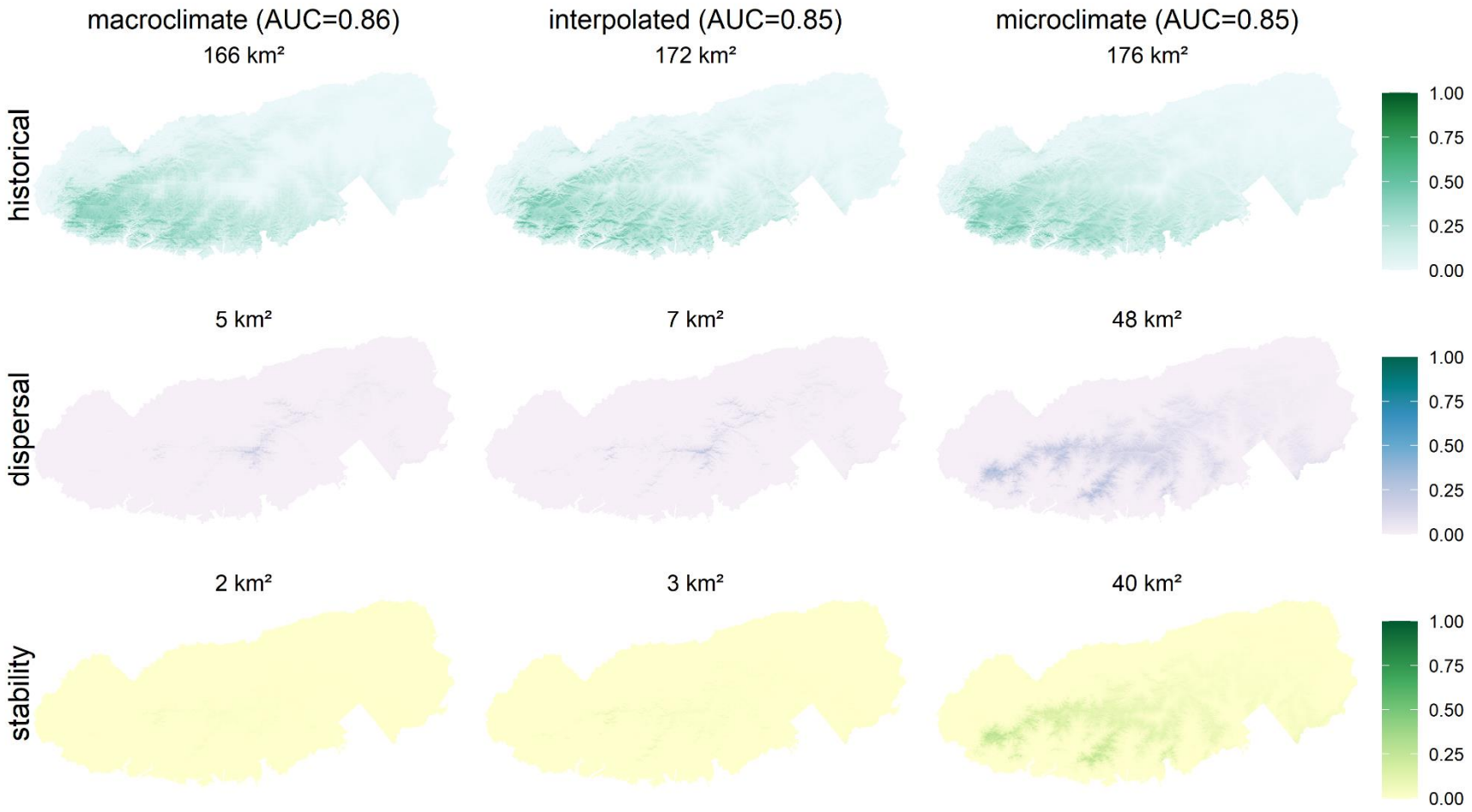

Fig S27. Probability of COREMAJ occurrence

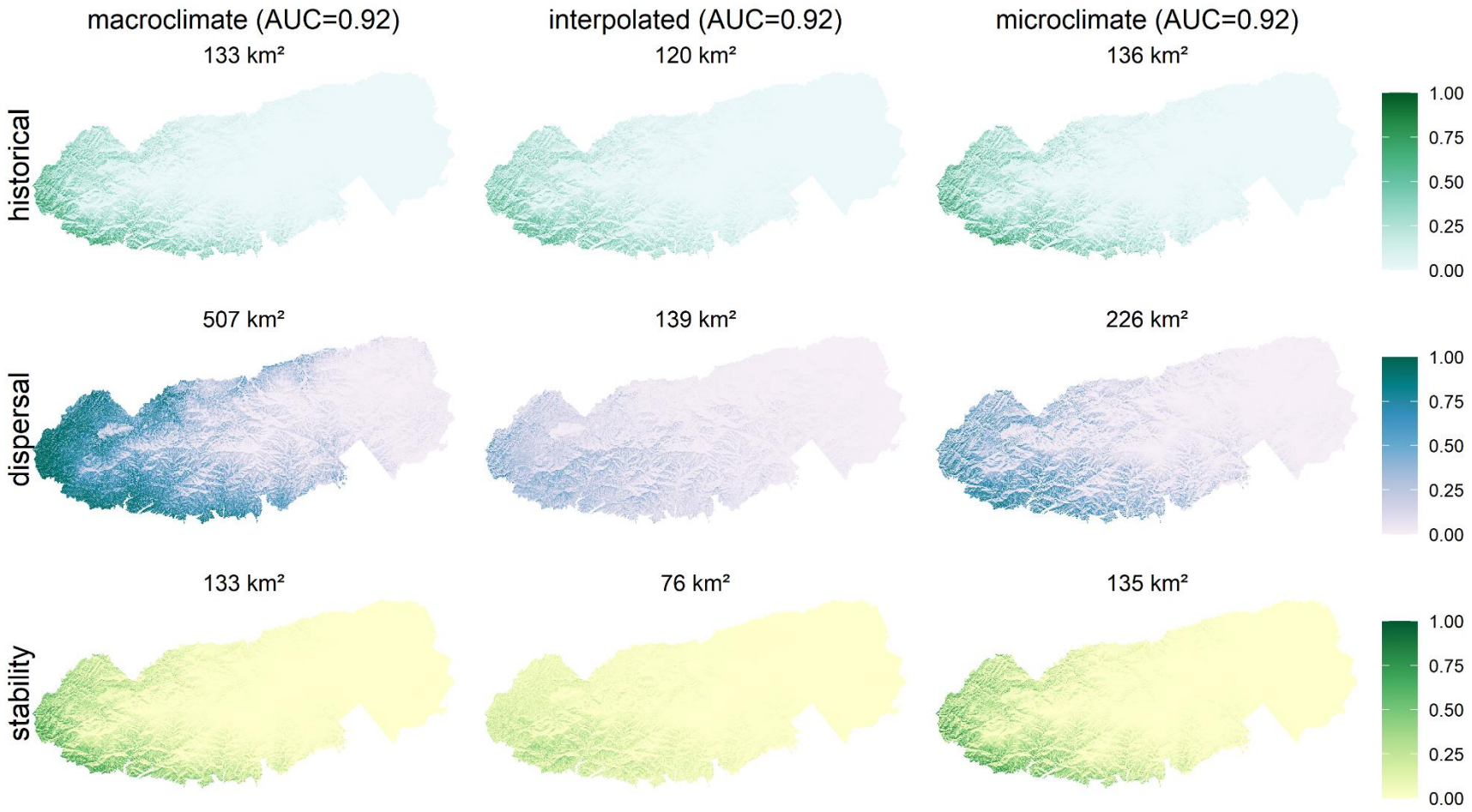

Fig S28. Probability of CORNFLO occurrence

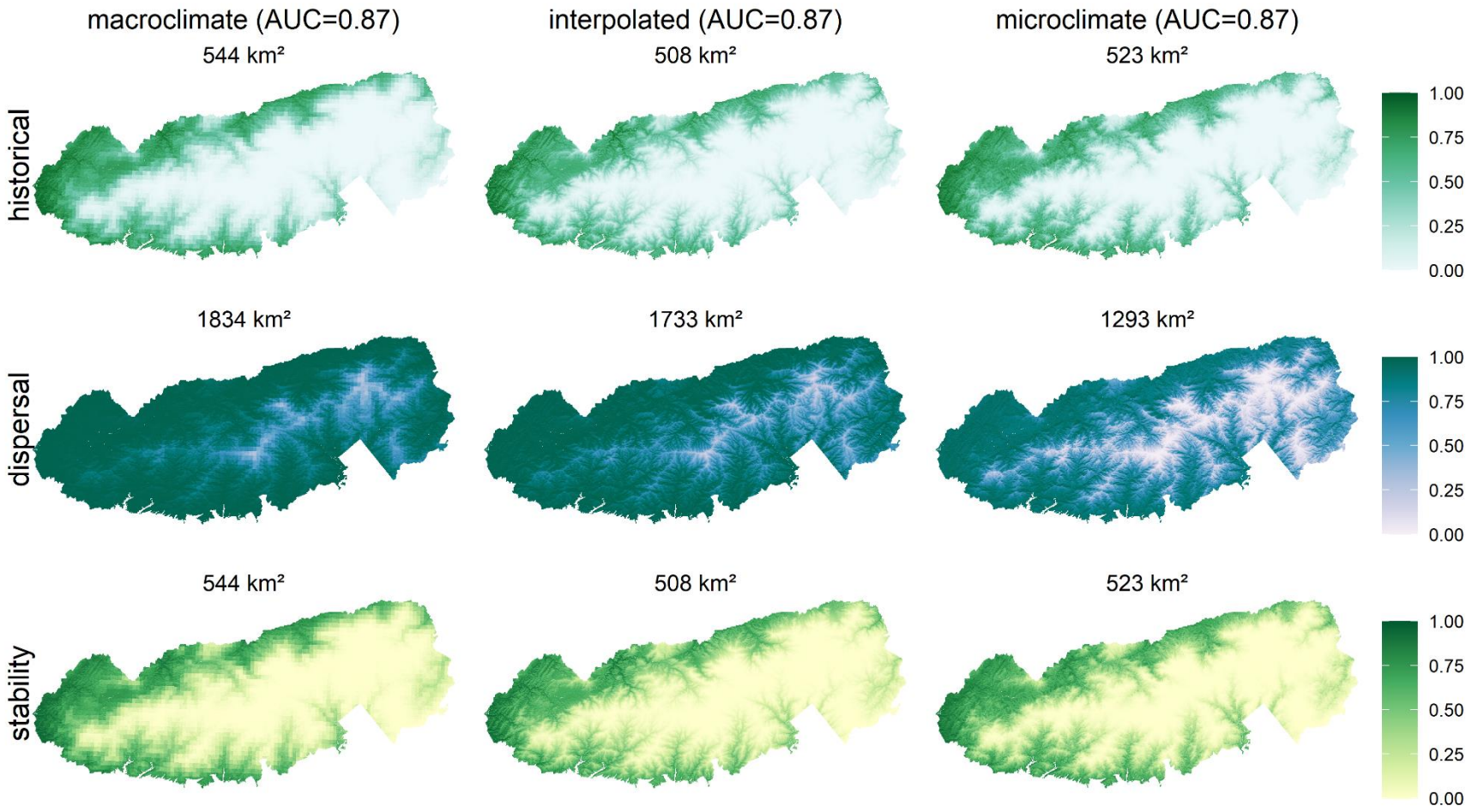

Fig S29. Probability of CYSTPRO occurrence

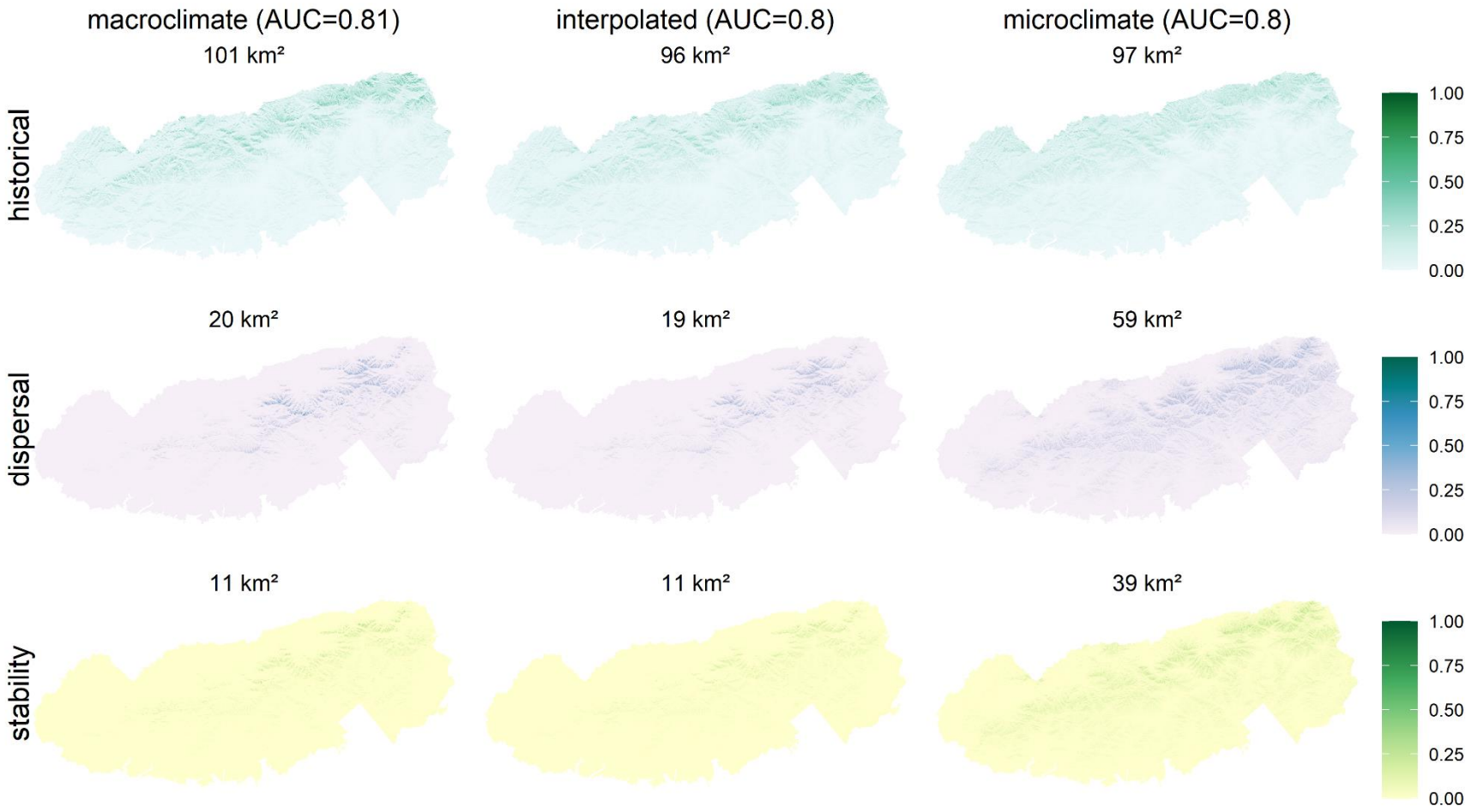

Fig S30. Probability of DEPAACR occurrence

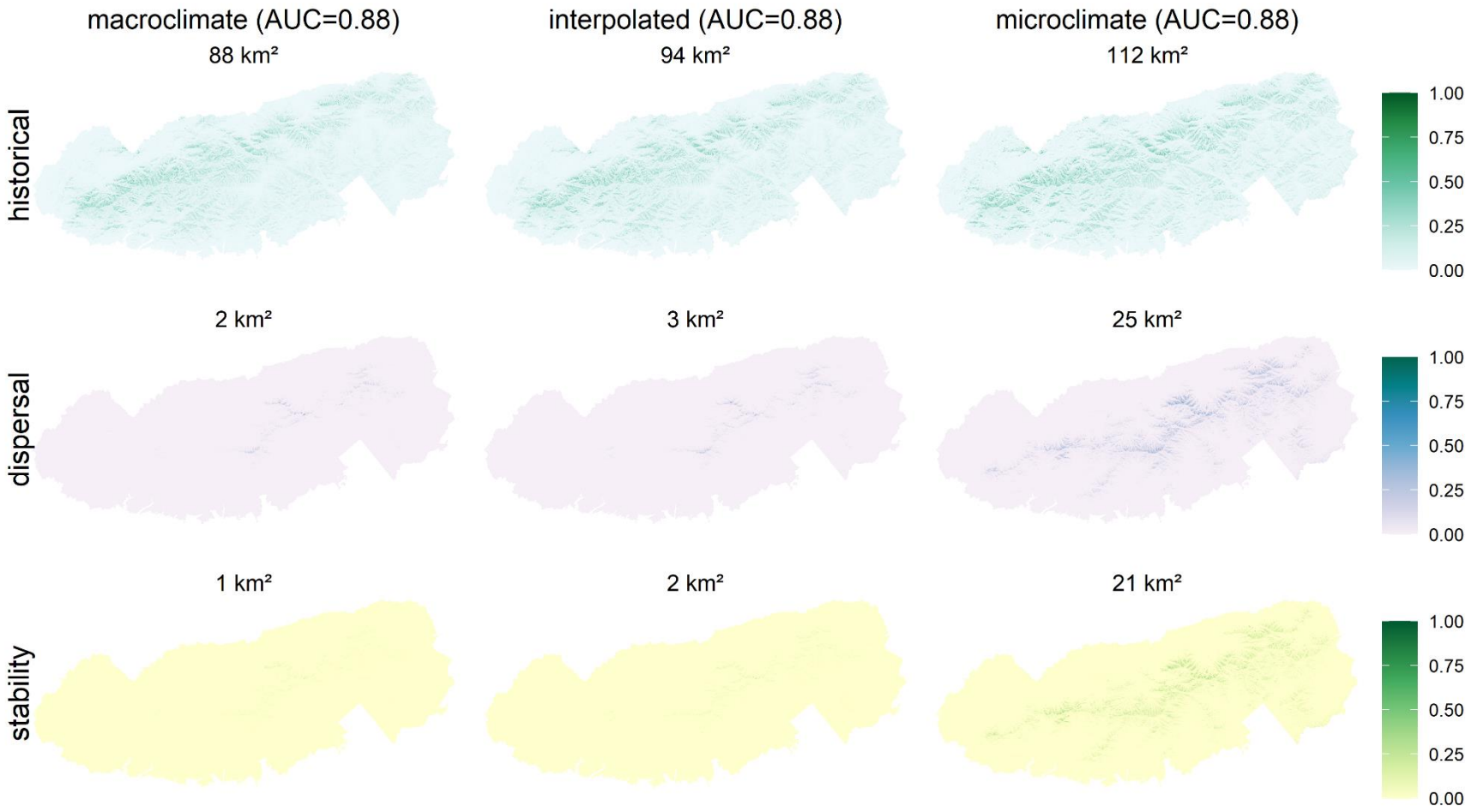

Fig S31. Probability of DESMNUD occurrence

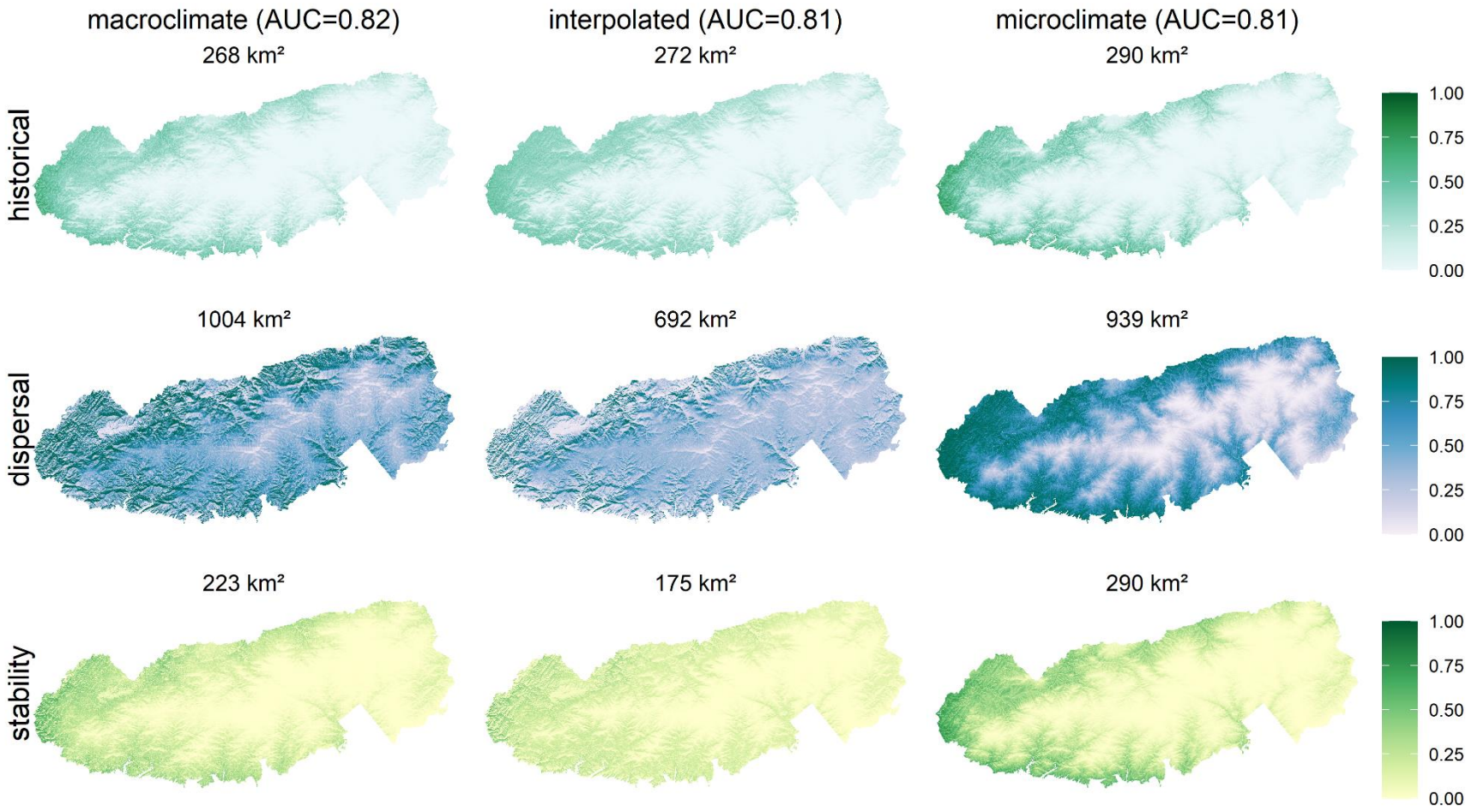

Fig S32. Probability of DICHCMM occurrence

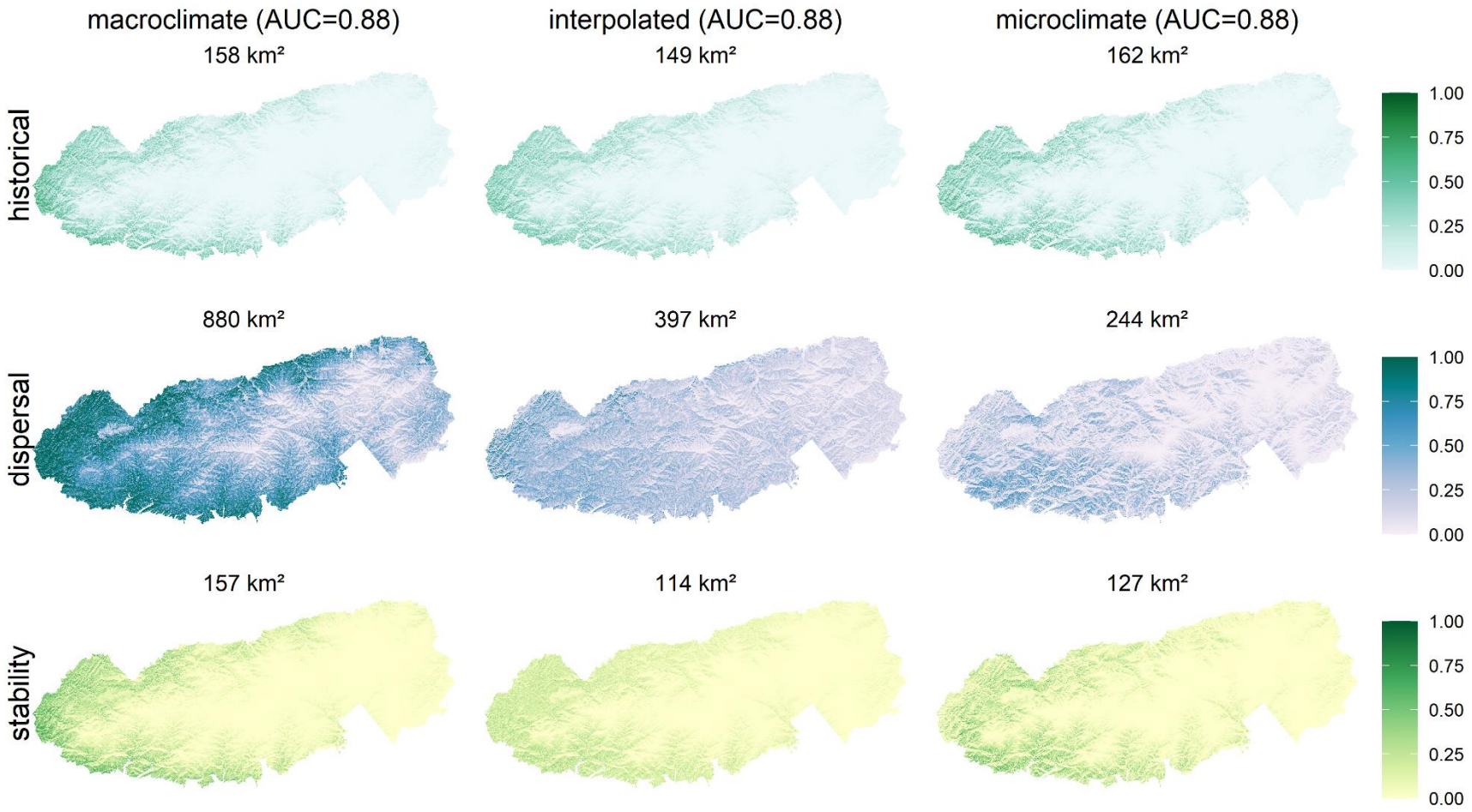

Fig S33. Probability of DRYOINT occurrence

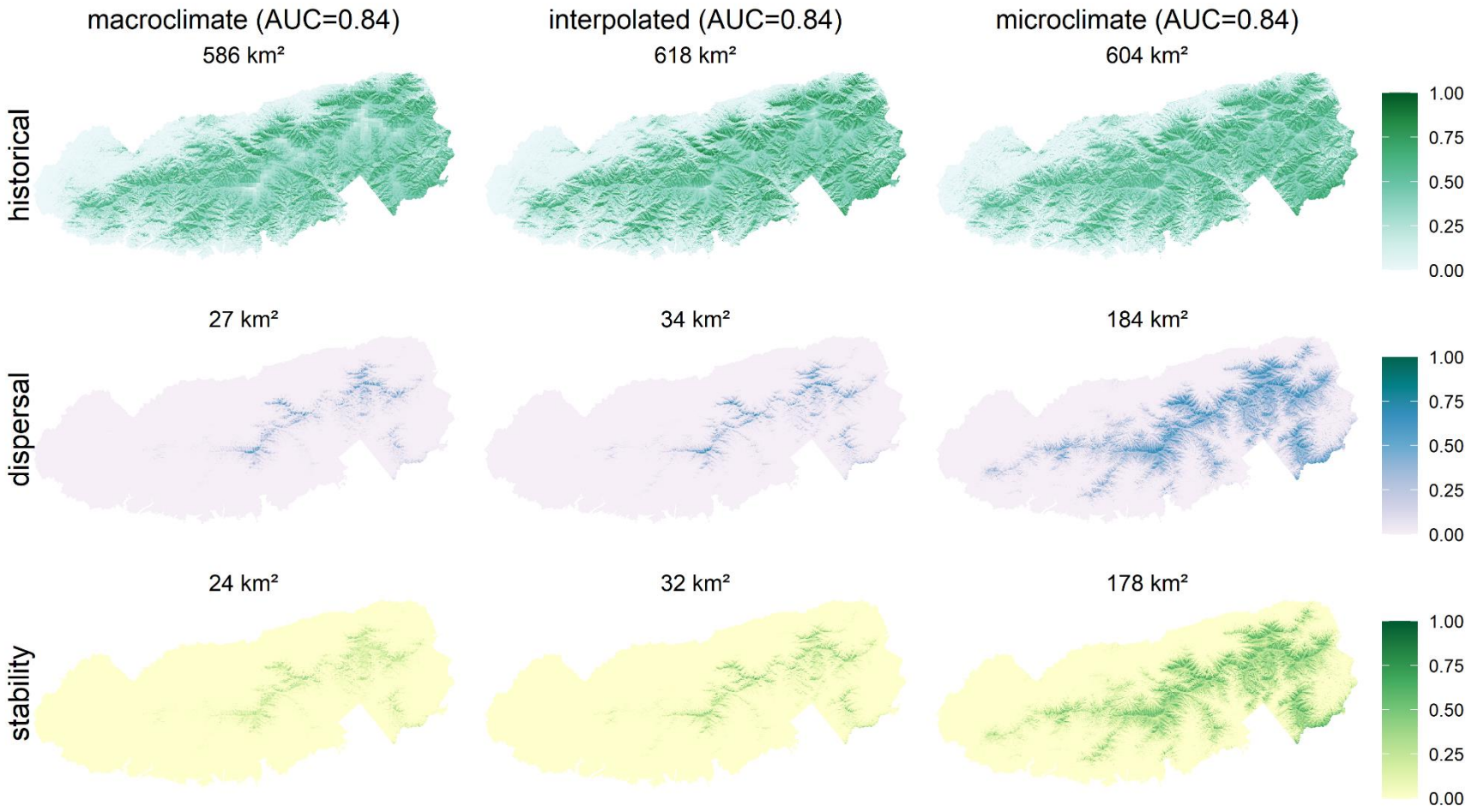

Fig S34. Probability of DRYOMAR occurrence

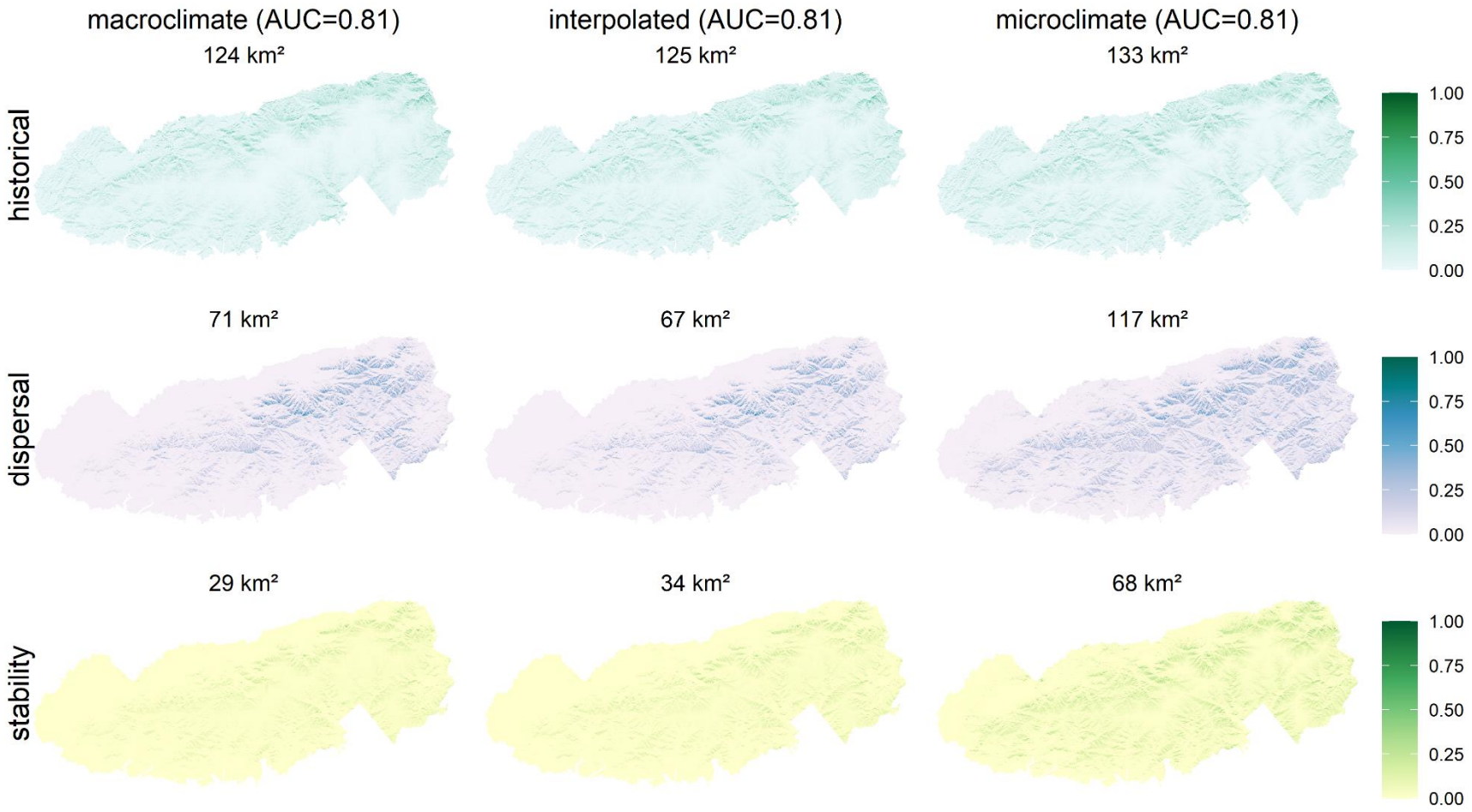

Fig S35. Probability of EPIGREP occurrence

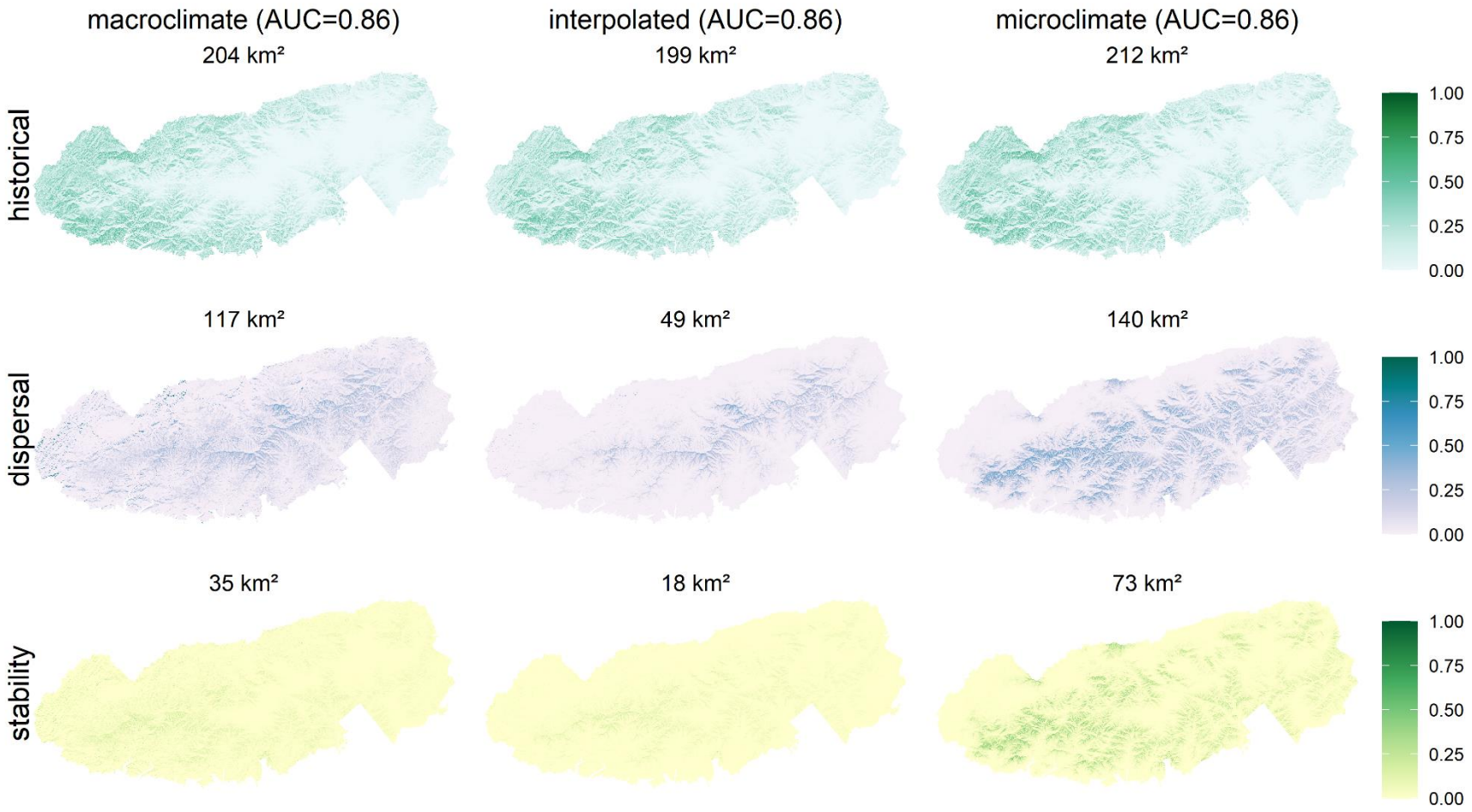

Fig S36. Probability of EUONAME occurrence

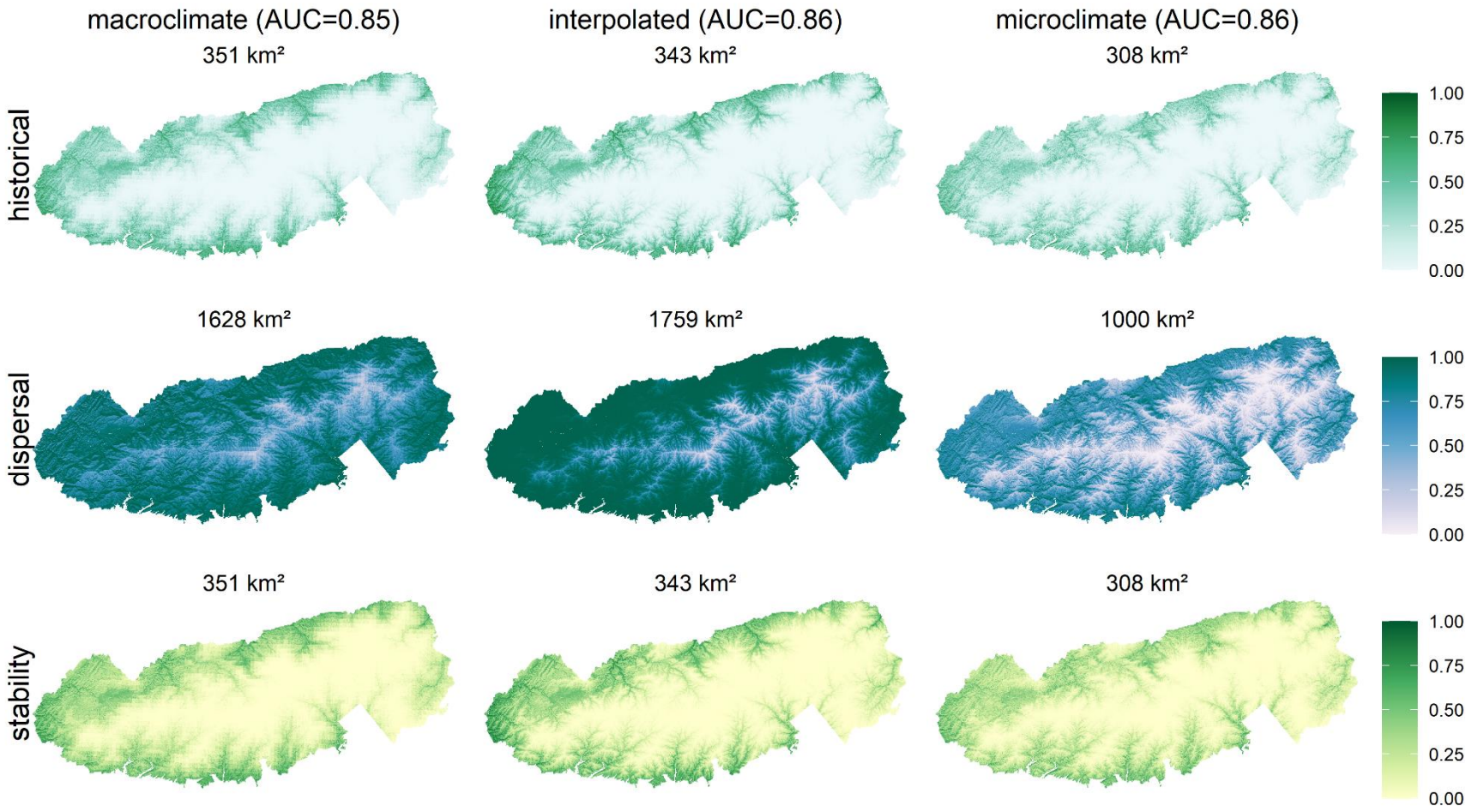

Fig S37. Probability of GALAURC occurrence

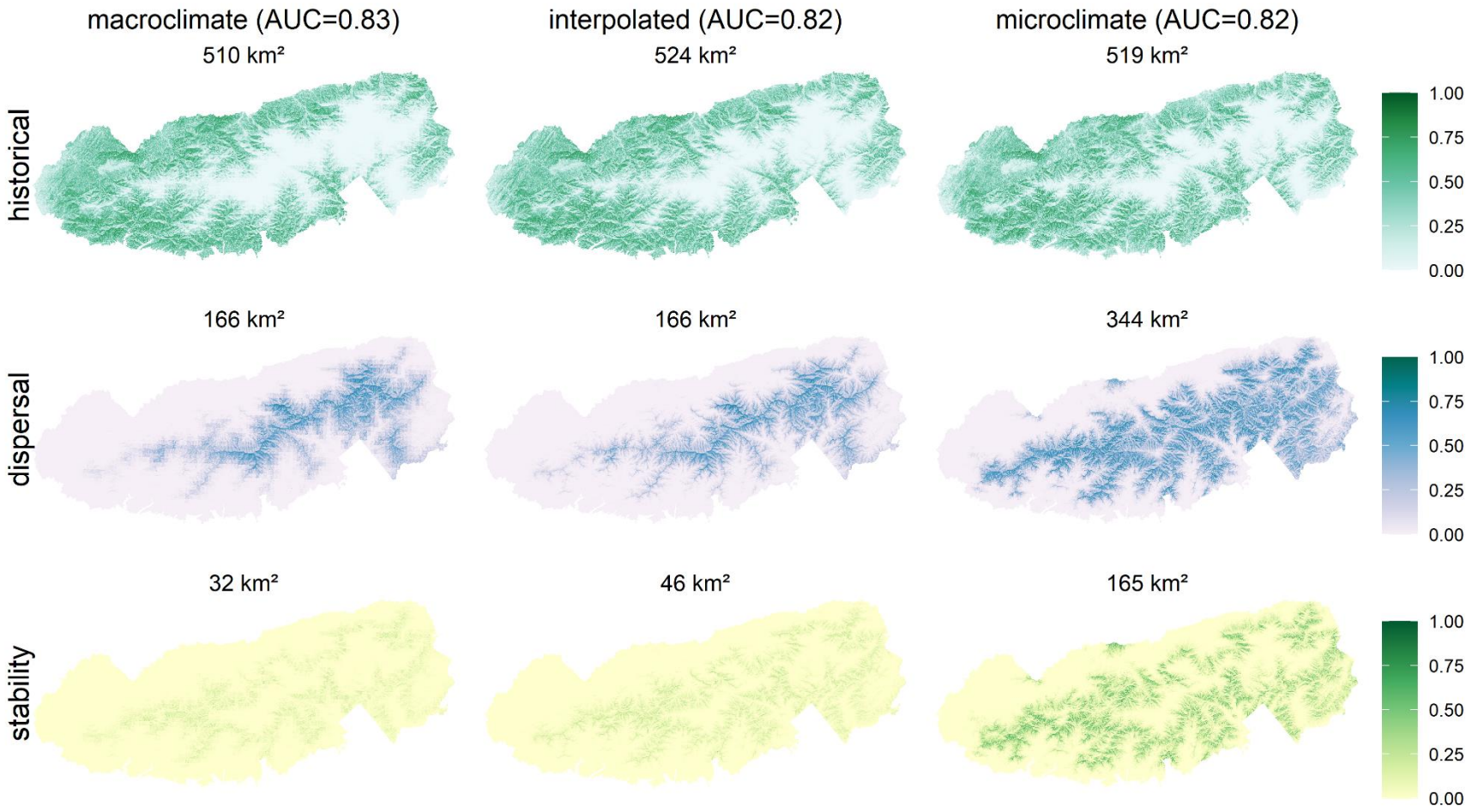

Fig S38. Probability of GALICRC occurrence

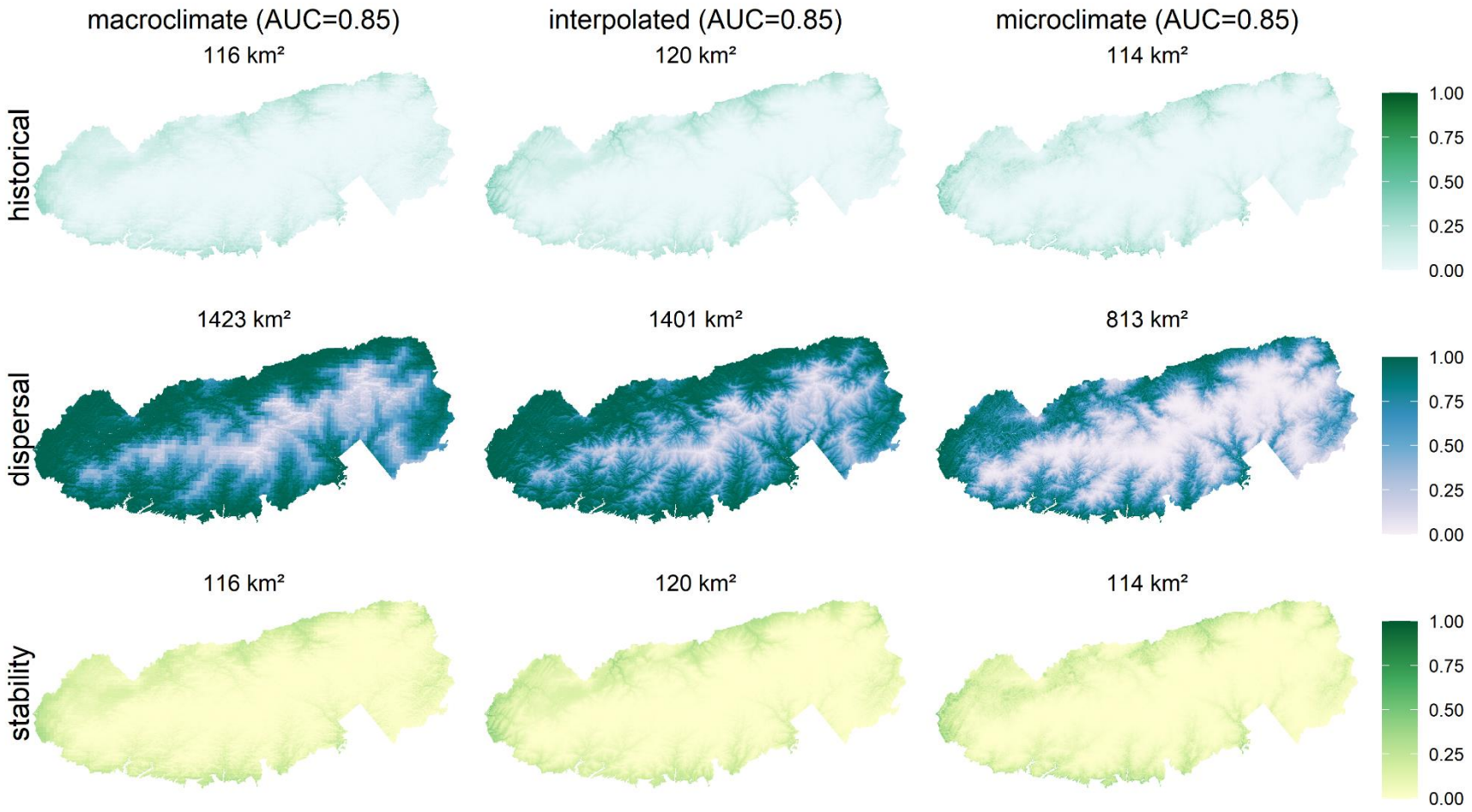

Fig S39. Probability of GAULPRO occurrence

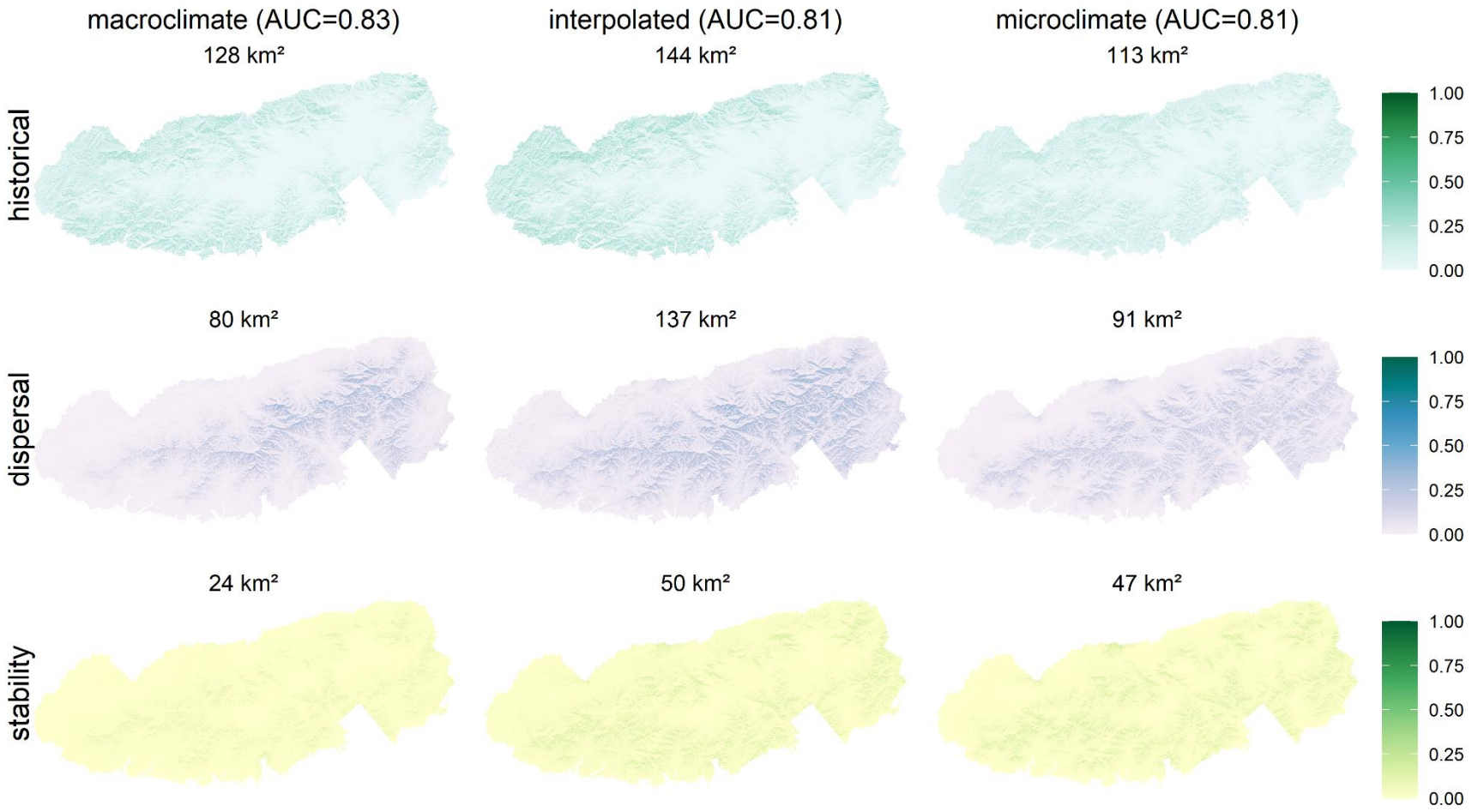

Fig S40. Probability of GAYLBAC occurrence

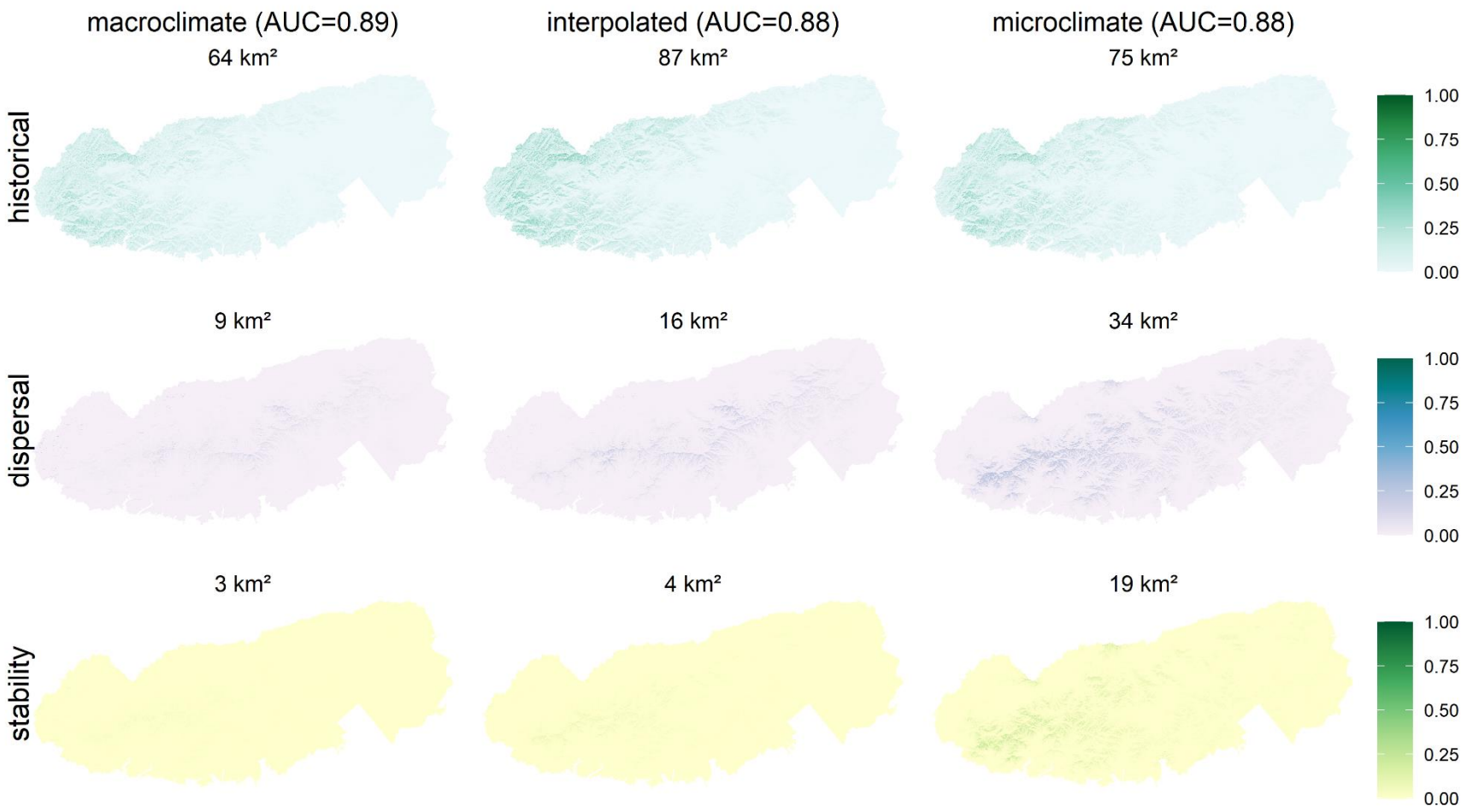

Fig S41. Probability of GAYLURS occurrence

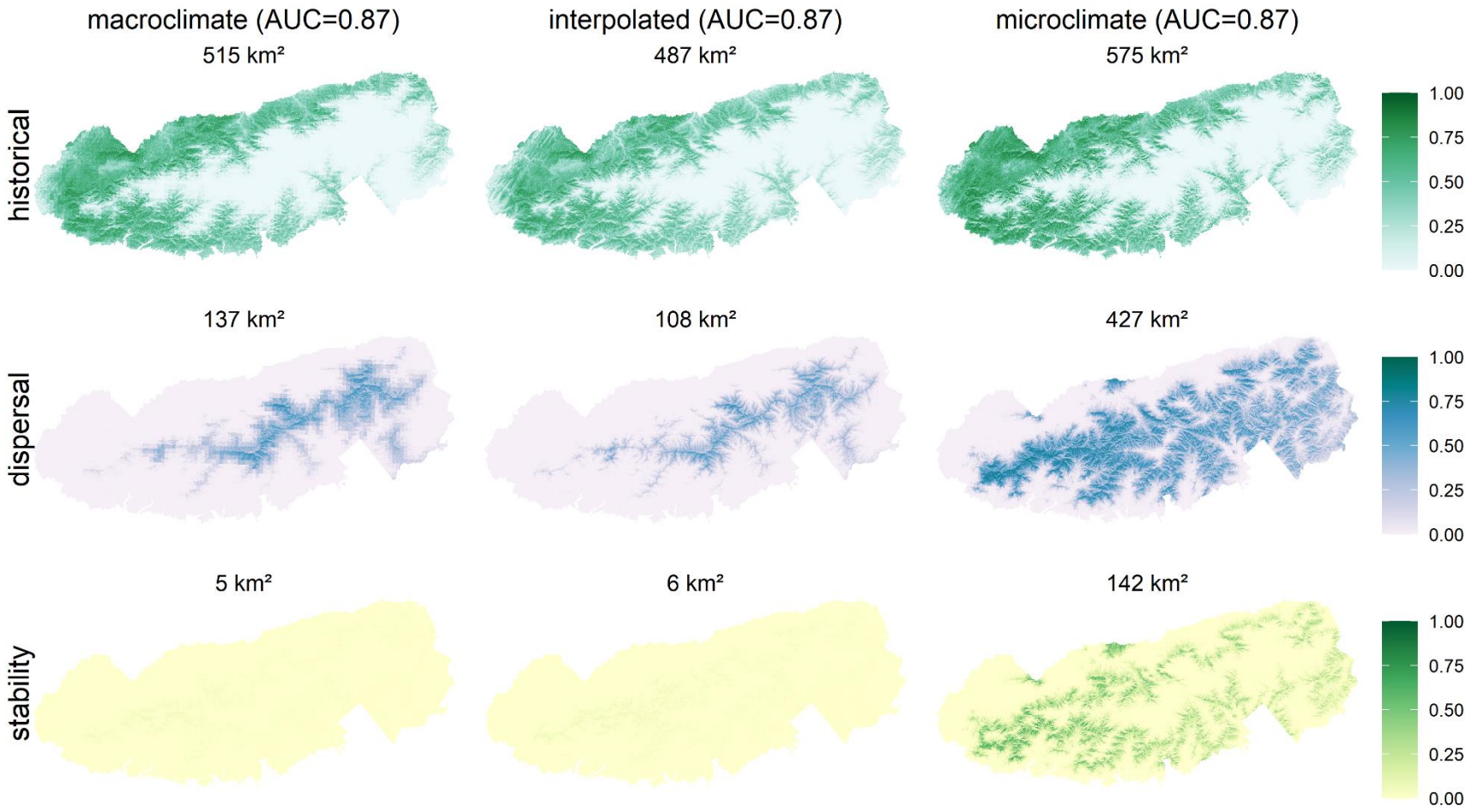

Fig S42. Probability of HALETETM occurrence

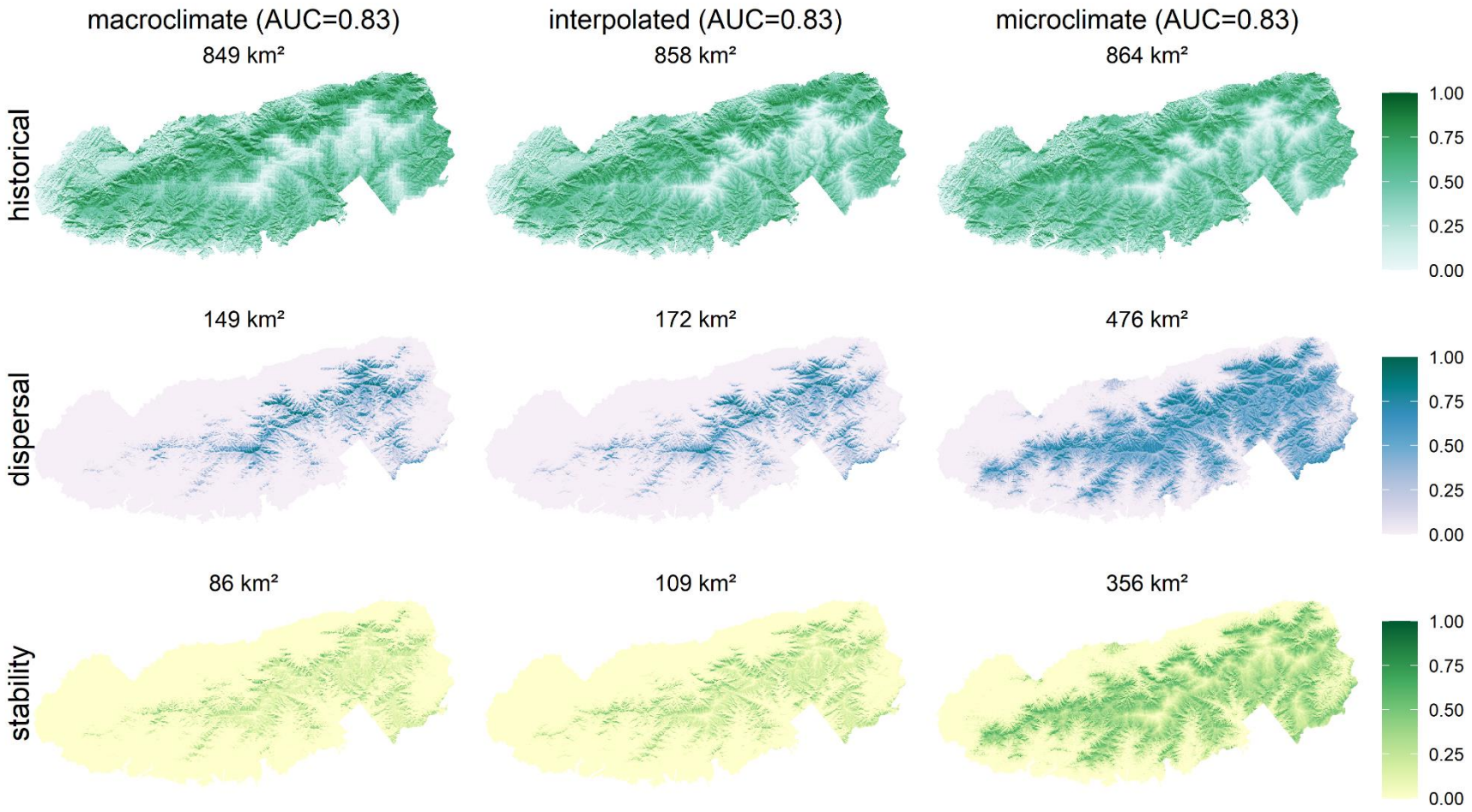

Fig S43. Probability of HOUSSER occurrence

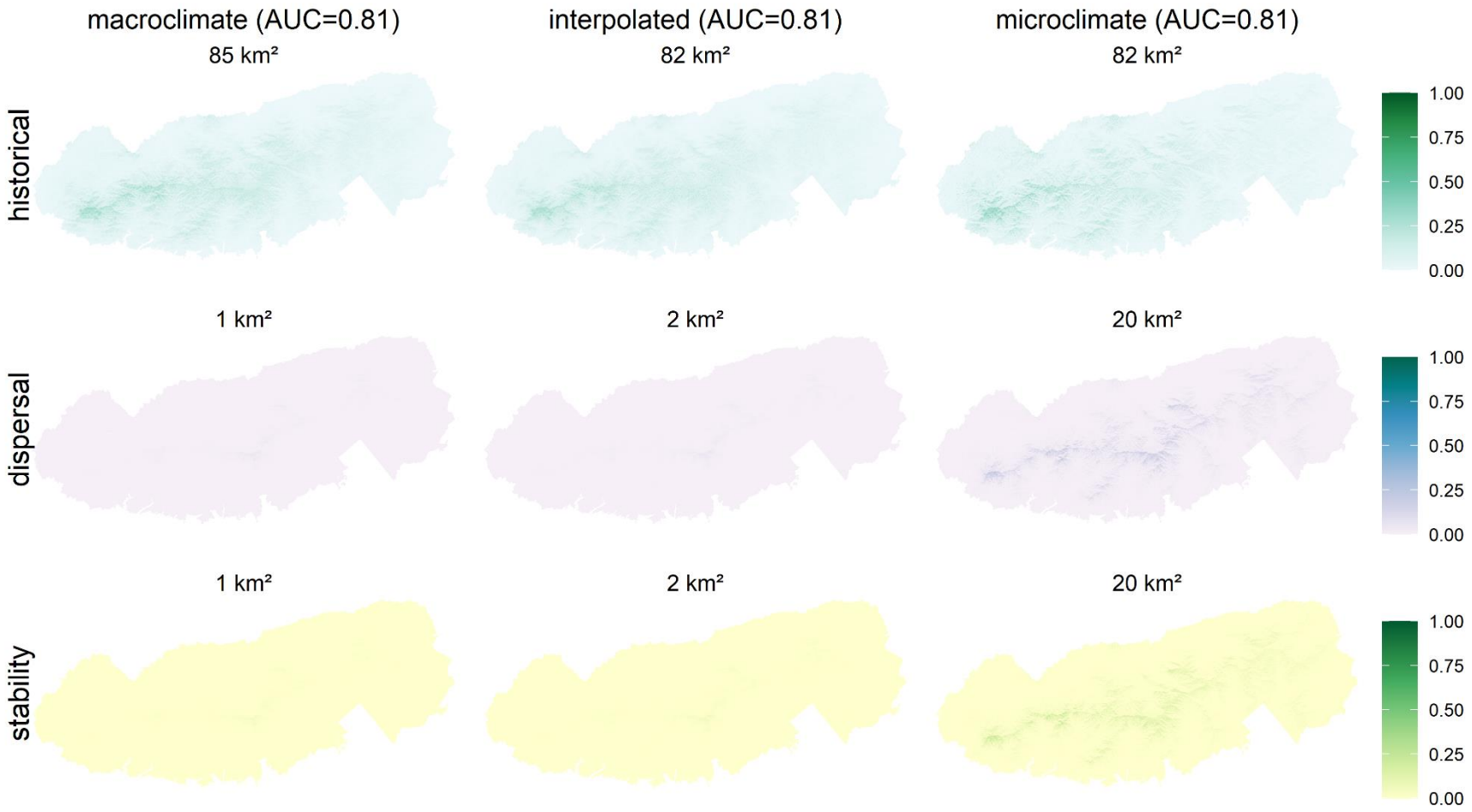

Fig S44. Probability of HUPELUC occurrence

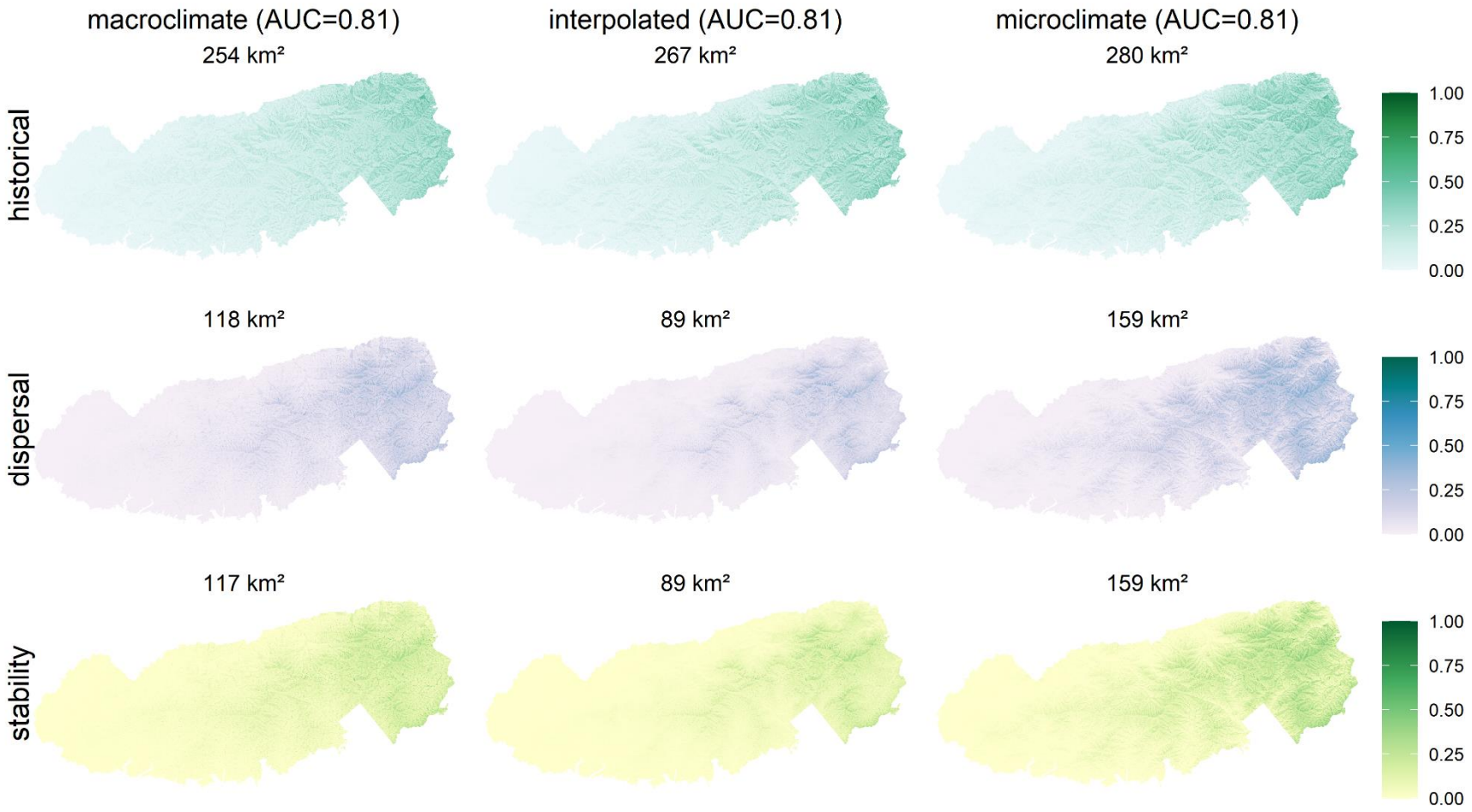

Fig S45. Probability of ILEXOPAO occurrence

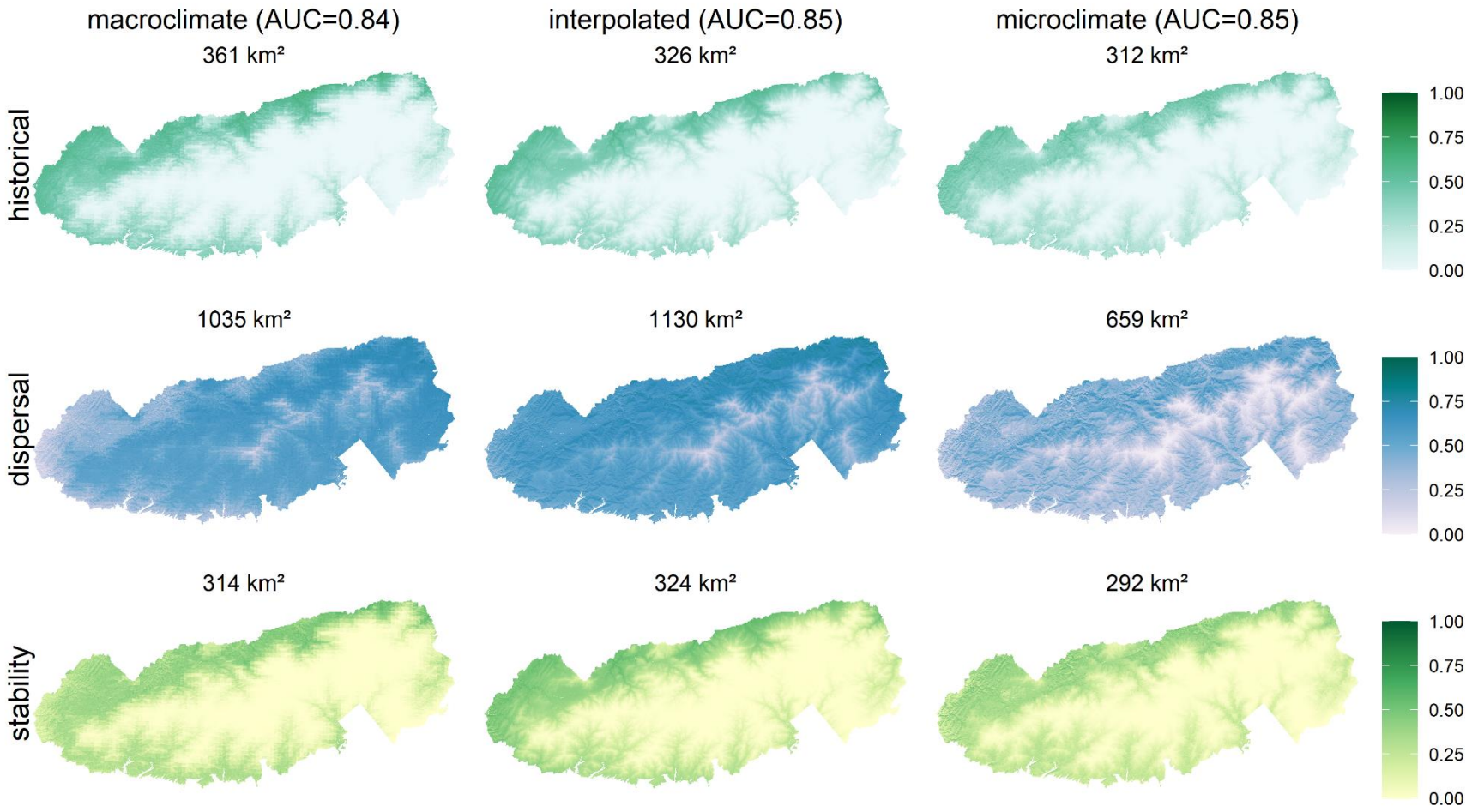

Fig S46. Probability of KALMLAT occurrence

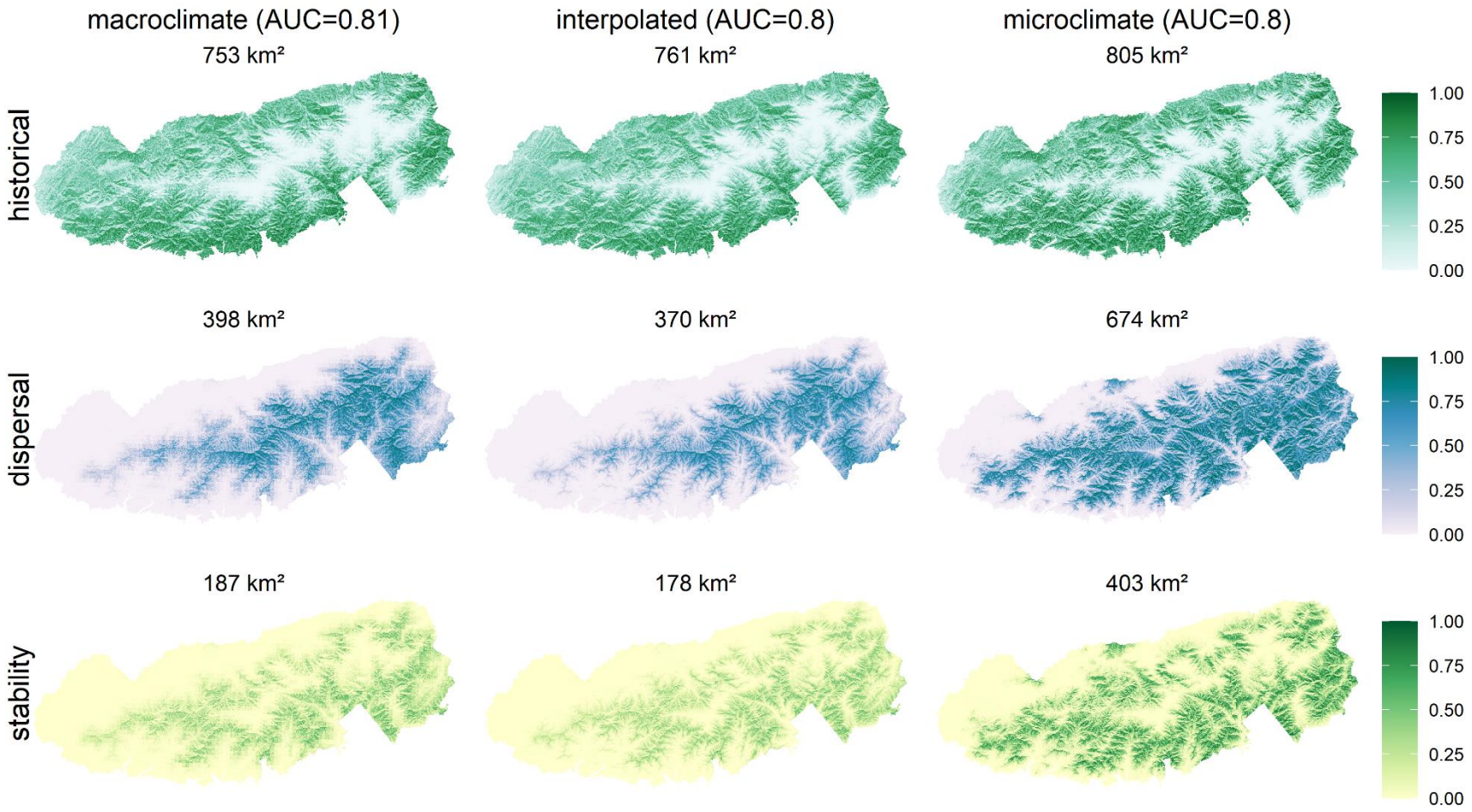

Fig S47. Probability of LAPOCAN occurrence

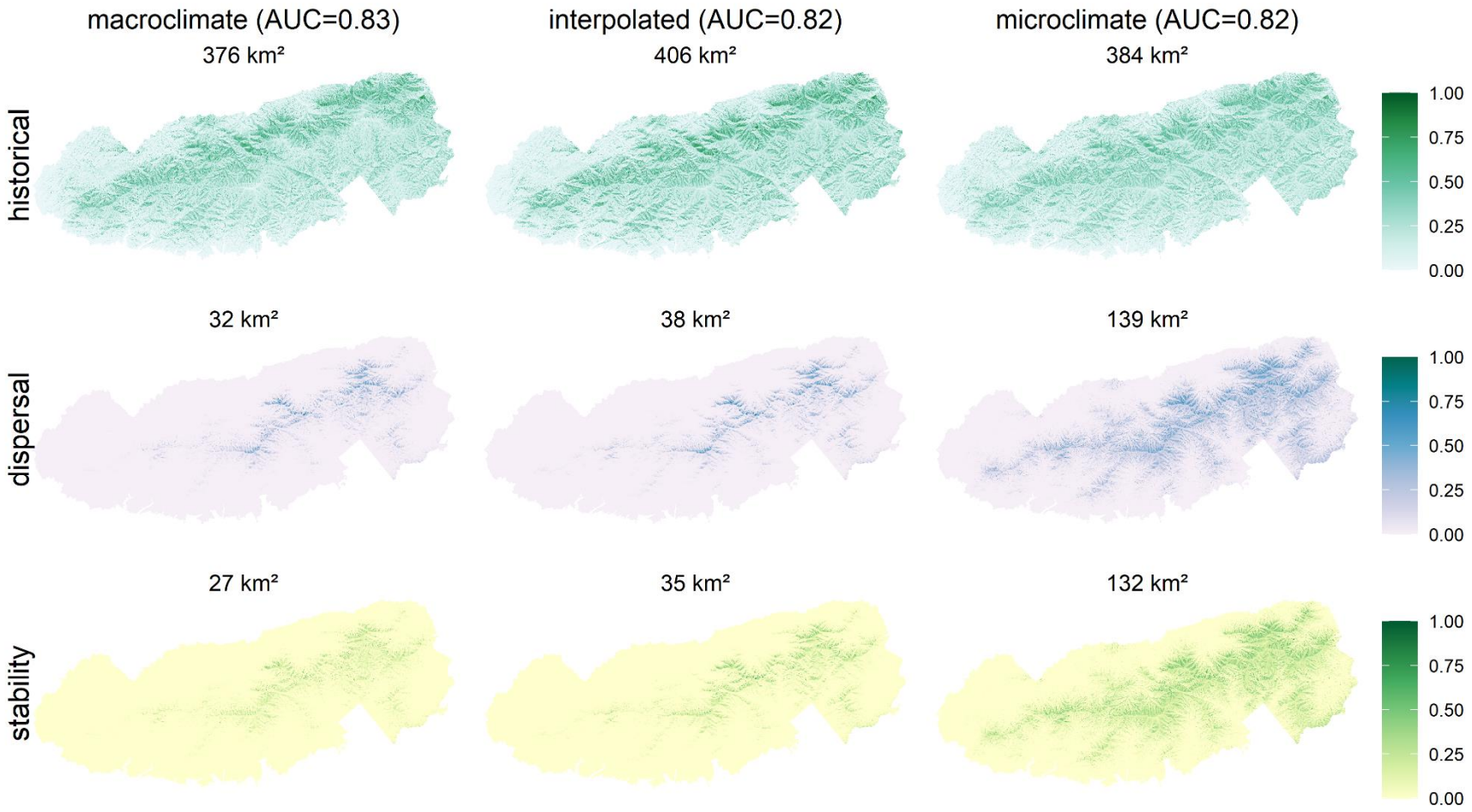

Fig S48. Probability of LINDBEN occurrence

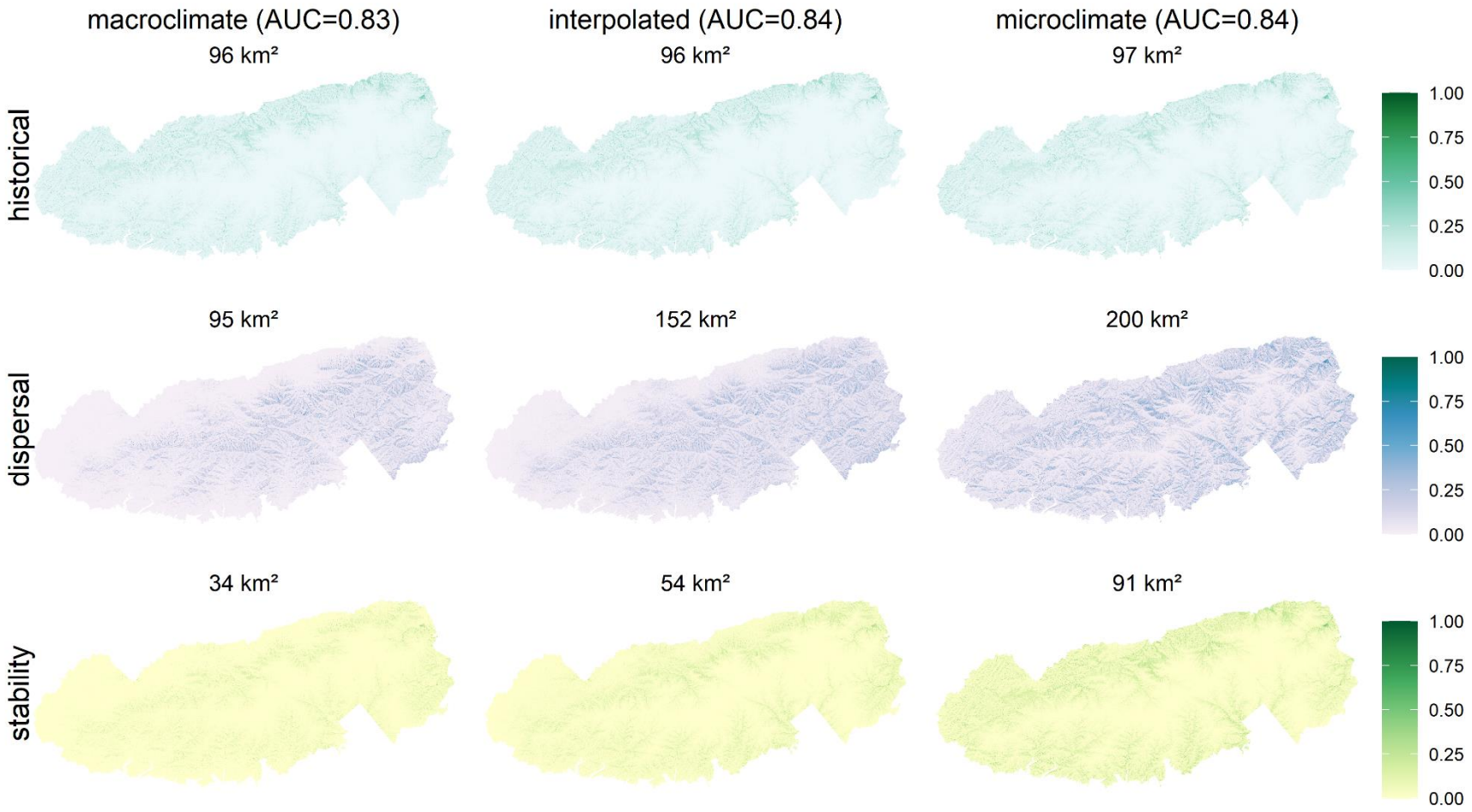

Fig S49. Probability of LIRITUL occurrence

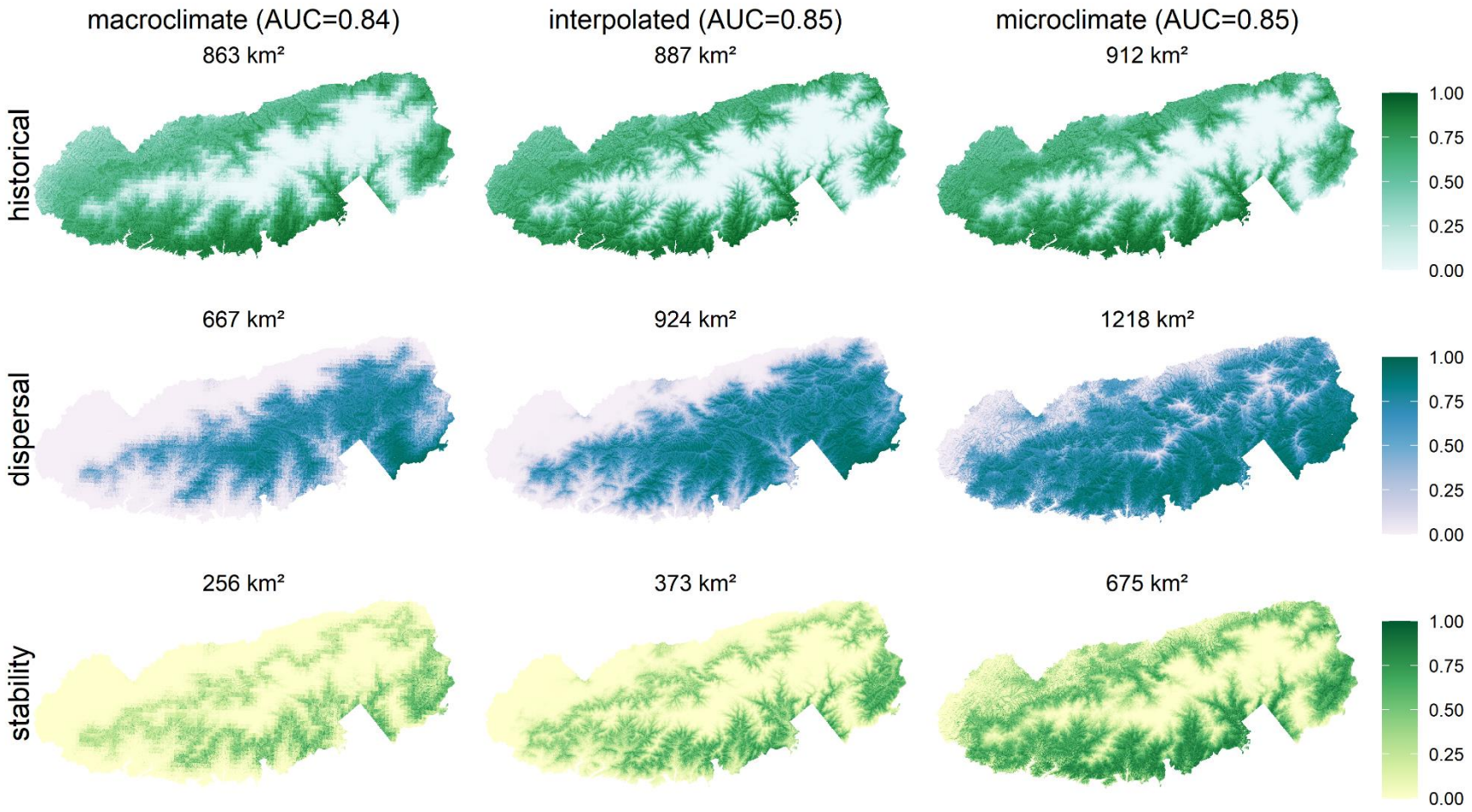

Fig S50. Probability of MAGNACU occurrence

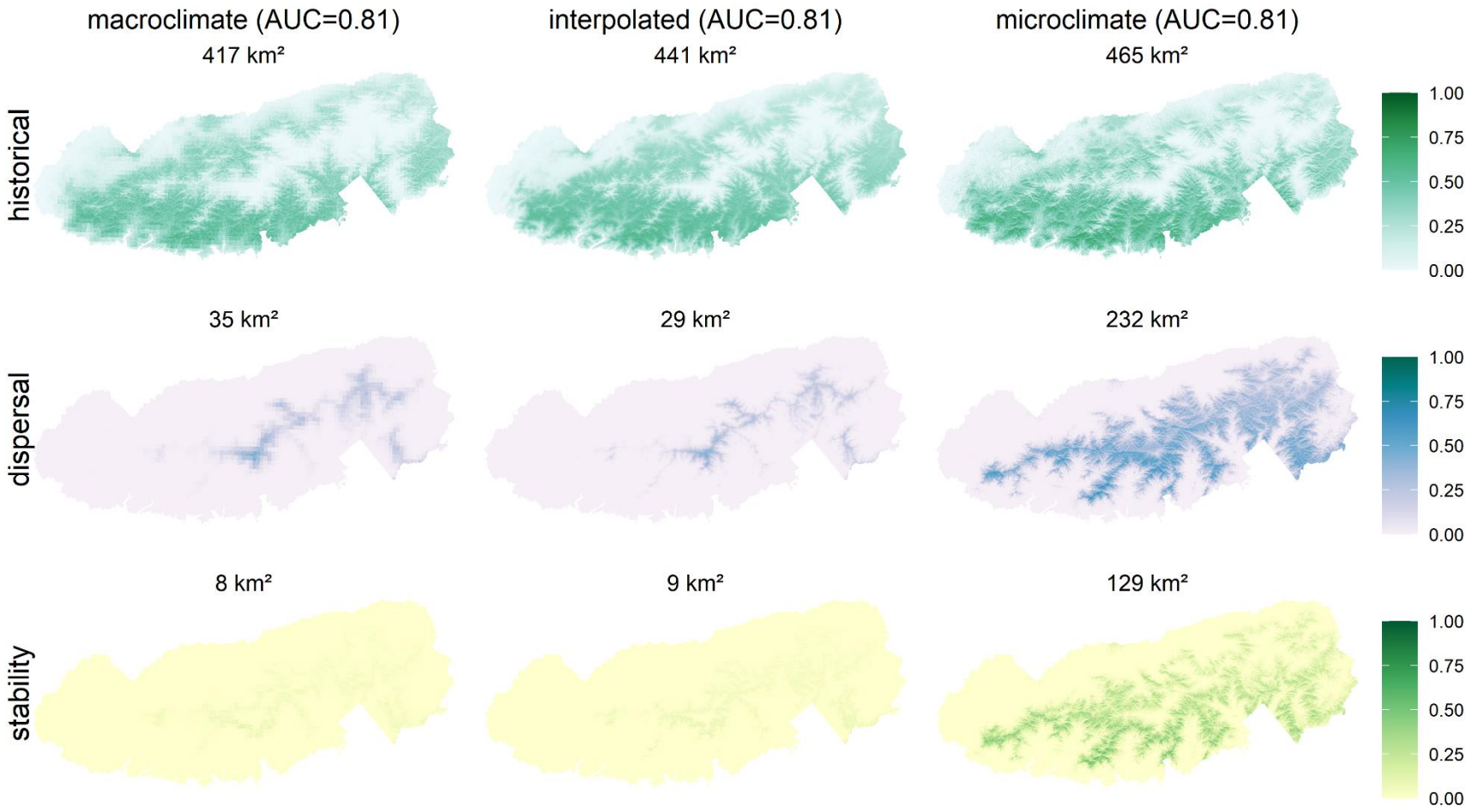

Fig S51. Probability of NYSSSYL occurrence

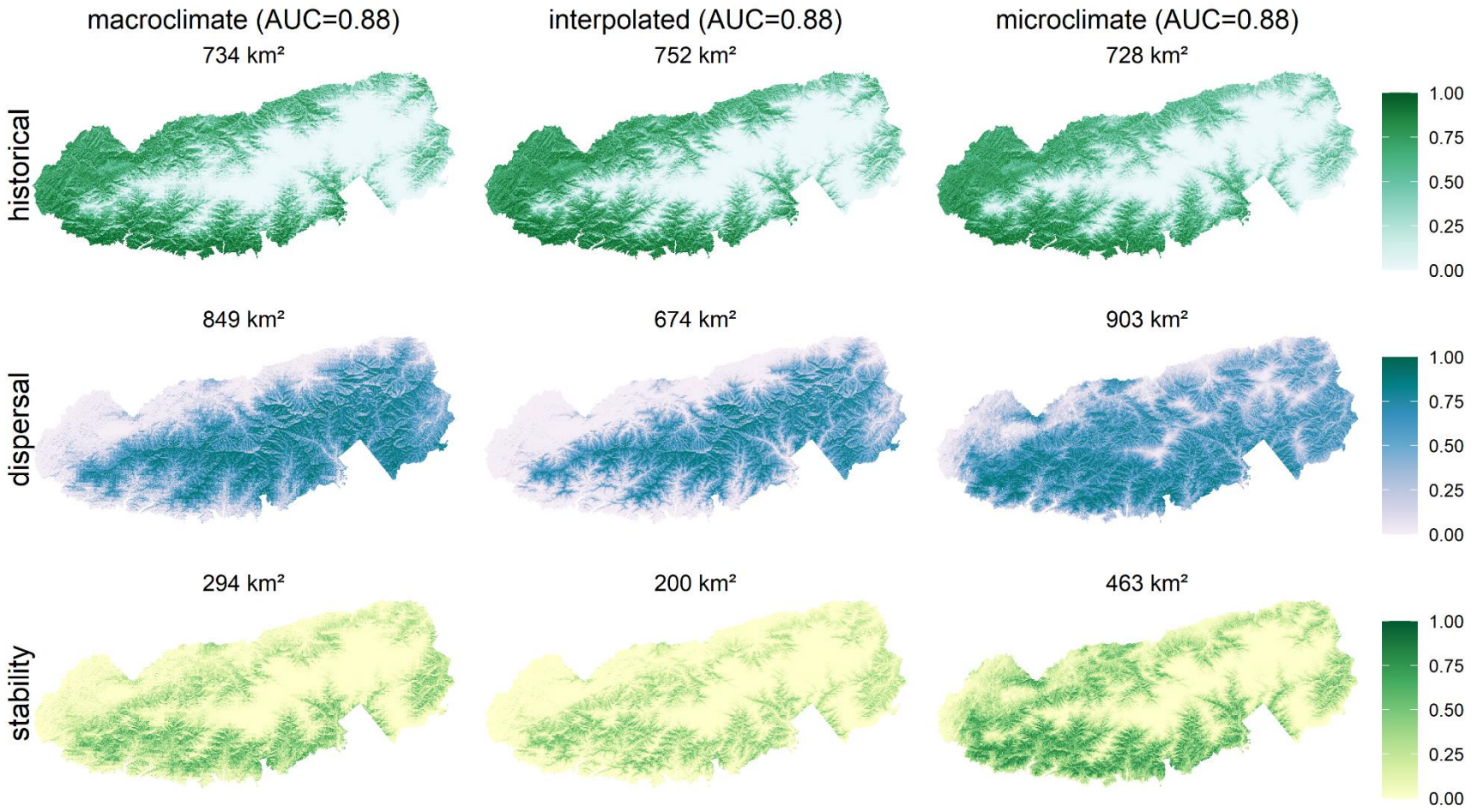

Fig S52. Probability of OSMOCLA occurrence

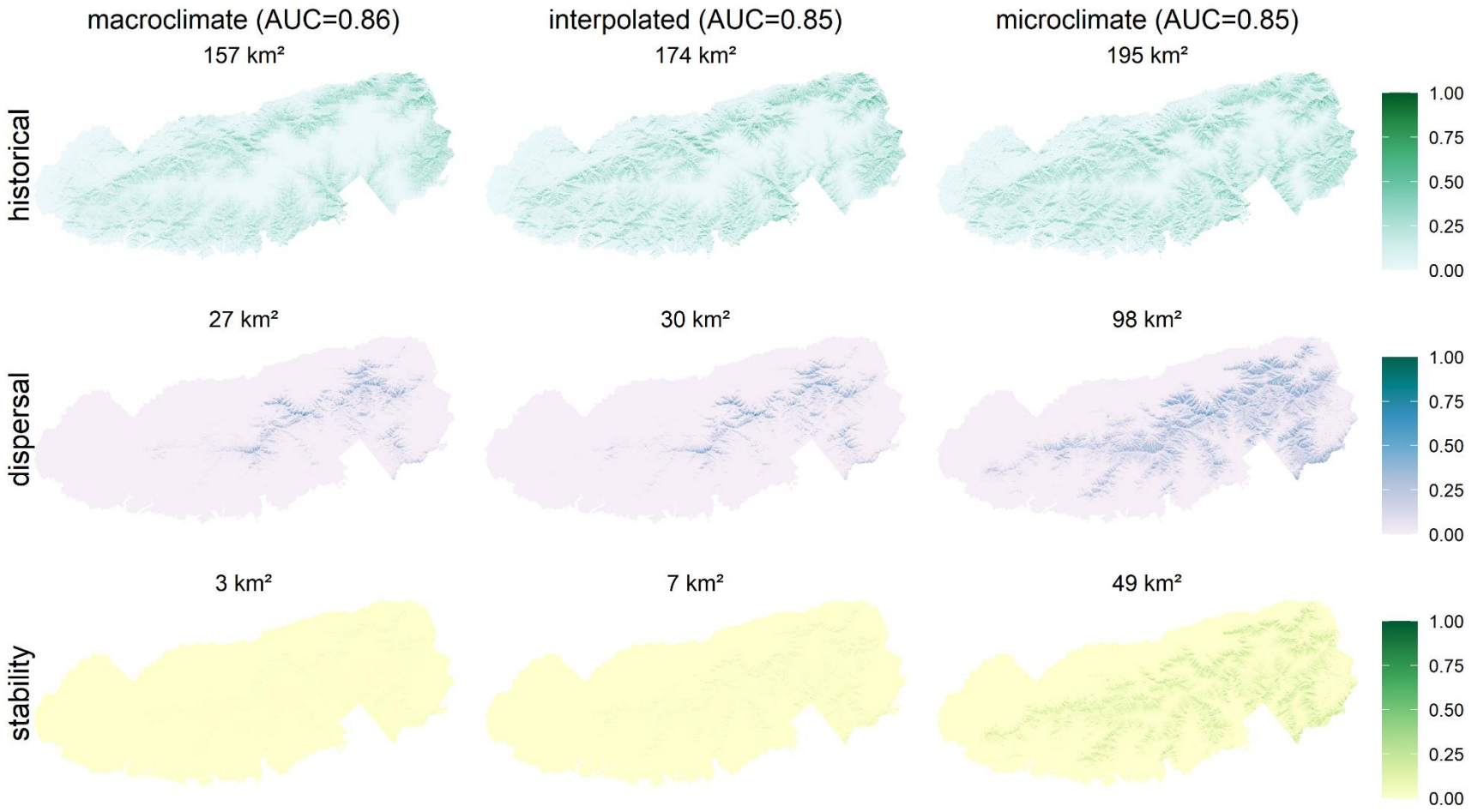

Fig S53. Probability of OXALMON occurrence

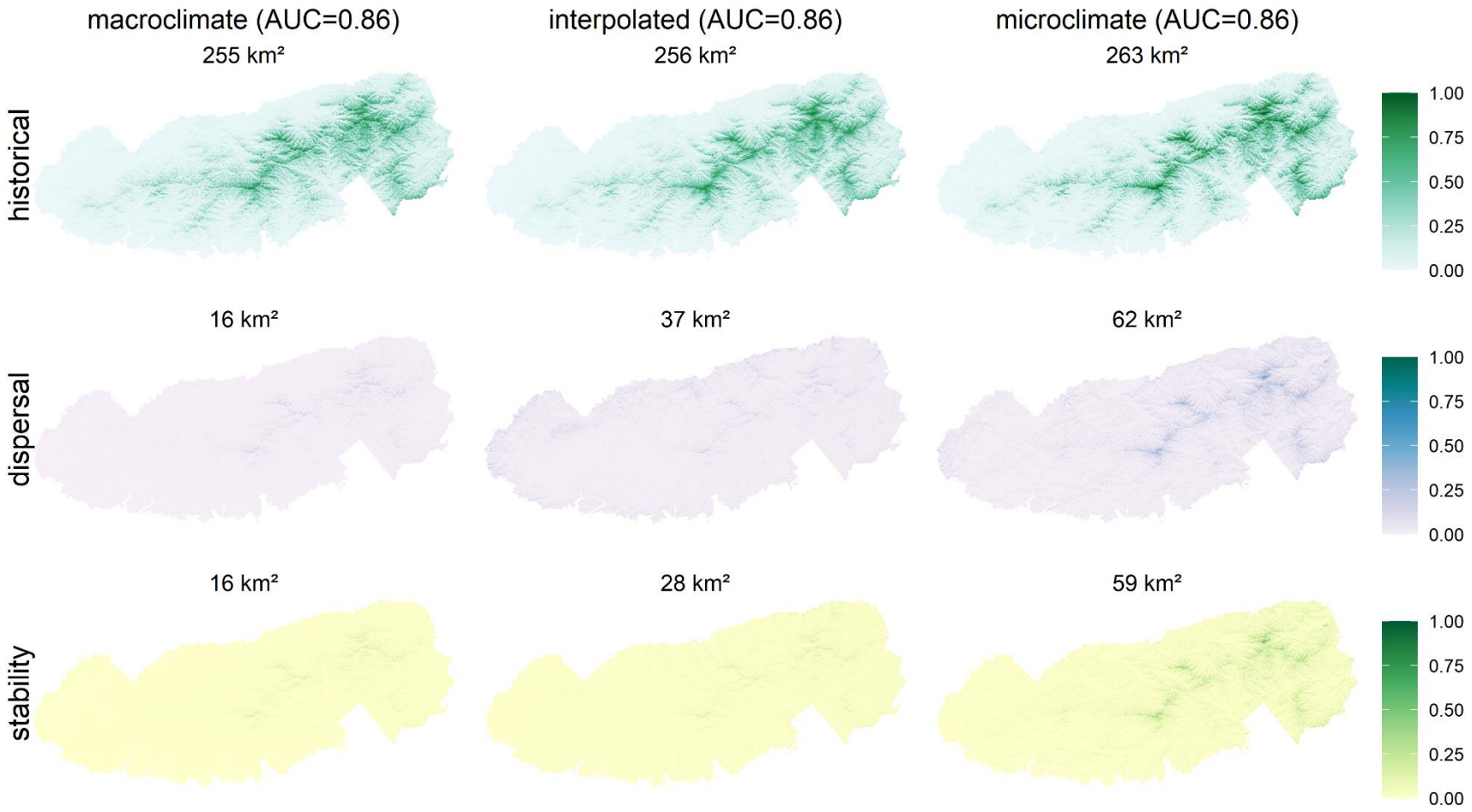

Fig S54. Probability of OXYDARB occurrence

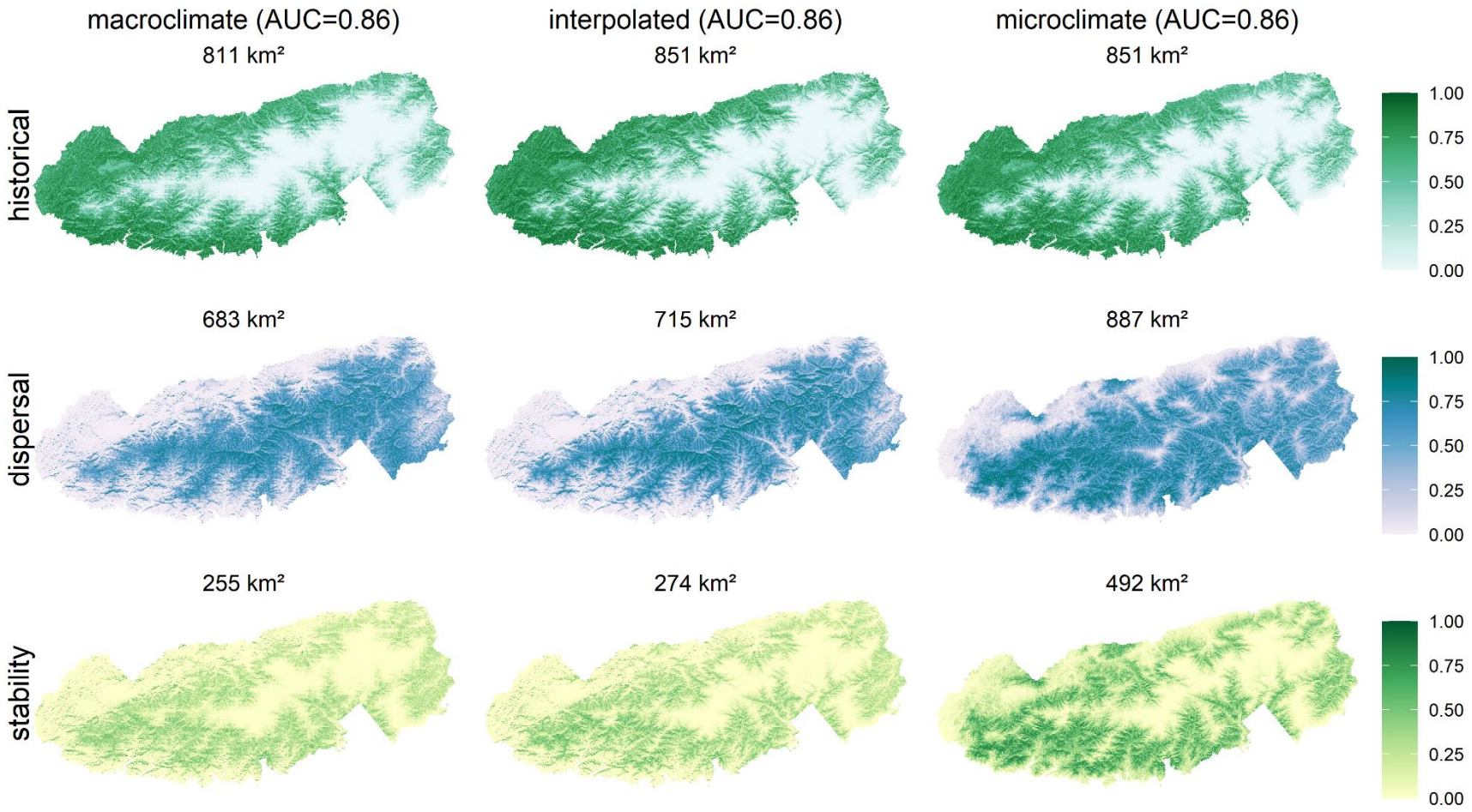

Fig S55. Probability of PARTQUI occurrence

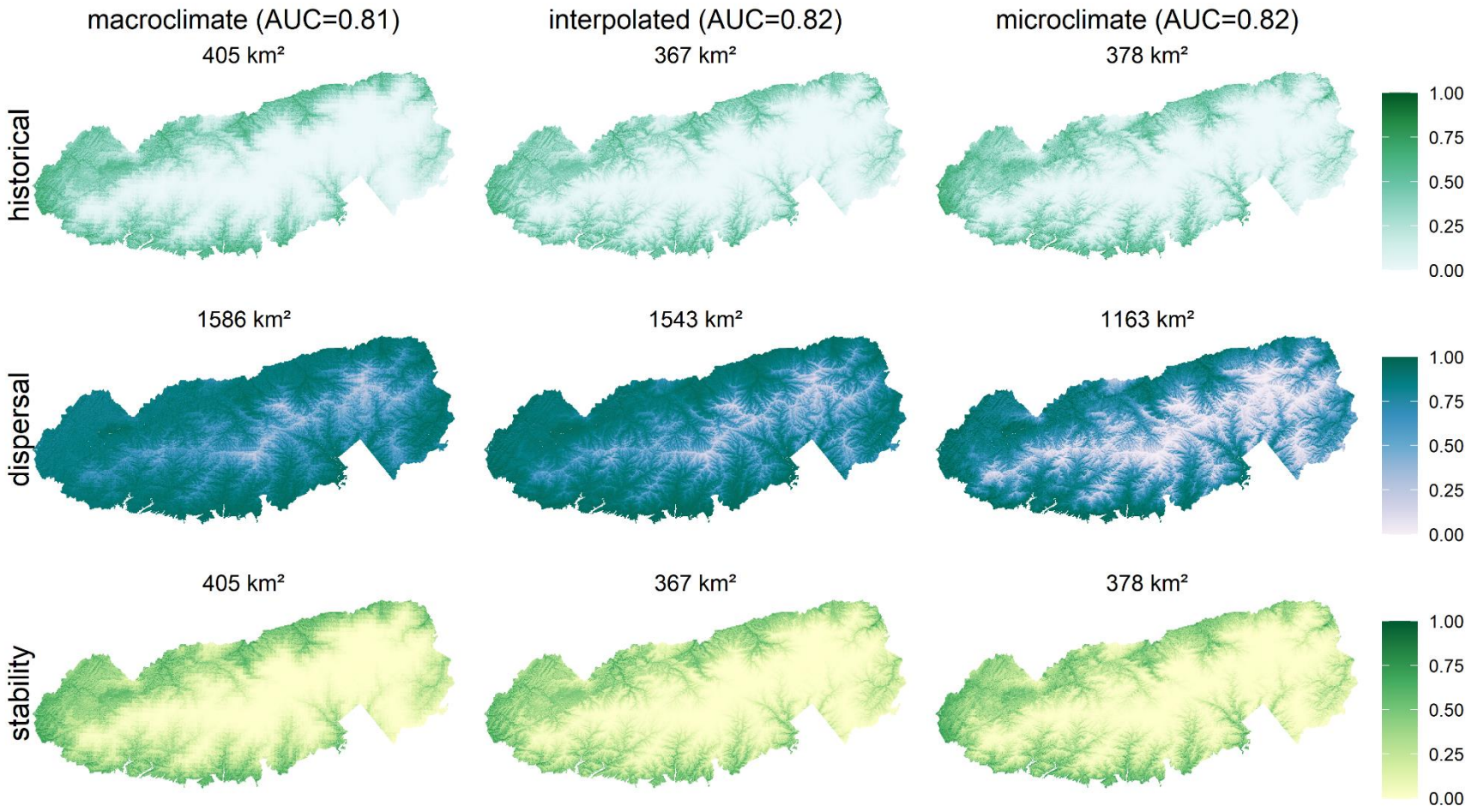

Fig S56. Probability of PHEGHEX occurrence

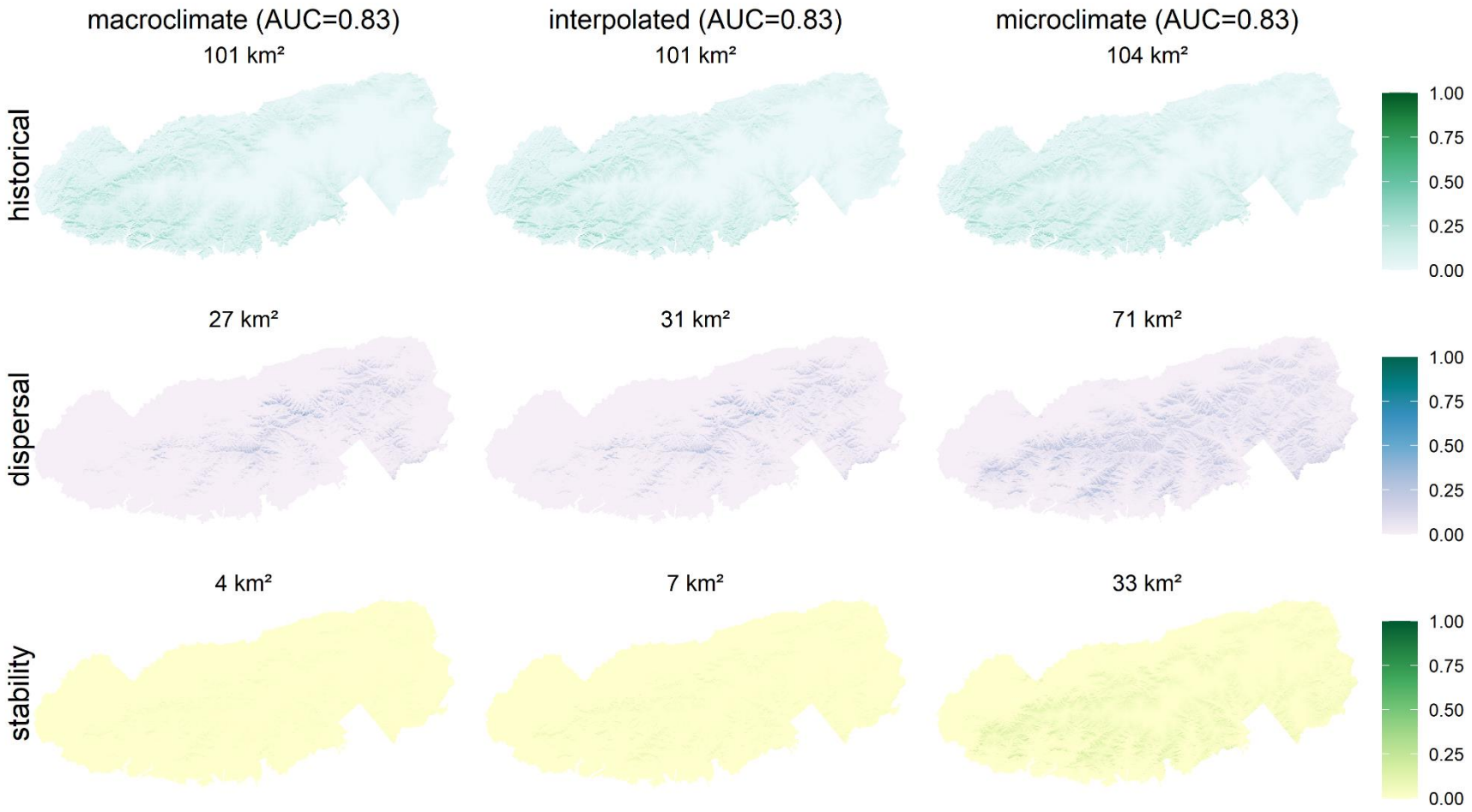

Fig S57. Probability of PICERUB occurrence

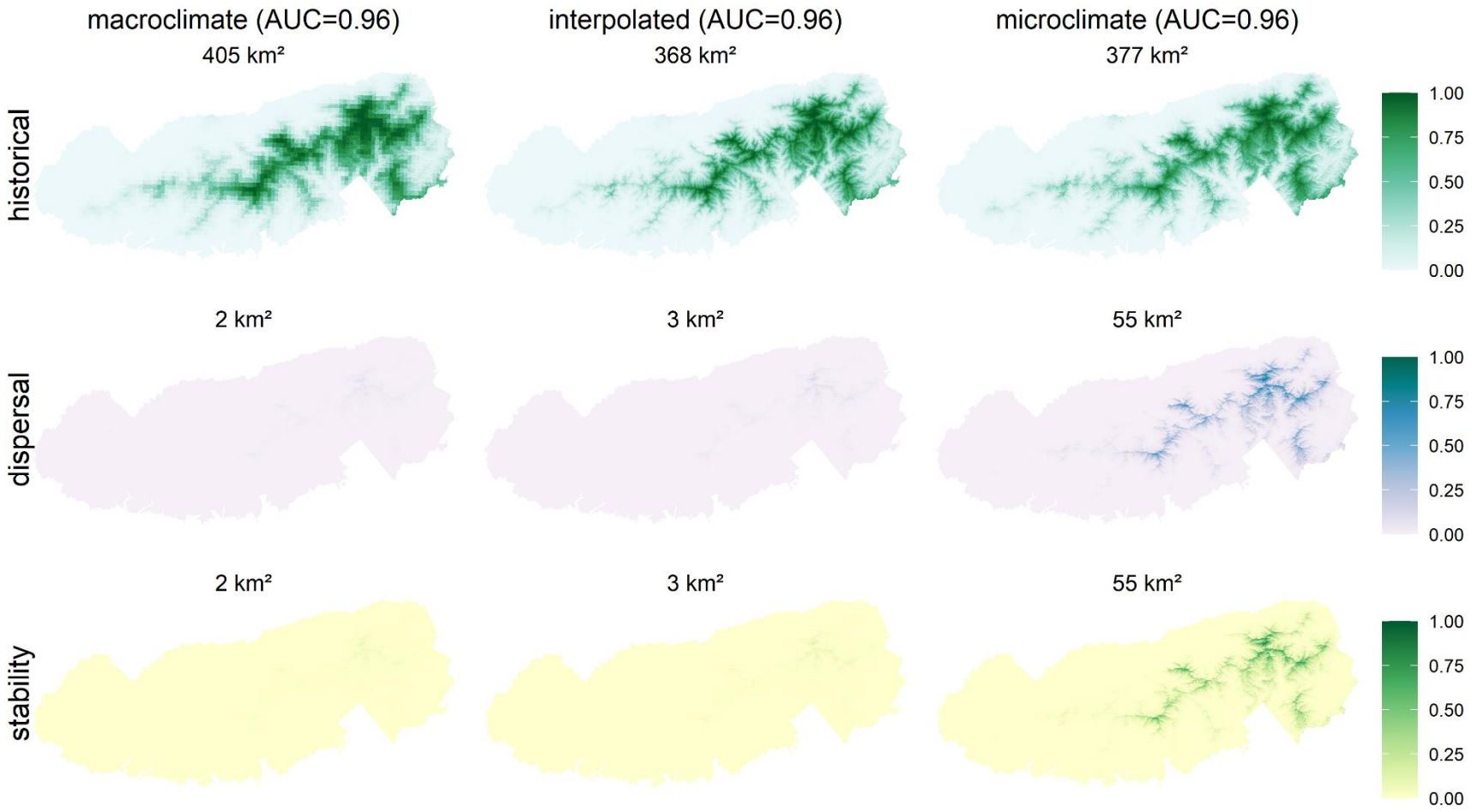

Fig S58. Probability of PINUPUN occurrence

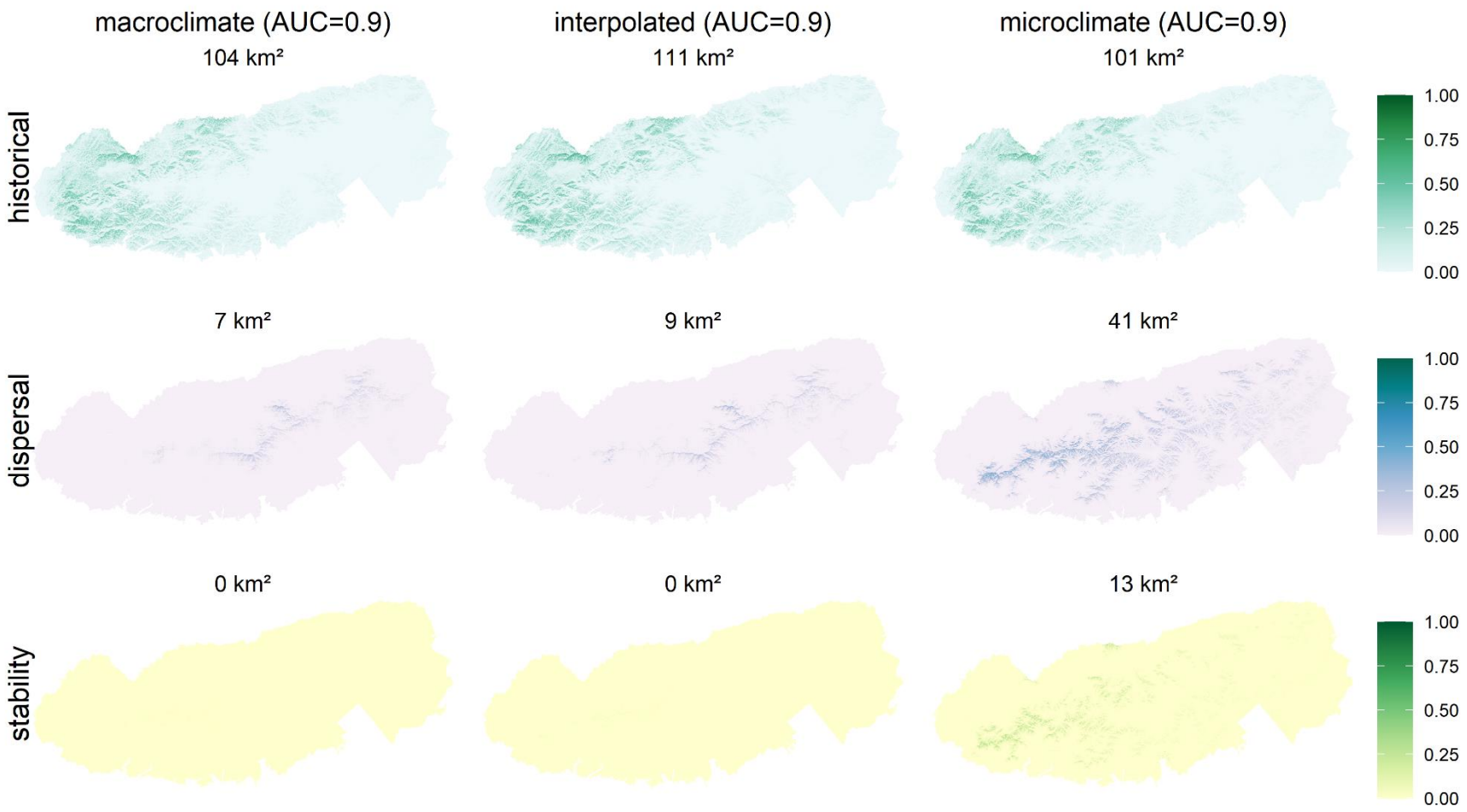

Fig S59. Probability of PINURIG occurrence

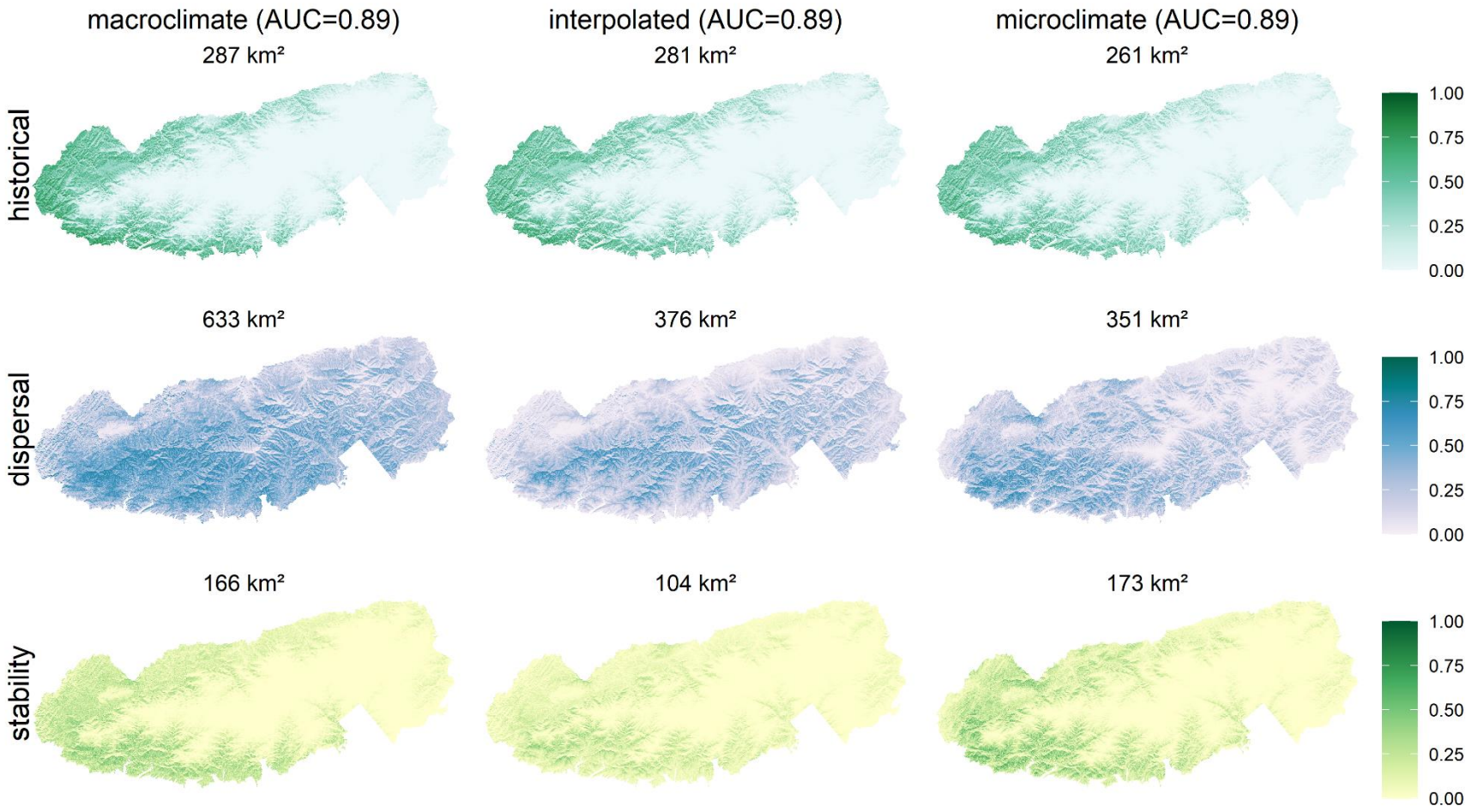

Fig S60. Probability of PINUSTR occurrence

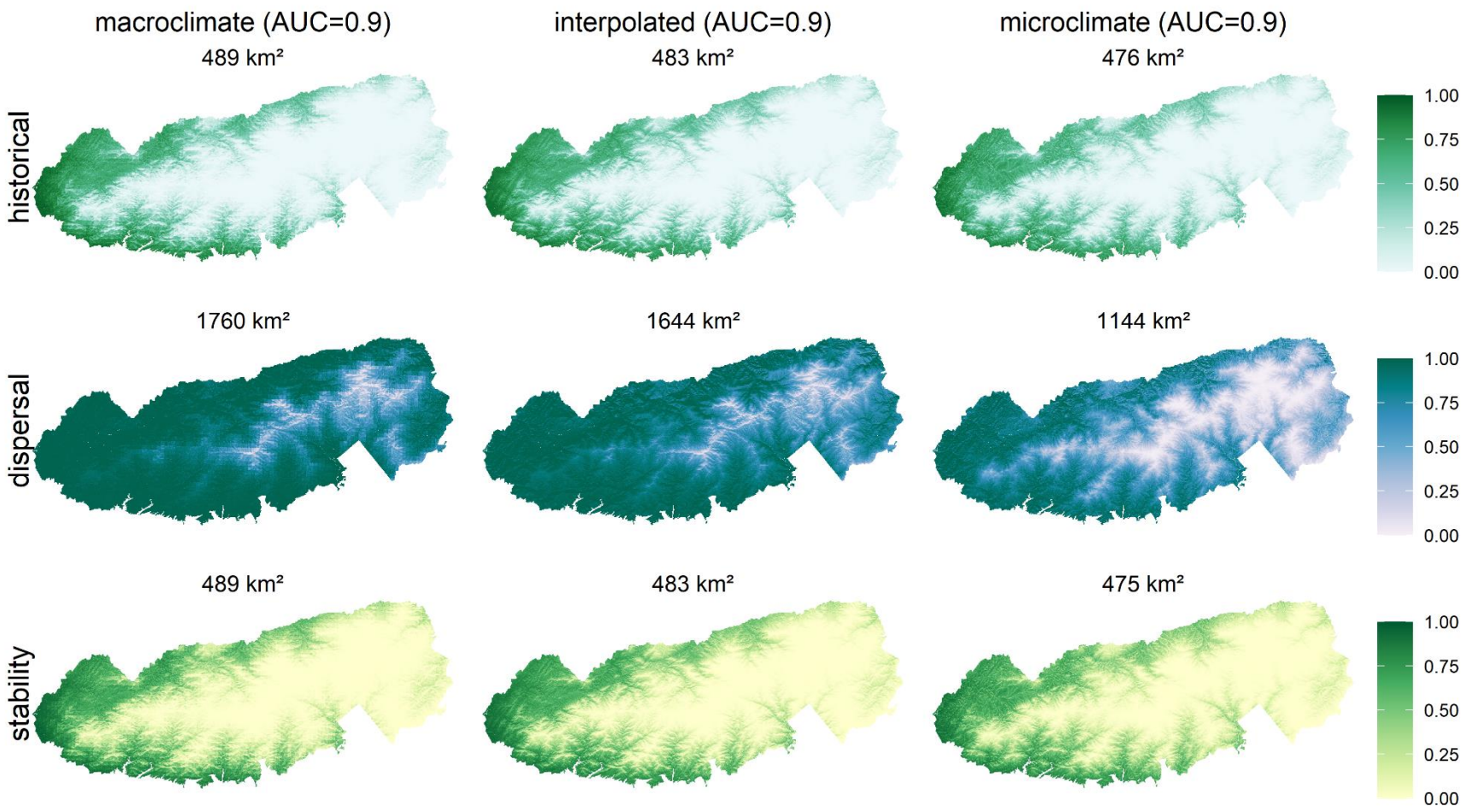

Fig S61. Probability of PINUVIR occurrence

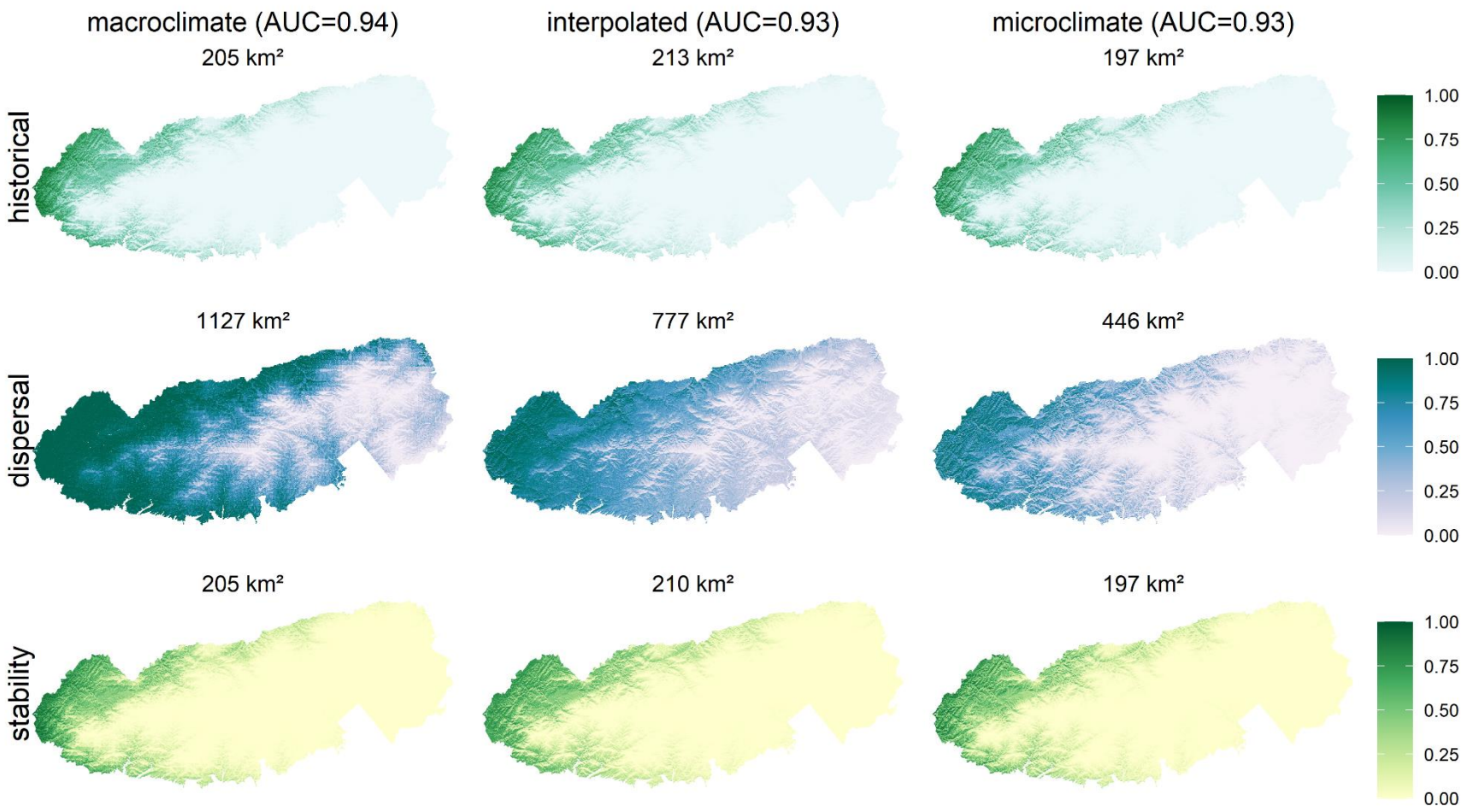

Fig S62. Probability of POLYPUB occurrence

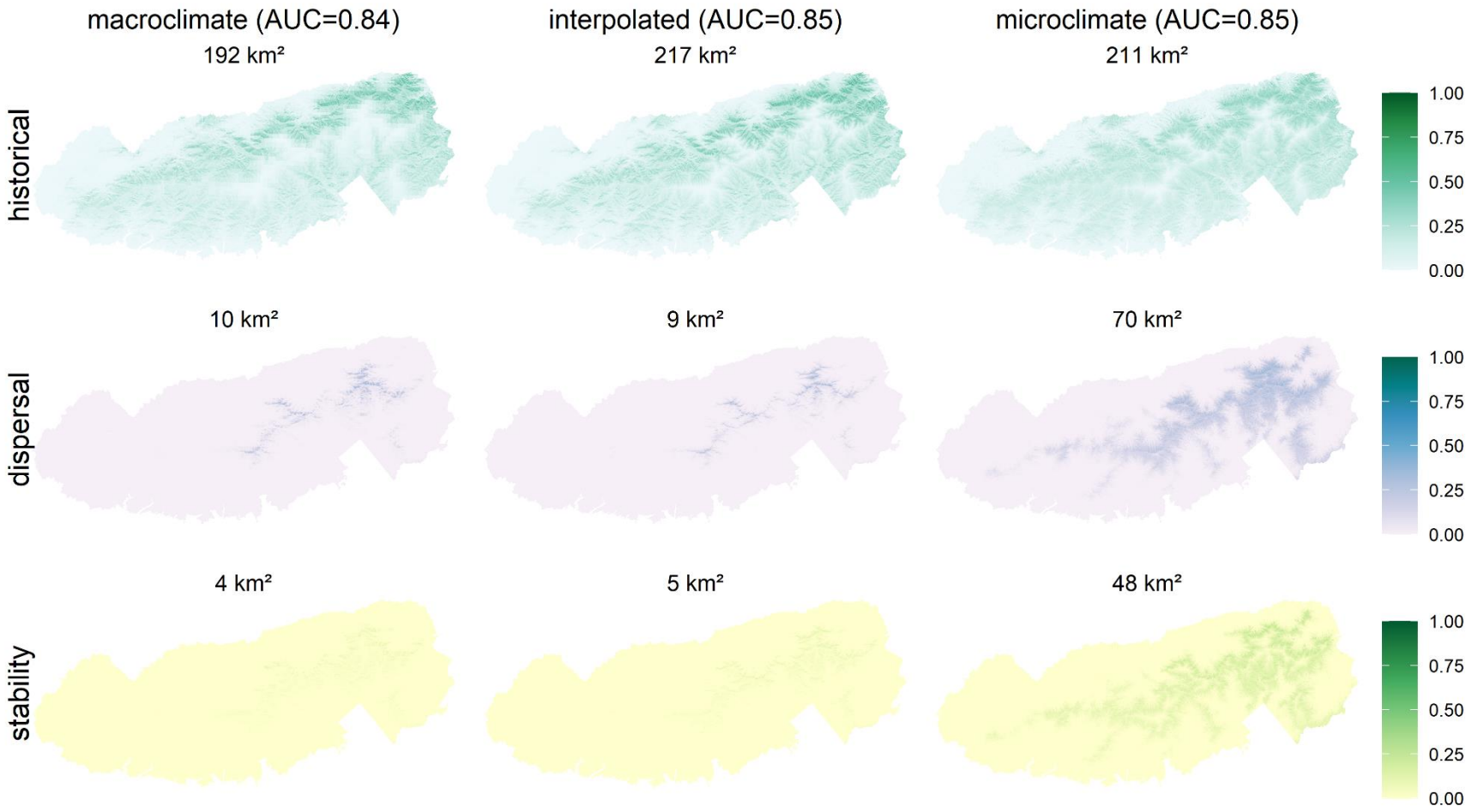

Fig S63. Probability of POTECND occurrence

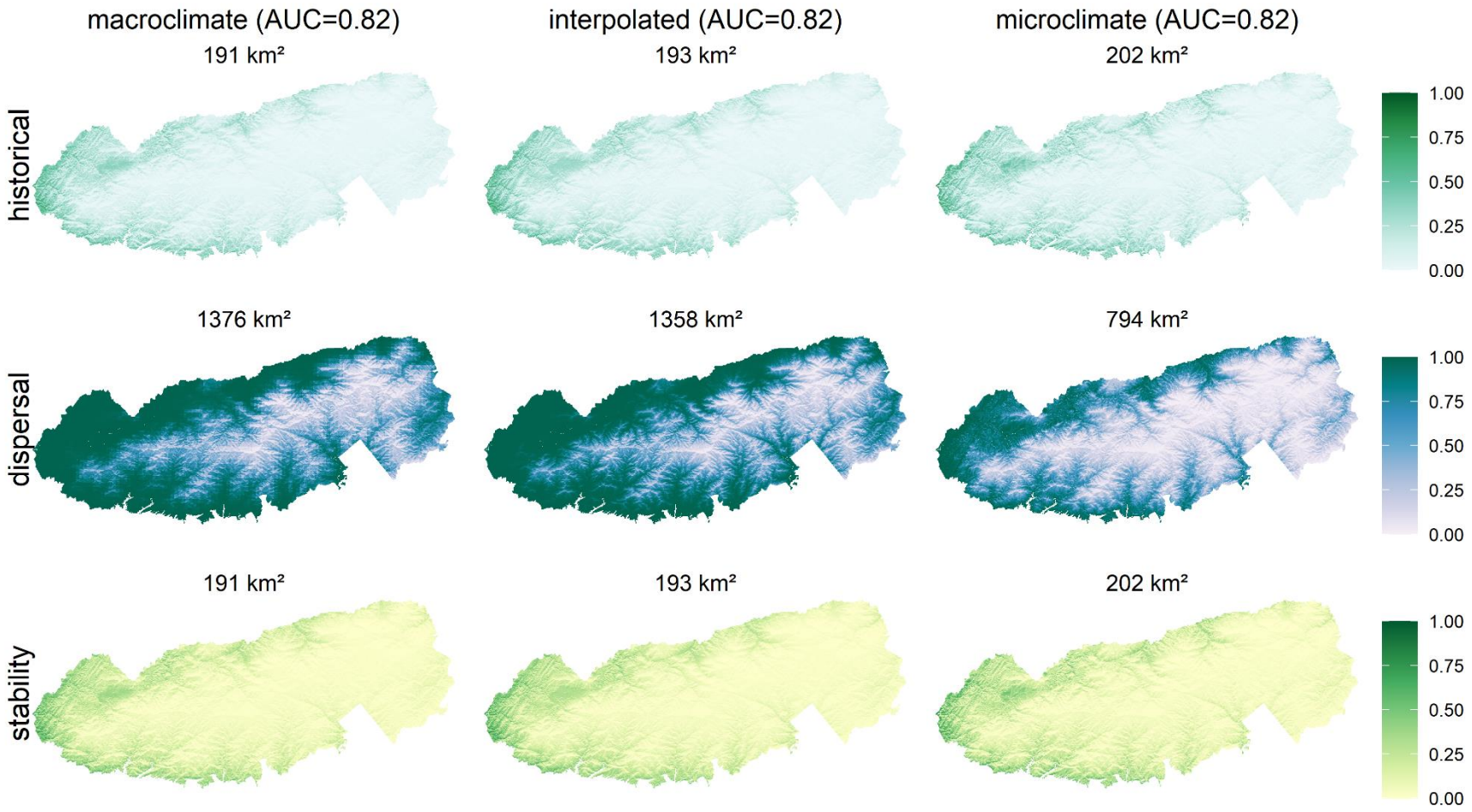

Fig S64. Probability of PROSLAN occurrence

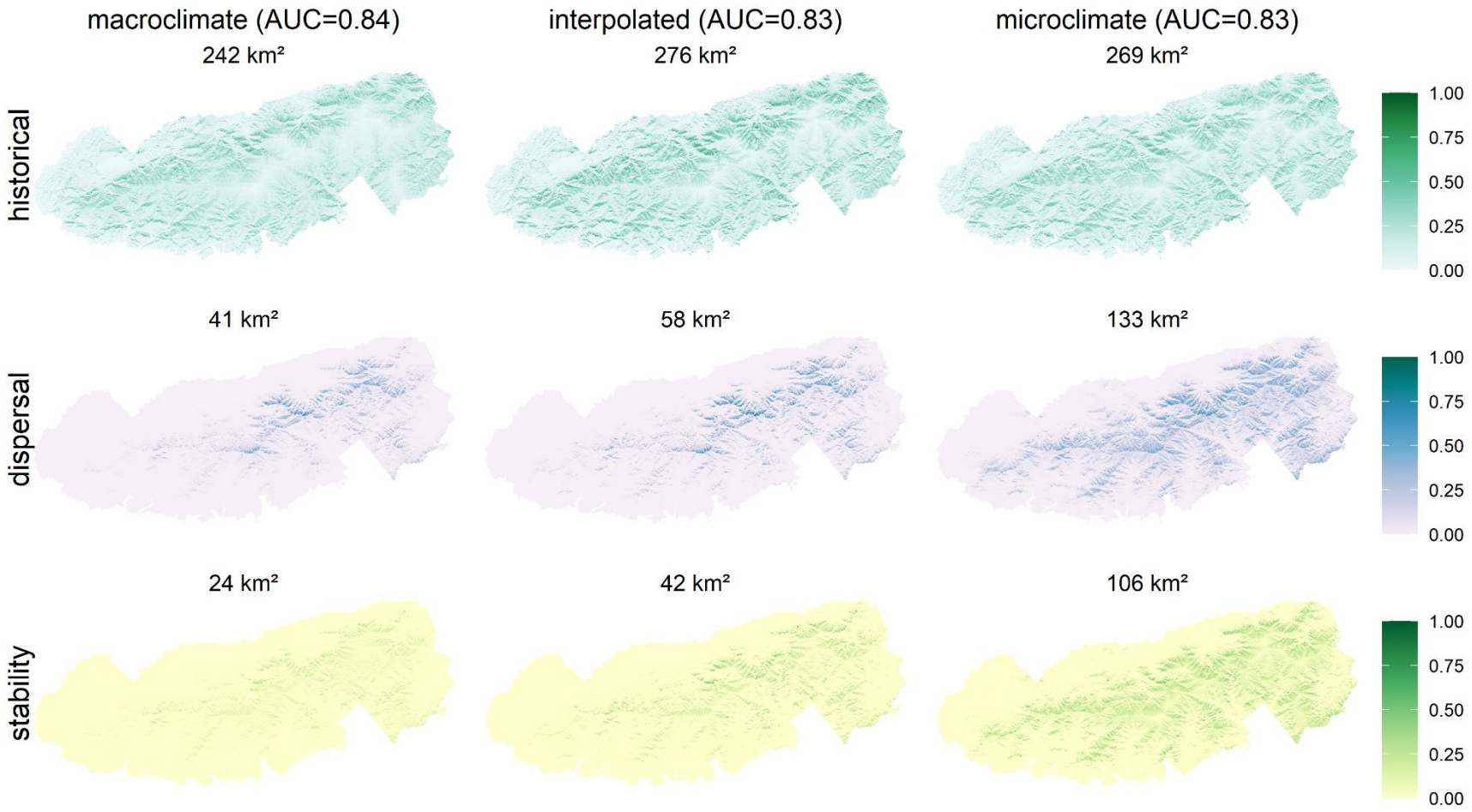

Fig S65. Probability of PRUNPEN occurrence

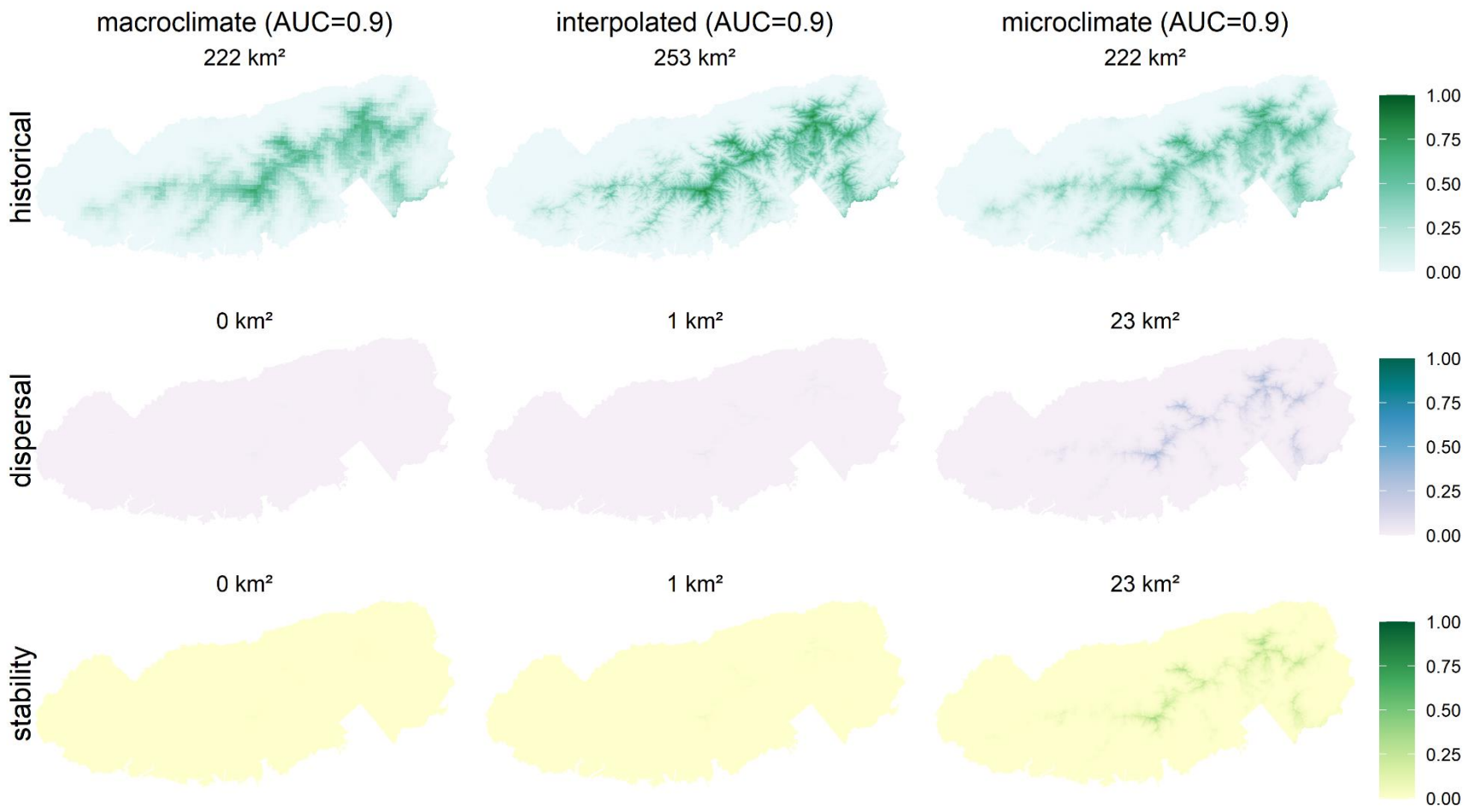

Figs S51 – S65

Jordan R. Stark, Jason Fridley

Fig S51. Probability of NYSSSYL occurrence

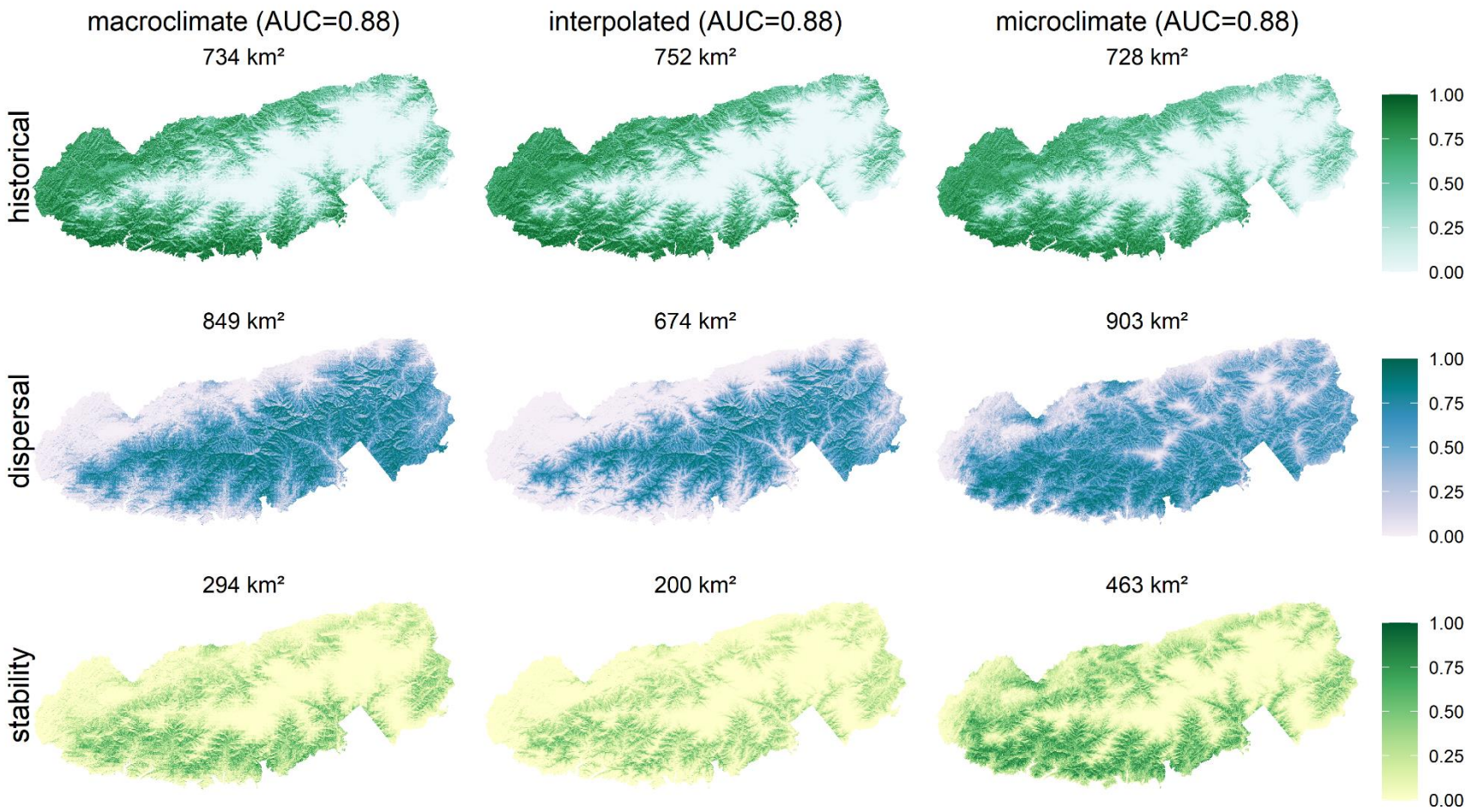

Fig S52. Probability of OSMOCLA occurrence

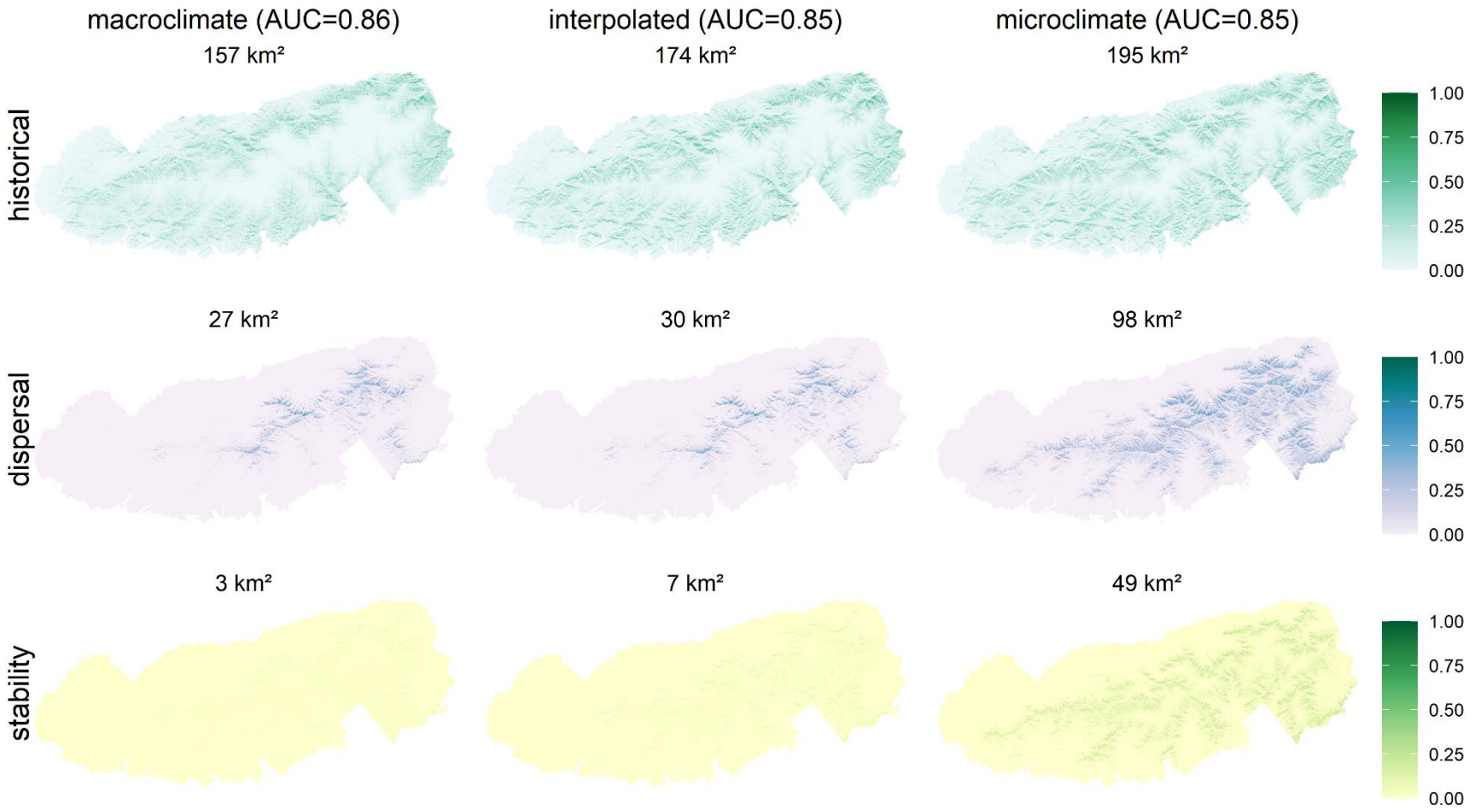

Fig S53. Probability of OXALMON occurrence

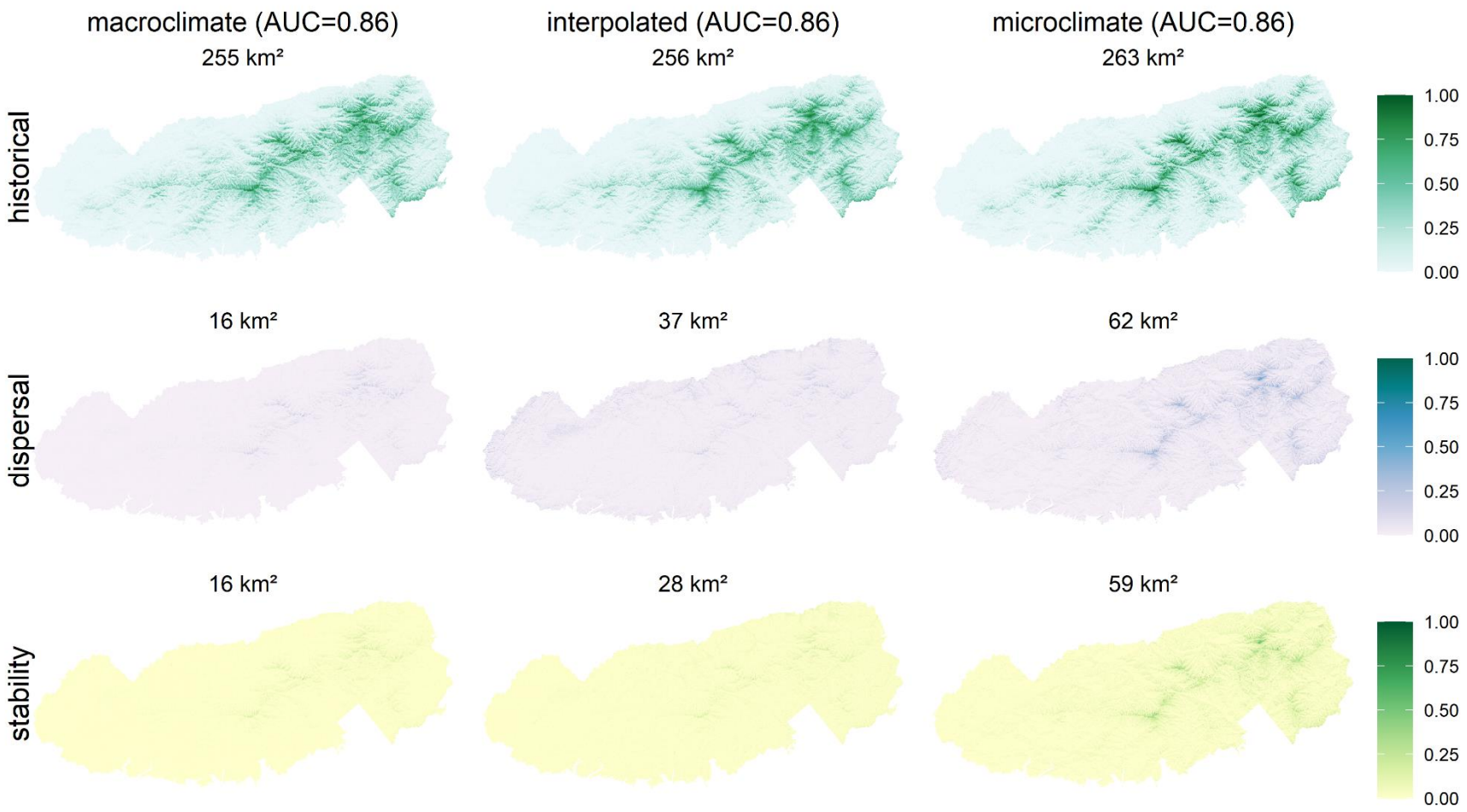

Fig S54. Probability of OXYDARB occurrence

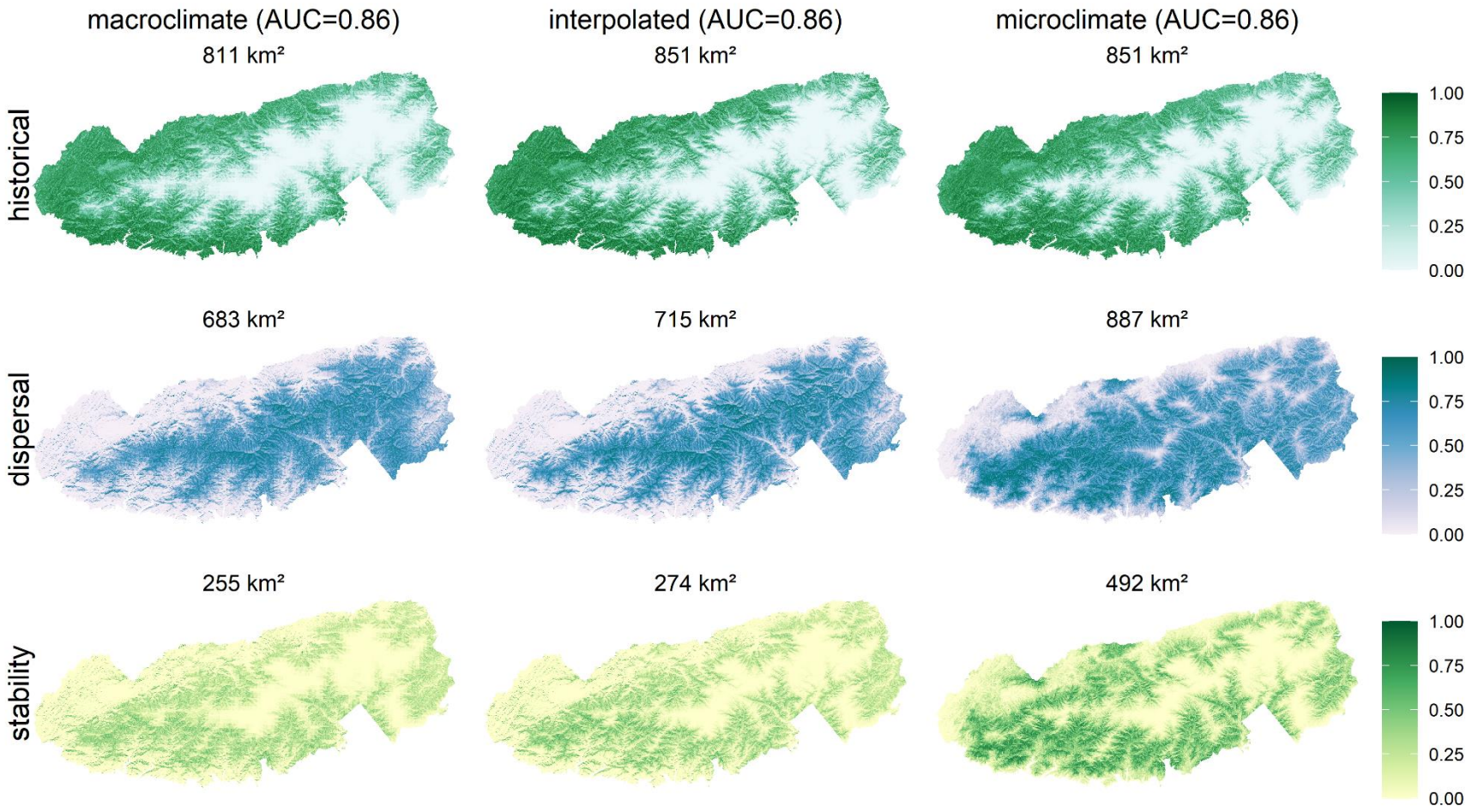

Fig S55. Probability of PARTQUI occurrence

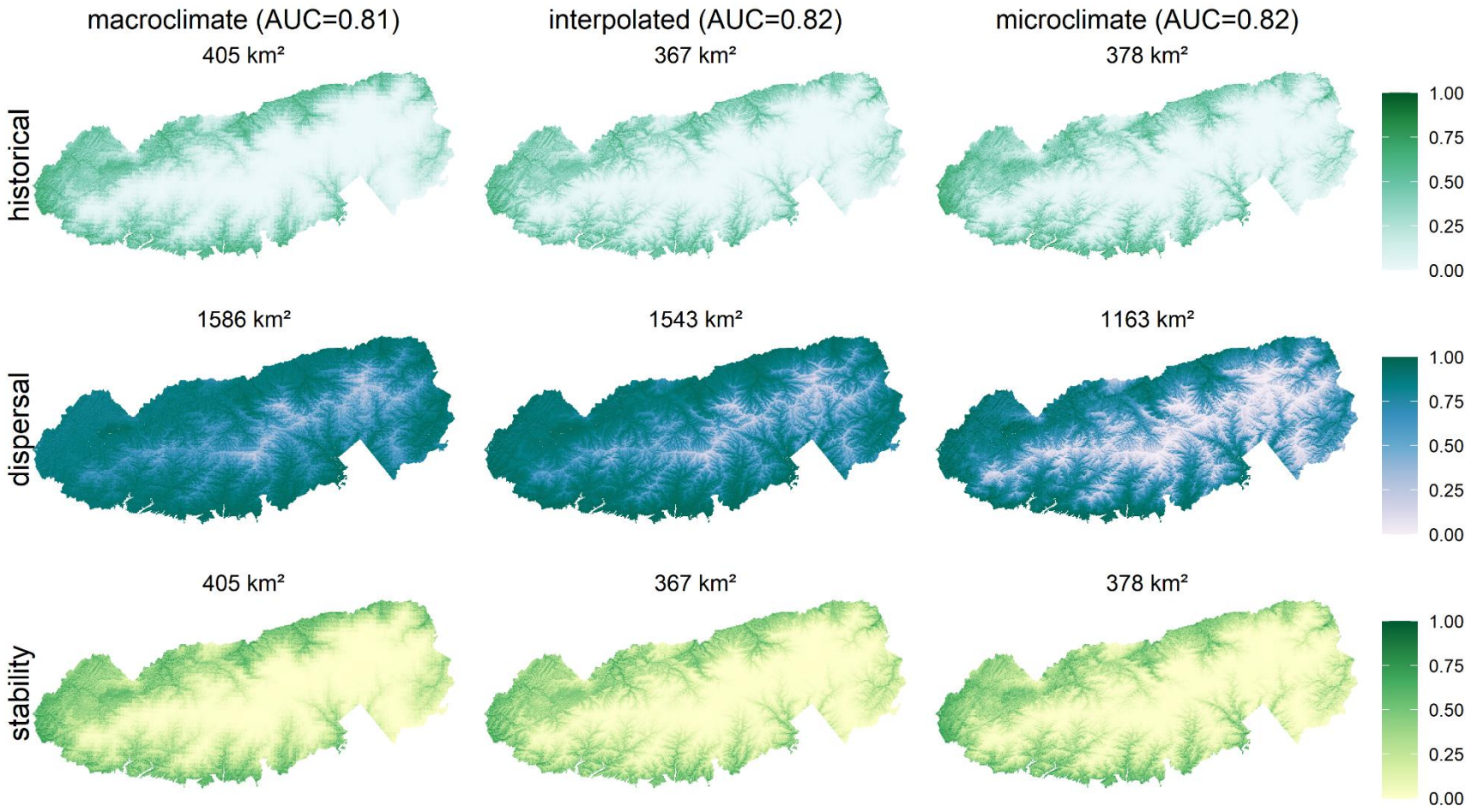

Fig S56. Probability of PHEGHEX occurrence

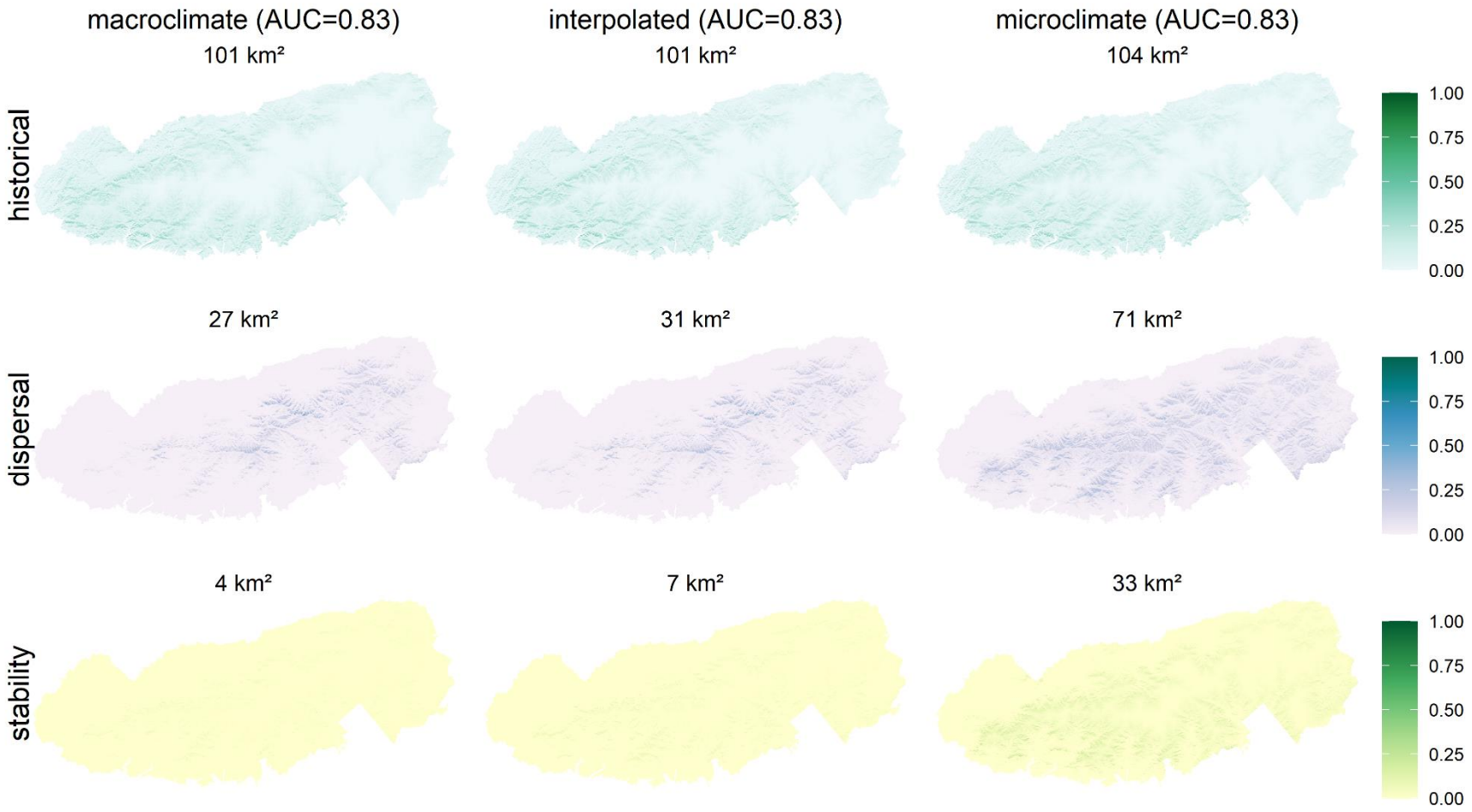

Fig S57. Probability of PICERUB occurrence

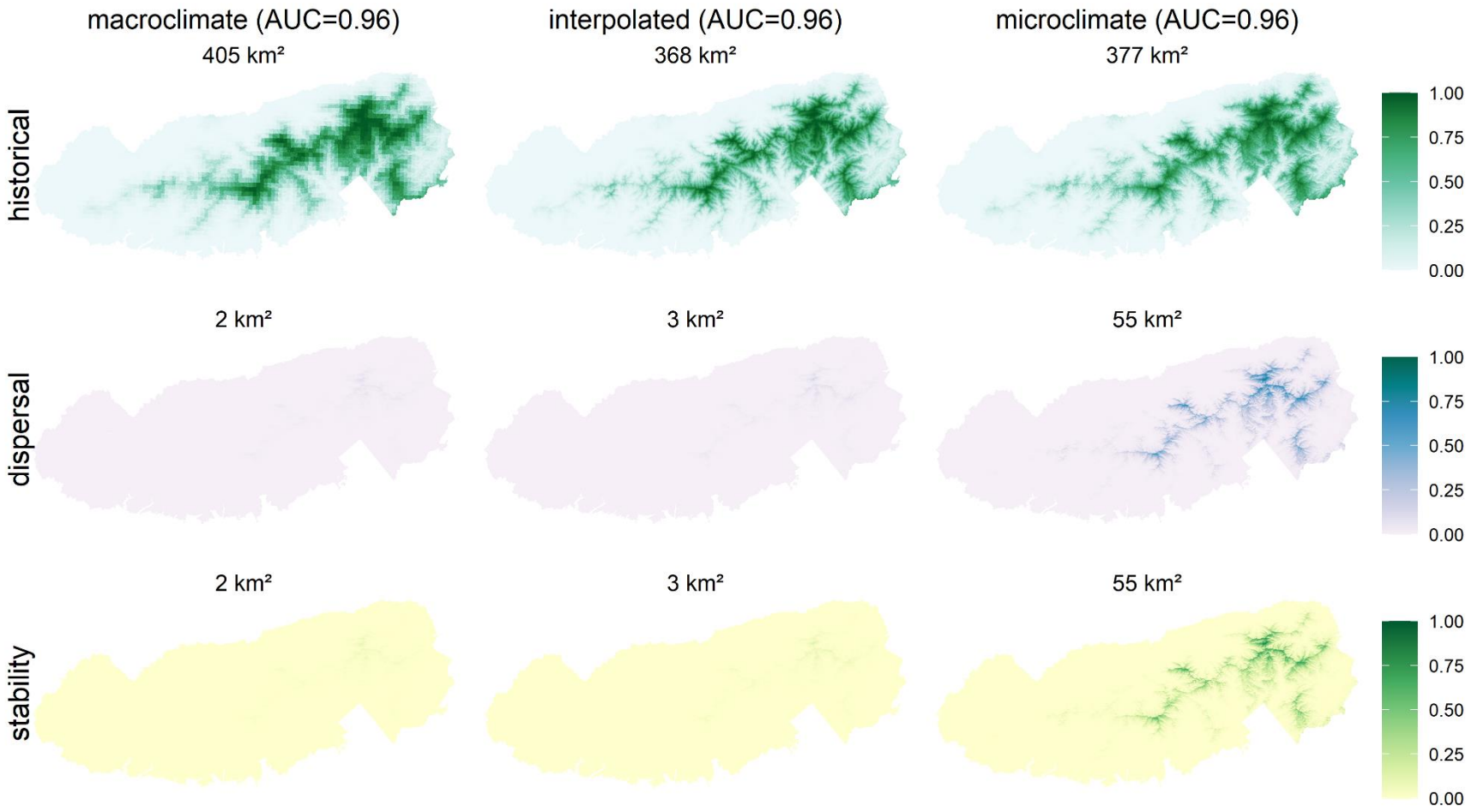

Fig S58. Probability of PINUPUN occurrence

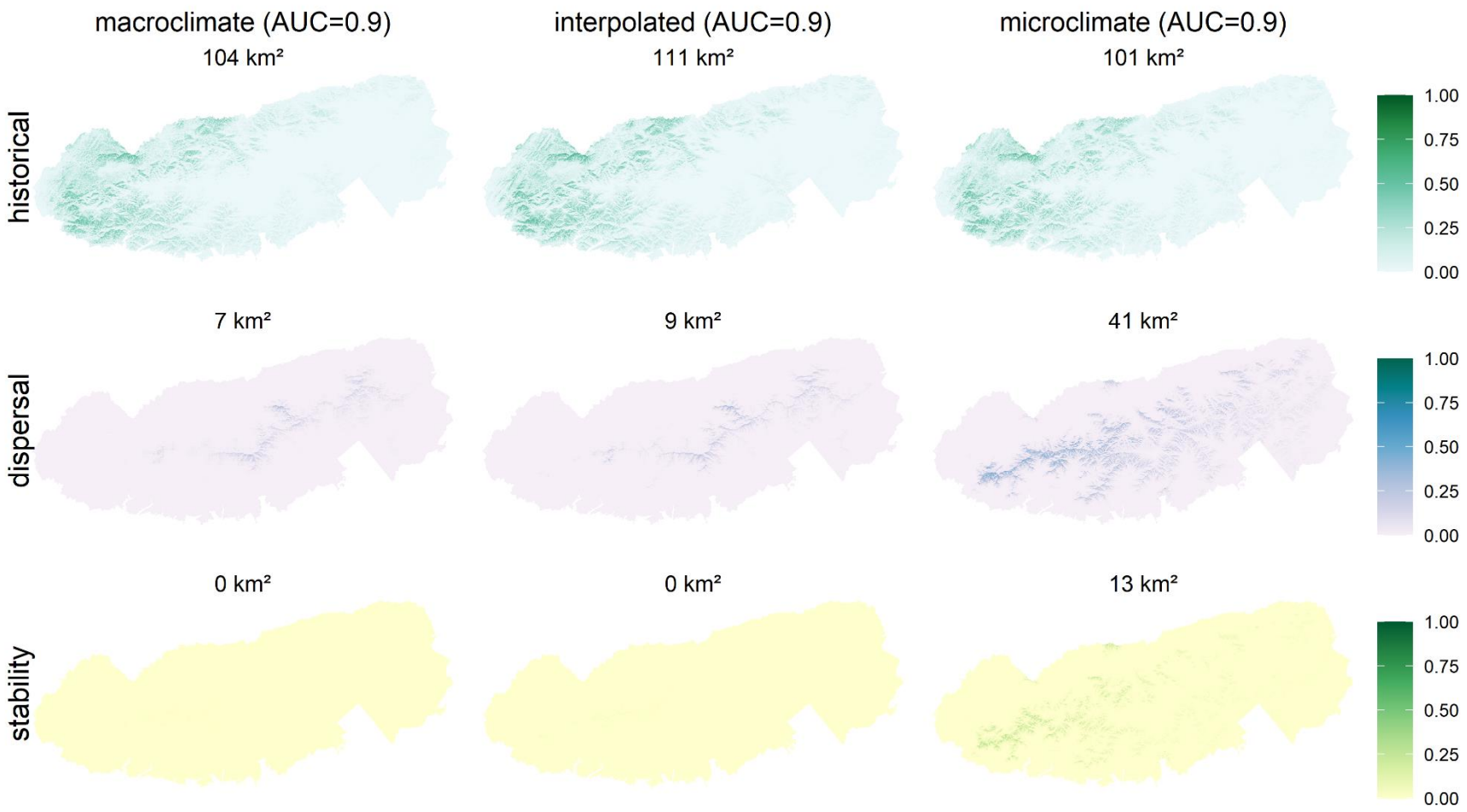

Fig S59. Probability of PINURIG occurrence

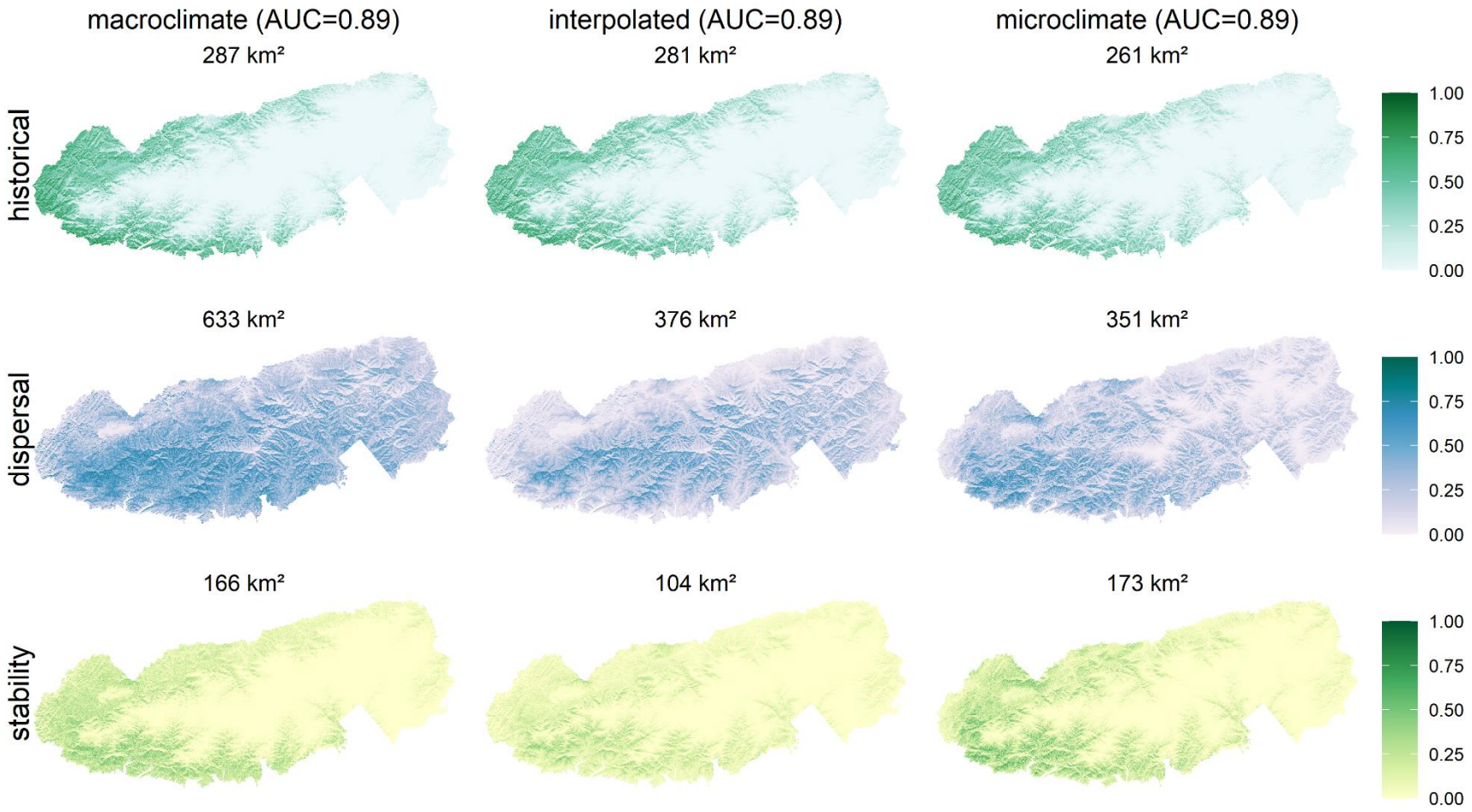

Fig S60. Probability of PINUSTR occurrence

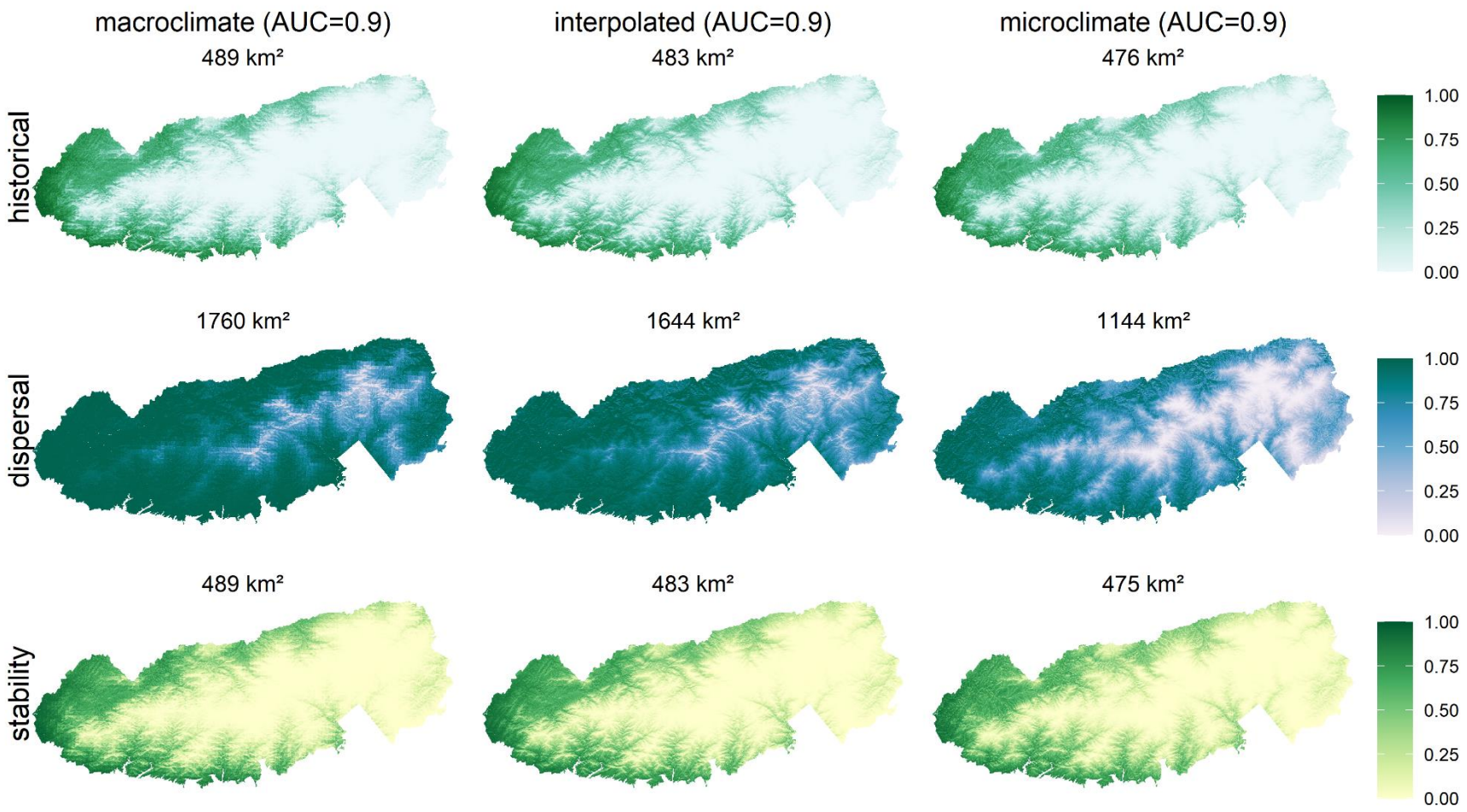

Fig S61. Probability of PINUVIR occurrence

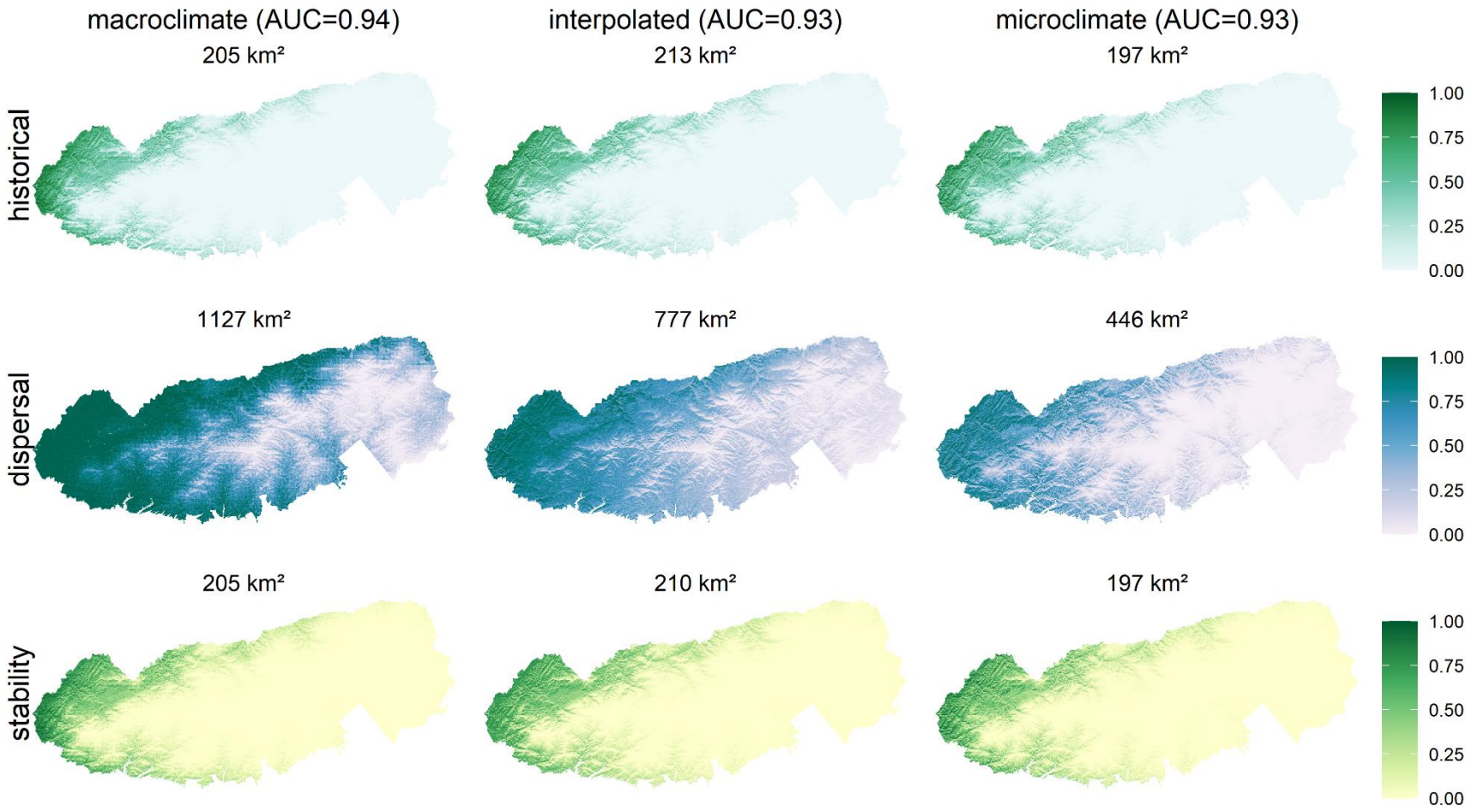

Fig S62. Probability of POLYPUB occurrence

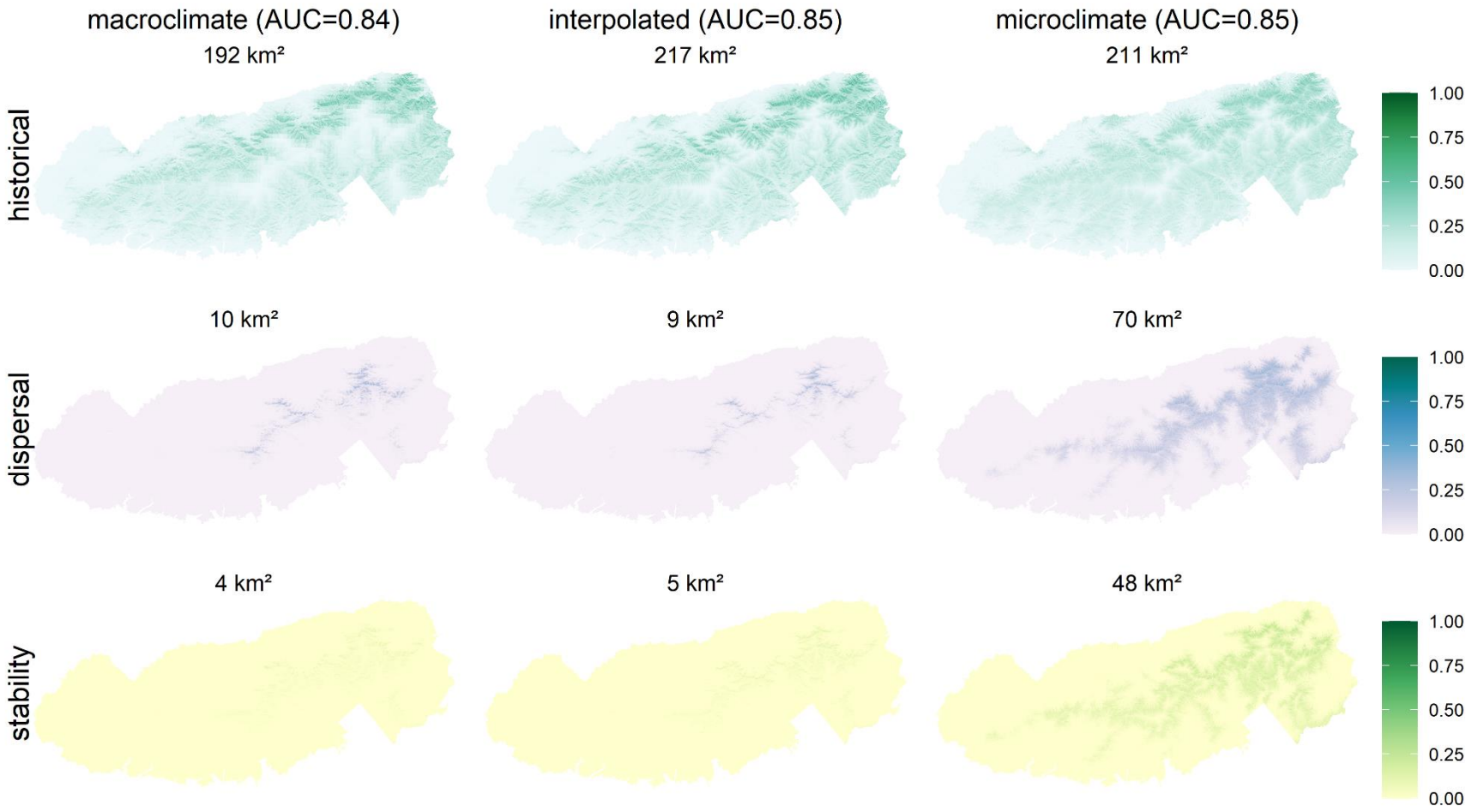

Fig S63. Probability of POTECND occurrence

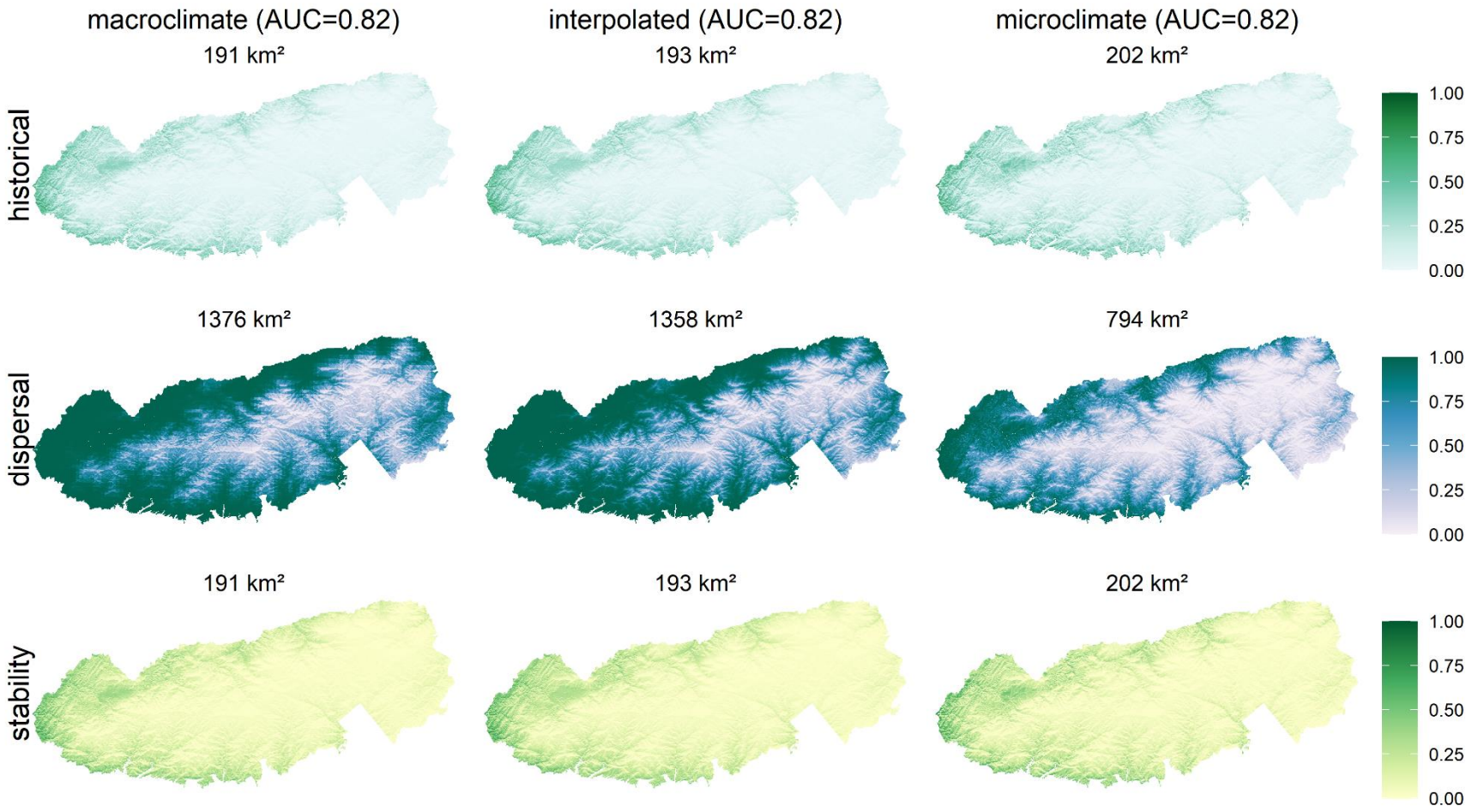

Fig S64. Probability of PROSLAN occurrence

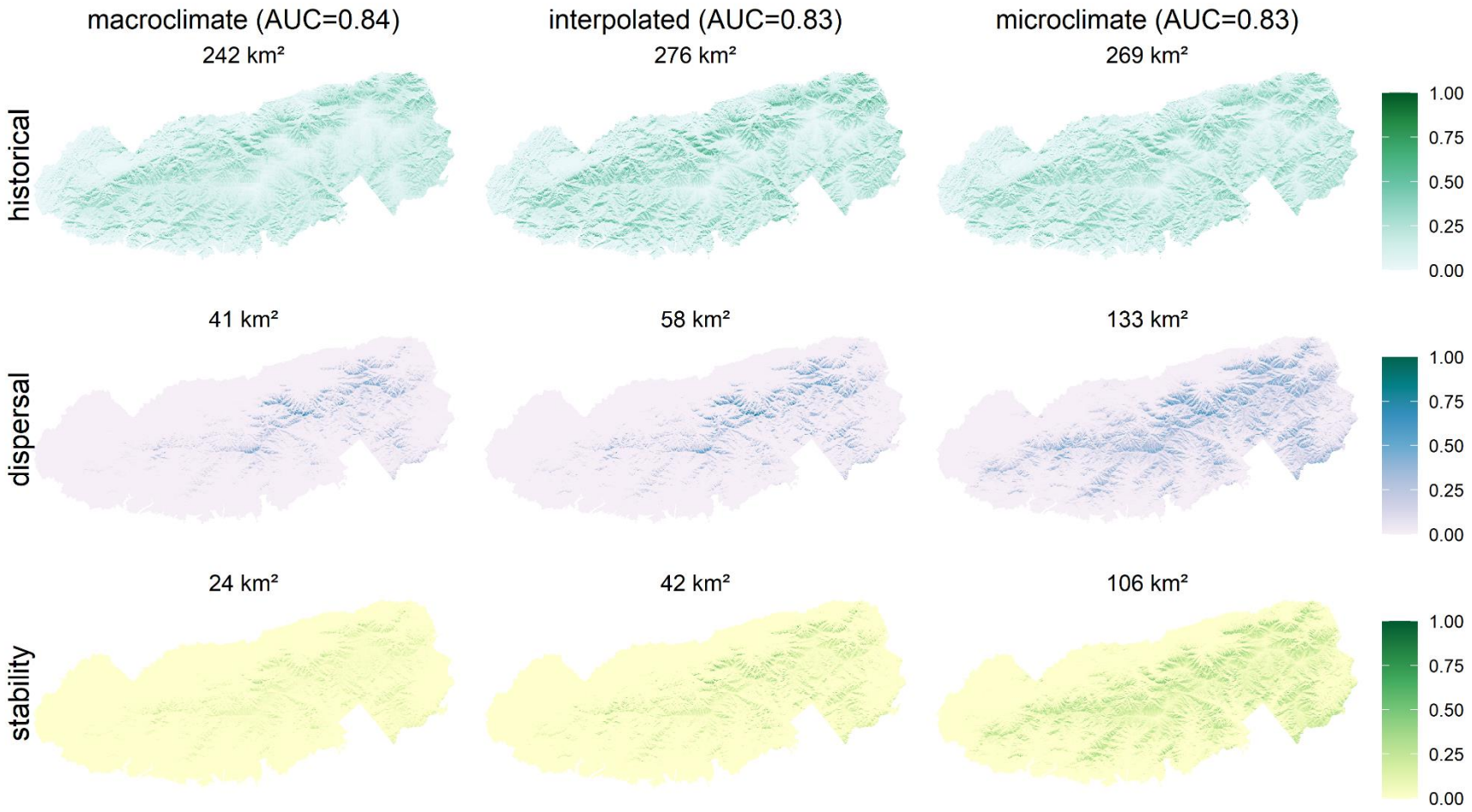

Fig S65. Probability of PRUNPEN occurrence

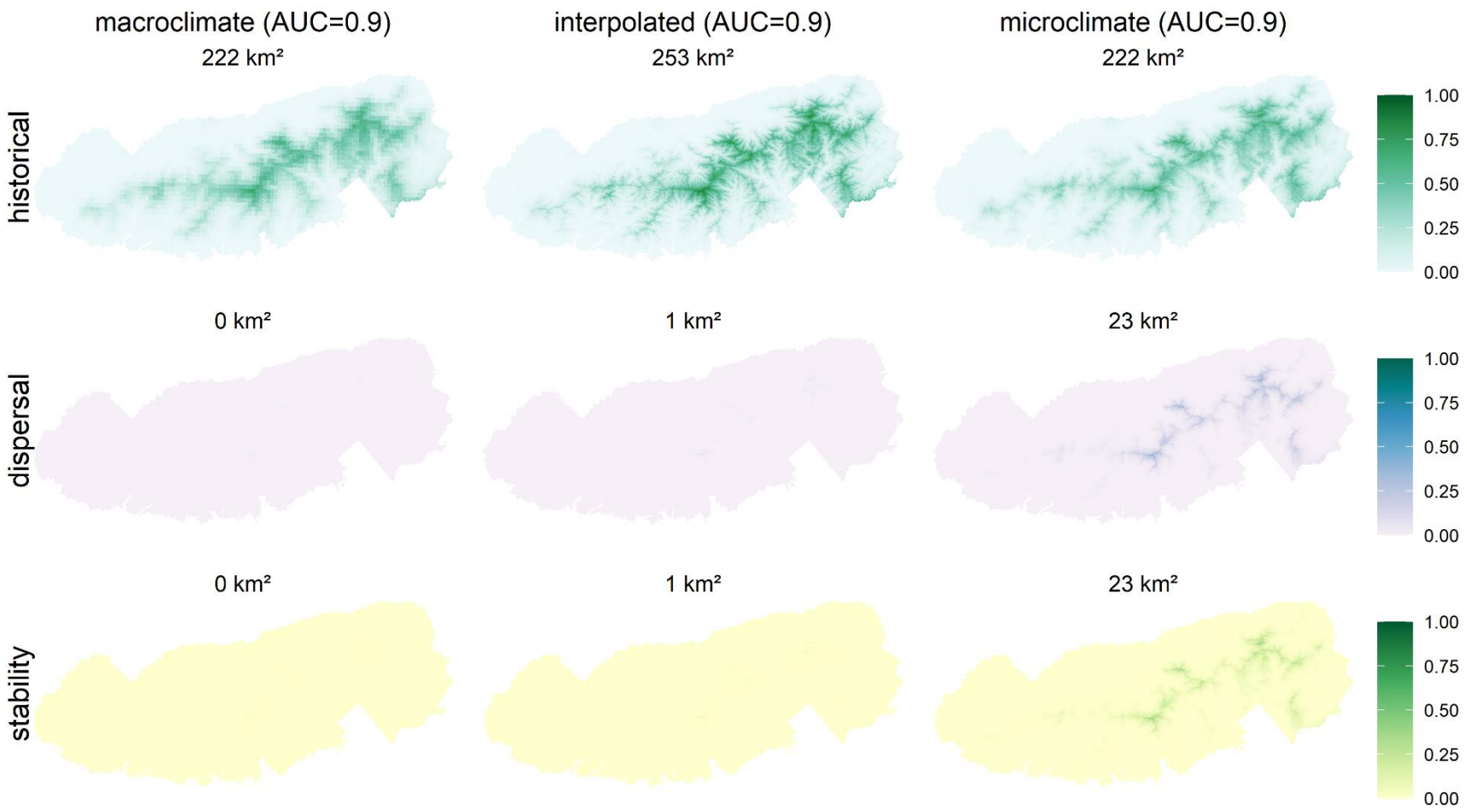

Fig S66. Probability of PTERAQU occurrence

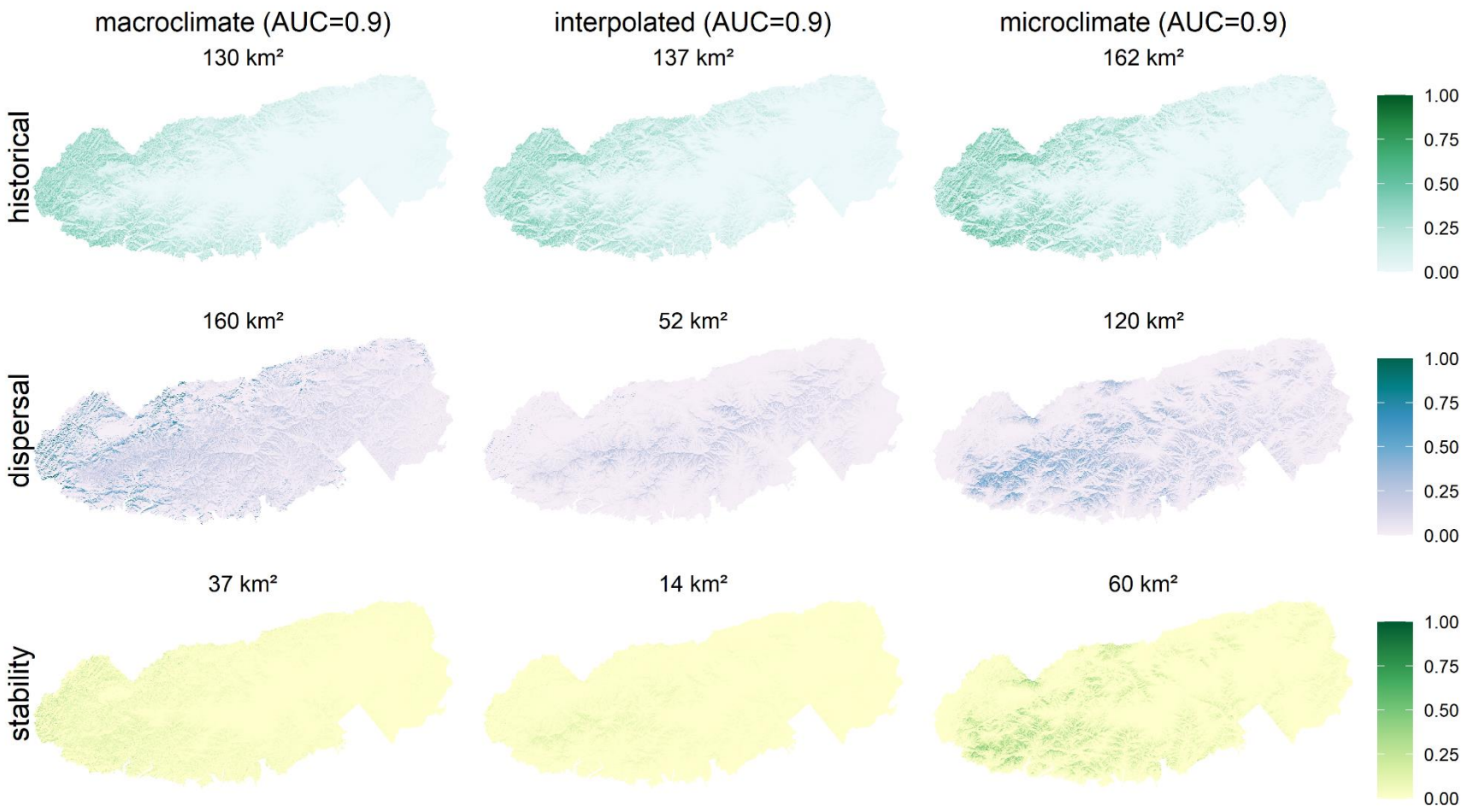

Fig S67. Probability of QUERALB occurrence

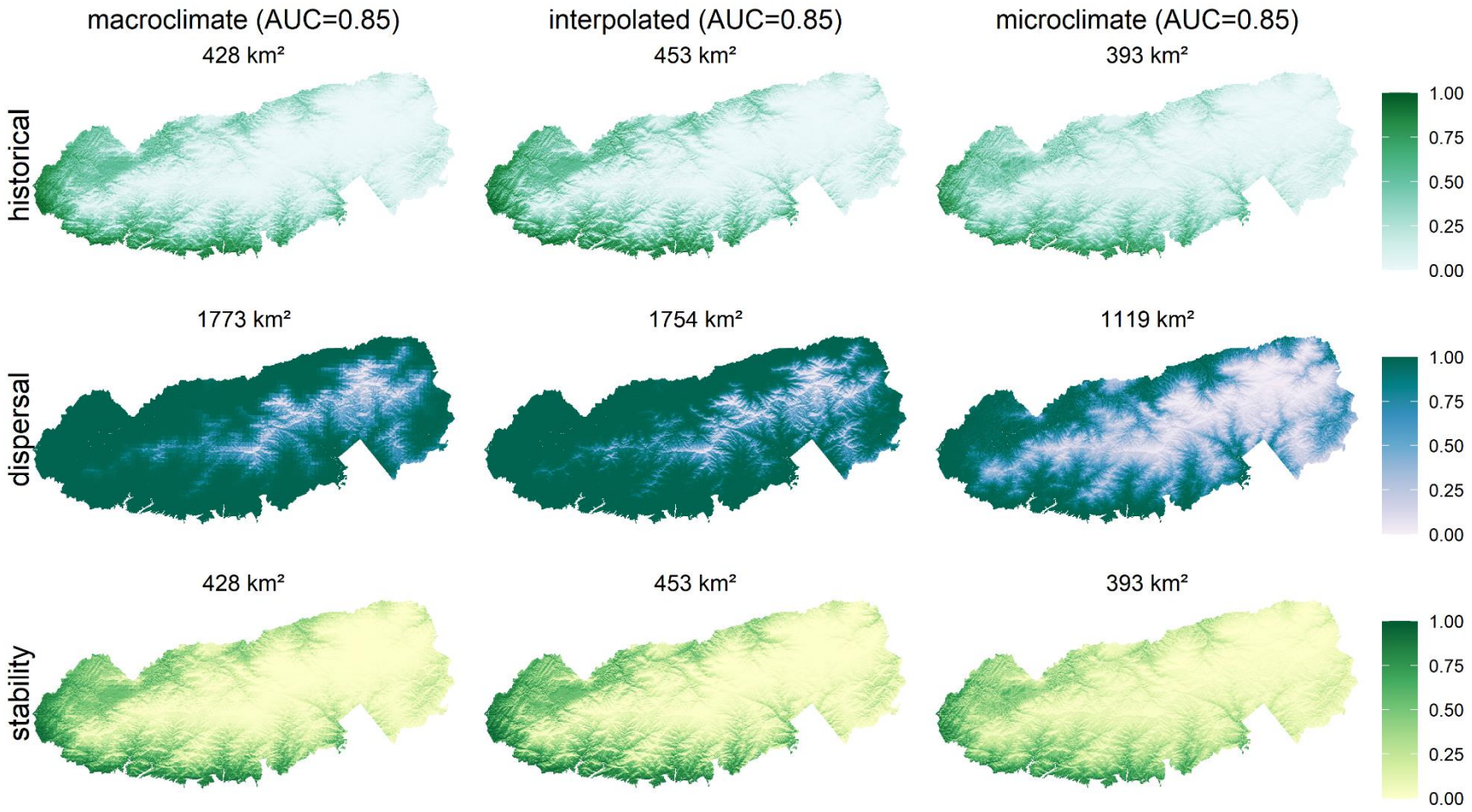

Fig S68. Probability of QUERCOCC occurrence

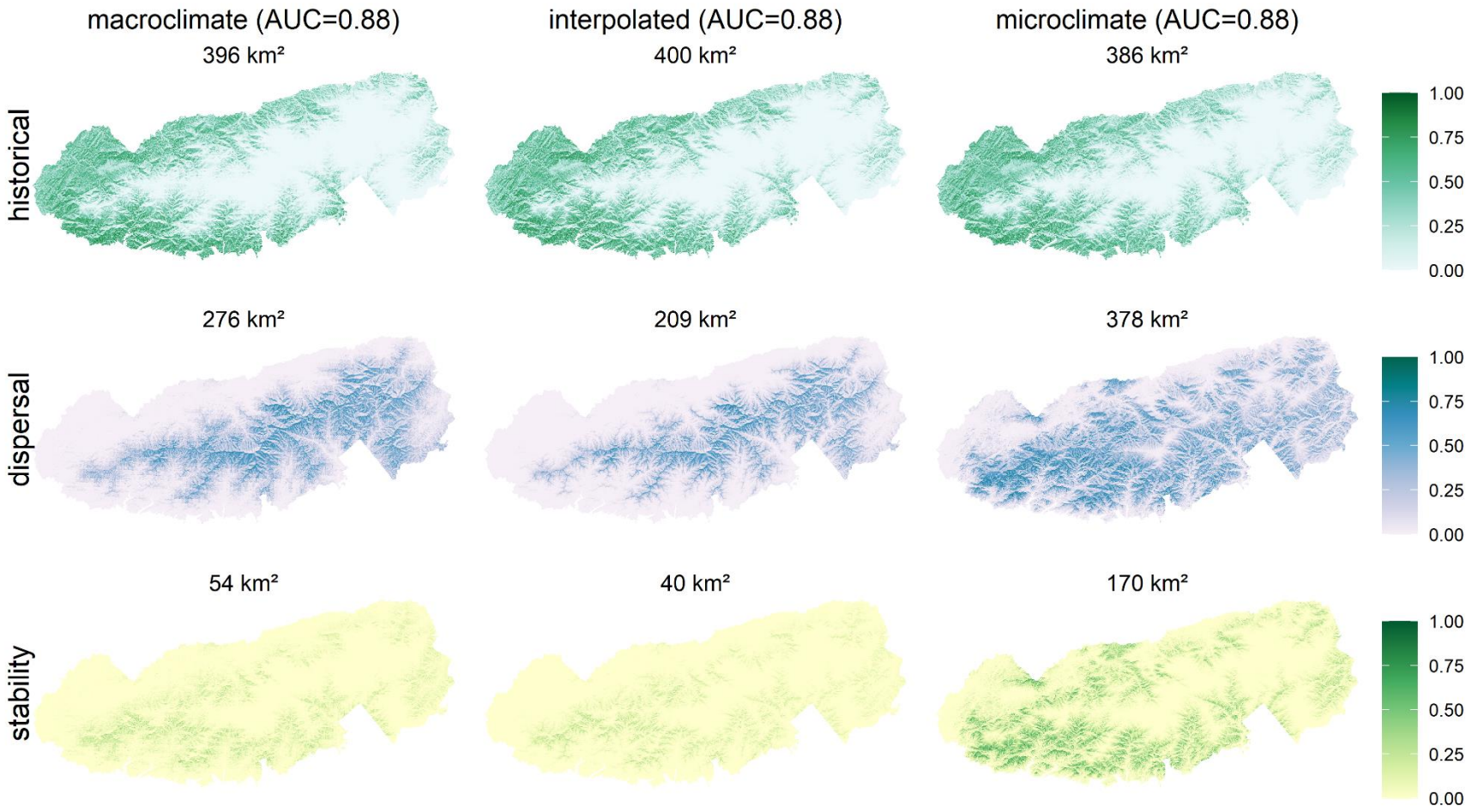

Fig S69. Probability of QUERMON occurrence

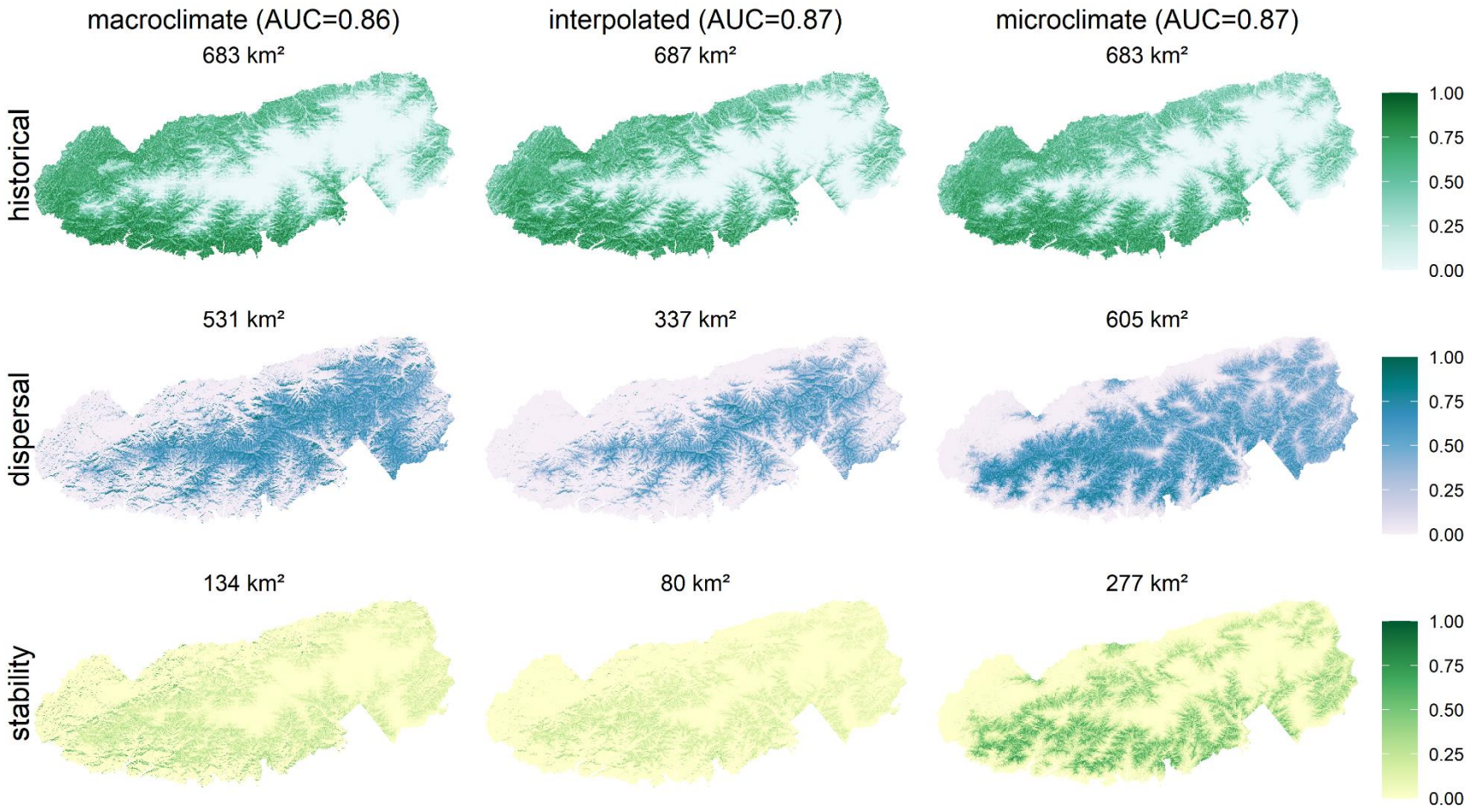

Fig S70. Probability of QUERVEL occurrence

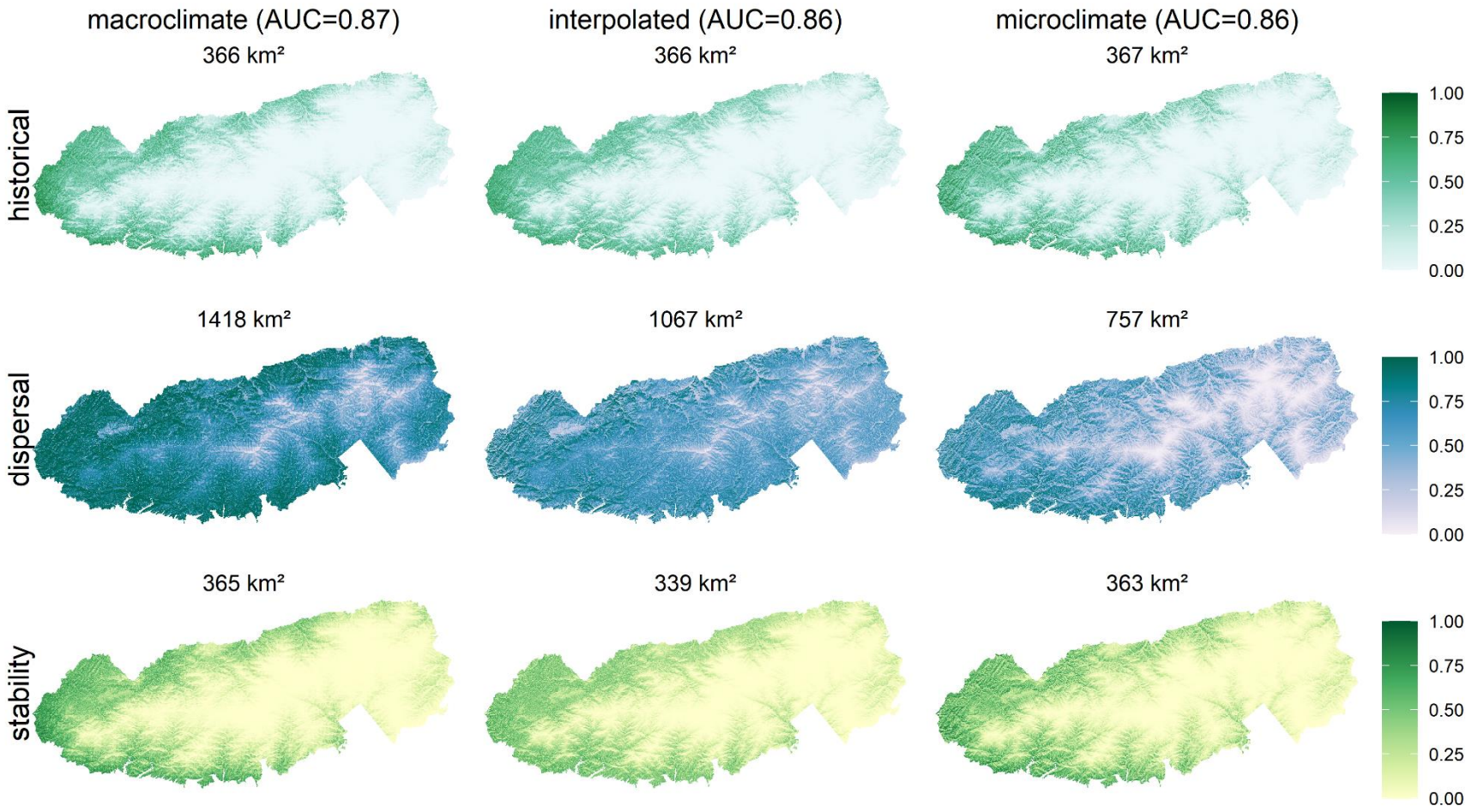

Fig S71. Probability of SANGCND occurrence

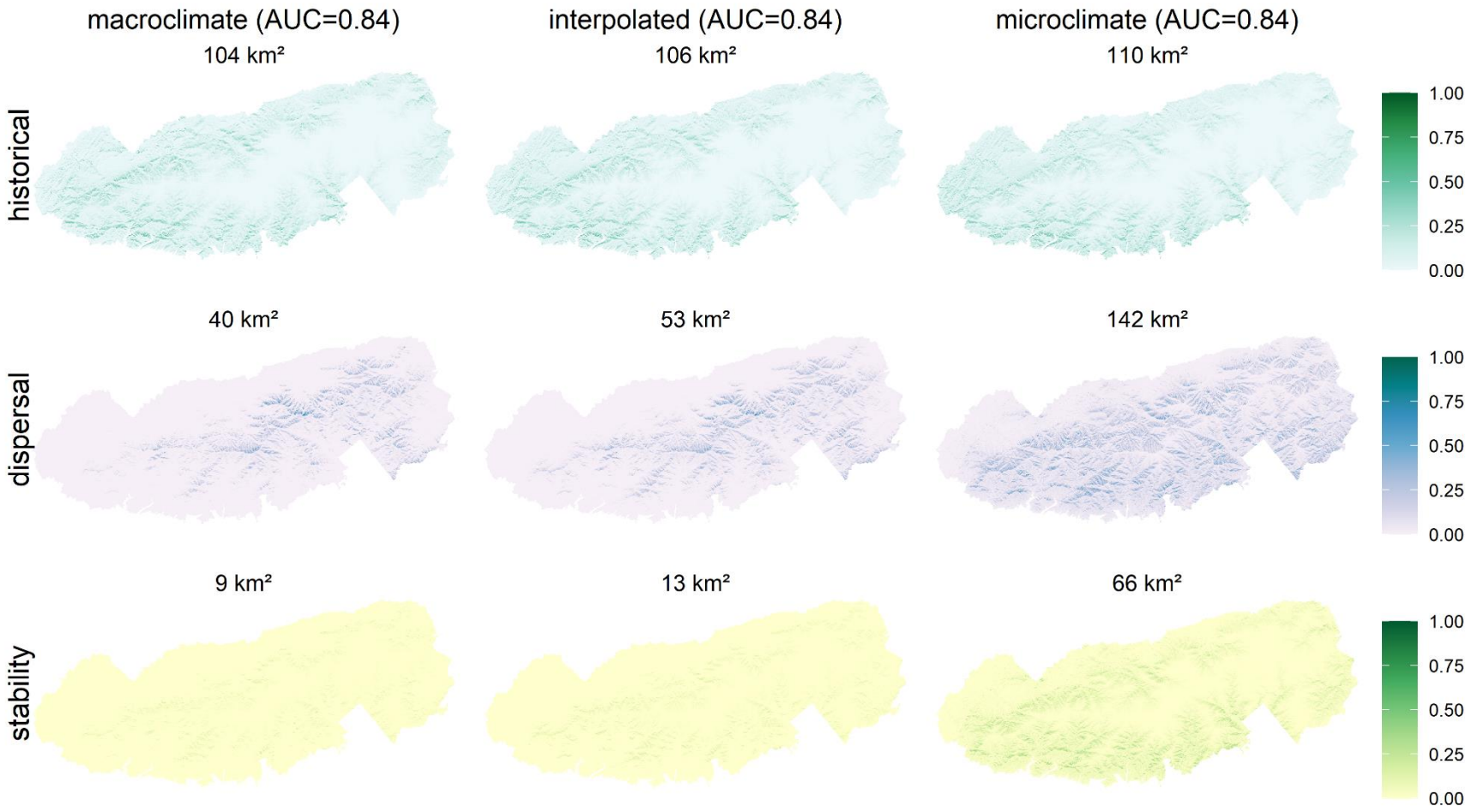

Fig S72. Probability of SANICANC occurrence

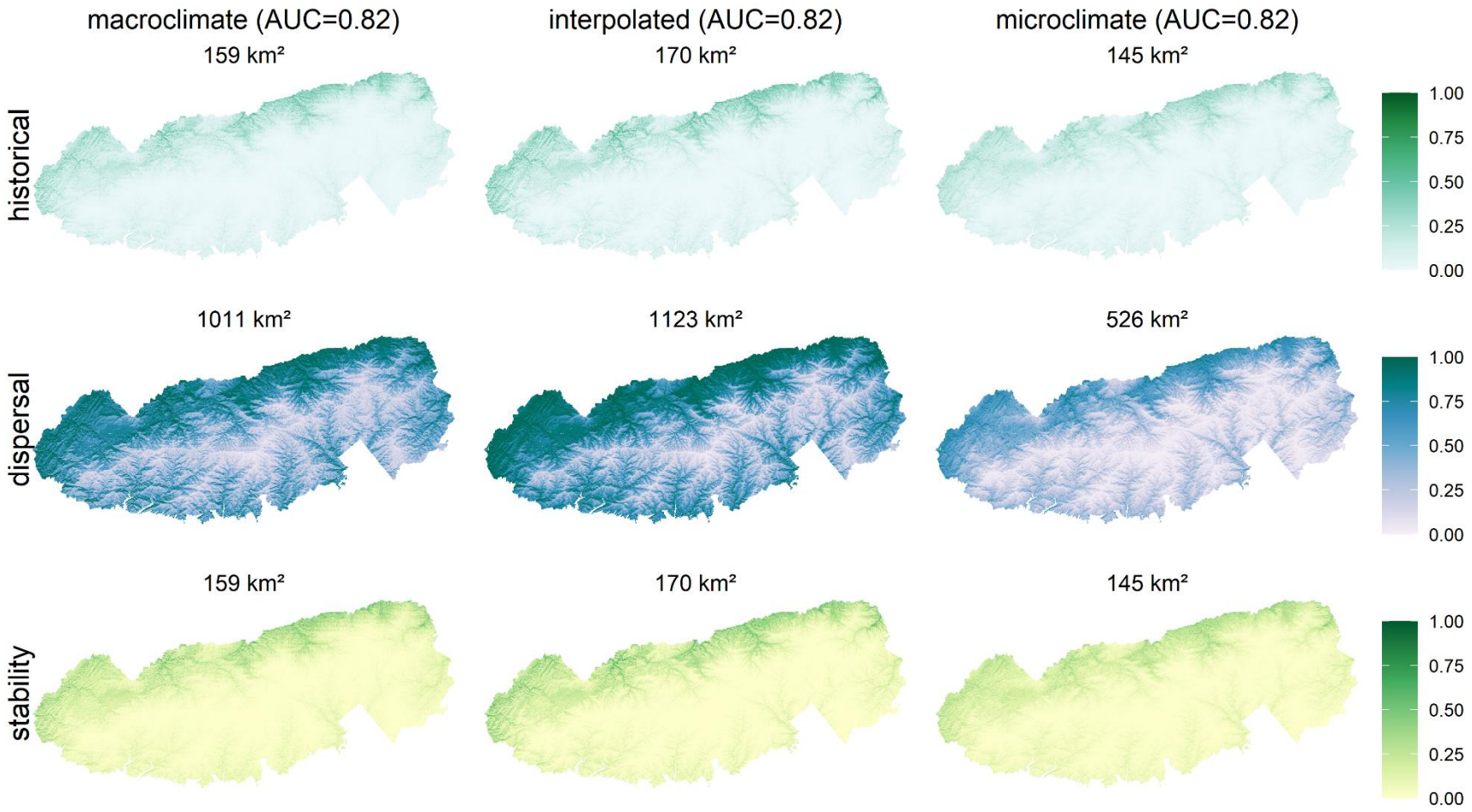

Fig S73. Probability of SASSALB occurrence

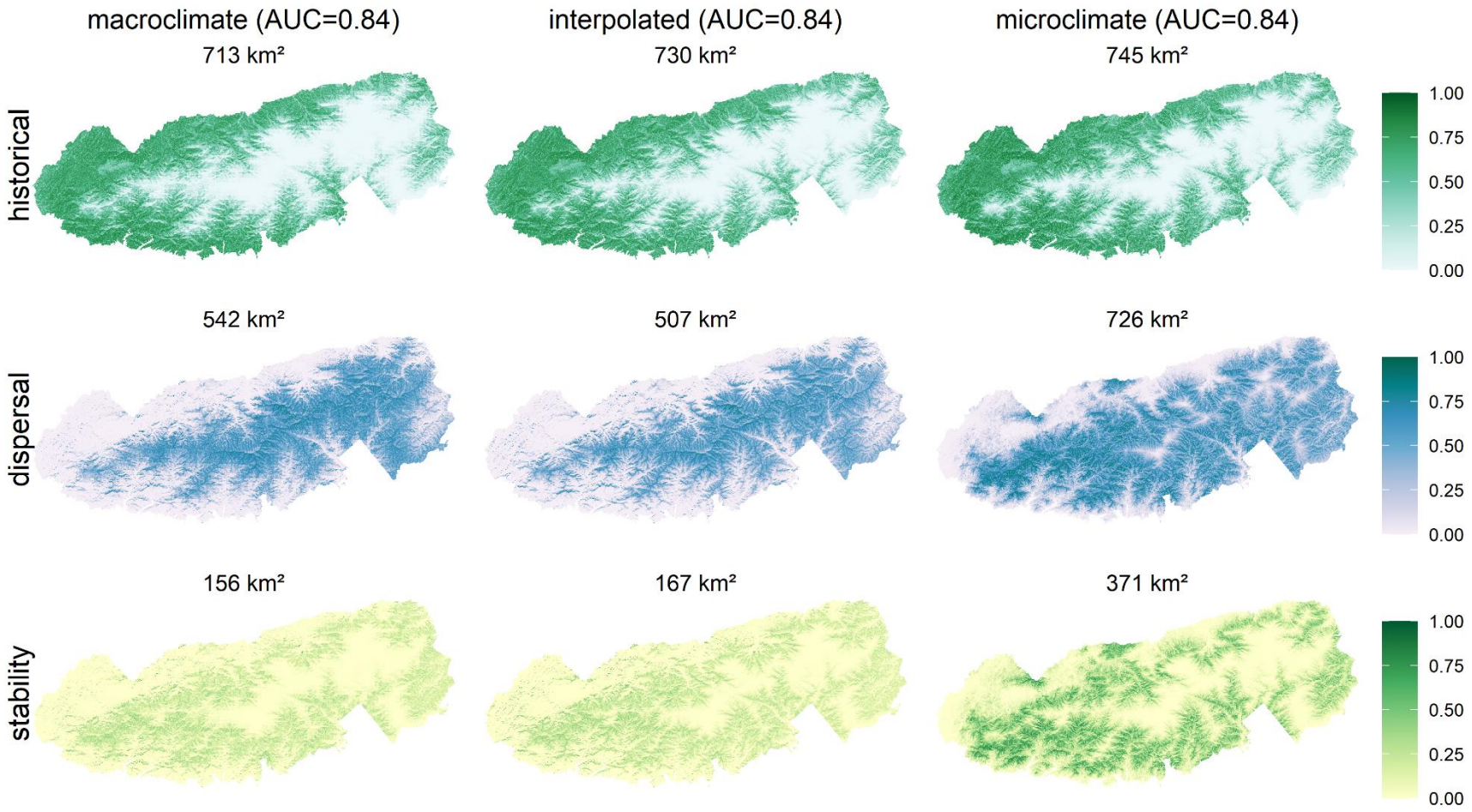

Fig S74. Probability of SMILGLA occurrence

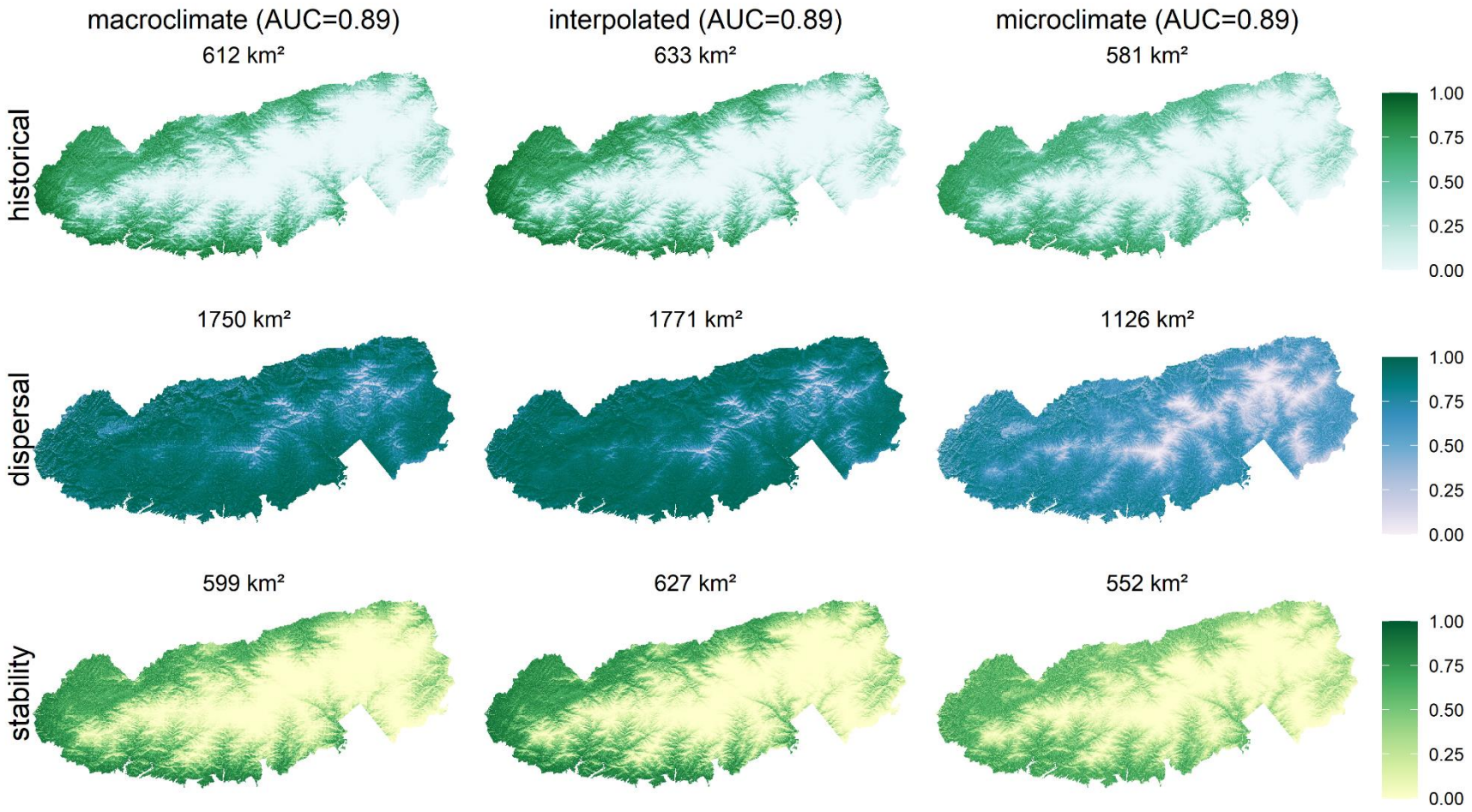

Fig S75. Probability of SMILHER occurrence

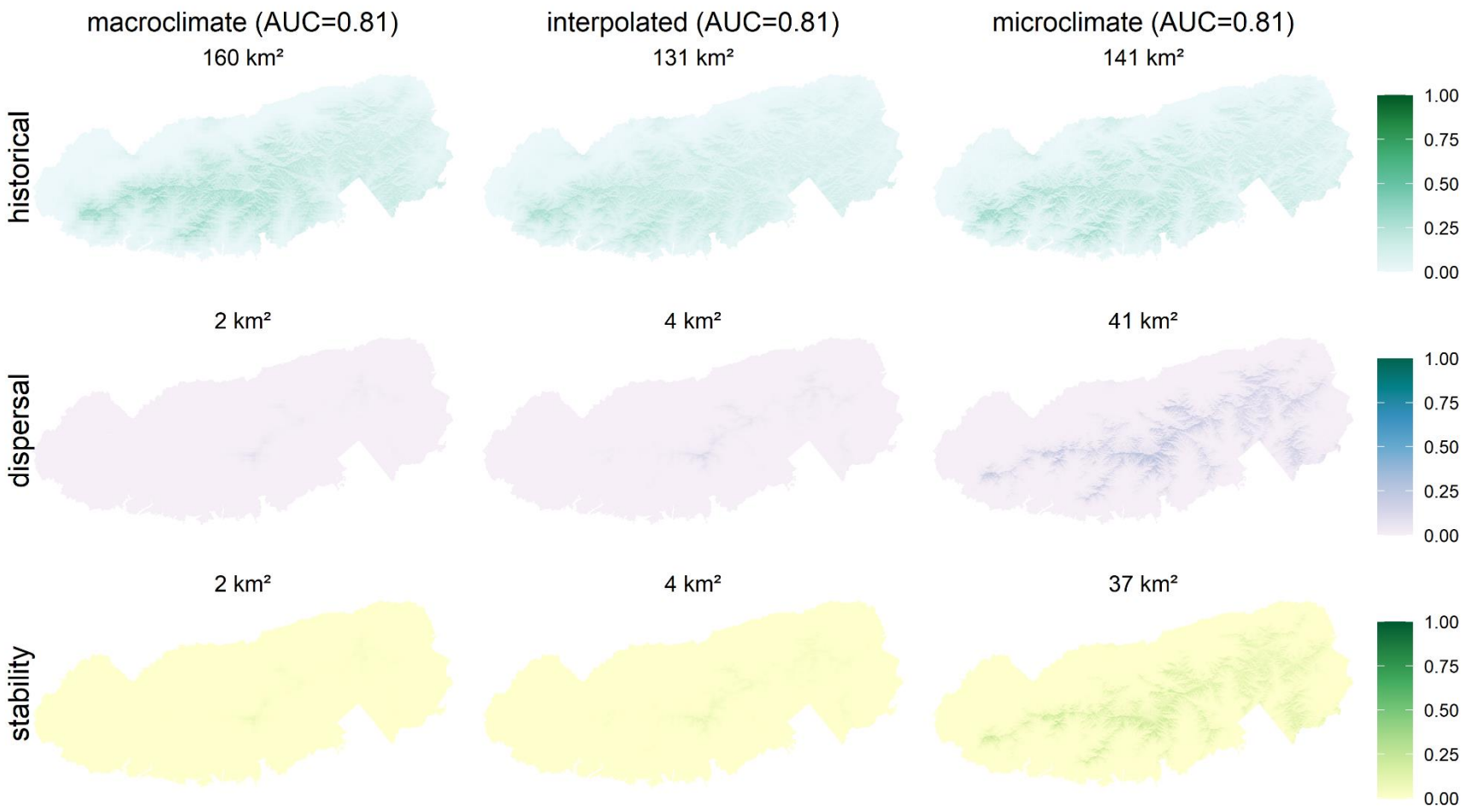

Fig S76. Probability of SMILROT occurrence

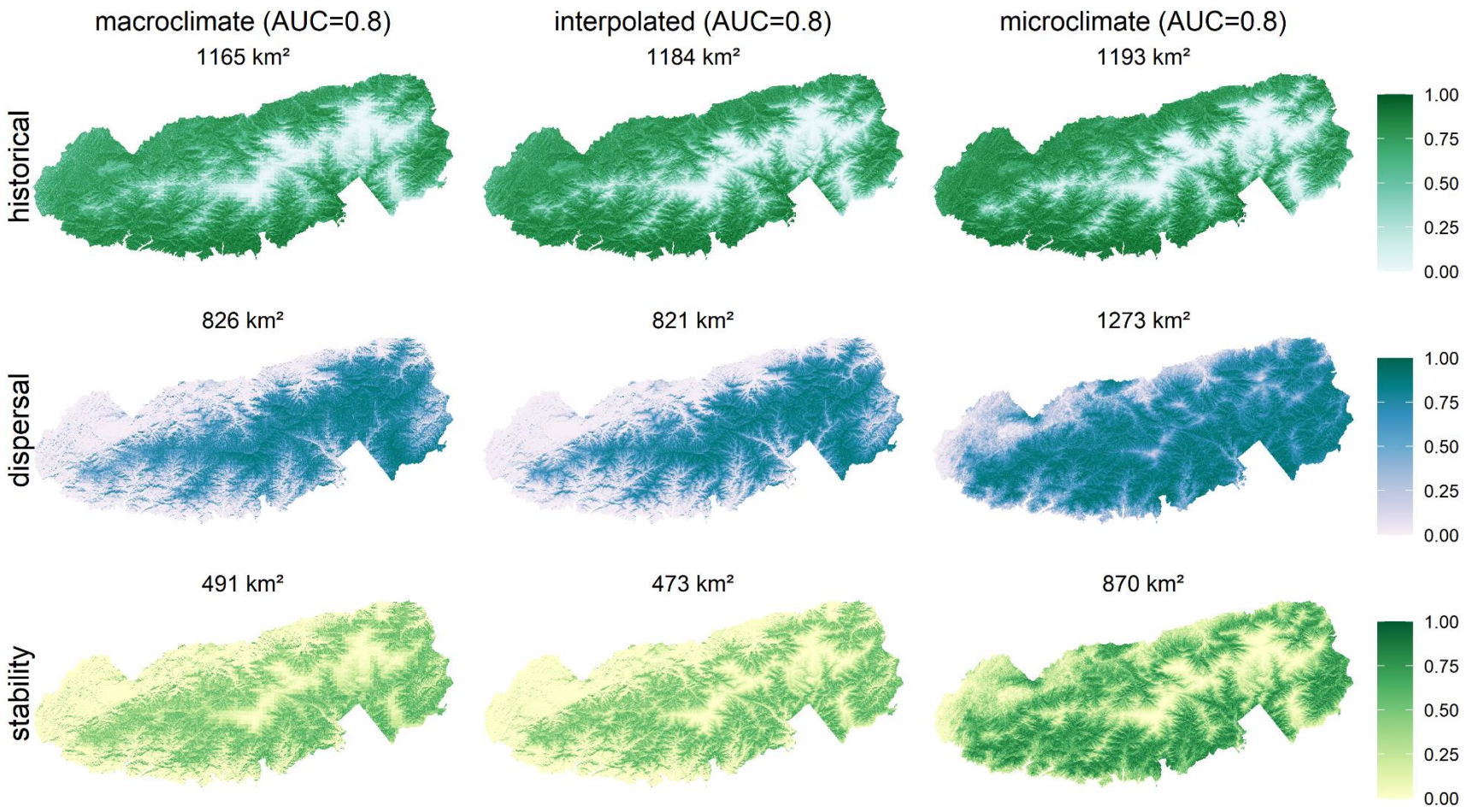

Fig S77. Probability of SMILTMN occurrence

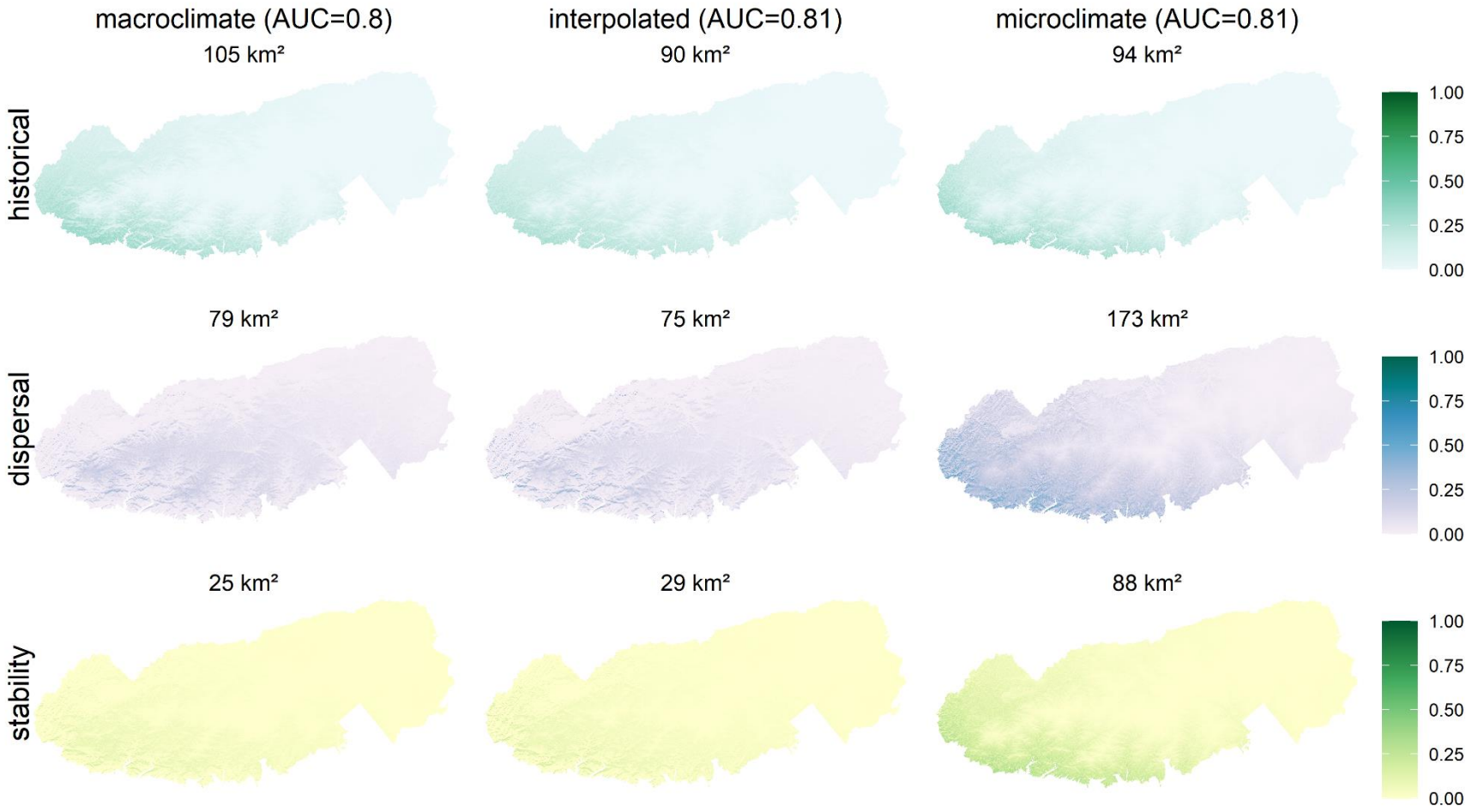

Fig S78. Probability of STELPBR occurrence

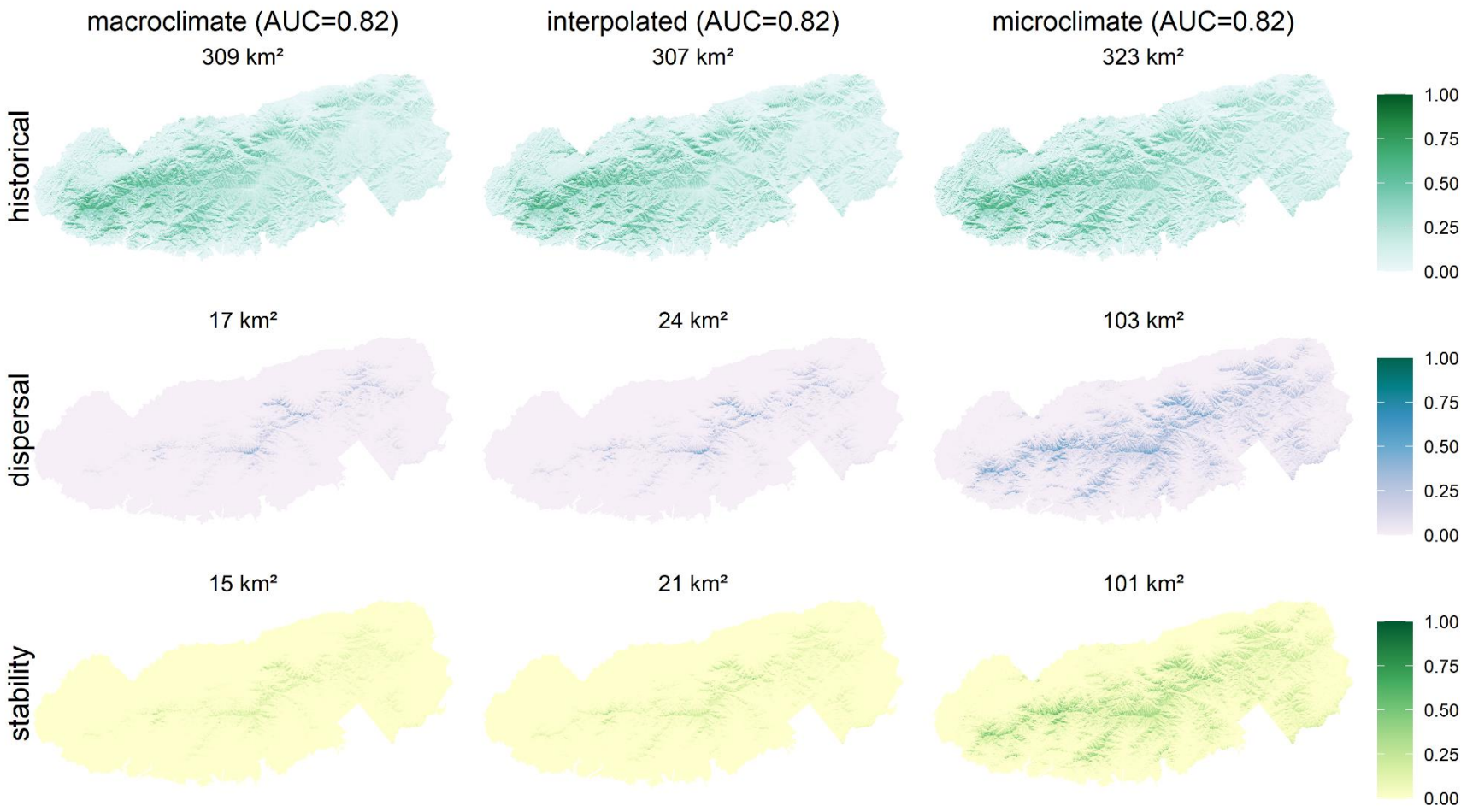

Fig S79. Probability of THALTHA occurrence

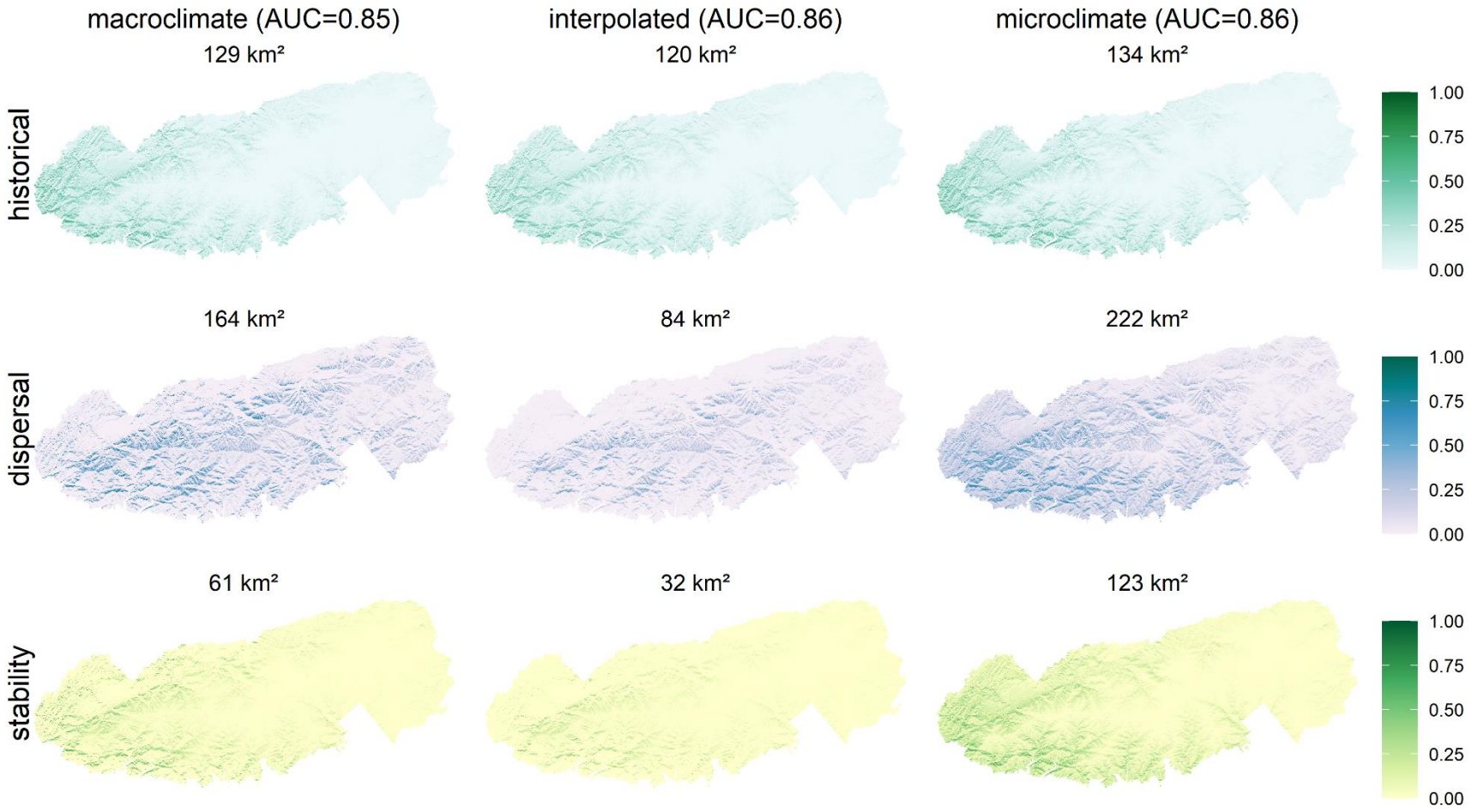

Fig S80. Probability of TIARCOR occurrence

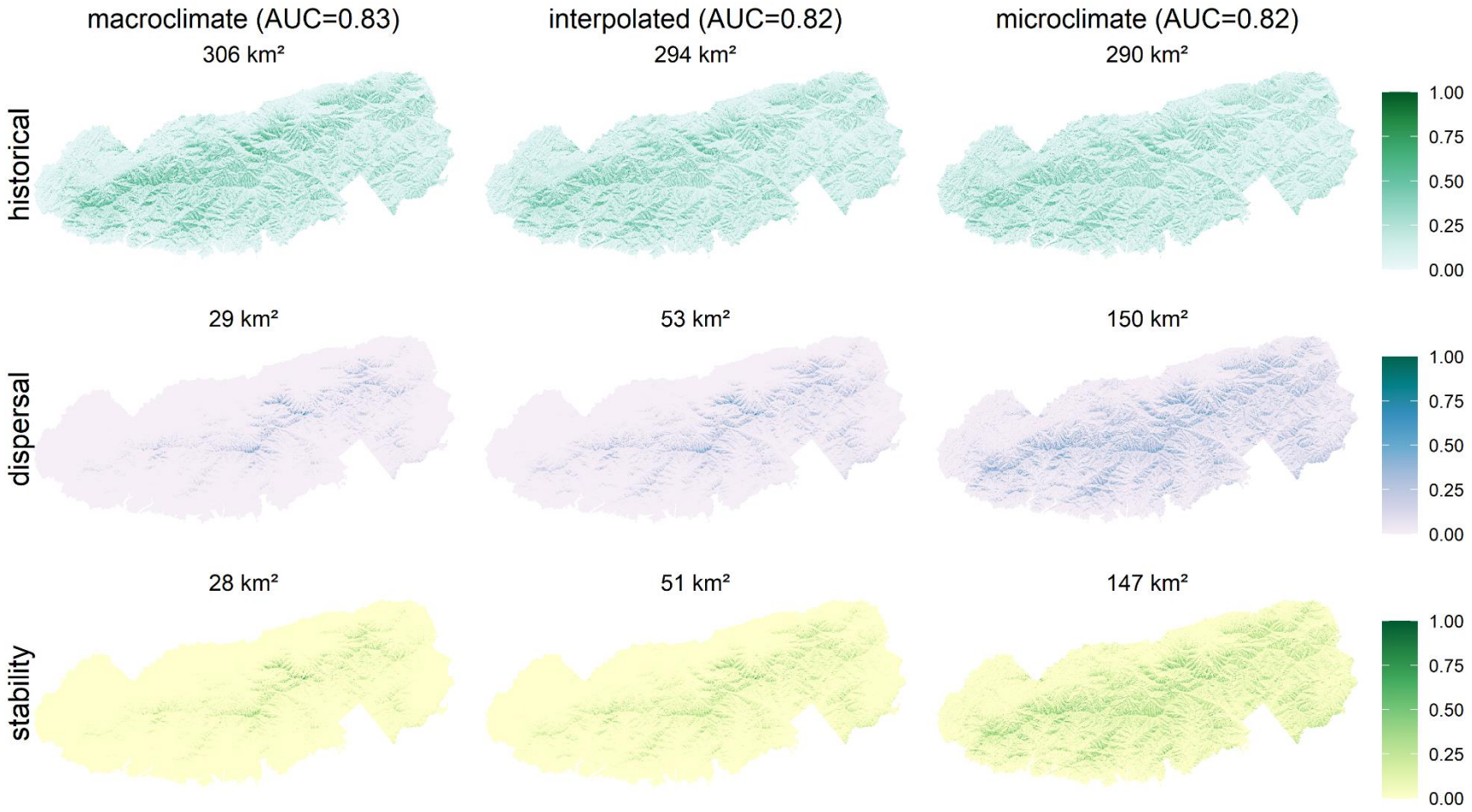

Fig S81. Probability of TILIAME occurrence

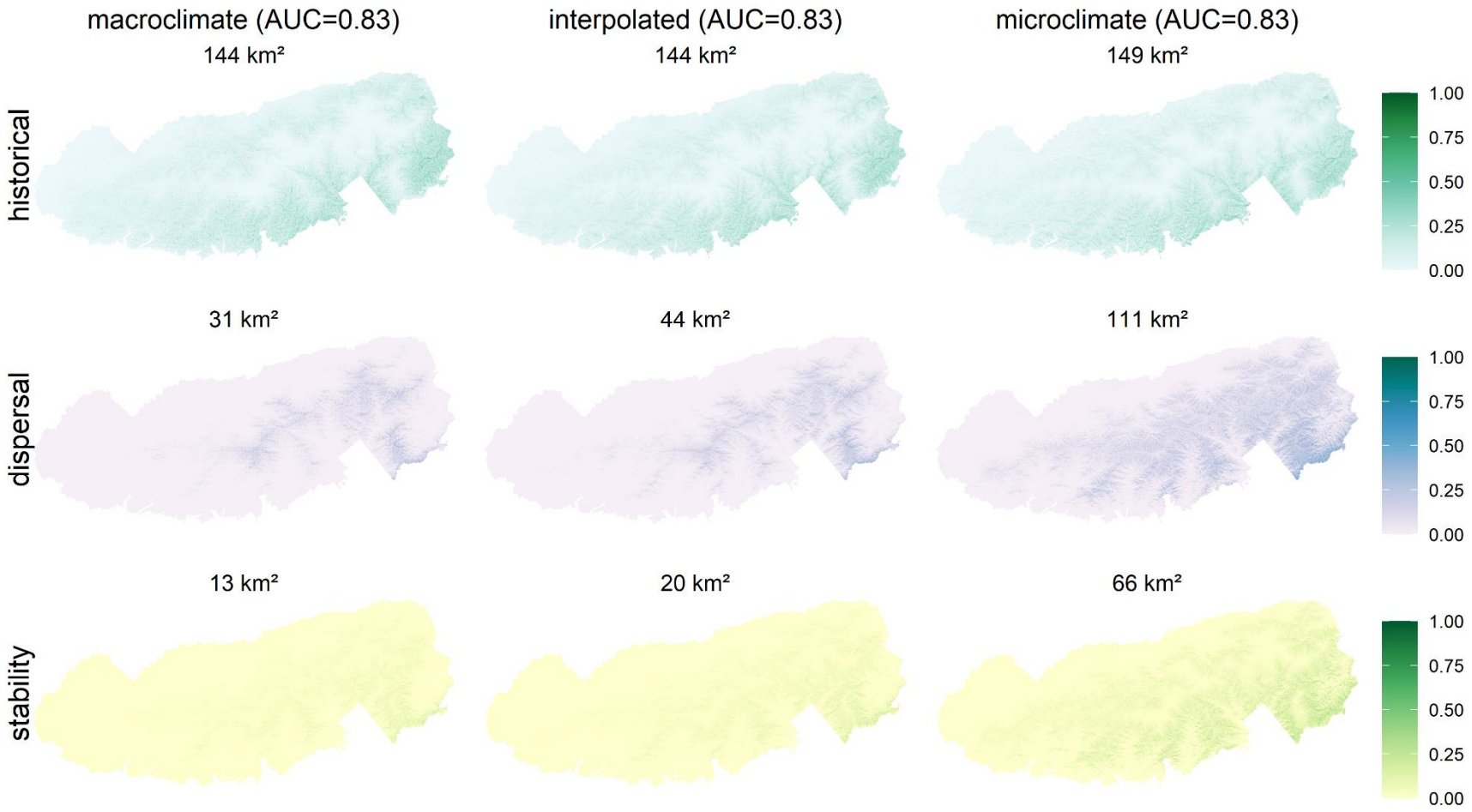

Fig S82. Probability of TILIAMEH occurrence

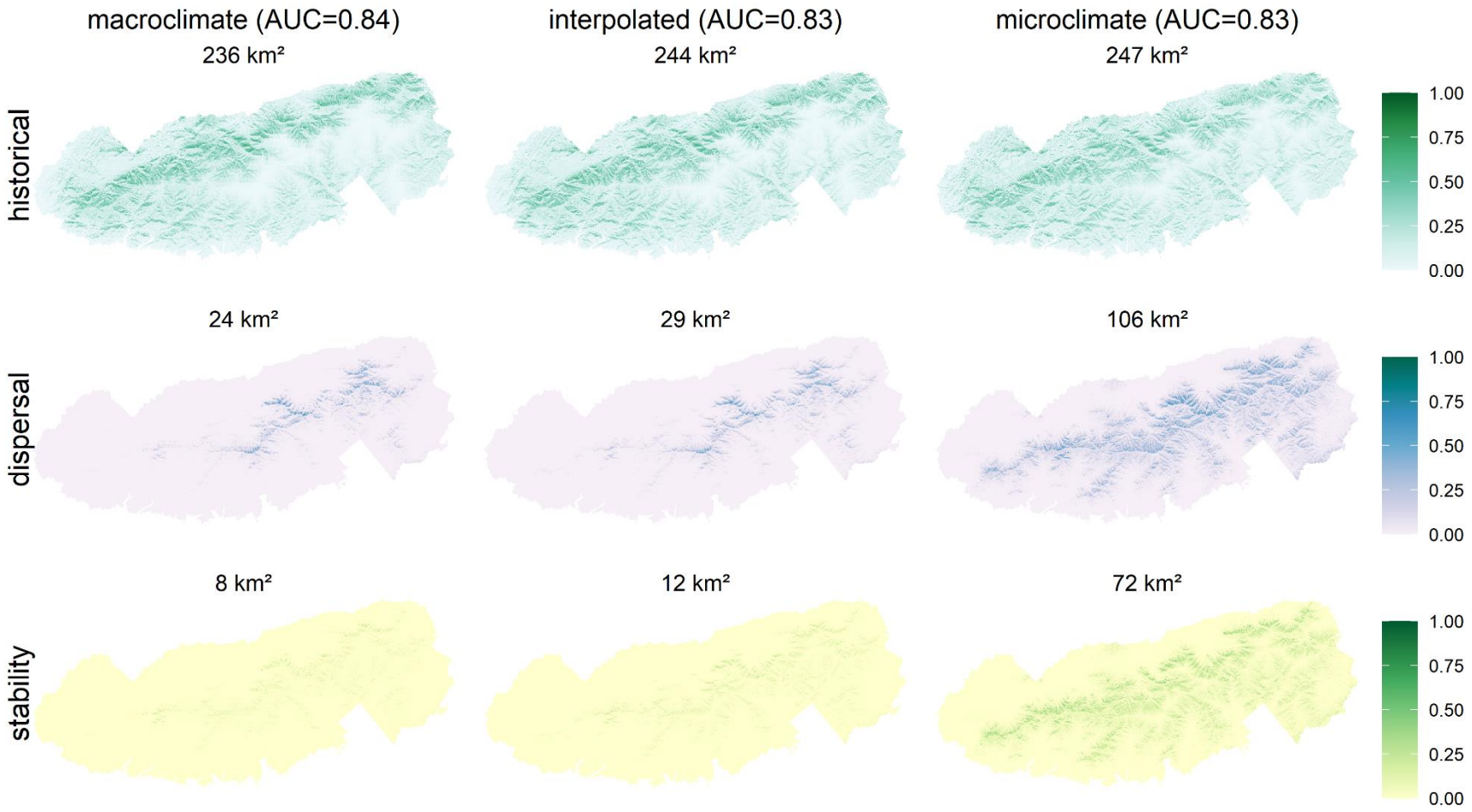

Fig S83. Probability of TOXIRAD occurrence

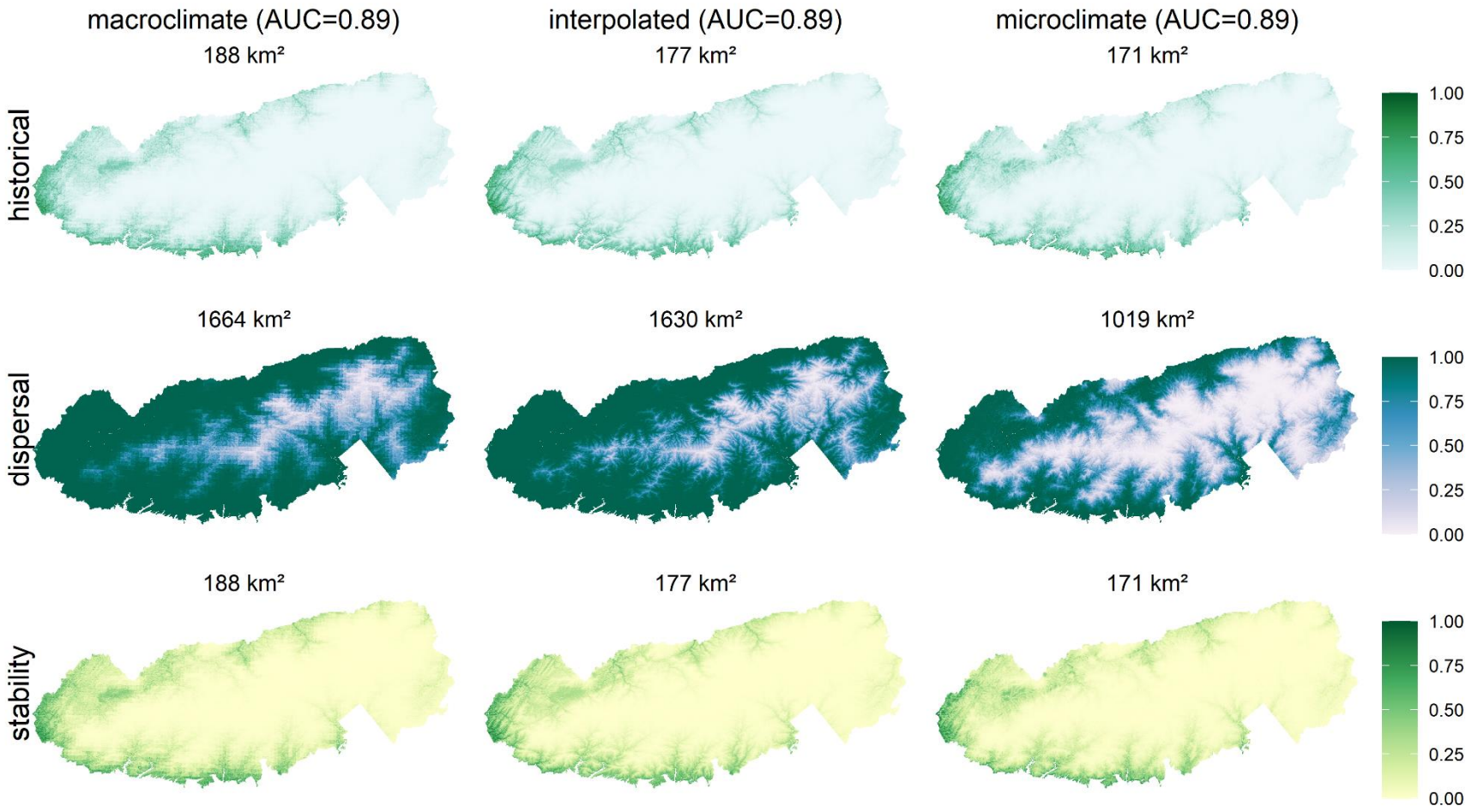

Fig S84. Probability of VACCERY occurrence

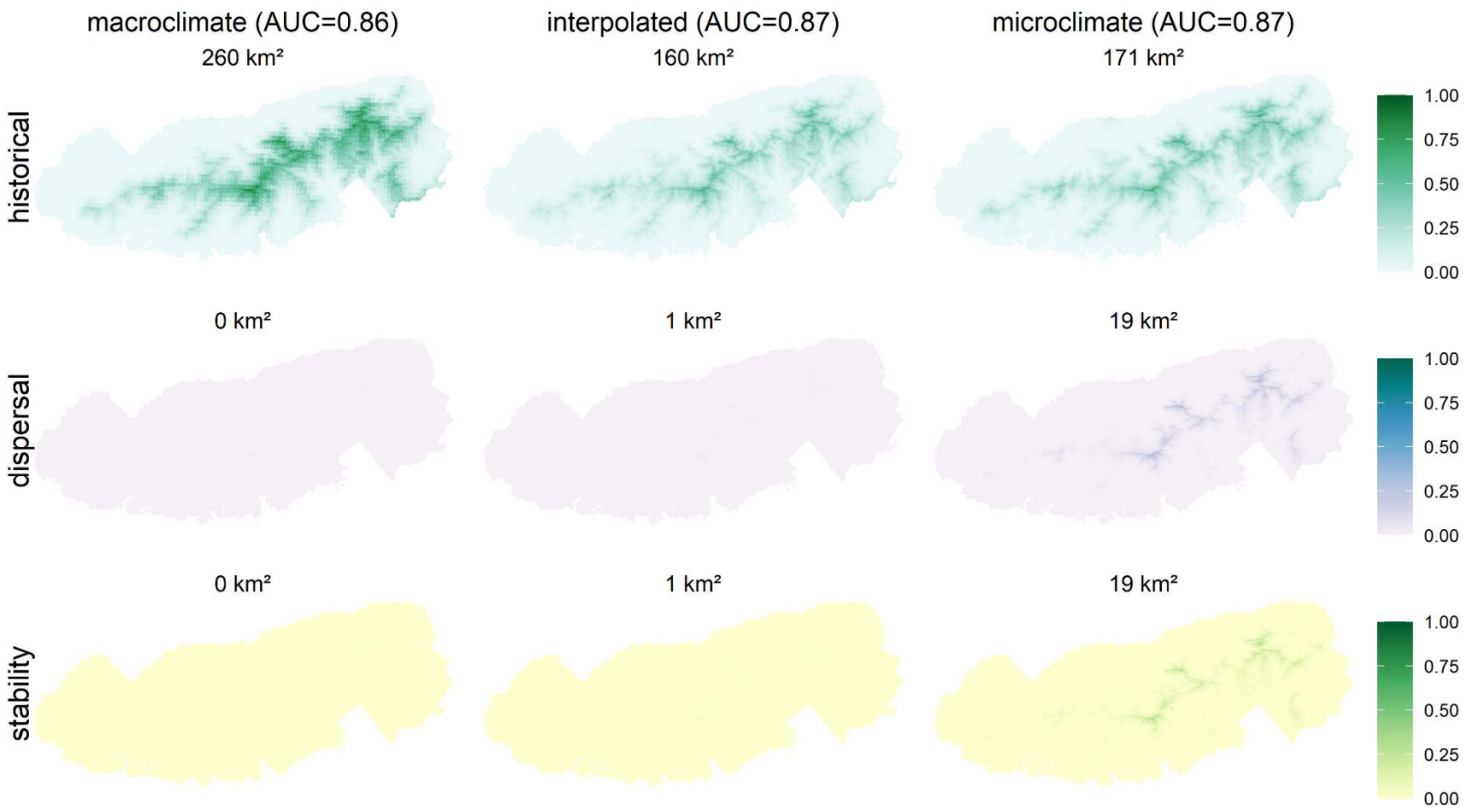

Fig S85. Probability of VACCHIR occurrence

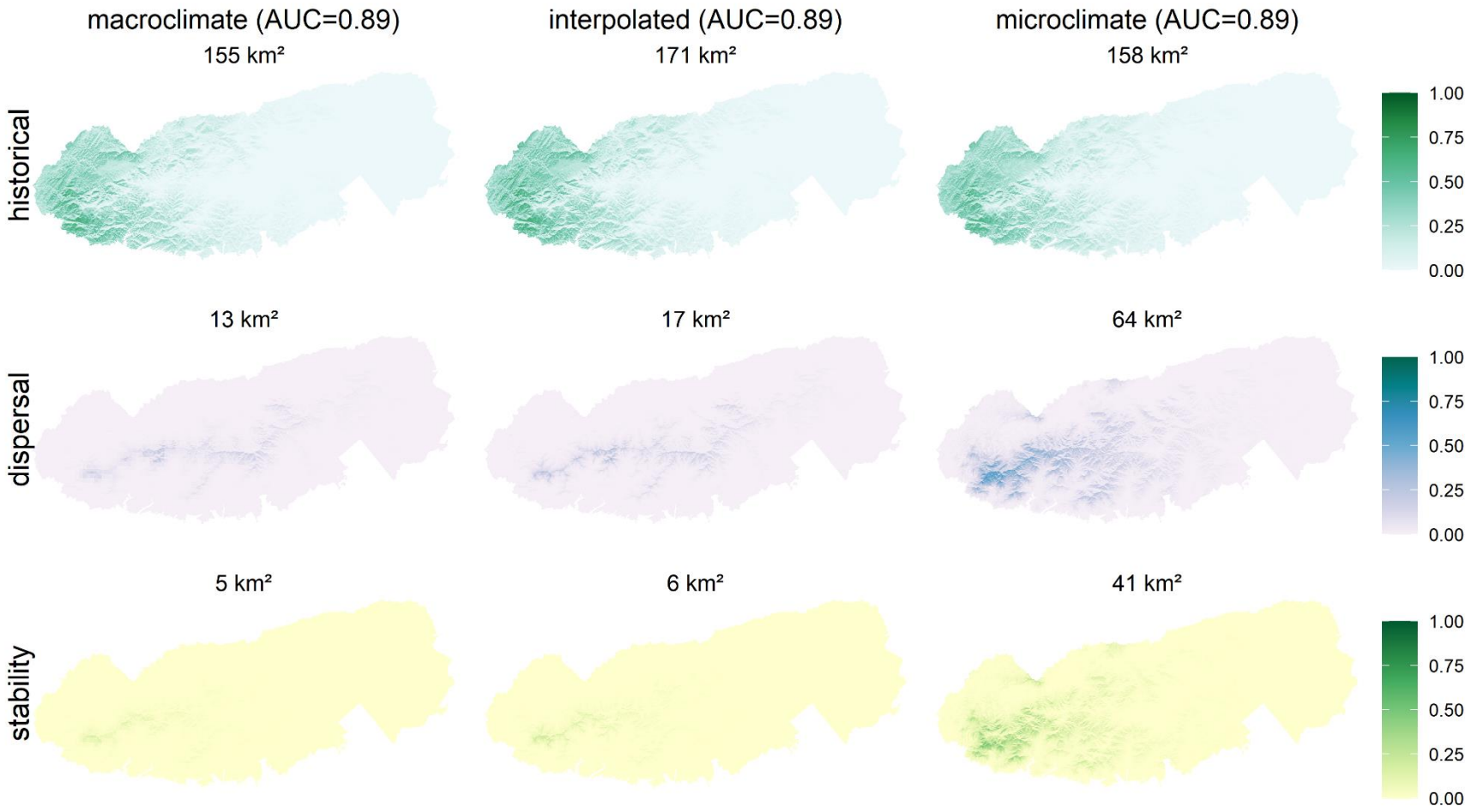

Fig S86. Probability of VACCPAL occurrence

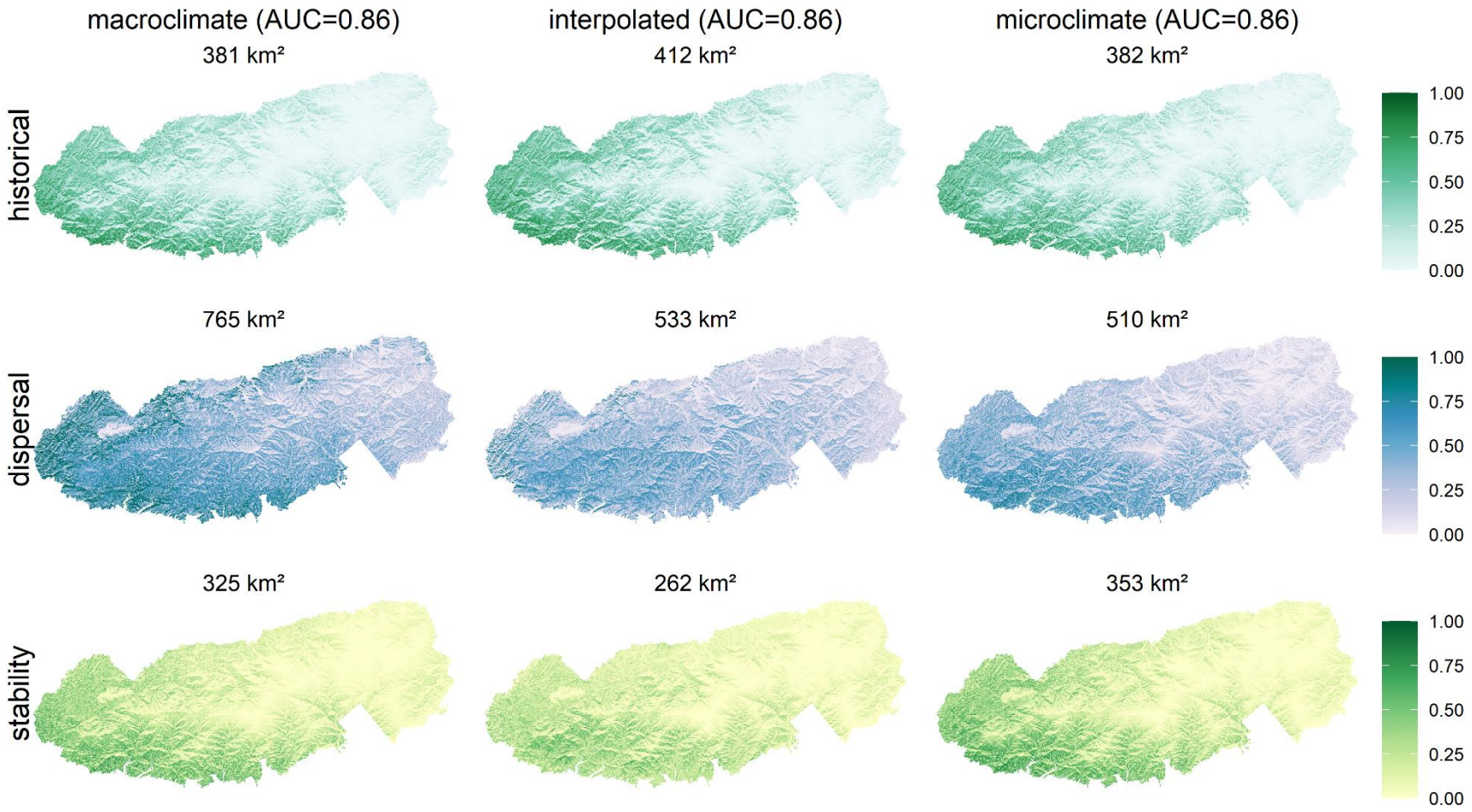

Fig S87. Probability of VACCSIM occurrence

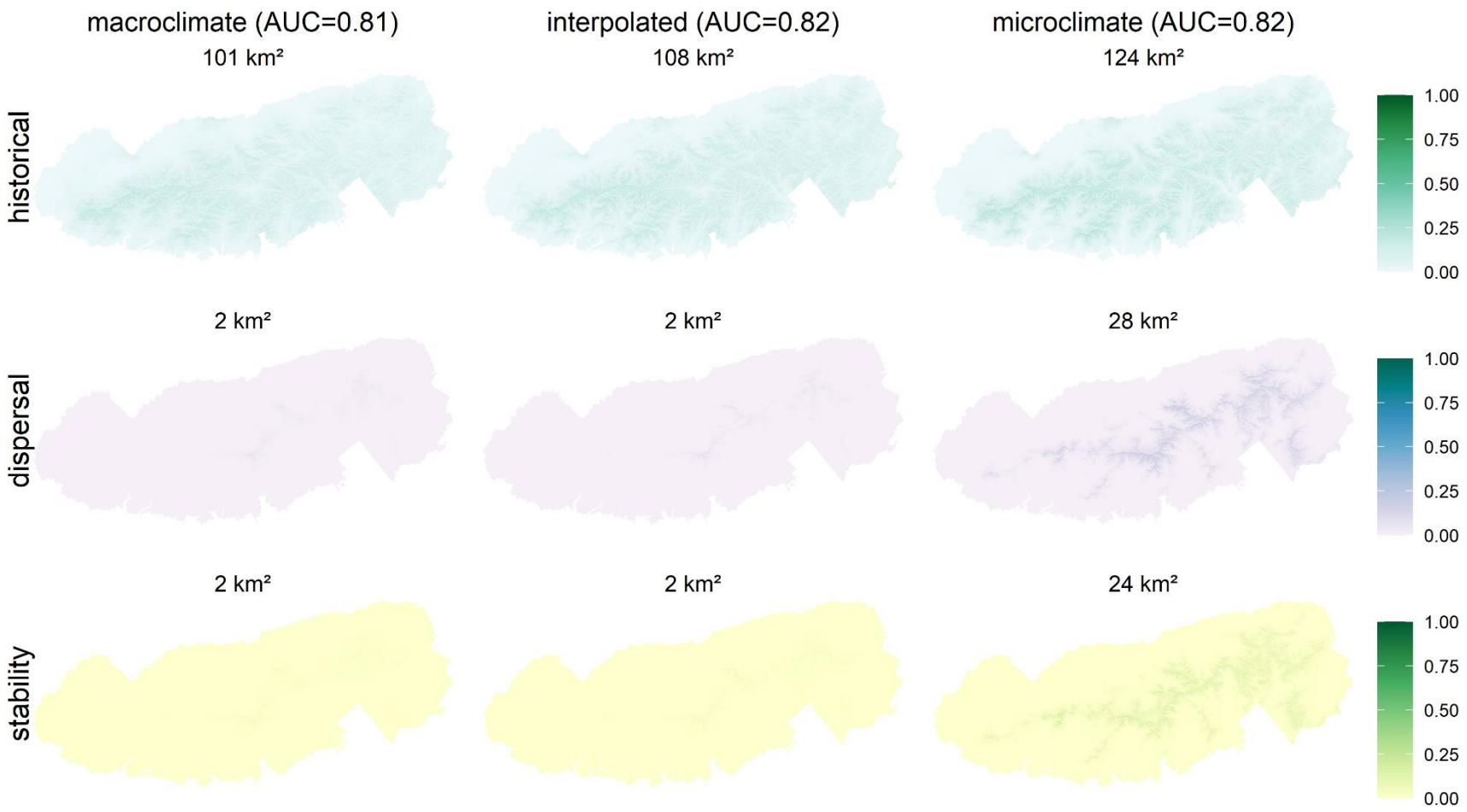

Fig S88. Probability of VACCSTA occurrence

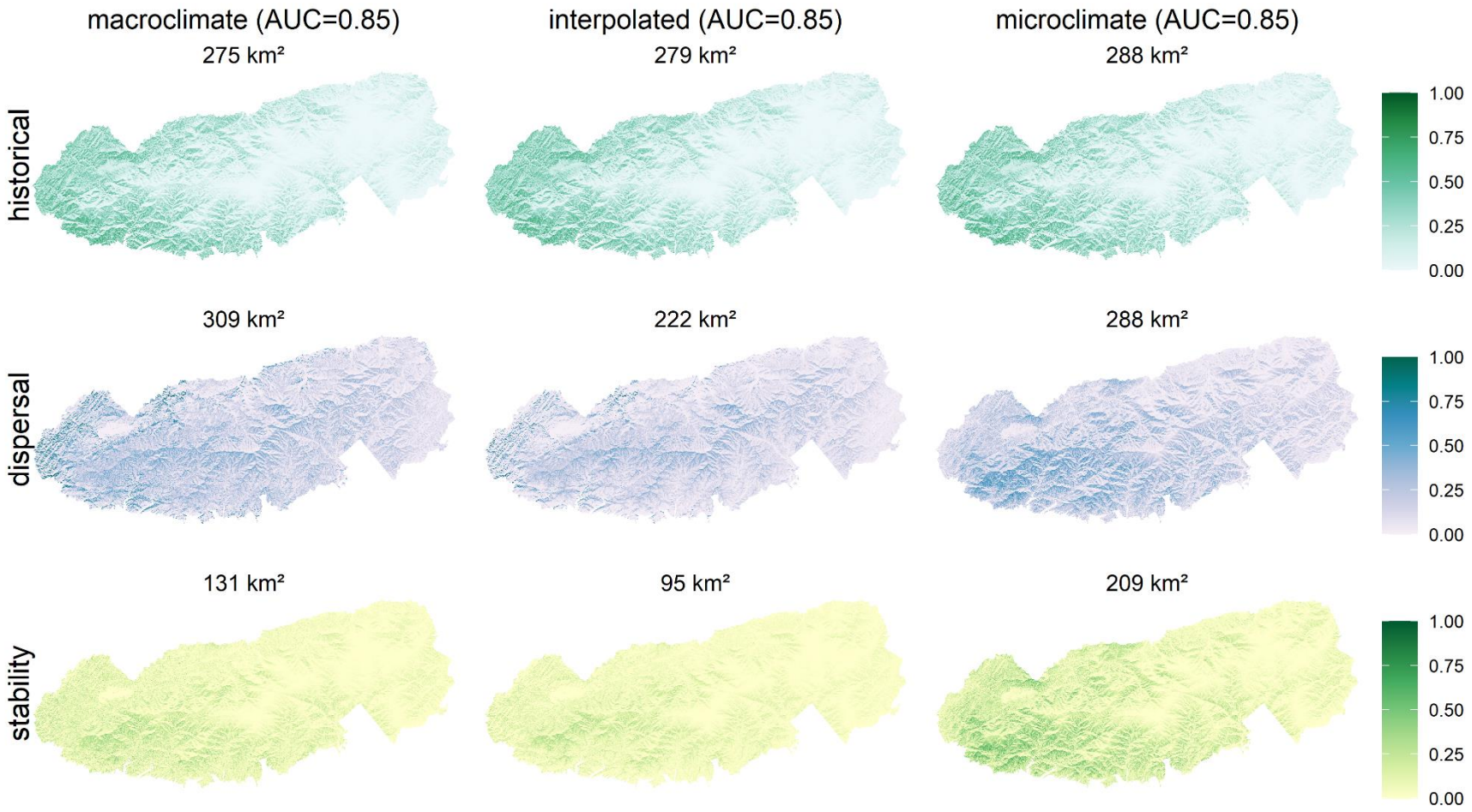

Fig S89. Probability of VIBULAN occurrence

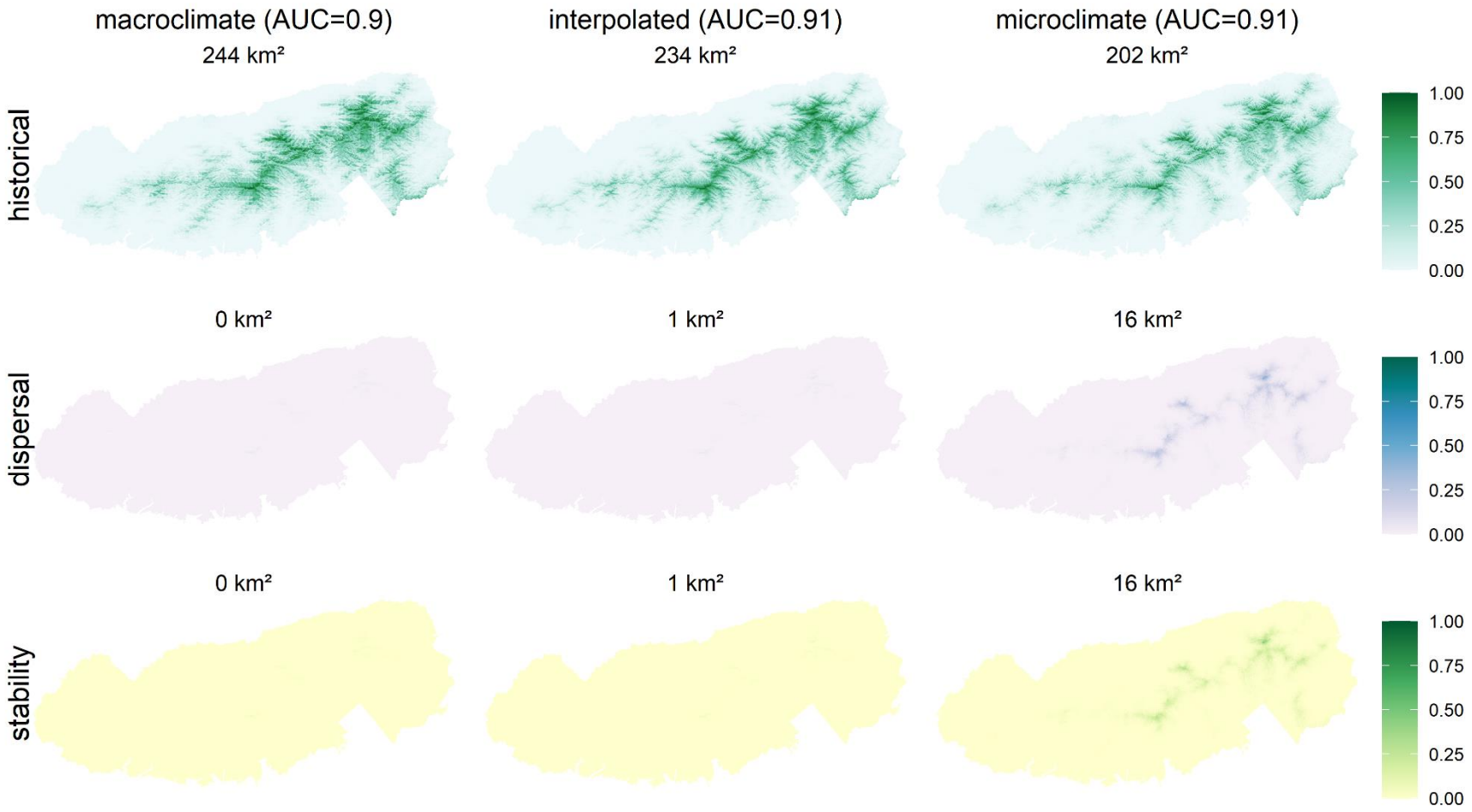

Fig S90. Probability of VIOLROT occurrence

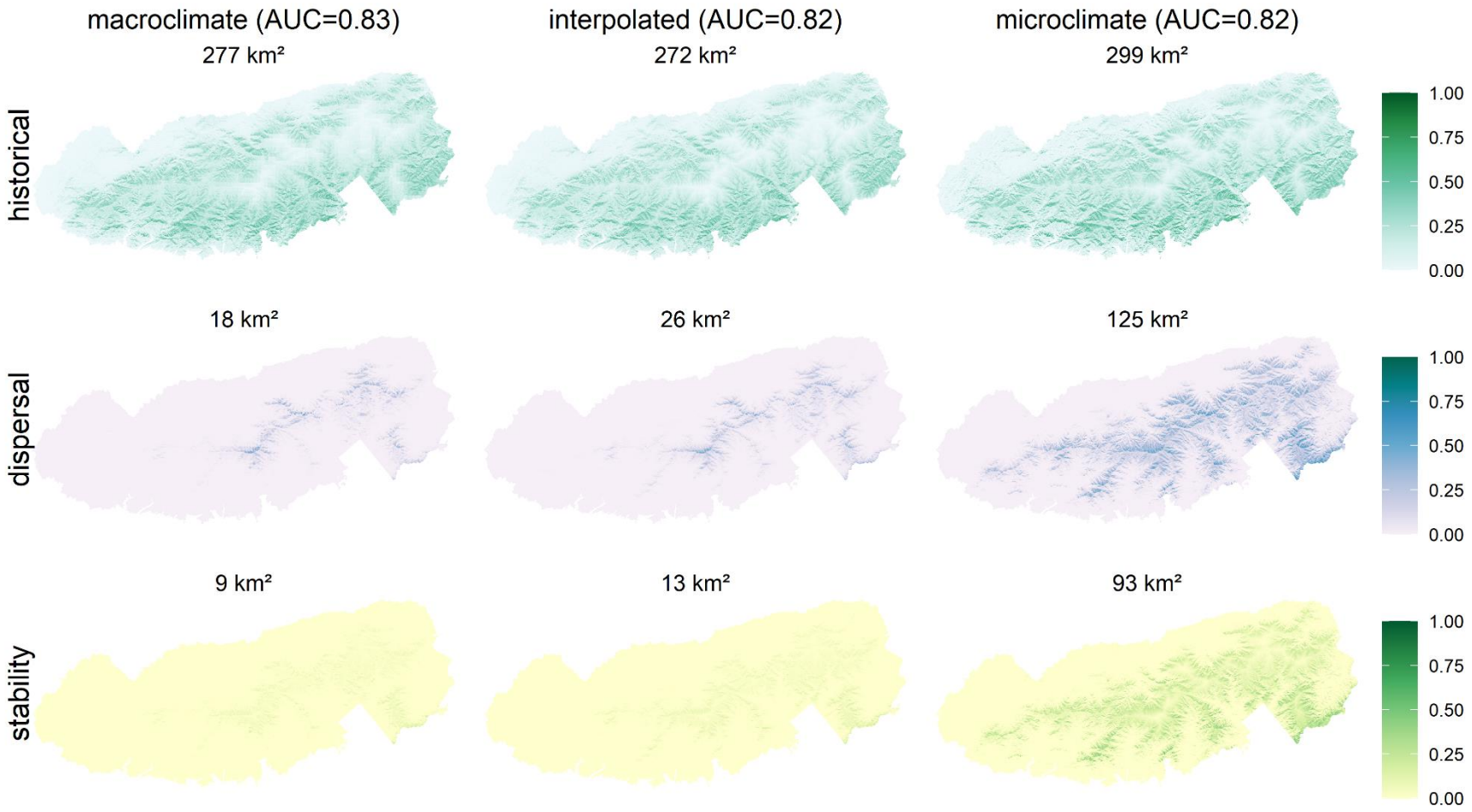

Fig S91. Probability of VIOLSOR occurrence

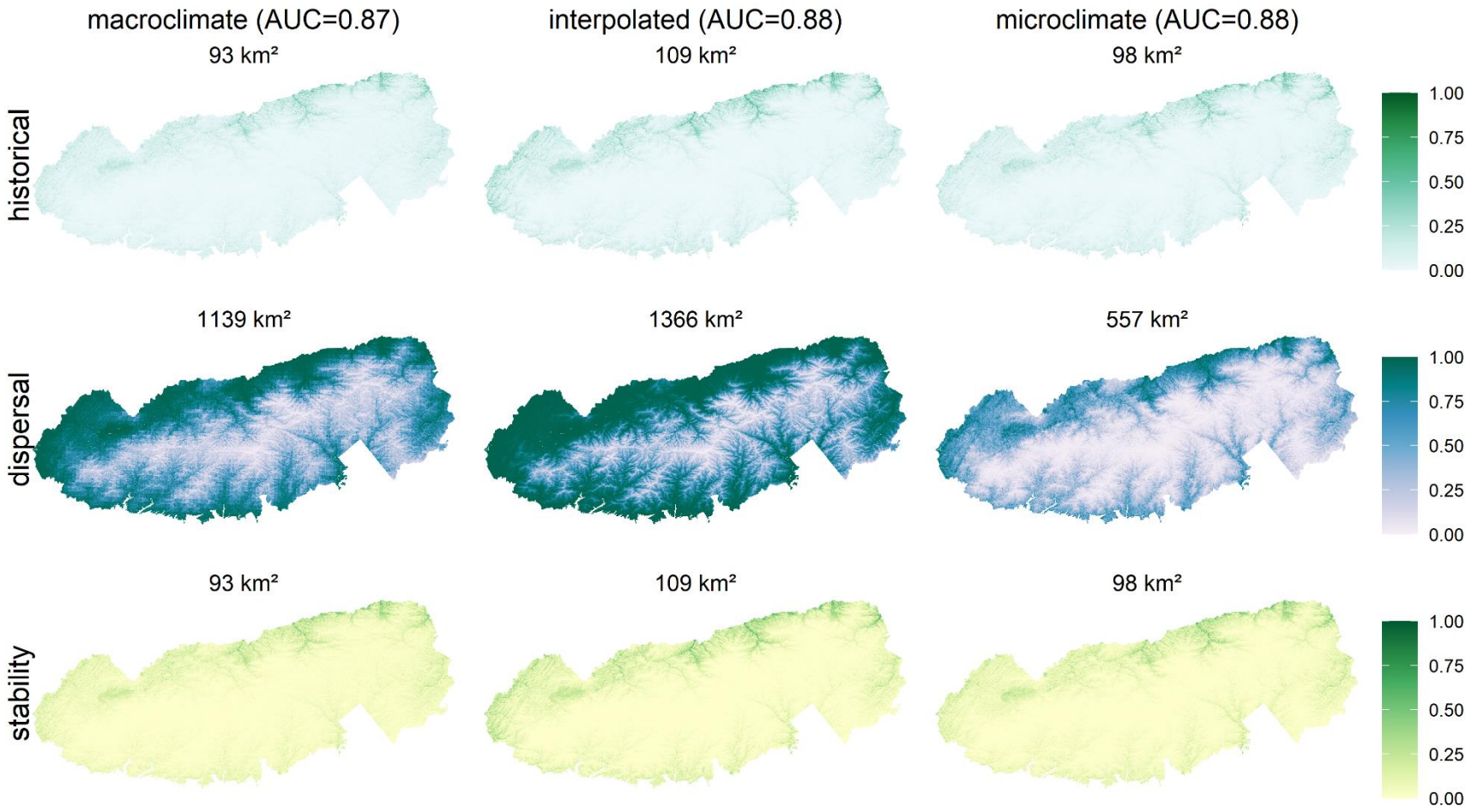

Fig S92. Probability of VITIAES occurrence

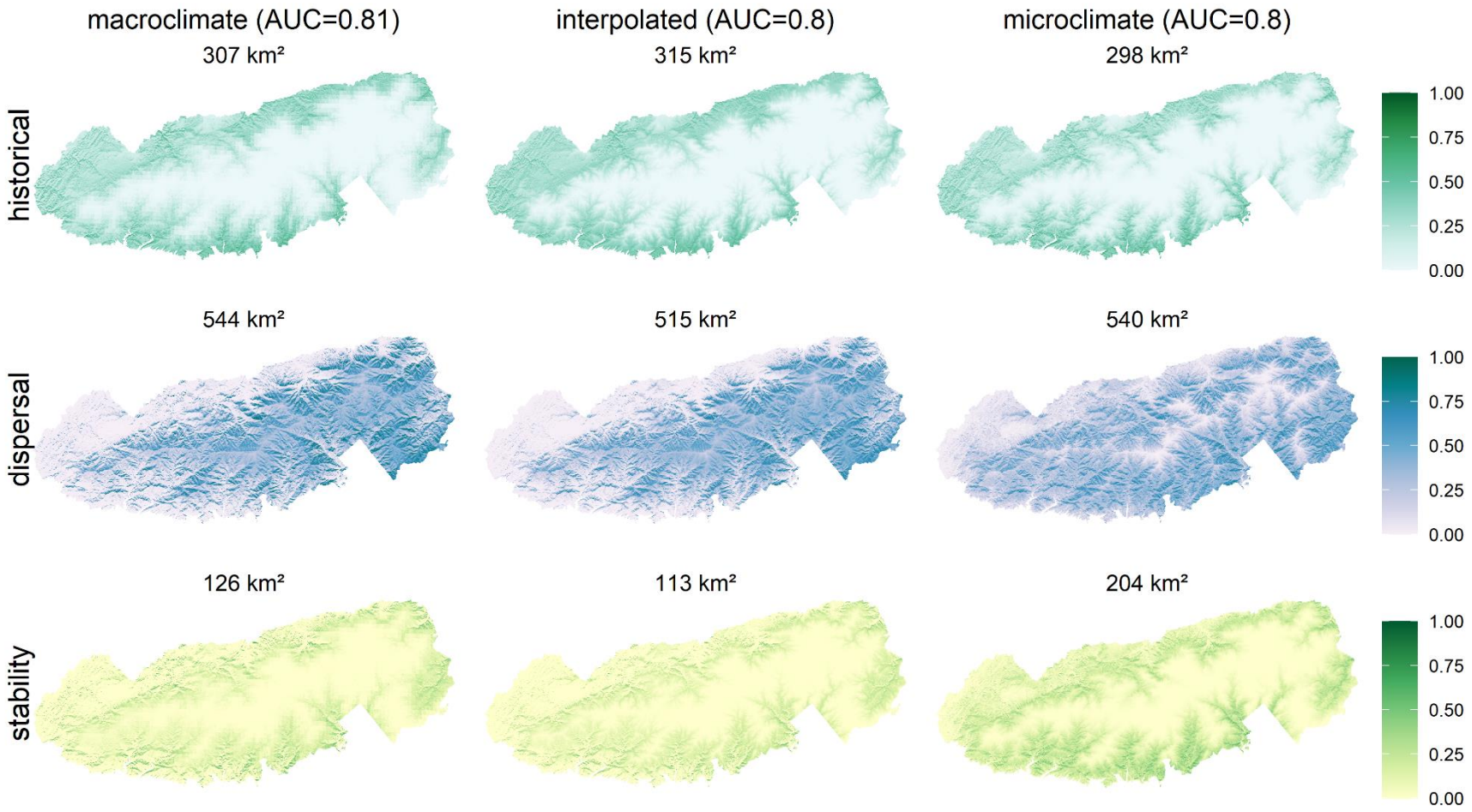

Appendix 2: Sensor design and construction

The following design is based on the Environmental Microcontroller Units (EMUs) of James Mickley and colleagues at UCONN. See https://github.com/mickley/EMU and:

Mickley, J. G., T. E. Moore, C. D. Schlichting, A. L. DeRobertis, E. Mason, & R. Bagchi (2018). Measuring Microenvironments for Global Change: DIY Environmental Microcontroller Units (EMUs). Methods in Ecology and Evolution. 1-7. doi: 10.1111/2041-210X.13128

The below modifications include programming and data access via Arduino IDE rather than Lua; more robust external wiring and housing, soldered connections on a pre-printed circuit board in place of a breadboard; a soil temperature sensor; and two rather than one soil moisture sensors. Total per-unit cost is about $20.

This 'B' version of sensors was primarily designed to be completely belowground and not detected by animals in the field, but it contains several other improvements compared to the 'A' version including (1) pre-printed circuit boards which reduce construction time and improve reliability, (2) improved housings constructed from PVC for lower cost and increased water resistance, and (3) new code that allows sensor to enter 'deep sleep' if there is an error with the RTC and allows data download without uploading a different program. All Arduino scripts as well as data processing scripts are available at github.com/jordanstark/Soil_temp_moisture_EMU/ .

The Arduino code was written with Arduino IDE version 1.8.9. The board manager was used to install 'esp8266' version 2.5.2 (note that more recent versions may be incompatible with the SPIFFS storage!). The following Arduino libraries are also required: 'RTClib', 'uRTClib', 'OneWire', 'DallasTemperature', and 'Adafruit_1x15'. Drivers to install and communicate with the microcontrollers are available from https://www.wemos.cc/en/latest/ch340_driver.html .

Wiring & testing components

For testing, it is useful to have a copy of the printed circuit board on a breadboard—wired as in this diagram. A battery pack can be attached to the lower power rails to provide power. I generally test (1) microcontrollers-just make sure that they turn on; (2) RTCs, both to check that the time can be set and that the alarm function works; (3) MOSFETs, to make sure they work with the alarm. I have not had issues with other components but they could also be checked using this wiring.

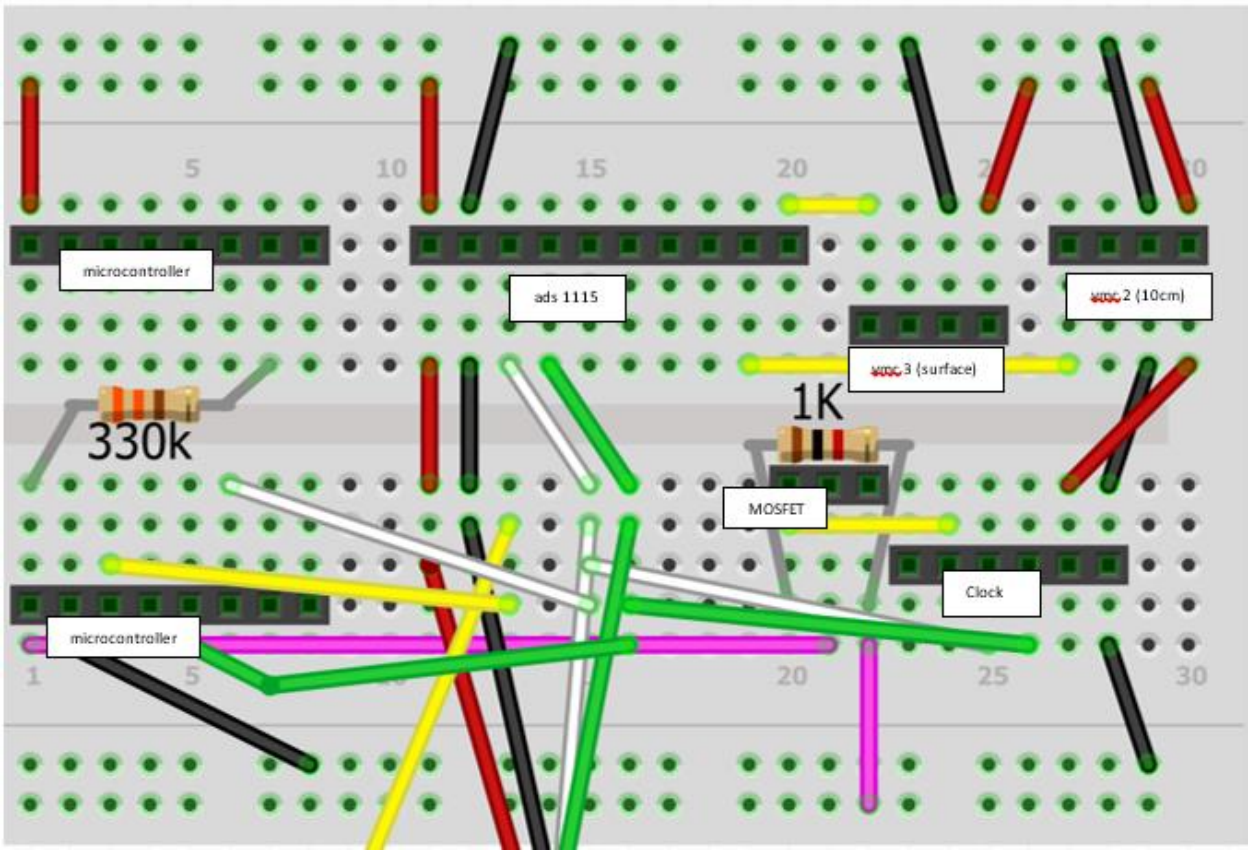

Fig S93. Fritzing circuit diagram for use with a breadboard.

1. Circuit board – upgraded to a custom printed circuit board – design attached. We ordered these from JLCPCB for ~$0.50 per board--they decrease cost and time. If you are only

making a few, you could solder these instead (see ‘A’ protocol at https://sites.google.com/site/fridleylab/home/protocols).

Gerber design files in ‘Construction’ folder; download ‘B sensor PCB Gerber.zip’.

i. Solder ~10 cm of color-coded wires to the “1wire” section of the board (red to 3v, black to gnd, yellow to OneWire). If using any I2C probes (not described in this protocol but see Mickley et al. or the ‘A’ sensor protocol) additional wires can be soldered to the I2C section

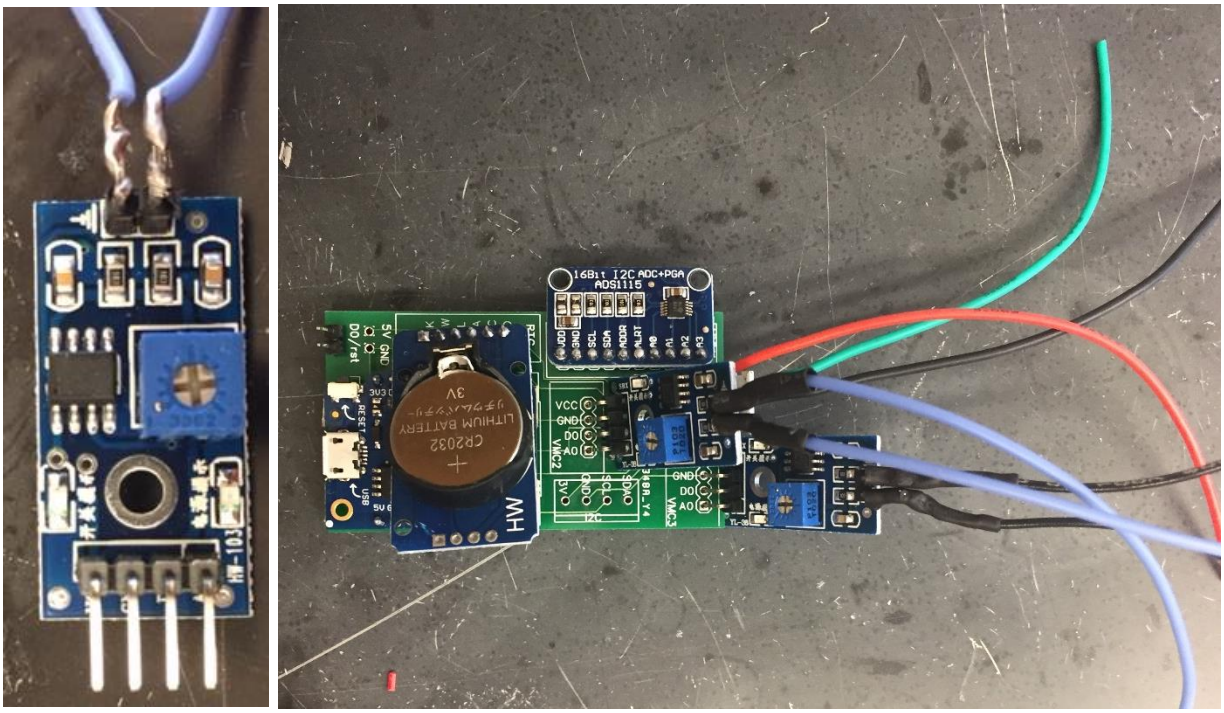

Fig S94. Printed circuit board with soldered components

2. Other components soldered to circuit board

These components (pre-tested) can be wired into their correct locations on the circuit board above:

i. microcontroller – lolin d1 mini

Use short pins with black plastic part underneath. Test to make sure that the microcontroller can be programmed by uploading any sketch.

ii. real-time clock – ds3231sn

Remove upper-left resistor marked "102" and 4x472 resistor across from vcc. Remove LED lights to save power. MAKE SURE TO TEST THESE-about 25% do not work (either cannot accept time input or will not enable alarm). I am setting and checking the time with board_config.ino and then running test_clock_blink.ino which should turn the microcontroller on once per minute and blink the onboard LED 3x.

iii. analog-to-digital converter – ads1115

Solder to pins. I haven't had any issues with these.

iv. P-mosfet

Test these with test_clock_blink.ino sketch to make sure they work before soldering in! The front (where the black box sticks out) should point in the direction of the arrow on the circuit board.

v. Battery pack

Solder to '5V' (red) and 'GND' (black) near the RTC and d1 mini.

vi. Chip for soil moisture sensors (x2)

Attach ~15 cm leads and cover each top pin with heat shrink before soldering to board. Do not insert completely into board—you want to be able to bend the chips back slightly to fit in the PVC housing. Remove the LEDs to save power.

vii. Pins for jumper

Use extra pins from microcontrollers or other components, cut to only 2 pins.

viii. Resistors

1k and 330k resistors-easiest to wire these on the back of the board and cover connections with a piece of electrical tape to avoid accidental shorts. Can wire on the front if careful…

3. Sensors

i. soil temp – ds18b20

Cut wire to 50 cm length. Remove ~3cm of shielding and strip ~ 1cm of each wire.

ii. soil moisture (x2)

Remove pins, taking as much solder out of pin holes as possible with solder sucker. To make the shallow probe, cut excess wire from soil temp probe to 40 cm. Cut off excess yellow wire and solder red and black wires to probe; direction does not matter. Strip as little of the wire as possible. To make the deep probe, use 50cm of 2-strand 24awg wire. After soldering wires to probes, cover connection between wire and probe generously with 100% silicone and let dry at least overnight—this often requires touching up on the side the wire was resting on the next day. Paint modified silicone sealant over soldered connections on the other side. Remove ~2 cm of exterior shielding from the other end and strip 1-2cm.

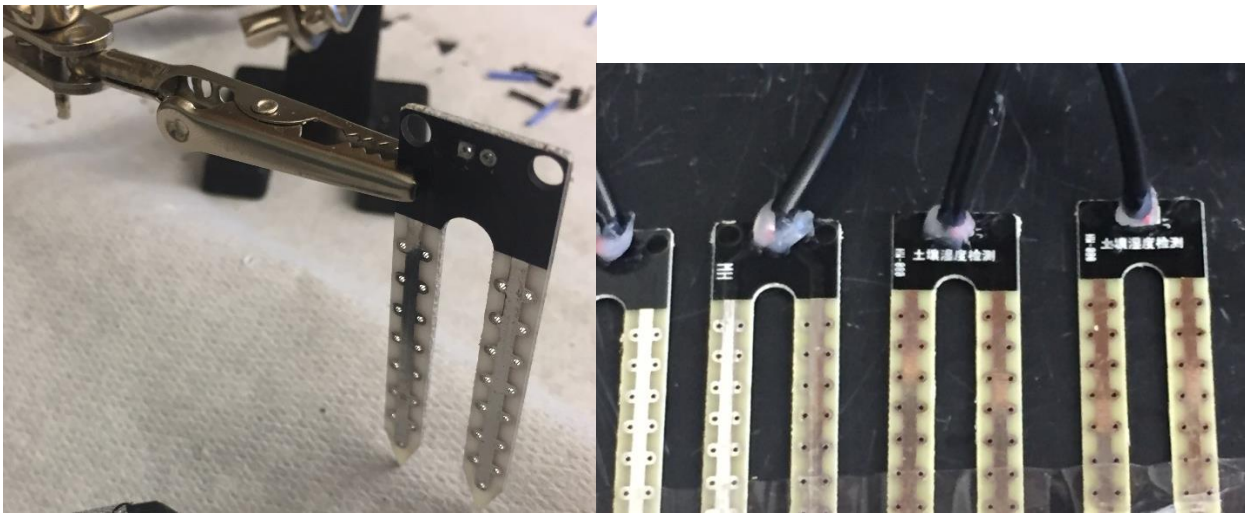

Fig S95. Preparation of soil moisture sensors. Panel A (left) shows removal of pins and solder; panel B (right) shows moisture sensors with new wires attached and waterproof silicone around connections.

Housing and assembly

1. PVC and fittings – 2” FTP cap, 2” adapter, 2” x ½” bushing, PG13.5 cable gland

Use PVC primer and cement to permanently attach adapter to bushing. When dry, coat cable gland threads with 100% silicone and tightly screw into bushing. Apply thin layer of 100% silicone around the connection between cable gland and PVC. Let dry again.

2. Sensor attachment to circuit board

Insert wires from soil moisture and temperature probes through cable gland. Solder the wires from the 50 cm long moisture probe to the chip in the ‘VMC2’ slot and the 40 cm long moisture probe to the chip in the ‘VMC3’ slot. Solder wires from temp probe to respective wires from ‘onewire’ slots (yellow- OneWire, red- 3V, black – gnd). Cover connections with heat shrink to avoid shorts. Solder wires for battery pack onto their connectors.

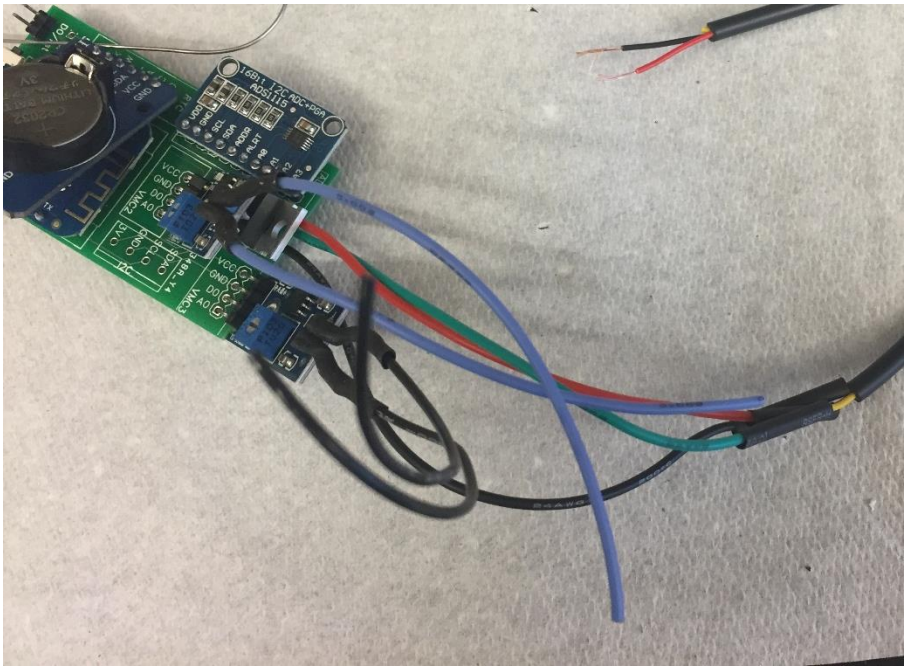

Fig S96. Soldering sensor wire to prepared circuit board. Note that it is generally easiest to install circuit boards in housing before attaching sensors since the moisture sensor will not fit through cable glands.

3. Waterproofing

Position wires for soil sensors so that the stripped portion of wire is just inside of the PVC housing. Remove the outer screw cover of the cable gland and fill the inner ring around the wires with 100% silicone. Let dry at least 24h.

Fig S97. Nearly assembled sensors

Testing, software and assembly

1. Board and clock configuration: files at https://github.com/jdfridley/Sensors

Run board_config.ino with SPIFFS set to 3M to format SPIFFS and set the clock time.

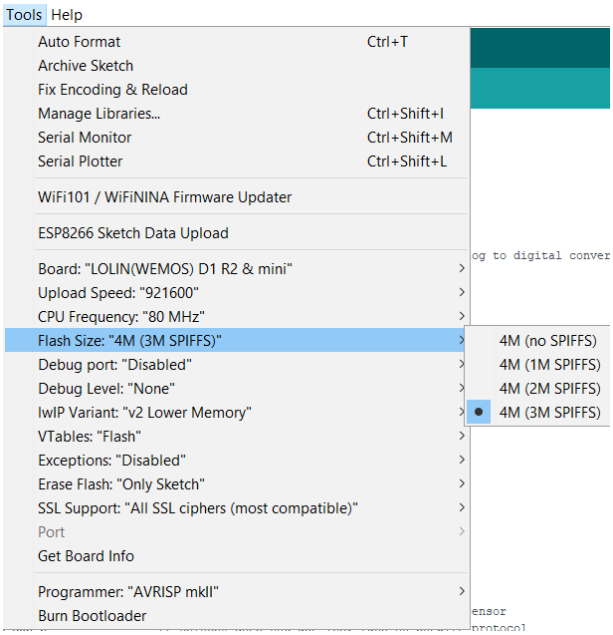

Fig S98. Settings configuration for SPIFFS in Arduino IDE

2. ESP8266 code

Upload B_sensor_read_dl.ino to microcontroller. Make sure to edit the sensor number! This code will write data from each sensor to SPIFFS every hour. Check back in several days to make sure all sensors are reading reasonable values (see 'data download' section below). For sensors with unusual values, check wiring/sensors/etc to determine cause. This program will continue reading after downloading data; to stop reading remove one or more batteries. DO NOT store using board_config.ino program as this will drain batteries.

Assembly

Wrap battery pack in duct tape (electrical tape also works) to avoid damaging batteries by scraping against electrical components. Place battery pack between clock and D1 mini and insert all into PVC housing (it is a tight fit!). Place jumper over pins on circuit board. Wrap threads with PTFE tape. Place two silica gel packets in housing and seal tightly.

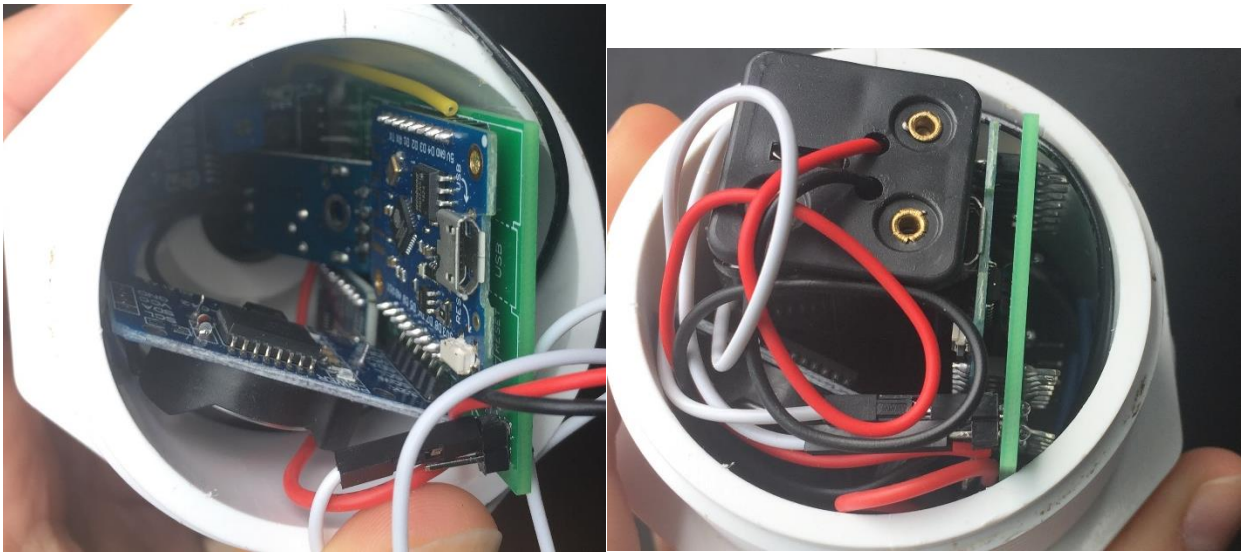

Fig S99. Final sensor assembly. Panel A (left) shows circuit board inside sensor housing without battery pack; Panel B (right) shows circuit board and battery pack inside sensor housing.

Sensor installation

Use tulip bulb planter to create a hole slightly deeper than sensor housing and place sensor housing tightly in hole. Install soil moisture sensors upslope and to the left, with wires in a shallow trench leading back to housing. Pack soil back around housing and cover with removed leaves. Flag trees on either side of the sensor and note position between trees (ie center, or 3 feet

from right tree looking upslope). Sensors are easily detected for data retrieval using a metal detector.

Data download and processing

1. Downloading data with PuTTY

To download data, remove the jumper, plug microcontroller into computer and save serial input using PuTTY (input will start as soon as the microcontroller is plugged in). Files are saved as a raw text file (you can use the .txt extension to open in notepad or another text program).

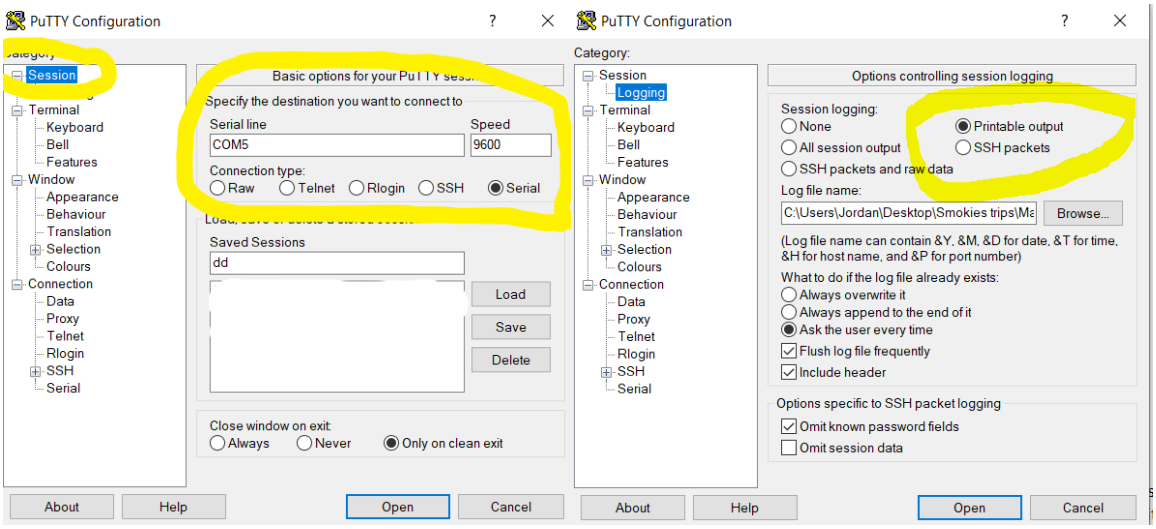

Fig S100. Configuration of PuTTY for data download. Note that the COM port may not be COM5 on all systems.

2. Converting raw files to .csv (in R)

For anything but a very small dataset, it is most convenient to process the files into a more standard format that can be read into R or other data analysis programs. To do this, place all of the raw data files in an otherwise empty folder. In a separate folder, save the calibration

coefficients (calib_coefs.csv) that convert raw readings from the soil moisture probes and soil temperature probe to volumetric soil moisture. You can then run the R script 'ReadBSensors.R'; edit the 'data_path' at the top to the folder with sensor files in it, the 'Metadata_path' to the folder with calib_coefs.csv in it, and the 'Out_path' to the folder where you would like to save the finished .csv file with all of the data. The file will be saved as 'sensordata.csv' unless you edit the last line of code to include some other name. Note that this script assumes the temperature is the same for both of the soil moisture probes and the soil temperature probe; if they are installed at different depths you may want to calculate a temperature correction. Additional R scripts for removing dates when sensors were not deployed in the field and identifying malfunctioning sensors are available at https://github.com/jordanstark/Soil_temp_moisture_EMU/DataCleaning

Useful links and resources

The components and connections in this design are based largely on **Mickley, J. G., T. E. Moore, C. D. Schlichting, A. L. DeRobertis, E. Mason, & R. Bagchi (2018). Measuring Microenvironments for Global Change: DIY Environmental Microcontroller Units (EMUs).** ***Methods in Ecology and Evolution*****. 1-7. doi: 10.1111/2041-210X.13128 .**

In addition to this paper, Mickley et al have a fantastic github resource for EMUs with troubleshooting and calibration information: https://github.com/mickley/EMU

Many thanks to Fernanda Santos at Oak Ridge National Lab for comments on this protocol.

Vita

Education

Syracuse University, Syracuse NY — Anticipated Dec 2021

Master of Science, Biology

Thesis: Drivers and effects of microclimate variation in Great Smoky Mountains National Park

Skidmore College, Saratoga Springs NY — May 2015

Bachelor of Arts, Environmental Studies/Science Track, *summa cum laude*, Phi Beta Kappa

Publications

In review: Stark JR, Fridley J. Microclimate-based species distribution models in complex terrain indicate widespread cryptic refugia under climate change.

In review: Beslity J, Shaw SB, Drake J, Stark JR, Fridley J, Stella J. A low cost, low power sap flux probe for distributed and intensive monitoring of tree transpiration.

In prep: Stark JR¸ Fridley J. Expanding microclimate beyond temperature: new tools and models allow prediction of fine-scale, landscape-wide soil moisture variability in complex terrain.

Griffin-Nolan RJ, Mohanbabu N, Araldi-Brondolo S, Ebert AR, LeVonne J, Lumbsden-Pinto JI, Roden H, Stark JR, Tourville J, Becklin KM, Drake JE, Frank DA, Lamit LJ, Fridley JD. 2021. Friend or foe? The role of biotic agents in drought-induced plant mortality. Plant Ecology 222(5): 537-548.

Stark JR, Cardon ZG, L. Peredo E. 2020. Extraction of high-quality, high-molecular-weight DNA depends heavily on cell homogenization methods in green microalgae. Applications in Plant Sciences 8(3): e11333

Stark JR, Lehman R, Crawford L, Enquist BJ, Blonder B. 2017. Does environmental heterogeneity drive functional trait variation? A test in montane and alpine meadows. Oikos 126:1650-1659.

Ness JH, Pfeffer M, Stark JR, Guest A, Combs LJ and Nathan E. 2016. In an arid urban matrix, fragment size predicts access to frugivory and rain necessary for plant population persistence. Ecosphere 7:6

Dávalos A, Nuzzo V, Stark JR, Blossey B. 2013. Unexpected earthworm effects on forest understory plants. BMC Ecology 13:48.

Experience

Research Assistant, Syracuse University, Syracuse, NY

June 2019-present

Teaching Assistant, Syracuse University, Syracuse, NY

3 semesters, June 2019-present

Research & Teaching Assistant, MBL, Woods Hole MA

Aug 2017-May 2019

Lab & Field Assistant, UC Berkeley, El Verde Field Station, Puerto Rico

Aug 2016-Aug 2017

Crew Leader/ Science Technician, Center for Natural Lands Management, Olympia WA

Oct 2015-Aug 2016

Research Assistant, Rocky Mountain Biological Lab/University of Arizona, Gothic CO

Summers 2014, 2015

Field Assistant, Racine-Johnson Aquatic Ecologists, Ithaca NY

Summer/Winter 2012 - 2014

Outreach and presentations

Fridley J, Stark JR. "Climate change and the future forests of Great Smoky Mountains National Park". Presentation to the Highlands Biological Foundation, June 2021.

Workshop: Intro to DIY sensors for measuring the environment, with J. Beslity and J. Fridley; 25 May 2021. 15 participants with various backgrounds including undergraduates and professors from several institutions.

Stark JR. "Plants, and EMUS, and Bears, Oh My". Outreach presentation on ecological and microclimate research to intermediate biology students interested in joining research labs, March 2021

Becklin K, Fridley J, Stark JR. Meet and greet session with Onondaga Community College students interested in research at Syracuse University, March 2021

Stark JR, Fridley J. 2020. Bringing climate down to the forest floor: Low-cost, high resolution sensors for microclimate modeling. Great Smoky Mountains National Park Science Colloquium.

Bachrach H, Gubbins A, Pfeffer M, Stark JR, Turner S and C Gibson. 2015. Small things in small streams in small towns causing big problems. Society for Freshwater Science Annual Meeting.

Ness JH, M Pfeffer, L Combs, E Nathan, A Guest and JR Stark. 2014. Habitat fragmentation induced by urban sprawl compromises interactions between desert plants and fruit-consuming mammals. Ecological Society of America Annual Meeting.